DOTTORATO DI RICERCA IN SCIENZE CHIMICHE

CICLO XXXII

COORDINATORE Prof. PIERO BAGLIONI

GELS BASED SYSTEMS FOR THE DEVELOPMENT OF FUNCTIONAL MATERIALS

Settore Scientifico Disciplinare CHIM/02

Dottorando
Dott. Marta Rossi

_____
(firma)

Tutore
Prof. Emiliano Fratini

_____
(firma)

Coordinatore
Prof. Piero Baglioni

_____
(firma)

Anni 2016/2019

Index

Abstract

The investigation of gel systems is interesting for a wide variety of applications, spanning from chromatography to membrane separation, artificial tissues for wound dressing, drug delivery, sensing and catalysis. Recently, they have been employed also for the cleaning and conservation of works of art, thanks to their ability of ensuring a controlled and selective cleaning action, in order to maintain the comprehensibility of artworks and prevent their degradation. For many of these purposes, it is necessary to improve already existent gel systems and develop innovative ones, understanding the correlation between their structural properties and the diffusion processes of molecules and macromolecules through them. Therefore, macroscopic poly(2-hydroxyethyl methacrylate) (pHEMA) based hydrogels and poly(N-isopropylacrylamide) (PNIPAM) and poly(methyl methacrylate) (PMMA) microgels were prepared and deeply characterized. In particular, the effect of water content and state, cross-linker concentration and topology, and finally the monomer/polymer ratio were investigated in respect of the final properties of classical pHEMA and even semi-interpenetrating with poly acrylic acid (pHEMA/PAA) hydrogels. Calorimetric techniques were carried out to evaluate the equilibrium water content and the ratio between free and bound water, while Small Angle X-rays Scattering (SAXS) to characterize the polymer topology at the nanoscale. Moreover, Fluorescence Recovery After Photobleaching experiments, with model probes differing in size (FITC and FITC-dextrans), were performed to monitor the diffusion processes and interactions in the hydrogel matrix.

One of the pHEMA/PAA hydrogels studied, with ideal mechanical properties and retentiveness, together with a semi-interpenetrating pHEMA network with poly(vinyl pyrrolidone) (PVP), were selected and uploaded with

tetraethylenpentamine (TEPA) to be tested for the removal of Cu(II) alteration products (i.e. copper oxychlorides) from bronze artefacts. In order to understand the influence of structural and chemical changes of pHEMA/PVP and pHEMA/PAA hydrogels and the role of TEPA in the coordination of Cu(II) ions, the semi-IPNs were swollen in water at different pH values (6, 8, 12), and in a water solution of TEPA (pH 12), and characterized through SAXS, Scanning Electron Microscopy (SEM), Fourier Transformed Infrared Spectroscopy with Focal Plane Array (FTIR-FPA) and calorimetric techniques. Finally, both hydrogels, loaded with TEPA, were applied on artificially aged bronze coins, to investigate, by means of FTIR-FPA chemical mapping, their ability to solubilize and remove copper oxychlorides.

In order to easily synthesized PMMA and PNIPAM microgels, already used surfactant free emulsion polymerization methods were modified and adapted to obtain monodisperse micron-sized particles. Microgels respond much faster than bulk gel to external stimuli, tuning their structural and physicochemical properties, thus they can be used in a lot of applications in biomedical field, electronics, and fundamental research. Anyway, since they are not easy to handle, macroscopic systems (i.e. macrogels) with different cross-linker concentration and PNIPAM/PMMA ratio were developed, in order to obtain materials that maintain all the properties of the microscopic gels, combining the characteristic of the two different particles. These hydrophilic-hydrophobic macrogels can swell in organic solvent and water, leading the possibility of loading and releasing hydrophilic and hydrophobic drugs. This feature makes them suitable systems for biomedical applications and for the preservation and restoration of cultural heritage.

Moreover, PNIPAM and the more hydrophilic PNIPAM-poly(ethylene glycol) microgels were employed as model systems to study the diffusion inside macroscopic cryogels, with pore dimensions similar to the size of the

microparticles, through the use of particle tracking analysis at different temperatures. The obtained results ma may provide important information to understand the diffusional properties of many natural and industrial processes, such as biomolecules and macromolecules that moves through cells or other biological fluids, and drugs confined in nanocomposite materials.

List of abbreviations

AIBN	Azobisiosbutyronitrile
APS	Ammonium persulfate
Cg	Chemical gel
CLSM	Confocal laser scanning microscope
DSC	Differential scanning calorimetry
EDTA	Ethylenediaminetetraacetic acid
EGDMA	Ethylene glycol dimethacrylate
ESC	Equilibrium solvent content
EWC	Equilibrium water content
FITC	Fluorescein isothiocyanate
FPA	Focal plane array detector
FTIR	Fourier transform infrared spectroscopy
FWI	Free water index
FRAP	Fluorescence recovery after photobleaching
MBA	N,N'-Methylenebis(acrylamide)
MSD	Mean square displacement
PAA	Poly(acrylic acid)
PEG	Poly (ethylene glycol)
Pg	Physical gel
PGD	Poly(ethylene glycol) dimethacrylate
pHEMA	Poly(2-hydroxyethyl methacrylate)
PMMA	Poly(methyl methacrylate)
PNIPAM	Poly(N-isopropylacrylamide)
PVA	Poly(vinyl alcohol)
PVP	Polyvinylpyrrolidone
SAXS	Small angle x-ray scattering
SEM	Scanning electron microscopy
Semi-IPN	Semi-interpenetrating polymeric network
TEPA	Tetraethylenepentamine
TGA	Thermogravimetric Analysis

Chapter I

Introduction

Gels

According to the international Union of Pure and Applied Chemistry (IUPAC), a gel is a "non fluid colloidal network or polymer network that is expanded throughout its whole volume by a fluid"[1]; in other words gels can be defined as a two- or multi-component system consisting of a three dimensional polymer network chains with a fluid that fills the space between the macromolecules. Thus, their physical properties are in-between those of a solid and of a liquid.

The investigation of gels has attracted interest over the past decades due to their application in electronics[2], gel electrophoresis and size exclusion chromatography, and in biological and biomedical contexts, as biosensor, artificial tissue scaffolds, wound dressing[3], contact lenses, and drug delivery systems[4].

Recently, they have been employed also in art conservation for the cleaning of cultural heritage, where it is necessary to develop systems able to ensure a controlled and selective cleaning action. In fact, the removal of unwanted layers (dirt, soil, aged adhesives, varnishes, and corrosion products) is fundamental in the conservation practice to maintain the health state of artworks and prevent their degradation. Because most artworks surfaces are sensitive to aqueous solutions or organic solvents, the cleaning fluids can be confined in gels that are able to ensure a controlled release and a non-invasive removal of the unwanted layers, without affecting the original components of the artefacts[5].

1.1 Gelation theories and polymeric network structure

Statistical approaches were applied for the development of the gelation theories by Flory and Stockmayer[6], who postulated the "classical statistical theory", and by Zallen and Stauffer with the "percolation model"[7],[1].

According to the Flory-Stockmeyer model, multifunctional molecules lead to the formation of covalent bonds between them to yield a network structure. Considering that the formation or not-formation of covalent bonds between monomers is a random event, with a given probability p, the system can exist in a *sol* phase consisting of finite polymers (monomers, dimers, trimers, oligomers, etc), if p is small, otherwise, if p exceeds a critical threshold value, p_c, a single molecule, which is infinite in spatial extension ("infinite network"), is formed. This latter situation corresponds to the gel phase. Using a combinatorial approach, it was possible to derive an expression for the molecular weight (Mw) distribution and for p_c, at which $M_w \rightarrow \infty$ (gel point).

The Flory-Stockmayer theory is based on some assumptions that affect the accuracy of this model:

i. The reactivities of all functional groups of the same type are equal and independent of each other;
ii. The intermolecular reactions between molecules of the same cluster are not allowed;
iii. Monomers are assumed to be point-like (without steric hindrance, and excluded volume effects);
iv. Solvent molecules are absent;
v. There is no correlation between molecules.

As a consequence of these assumptions, a conversion slightly higher than that predict by the theory is usually necessary to create a polymer gel[1].

The "percolation model" takes into account the presence of a solvent, the correlations between the molecules of the system, and does not imply unlimited mobility and accessibility of all groups.

Considering a solvent molecule (A) and a monomer (B), the particle-particle interactions can be approximated to the following four types of nearest-neighbor interactions:

-W_{AA} = solvent-solvent interactions;

-W_{AB}= solvent-polymer interactions;

Monomer-monomer interactions occur through van der Waals interactions and directional interactions leading to the formation of tie-points (e.g. covalent bonds):

-W_{BB} = monomer-monomer van der Waals interactions, with weight ρ;

-E = bonding energy between monomers, with weight 1-ρ.

According to this description, the gel phase is defined as the phase where a non-zero finite fraction of monomers is bonded together via chemical bonds to form a macroscopic molecule[9].

In order to calculate the gelation threshold φ_g, the requirements for considering a pair of monomers as bonded must be defined: (i) they must be nearest neighbors and (ii) their relative interaction must be –E. Thus, the probability, p, that a pair of neighboring monomers can be considered as bonded is given by:

$$p = \frac{(1-\rho)^{\frac{E}{KT}}}{\rho^{\frac{W_{BB}}{KT}} + (1-\rho)^{\frac{E}{KT}}} \qquad \text{(Eq. 1.1)}$$

For simplicity, previous discussion considers systems made up by monomers whose directional interactions are the covalent bond between them. Obviously, this approach can be extended to systems of polymer chains of M monomers.

In the case of thermoreversible gel systems, the directional interaction leading to network formation might be of different nature than covalent bonds (e.g. hydrogen bonds)[10].

The gelation threshold, φ_g, is given by:

$$\varphi_g = \frac{Rz^2\sigma}{[(1+R)\sigma-1]z^2+(\sigma-1)^2} \qquad \text{(Eq. 1.2)}$$

where R is a parameter depending on the coordination number f (i.e. the number of interactions per polymer segment and per solvent molecule) and the number of monomers M; z depends on the respective weight of van der Waals or directional interactions between monomers (ρ and 1-ρ); σ depends on M, f and the probability of bond formation between monomers p. For the procedure to get to Eq. 1.2, the reader is referred to Coniglio *et al*[11].

In order to have a detailed picture of gel topology , it is important to define three characteristic parameters:

1. Polymer volume fraction in the swollen state ($v_{2,s}$);
2. Molecular weight of the polymer chain between two neighbouring cross-linking points (M_c);
3. Corresponding mesh size or correlation length (ξ).

Figure 1.1 (a) shows the schematic structure of a gel.

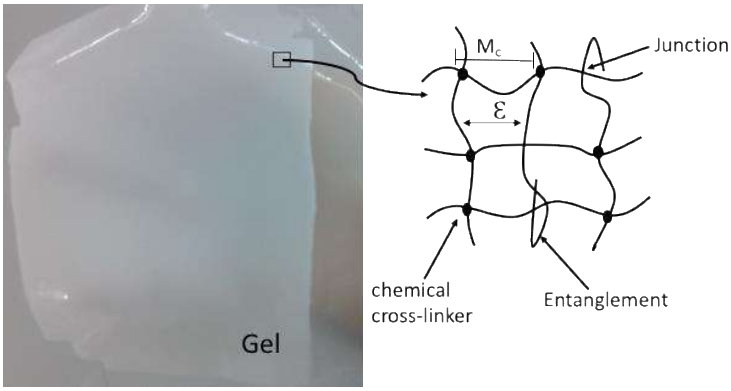

Figure 1.1 (a). Left) Macroscopic appearance of a gel. Right) Schematic representation of the internal structure of a gel.

The polymer volume fraction in the swollen state is a measure of the amount of fluid imbibed and retained by the hydrogel.

$$v_{2,s} = \frac{volume\ polymer}{volume of swollen\ gel} = \frac{V_P}{V_{Gel}} = \frac{1}{Q} \qquad \text{(Eq. 1.3)}$$

This parameter can be determined by using equilibrium swelling experiments. The molecular weight between two consecutive cross-links M_c, which can be either of a chemical or physical nature, is a measure of the degree of cross-linking of the polymer.

$$X = \frac{M_0}{M_C} \qquad \text{(Eq. 1.4)}$$

where M_0 is the molecular weight of the repeating units building the polymer chains. It is important to mention that, due to the random nature of the

polymerization process itself, only average values of M_c can be calculated. The network mesh size represents the distance between consecutive cross-linking points and provides a measure of the porosity of the network.
These parameters, which are not independent, can be determined theoretically or through a variety of experimental techniques[11].

1.2 Classification of gels

Gels can be classified in different ways depending, for example, on the nature of the cross-linking (physical and chemical gels), on the medium in which the polymeric network is dispersed (xerogel/aerogel, organogel, and hydrogel), and on the basis of the polymer composition (homopolymer, copolymer, interpenetrating polymer network).

1.2.1 Physical and Chemical gels

Physical gels are polymeric systems that form a 3D network thanks to the presence of non-covalent interactions (i.e. hydrophobic, electrostatic, and Van der Waals interactions, or hydrogen bonds) between the macromolecular chains (see Figure 1.2.1 (a)). Due to the weak nature of these interactions (1-120 kJ/mol), it is possible to break and reform them in certain conditions. In fact, almost all types of physical gels are thermoreversible; increasing the temperature over a given threshold (depending on the chemical nature of the gellant and the liquid phase) causes the melting of the supramolecular structure, leading to the redispersion of the single molecules in the solvent bulk phase. By cooling back

to the original temperature, a sol-gel transition occurs, and the polymer network is reformed.

There are various methods for obtaining physically cross-linked gels:

- Freeze-thawing, where the physical cross-linking is achieved through repetitive freeze-thaw cycles that causes a phase separation. Poly(vinyl alcohol) (PVA) is a popular example. When the water freezes, the ice crystals brings closer the PVA chains that form hydrogen bonds among the hydroxyl groups, leading to the formation of polymer crystallites[5];
- Stereo complex formation, easily prepared by dissolving each product in the solvent and mixing the solution;
- Ionic interaction, where ionic polymers are cross-linked through the addition of di- or tri-valent counter ions;
- H-bonding, in which the gel-like structure creates thanks to the formation of hydrogen bonding interactions;
- Maturation, where the heating induces an aggregation process that results in gel formation[12].

Chemical gels are constituted of cross-linked polymer networks built up through covalent bonds (see Figure 1.2.1(a)). In this case the polymer network forms a single macromolecule with a very high molecular weight (Mw). The permanent nature of the covalent bonds connecting polymer chains (binding energy 200-650 kJ/mol) makes chemical gels thermally irreversible materials: only over a critical temperature the bonds can be break, but after cooling, the systems are not able to reproduce the original structure. Their behavior is similar to solids, in fact, chemical gels are able to load high amounts of solvent without undergoing polymer solubilization. Different methods are used for obtaining chemical gels:

- Chemical cross-linking, where covalent linkages between polymer chains can be established by the reaction of functional groups;

- Grafting, that involves the polymerization of a monomer on the backbone of a preformed polymer;
- Radical polymerization, according to which low-molecular-weight monomers in the presence of a cross-linking agent bring to the gel synthesis through radical polymerization by thermal or UV activation. This is one of the most widely used methods that, even under mild conditions, results in the rapid formation of the gel.
- Condensation reaction, that usually involves reactions between hydroxyl /amines groups and carboxylic acids or their derivatives. These gels typically contain amide bonds in their cross-links.
- Enzymatic reaction, where an enzyme catalyzes and yields a linkage between two polymers;
- High energy radiations, that require the use of gamma (γ) or electron beam radiations. Thus, unsaturated compounds can be polymerized thanks to the formation of radicals on the polymer chains by the homolytic scission. The advantage of this method is that the process can be done in water under mild conditions (room temperature and physiological pH) without using toxic cross-linking agents.

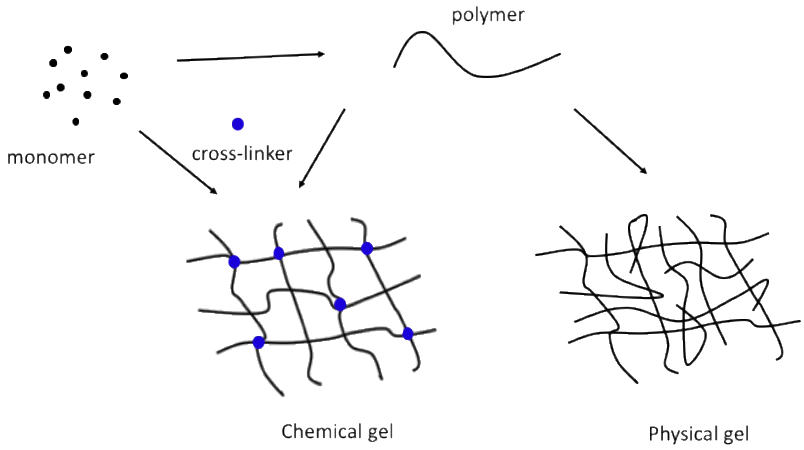

Figure 1.2.1 (a). Synthesis of chemical gels, through polymerization and cross-linking reaction (left), and physical gels, through association of polymer chains (right). Readapted with permission from Bonelli et al. (2016). Copyright © 2016, Atlantis Press[13].

1.2.2 Xerogels/Aerogels, Organogels, Hydrogels

A xerogel is a solid formed from a gel by drying with unhindered shrinkage. Xerogels usually retain high porosity (15–50%) and enormous surface area (150–900 m^2/g)[14], along with very small pore size (1–10 nm). When solvent removal occurs under supercritical conditions, the network does not shrink and a highly porous, low-density material, known as an aerogel, is produced. Heat treatment of a xerogel at high temperature produces viscous sintering and effectively transforms the porous gel into a dense glass.

An organogel can be considered as a semi-solid preparation which has an immobilized external apolar phase trapped inside spaces of a three-dimensional network. Organogels can be classified as low molecular weight (LMW) or polymeric gelators, depending on the nature of the gelling molecules. In the latter, polymers immobilize the organic solvent by forming a network of cross-linked chains, in chemical gels, or entangled chains, in physical gels, in which interactions such as hydrogen bonding, van der Waals forces and π-stacking are established. Considering LMW organogelator, their self-assembly depends on physical interaction for the formation of aggregates sufficiently long to overlap and induce solvent gelation. Depending on the kinetic properties of aggregates, an important distinction is made between those composed of solid (or strong) versus fluid (or weak)[15].Their thermodynamic stability has been attributed to spontaneous formation of fibrous structure by virtue of which the organogels reside in a low energy state. Thus, it is necessary to provide external energy to disrupt the three-dimensional structure and subsequently transform the gelled state to the sol state above room-temperature. Some common examples of gelators include sterol, sorbitan monostearate, lecithin and cholesteryl anthraquinone derivatives[16].

Hydrogels have been defined as two- or multi-component systems consisting of a three-dimensional network chains and water that fills the space between the macromolecules. Depending on the properties of the polymers used, as well as on the nature and density of the network joints, these structures can contain various amounts of water; usually, in the swollen state, the mass fraction of water in hydrogel is much higher than the mass fraction of the polymer. Hydrogels may be synthesized through one-step procedures, like polymerization and parallel cross-linking of multifunctional monomers, or through multiple step procedures, involving synthesis of polymer molecules having reactive groups and their subsequent cross-linking[17].

1.2.3 Homopolymer, Copolymer, Interpenetrating Polymer Network

The homopolymer gels are formed by a polymer network derived from a single species of monomer, which is the structural unit comprising of any polymer network. Depending on the nature of the monomer and on the polymerization technique, they may have a cross-linked skeletal structure.

The copolymer networks are formed by two or more different monomer species arranged in a random, block or alternating configuration along the chain of the polymer network.

The interpenetrating polymer networks (IPN) are an important class of gels constituted by two independent cross-linked synthetic and/or natural polymer components, organized in a 3D network structure. The semi-IPN gels have the same structure, but one component is a cross-linked polymer and the other component is a non-cross-linked polymer[17].

The schematic reactions to obtain these gels are reported in Figure 1.2.3 (a).

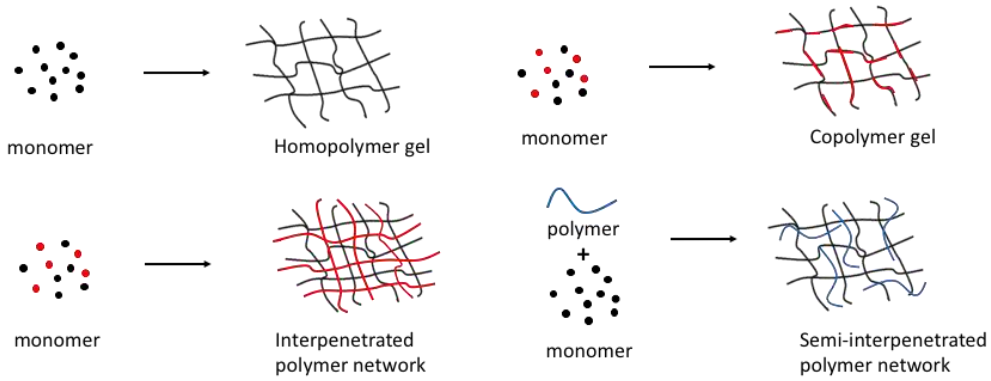

Figure 1.2.3 (a). Synthetic approach to obtain homopolymer gel (top, left), copolymer gel (top, right), interpenetrated polymer network (bottom, left), and semi-interpenetrated polymer network (bottom, right).

1.2.4 Microgels and Macrogels

Considering the size, gels can be in the form of macroscopic networks (i.e. macrogels) or confined to smaller dimensions as in the case of microgels, which they are known as nanogels if their size is in in the submicron range. Microgels consist of one to several polymer molecules in which each of the polymers holds cross-linked units. This makes them fundamentally different from polymer solutions (sols) that are homogeneously dissolved in the solvent as molecules, without having cross-linked units. There are various synthetic strategies for the preparation of microgels that include photolithographic and micromolding methods, microfluidics, free radical heterogeneous polymerization in dispersion, precipitation, inverse (mini)emulsion, and inverse microemulsion[18].

In general, when the distance between polymer molecules is long enough to make intermolecular cross-linking more difficult, intramolecular cross-linking of the same polymer chain occurs. The spreading of molecules, due to cross-linking, leads to local concentration fluctuations. Consequently, the probability of contact with other cross-linked polymer chains decreases, leading to the formation of microgels. The compatibility of microgels with solvents diminishes as cross-linking progresses.

Macrogels are typically bulks, made of a single, giant molecule consisting of polymer chains connected by cross-links. The distribution of cross-linked units inside macrogels is not uniform, in fact, when crosslinking is induced by light,

the energy flux is higher on the surface than in the bulk, creating higher cross-linking density on the outside. This allows the creation of a skin-core morphology in the gel. When a gel is formed by simultaneous polymerization of monomer and cross-linkers, it is necessary to evaluate the reaction conditions, including concentration, temperature, and the reactivity ratio of the monomer and cross-linking agent. When their reactivity is very different, a preferential cross-linking reaction takes place at the beginning and at the end of the polymerization. This creates localized cross-links in the macrogel that lead to the formation of a heterogeneous network (see Figure 1.2.4(a)).

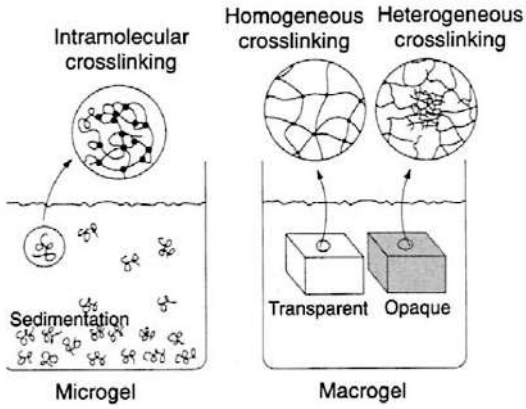

Figure 1.2.4 (a). Microgels (left) and macrogels (right) morphological structure. (Shibayama and Norisuye, 2001, Copyright, Elsevier)[19].

In this thesis, chapter III is dedicated to macroscopic gels, in particular poly(2-hydroxyethyl methacrylate) (pHEMA) based hydrogels with their physico-chemical characterization and applications, while chapter IV is related to microgels, both hydrophilic and hydrophobic, used for the investigation of their diffusional properties and for the synthesis of hydrophilic-hydrophobic macrogels.

Chapter II

Main techniques of investigation

This chapter reports equations and instrumental conditions used for the physico-chemical characterization of the prepared gel systems (macro and microgels).

2.1 Water content and state

The investigation of the amount and type of water loaded in the gels give information on the absorption and permeation properties of the polymeric network.

In particular, the equilibrium water content (EWC) and the equilibrium solvent content (ESC) provide information on network hydrophilicity and they can be calculated as follows (Eq. 2.1):

$$EWC(ESC) = \frac{W - W_d}{W} \qquad \text{(Eq. 2.1)}$$

where W is the weight of the hydrated sample and W_d the weight of the dry sample. The values of W_d were experimentally determined from thermogravimetric analysis (TGA), considering the weight of the sample at c.a. 200 or 300 °C, for water and high boiling solvent respectively.

Experimentally, TGA was carried out with a SDT Q600 (TA Instruments). The balance sensitivity is 0.1 μg. Measurements were performed in a nitrogen atmosphere with a flow rate of 100 mL/min. The samples were put in an open alumina pan, and the analyses were performed with a heating rate of 10 °C/min from 25 °C to 450 °C.

Differential scanning calorimetry analysis (DSC) was performed with a Q2000 Calorimeter (TA Instruments) to determine the state of water in the hydrogels.

The temperature range was from -80 °C to 30 or 200 °C with a scan rate of 2 °C/min, using hermetic aluminum or sealed stainless steel pans respectively.

When a xerogel begins to absorb water, first molecules that enter into the matrix hydrate the most polar, hydrophilic groups, leading to 'primary bound water'. As soon as the polar groups are hydrated, the network swells and exposes hydrophobic groups, that weakly interact with water molecules, giving rise to 'secondary bound water', often combined with the primary one and simply called 'total bound water'. An additional swelling water, that is imbibed after the ionic, polar and hydrophobic groups, is related to 'free water' and is assumed to fill the space between the network chains. Experimentally, the free water undergoes thermal transition at temperature analogous to bulk water (at 0°C). On the contrary, the secondary bound water exhibits a first order thermal transition at a temperature lower than 0°C, while the primary bound water is related to the non-freezing water, which does not undergo thermal transition above -70°C[20].

Thus, from DSC curves it is possible to determine the free water index (FWI) or the fraction of free water (C_{free}) according to the following equations (Eq. 2.2 and 2.3):

$$FWI = \frac{\Delta H_{tr}}{\Delta H_f \times EWC} \qquad \text{(Eq. 2.2)}$$

$$C_{free} = \frac{\Delta H_{tr}}{\Delta H_f} \qquad \text{(Eq. 2.3)}$$

where ΔH_{tr} (J/g) is the heat of transition obtained by the integral of melting peaks around 0˚C in the DSC curves, and ΔH_f is the theoretical value of the specific enthalpy of fusion of water at 0 °C (333.6 J/g[21]).

The fraction of bound water (C_{bound}) was calculated from the difference between the EWC and C_{free} (Eq. 2.4).

$$C_{bound} = EWC - C_{free} \quad \text{(Eq. 2.4)}$$

2.2 Characterization of structural, morphological, and diffusional properties

The structure of the gels at the nanoscale level was analyzed through Small Angle X-ray Scattering (SAXS) measurements, carried out with a HECUS S3-MICRO camera (Kratkytype) equipped with a position-sensitive detector (OED 50M) containing 1024 channels of width 54 μm. Cu Kα radiation of wavelength λ = 1.542 Å was provided by an ultrabrilliant point microfocus X-ray source (GENIX-Fox 3D, Xenocs, Grenoble), operating at a maximum power of 50 W (50 kV and 1 mA). The sample-to-detector distance was 281 mm. The volume between the sample and the detector was kept under vacuum during the measurements to minimize scattering from the air. The Kratky camera was calibrated in the small angle region using silver behenate (d = 58.38 Å). Scattering curves were obtained in the q-range between 0.01 and 0.54 $Å^{-1}$, where q is the scattering vector, $q = 4\pi/\lambda \sin\theta$, and 2θ the scattering angle. Gel samples were placed into a 1 mm demountable cell, with kapton film used as windows. The temperature was set to 25 °C and was controlled by a Peltier element, with an accuracy of 0.1 °C. All the scattering curves were corrected for the empty cell and water contribution considering the relative transmission factor.

In the case of polymer gels, the scattering intensity I(q) is expected to be larger than that of the corresponding polymer solution, $I_{soln}(q)$. Thus, a way to describe them is to decompose I(q) into $I_{soln}(q)$ and an excess scattering function, $I_{ex}(q)$, by assuming simple additivity[22].

$$I(q) = I_{soln}(q) + I_{ex}(q) + B \qquad \text{(Eq. 2.5)}$$

B is the instrumental background independent from q.
The first contribution $I_{sol}(q)$ is a generalized version of the Ornstein-Zernicke equation 2.6:

$$I_{soln}(q) = \frac{I_{soln}(0)}{1+(\xi q)^m} \qquad \text{(Eq. 2.6)}$$

where ξ is the correlation length (or also mesh-size of the gel network) and $I_{soln}(0)$ the scattering intensity at q = 0, dependent from the contrast between the polymer and the solvent and from the volume fraction of the polymer in the gel, and m is the Porod exponent associated with the solvation term. The excess scattering, which appears at low q regions, is a steeply decreasing function with q. It was described by the model of Debye and Bueche[23], which represents the model of a two phase structure with a sharp boundary.

$$I_{ex}(q) = \frac{I_{ex}(0)}{(1+a^2q^2)^2} \qquad \text{(Eq. 2.7)}$$

where *a* is the length scale that characterizes the inhomogeneities in the gel. This function describes the additional fluctuations and/or solid-like inhomogeneities, that can be classified as:

- spatial inhomogeneities, that originate from nonuniform spatial distribution of cross-links;

-topological inhomogeneities, which are dependent on the topology of network, for examples loops, trapped entanglements, and dangling chains.

- connectivity inhomogeneities, related to the sizes and spatial distribution of clusters. Their significance becomes predominant at the gelation threshold as a percolation problem (see Figure 2.2 (a)).

- mobility inhomogeneities, that correspond to local variation of mobility, due to the introduction of cross-links[24].

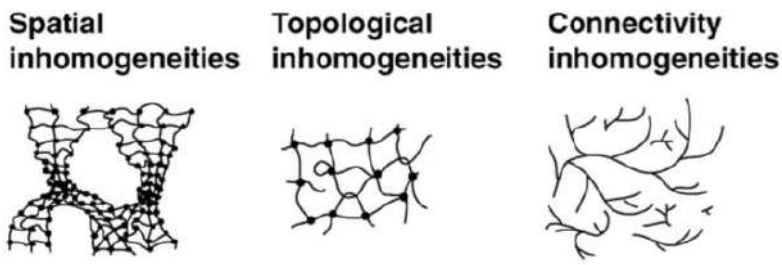

Figure 2.2 (a). Solid-like inhomogeneities in polymer gels. (Shibayama and Norisuye, 2002, Copyright, Chemical Society of Japan).

For the investigation on macroporosity, Scanning Electron Microscopy (SEM) analysis were performed on gels that were subjected to a freeze-drying process, to obtain xerogels whose porous structure is as close as possible to that of swollen gels. Images were acquired with a FEG-SEM ΣIGMA (Carl Zeiss, Germany). To increase the conductivity of the sample, a gold-metallization of xerogels was performed with an Agar Scientific Auto Sputter Coater.

Morphological characterization on the sub-micron and micron-scale is also possible through the use of Confocal Laser Scanning Microscopy (CLSM), after

loading the samples with fluorescent dyes. Measurements were performed with a laser scanning confocal microscope Leica TCS SP8 (Leica Microsystems GmbH, Wetzlar, Germany) equipped with a 63× water immersion objective. The 488 nm Ar^+ and 561 nm DPSS laser lines were used for the excitation of the fluorophores (i.e. Fluorescein and Rhodamine derivates, and Nile Red) and the emitted fluorescence was acquired, for the 2D and 3D imaging, in the microscope's xyz, xzy scan mode, using a photomultiplier (PMT) detector.

The investigation of gels diffusional properties was carried out through fluorescence recovery after photobleaching (FRAP) experiments. They were performed using 10 serial laser pulses (Δt=1.625 sec, power = 4 mW, Ar^+ lines at 458, 476 and 488 nm) focused on a circular spot (FRAP ROI) with a diameter of 35 μm. The diameter and the shape of the spot has been chosen in order to obtain diffusion coefficients independent from the geometry of the bleach region as reported in the work of Braeckmans et al.[1]. The fluorescence intensity in the FRAP ROI was normalized with respect to the fluorescence intensity of the background measured in a circular reference ROI with the same shape and dimension. The FRAP curves can be described with a model proposed by Soumpasis[27] (Eq. 2.8), that implies a diffusion-limited fluorescence recovery:

$$f(t) = a_0 + a_1 e^{\frac{2\tau_D}{t-t_{bleach}}}\left(I_0\left(\frac{2\tau_D}{t-t_{bleach}}\right) + I_1\left(\frac{2\tau_D}{t-t_{bleach}}\right)\right) \qquad \text{(Eq. 2.8)}$$

where a_0, a_1 are two normalizing coefficients introduced to account respectively for the non-zero intensity at the bleach moment and the incomplete recovery, t_{bleach} is the bleach time, τ_D is the characteristic timescale for diffusion, I_0, I_1 are the modified Bessel functions of the zero and first order (Eq. 2.9):

$$I_\alpha(x) = \frac{1}{\pi}\int_0^\pi exp(x \cdot cos\theta) \cdot cos(\alpha\theta)d\theta - \int_0^\infty exp(-x \cdot cosht - \alpha t)dt \quad (2.9)$$

where α is 0 for the 0-th order function and 1 for the 1-th order function, while x is defined as follow (Eq.2.10):

$$x = \frac{2\tau_D}{(t - t_{bleach})} \qquad \text{(Eq. 2.10)}$$

The diffusion coefficient for a bleach spot of radius *w* can be calculated from τ_D according to Eq. 2.11:

$$\tau_D = \frac{w^2}{4D} \qquad \text{(Eq. 2.11)}$$

Diffusion of microgels in macroscopic gels were performed with a confocal laser scanning microscope Zeiss LSM 710 equipped with a 63× oil immersion objective, using the 488 nm Ar^+ laser line for the excitation of the fluorophore (i.e. Fluorescein derivates). In order to determine the dynamics of the particles, the emitted fluorescence, in a 2D plane, was acquired every 0.39 s through a photomultiplier (PMT) detector. From the trajectories of the microparticles it was possible to calculate the mean square displacement (MSD, eq. 2.12) using the MSD.PRO function of the IDL program, developed by Crocker J. C. and Grier D. J[28].

$$MSD = \langle (x - x_0)^2 \rangle = \frac{1}{N} \sum_{n=1}^{N} \big(x_n(t) - x_n(0)\big)^2 \qquad \text{(Eq. 2.12)}$$

where N is the number of particles to be averaged, $x_n(0) = x_0$ is the reference position of each particle, $x_n(t)$ is the position of each particle at time t[29].

2.3 Analysis of composition and chemical structure

In order to determine the composition of the xerogels and the oxidized surface of the bronze coins, 2D FTIR imaging analysis was carried out using a Cary 620-670 FTIR microscope, equipped with a focal plane array (FPA) 128 x 128 detector (Agilent Technologies). This set up allows the highest spatial resolution currently available to FTIR microscopes. The spectra were recorded directly on the surface of the samples (gels, corroded bronze coins, or the Au background) in reflectance mode, with open aperture and a spectral resolution of 4 cm^{-1}, acquiring 128 scans for each spectrum. A ‘‘single-tile” analysis results in a map of 700 x 700 μm^2 (128 x 128 pixels), and the spatial resolution of each imaging map is 5.5 μm (i.e. each pixel has dimensions of 5.5 x 5.5 μm^2). Multiple tiles can be acquired to form mosaics. In order to improve the readability of the spectra, the background noise was reduced using the ‘‘smooth” tool (set at 11) of the Igor Pro software (Wavemetrics), taking care not to alter any diagnostic information deemed useful to this investigation. In each 2D map, the intensity of characteristic bands of the gels, or of bronze corrosion products, was imaged. The chromatic scale of the maps shows increasing absorbance of the bands as follows: blue < green < yellow < red.

Chapter 3

Macroscopic gels

pHEMA based hydrogel

pHEMA hydrogels were first prepared and described for biological use by Wichterle and Lim[30].

A three dimensional polymer network was obtained polymerizing the monomer 2-hydroxyethyl methacrylate (HEMA) (see Figure 3 (a)) in the presence of a cross-linking agent in aqueous solvent. Different approaches can be used to prepare pHEMA hydrogels:

1. bulk copolymerization of the monomer with a cross-linking agent;
2. cross-linking of the polymer in solution;
3. simultaneous copolymerization and crosslinking of a monomer with a cross-linking agent in solution.

The last method is preferable, since the polymerization can be carried out very quickly, and close to ambient conditions. Since the starting materials are in a liquid form, the formation of gels in a given shape can be readily obtained.

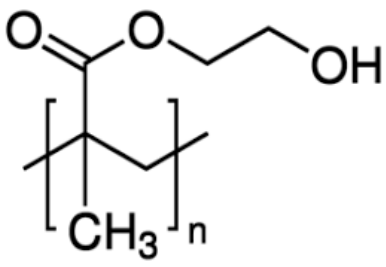

Figure 3 (a). pHEMA molecular structure.

The choice and concentration of the solvent during the polymerization determine the homogeneous or heterogeneous structure of the gel produced.

If water is used as the solvent, the concentration must be below a certain critical level to ensure the production of an optically transparent, homogeneous hydrogel. When the water content exceeds this limit, opaque, heterogeneous, macroporous hydrogels are obtained. The critical diluent concentration for water in the monomer mixture has been variously reported, in terms of the mass fraction, from 40% to 60%.

pHEMA gels were found to be resistant to acid hydrolysis and reaction with amines and incur alkaline hydrolysis significantly only at high pH and elevated temperature.

A variety of co-monomers or polymers are incorporated into the system to modify the chemical or mechanical properties of the hydrogel[31].

pHEMA hydrogels have been used or proposed for use as contact lenses, corneal replacement, synthetic prosthesis, artificial skin for wound dressing, and as drug delivery systems[32].

The particular suitability of pHEMA as biomaterial derives from the similarity of its physical properties to those of living tissues. This similarity is mostly based on its high water content, soft and rubbery consistence and low interfacial tension. The hydrophilicity is one of the most important factors for hydrogels in medical use, even if this characteristic may lead to poor mechanical strength, limiting their use in biomedical application. Moreover, also the high resistance to enzymatic digestion of pHEMA hydrogels, reflected in the unwillingness of normal cells to attach

themselves to their surfaces and to grow on them[33], has led to extensively use these systems as biomaterials.

3.1 Hydrogels preparation

All the reagents were purchased from Sigma Aldrich and used as received. Water was purified by using a MilliRO-6 Milli-Q gradient system (Millipore, resistance >18 MΩ cm)

Classical pHEMA hydrogels

Chemical pHEMA hydrogels were prepared adding HEMA monomer and various concentration of cross-linker to a beaker. In order to remove dissolved oxygen that could inhibit the polymerization, the solution was bubbled with N_2, then the initiator azobisisobutyronitrile (AIBN) and water, previously degassed, were sequentially added. The ratio HEMA/water was kept equal to 3:2 in all the prepared hydrogels, changing the amount and kind of cross-linker (i.e. ethylene glycol dimethacrylate (EGDMA) or poly(ethylene glycol) dimethacrylate (PGD)) see Table 3.1 (a). The mixture was transferred between two glassy covers, and the polymerization reaction occurred at 60°C for 4 hours. They were washed and placed in containers filled with water, that was renewed once a day for 7 days to remove unreacted monomers[34].

sample	cross-linker	cross-linker/HEMA molar ratio (*10^{-3})
H0	-	0
HE 13	EGDMA	13.1
HP 13	PGD	13.1
HP 10	PGD	10.0
HE 6	EGDMA	6.6
HP 5	PGD	5.0
HE 3	EGDMA	3.3
HE 2	EGDMA	1.6
HP 2	PGD	1.6
HE 1	EGDMA	0.8

Table 3.1 (a). Amount and type of cross-linker used in the preparation of chemical pHEMA hydrogels.

Physical gels (***pg***) with 10 to 41% hydration levels were prepared by adding the corresponding amount of H_2O (see Table 3.1 (b)) to poly(2-hydroxyethyl methacrylate) with an average molecular weight of 20000 Da. The so-obtained dispersions were centrifuged at 500 r.p.m. (8.3 Hz) till a homogenous transparent gel was obtained.

Sample	Water content %
pg11	11.5
pg18	18.4
pg20	20.4
pg25	24.9
pg27	26.6
pg28	28.0
pg41	41.3

Table 3.1 (b). % of hydration in physical pHEMA hydrogels.

Semi-IPN pHEMA hydrogels

To prepare the pHEMA/PAA semi-IPN hydrogels, an aqueous solution of poly(acrylic acid) (PAA) was added to a solution of EGDMA/HEMA molar ratio 0.006:1, AIBN and water before polymerization. The mixture, after sonication and degassing, was polymerized at 60°C for 4 hours. In order to remove any residue of unreacted monomers and free PAA molecules, the hydrogels were washed with water once a day for 7 days.
In particular, different semi-IPN hydrogels were obtained varying the ratio HEMA/PAA and the amount of water (see Table 3.1 (c)).
At macroscopic level the semi-IPN hydrogel with a water content of 60% is not transparent.

sample	HEMA wt%	H_2O wt%	PAA wt%	OH/COOH ratio
s-IPN60 8:1	36	60	3	8:1
s-IPN50 8:1	46	50	3	8:1
s-IPN38 8:1	57	38	4	8:1
s-IPN38 4:1	53.5	38	7.5	4:1
s-IPN38 2:1	48	38	13	2:1

Table 3.1 (c). Composition of semi-IPN pHEMA/PAA hydrogels. The OH/COOH ratio outlines the number of HEMA hydroxyl groups for each PAA carboxyl group.

The semi-IPN pHEMA/PVP gel was synthesized through radical polymerization as reported by Domingues et al [1]. Some variations in the synthetic process were adopted: the HEMA/PVP ratio was changed from 30/70 to 27.5/72.5 (% w/w), the water content in the pre-gel solution was 62.2% instead of 65%, while the cross-linker concentration was halved (see Table 3.1 (d)). These changes were adopted to obtain slightly softer and more flexible gel sheets that can be adapted to the rough surface of corrosion patinas. The semi-IPN was washed with water once a day for 7 days.

	pHEMA/PVP
HEMA (wt%)	10.3
Water (wt%)	62.2
MBA (wt%)	0.4
AIBN (wt%)	0.1
PVP (wt%)	27.0
HEMA/PVP ratio (%w/w)	27.5/72.5

Table 3.1 (d). Composition of the semi-IPN pHEMA/PVP hydrogel.

Hydrogel loading with probes

To investigate the diffusional properties of the classical pHEMA and semi-IPN pHEMA/PAA gels, small pieces (1x1x0.1 cm^3) of the different hydrogels were loaded with fluorescent molecules of various dimension: fluoresceine isothiocyanate FITC (hydrodynamic radius = 0.54 nm[35]), FITC-dextran 4 kDa (hydrodynamic radius = 1.4 nm[36]) and FITC-dextran 40 kDa (hydrodynamic radius = 4.5 nm[36]). The samples were incubated in $1 \cdot 10^{-4}$ M water solutions of the probes at least for two days. The concentration of FITC and FITC-dextran solutions was chosen to obtain a linear relationship between the fluorescence signal of the probe and its concentration, as verified by Braeckmans et al.[26].

Swelling and application of semi-IPNs for the cleaning of bronze mock-ups

In order to study the influence of structural and chemical changes and the role of tetraethylenpentamine (TEPA) in the coordination of Cu(II) ions, the pHEMA/PAA (s-IPN50 8:1) and the pHEMA/PVP gels were selected and swollen in water, reaching a stable pH of 6.3. Then, small pieces (5 x 5 x 0.2 cm^3) were cut and swollen with water at pH 8 and 12 (adjusted with a sodium hydroxide solution), and in a water solution of TEPA (20% w/w) for at least 5 days, using an excess of solution as compared to the gel's mass, to make sure that the semi-IPNs exchanged completely.

To evaluate the gels' effectiveness for the removal of Cu(II) alteration products from bronze artifacts, cleaning tests were carried out on an artificially aged bronze coin, which was provided by CNR-ISMN (Rome, Italy). The artificial aging procedure, developed by Ingo et al., produces corrosion patinas that are similar in appearance and composition to those of archeological bronze artifacts[38]. Small sheets of the two gels (1 x 1 x 0.02 cm^3), loaded either with a 20% (w/w) TEPA or with a 9.7% (w/w) EDTA (i.e. ethylenediaminetetraacetic acid) aqueous solution (both at pH 12), were applied twice on the coin surface for 45 minutes, covered with parafilm to limit the evaporation of fluid from the gels. EDTA was used as it is considered a reference complexing agent in the restoration practice; 9.7% is the maximum concentration of the compound at pH 12. During the application, the gels acquire a strong blue color that indicates the absorption of Cu(II) ions and the formation of Cu(II) complexes. After the treatment, the coin substrate was rinsed with water and air-dried. In order to check the presence of corrosion products and gel residues, 2D FTIR Imaging was carried out on the coin surface before and after the application of the gels.

3.2 Studies of structural and diffusional properties

Diffusion of molecules in hydrogels is an interesting study for a wide variety of applications, spanning from chromatography and membrane separation[39,40]to biomedical applications for encapsulation of cells or delivery of bioactive agents[41,42]. Since the transport of solute molecules in hydrogels takes place predominantly in the water-filled regions confined by the gel matrix[43], the interactions between the solute and the polymer network, arising from hydrodynamic friction, physical obstruction, electro-osmosis and specific binding[41,44] cause a slow down in the diffusion compared to bulk water. In particular, it is well known that increasing solute size[45] and decreasing the water fraction of the gel the mobility of the solute molecules decreases. Moreover, the cross linking process, that occurs during gelation, leads to the formation of a 3D network with a characteristic mesh size, which has a primary role in the diffusion process, if the solute size is comparable to the mean mesh size of the gel[46]. In fact, from previous studies, it was demonstrated that the release of a macromolecular drug from an hydrogel can be controlled adjusting the pore volume fraction and the pore size by changing the composition of the polymeric network and the amount of the cross-linker[47].

Several theoretical models try to describe the diffusion processes in gels[48]. The free volume theory defines the change in the diffusion rate as a function of the average free volume[49]; the obstruction assumes that the polymer chains are fixed and impenetrable segments immersed in a fluid[50];

the hydrodynamic presupposes that the solute, moving at a constant velocity in a continuum media, is obstructed by the frictional forces of the gel strands. Other models were developed merging different theories, however all these approaches do not consider the heterogeneity of the gel and the solute dimension. Thus, to overcome this limit, the aim of this study is to understand the diffusion properties of various solute molecules in hydrogels with different chemical composition, in order to determine a correlation between the hydrogels structure and the diffusion coefficient of the solute.

To improve the chemical and mechanical properties of pHEMA networks, a variety of co-monomers or polymers can be used during the synthesis of these hydrogels, leading to formation of interpenetrated (IPN) or a semi-interpenetrated (semi-IPN) polymeric networks with better capabilities of storing water and improved mechanical properties. For example, p(HEMA-co-sodium methacrylate)/chitosan and pHEMA/chitosan semi-IPN hydrogels have higher tensile and compressive moduli than classical pHEMA, which increase with the molecular weight of chitosan[51].

Also different kinds and amounts of cross-linkers can be used to tune the water content and the mechanical strength of the polymeric network, as demonstrated by Han et al.[51] studying p(HEMA-co-sodium methacrylate)/chitosan and pHEMA/chitosan semi-IPN hydrogels synthesized with two different cross-linkers.

Therefore, in this study, pHEMA hydrogels with various cross-linker/HEMA ratios and two different cross-linking agents, EGDMA and PGD, were formulated to investigate the effect of the amount and the chemical nature of the cross-linker on the water content of the gel and on the diffusional behaviour of solute molecules. Moreover, since only

classical "copolymer hydrogels" (pHEMA/PAA) have already been synthesized, new formulations of semi-IPN pHEMA/PAA hydrogels were developed and characterized to understand the influence of PAA on the physico-chemical and diffusional properties of the gels. In fact, while copolymer hydrogels have usually quite different characteristics from those resulting from the sum of single homopolymer[17], the semi-IPNs present properties similar to the average of the single homopolymer properties[34]. Therefore, all the prepared systems were investigated by means of SAXS to study the internal structure at the nanoscale level, while DSC and TGA were employed to investigate the hydration level and the state of water entrapped in the polymeric network. Finally, FRAP experiments were carried out to obtain the diffusion coefficient of probes with different size inside the polymeric network. All these results provide a complete description of the relationship between the structure and the hydration of the hydrogels with the diffusion properties of hydrophilic molecules.

3.2.1 Results and discussion

Structural characterization

SAXS curves of HE and HP hydrogels and their fitting parameters, obtained using the Ornstein-Zernike model, are reported in Figure 3.2.1 (a) and in Table 3.2.1 (a) respectively.

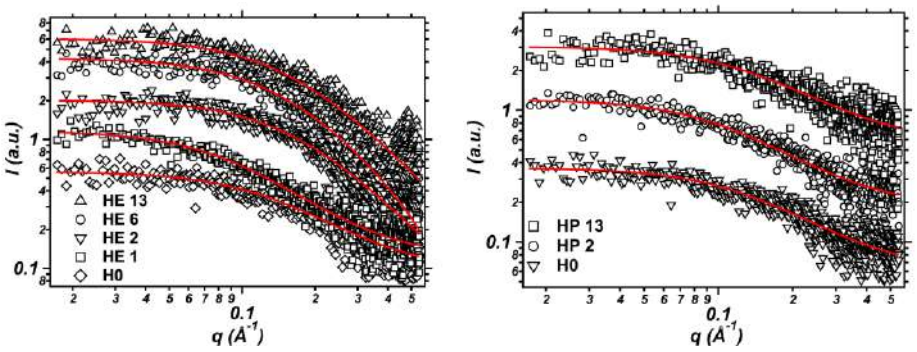

Figure 3.2.1 (a). SAXS curves of HE (left) and HP (right) hydrogels. Fitting curves are reported as continuous lines together with the experimental data (empty markers). The reported curves are offset along y-axes for clarity.

	$I_{sol}(0)$	ξ (nm)	Bkg
H0	0.74 ± 0.01	0.6 ± 0.1	0.13 ± 0.01
HE 13	1.39 ± 0.01	0.6 ± 0.1	0.11 ± 0.01
HE 6	1.45 ± 0.01	0.7 ± 0.1	0.11 ± 0.01
HE 2	1.26 ± 0.01	0.6 ± 0.1	0.12 ± 0.01
HE 1	0.86 ± 0.01	0.7 ± 0.1	0.10 ± 0.01
HP 13	0.60 ± 0.01	0.7 ± 0.1	0.13 ± 0.01
HP 2	0.77 ± 0.01	0.8 ± 0.1	0.13 ± 0.01

Table 3.2.1 (a). Fitting parameters obtained from the SAXS curves of HE and HP hydrogels.

Since the resolution of the experiment is about 5 Å, an increase in the cross-linker concentration does not affect the hydrogels mesh size, as it shown in

Table 3.2.1 (a). This result is in agreement with the study of T. Kanaya et al. [54], where they demonstrate that, in a semi-dilute polymer solutions, the polymer chains are overlapped each other before cross-linking, thus the cross-linking reaction has no influence on the gel structure.

Figure 3.2.1 (b) shows the SAXS curves of the semi-IPN hydrogels. Considering s-IPN 8:1 series, samples containing 50% and 60 %wt of water present solid-like inhomogeneities, whose average value is about 9.6 nm and 6.9 nm for s-IPN60 8:1 and s-IPN50 8:1 respectively, while the hydrogel with 38%wt of water does not have any appreciable inhomogeneity (see Table 3.2.1 (b)). The mesh size value is higher for the s-IPN60 8:1 (i.e. 1.7 nm), in agreement with other systems in which it was proved that the correlation length is proportional to the water content[42].

In pHEMA/PAA 38%wt series, the inhomogeneities and the mesh size values do not follow any particular trend. Concerning the average mesh size, the highest value was found for the s-IPN38 4:1 (around 1.0 nm), while s-IPN38 8:1 and s-IPN38 2:1 have comparable mesh size (0.7 nm) (see Table 3.2.1 (b)).

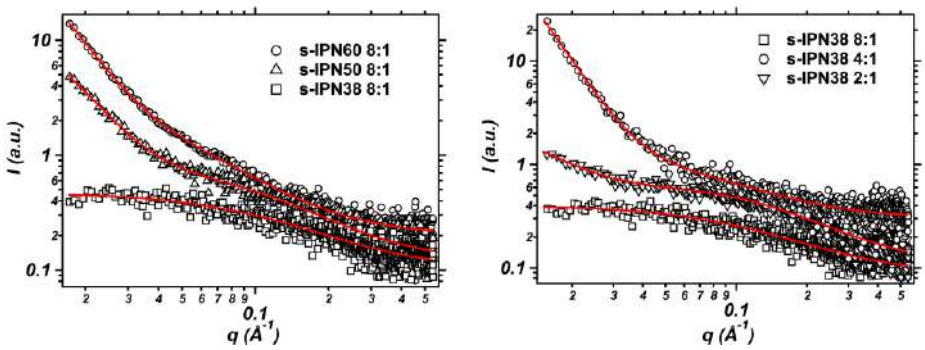

Figure 3.2.1 (b) SAXS curves of pHEMA/PAA hydrogels. Fitting curves are reported as continuous lines together with the experimental data (empty markers). The reported curves are offset along y-axes for clarity.

	$I_{sol}(0)$	ξ (nm)	a (nm)	Iex(0)	bkg
s-IPN60 8:1	0.70 ± 0.02	1.7 ± 0.1	9.6 ± 0.2	75.9 ± 4.5	0.09 ± 0.01
s-IPN50 8:1	0.90 ± 0.02	0.8 ± 0.3	6.9 ± 0.5	36.9 ± 2.1	0.18 ± 0.01
s-IPN38 8:1	0.45 ± 0.11	0.7 ± 0.1	-	-	0.18 ± 0.01
s-IPN38 4:1	0.45 ± 0.8	1.0 ± 0.1	14.5 ± 0.1	56.6 ± 0.1	0.21 ± 0.01
s-IPN38 2:1	0.80 ± 0.01	0.7 ± 0.2	6.3 ± 0.6	3.9 ± 0.8	0.16 ± 0.01

Table 3.2.1 (b). Parameters obtained from the fitting of pHEMA/PAA semi-IPN hydrogels.

Water in hydrogels

The investigation of the amount and state of water in hydrogels provides important information on the absorption, diffusion and permeation properties of these systems.

Preliminary studies on water state were carried out to compare the hydration properties in pHEMA physical and chemical classical hydrogels with different water content, to understand how the cross-linking process

influences the interaction with water molecules and between the polymer chain of the gel matrix. DSC curves (see Figure 3.2.1 (c) and (d)) show 2 fractions of water in pHEMA hydrogels with up to 40% wt of water content according to their diverse response to freezing/melting cycles: one fraction is bound, thus it does not freeze and melt, and one is free.

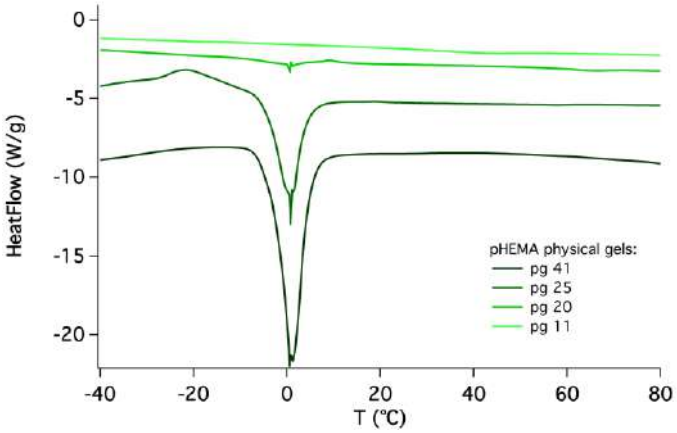

Figure 3.2.1 (c). DSC thermograms of physical pHEMA hydrogels with 10 to 40% water content. The reported curves are offset along y-axis for clarity.

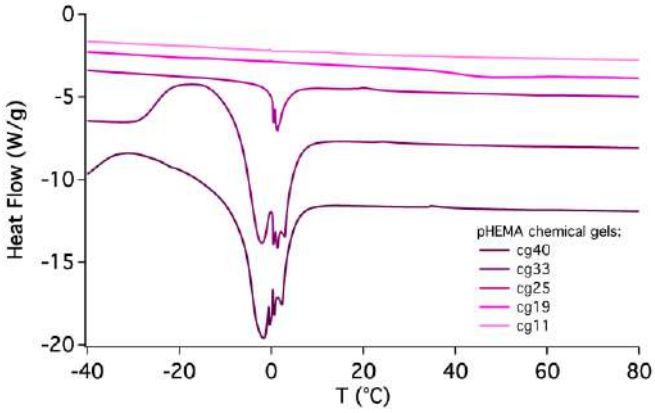

Figure 3.2.1 (d). DSC thermograms of chemical pHEMA hydrogels with 10 to 40% water content. The reported curves are offset along y-axis for clarity.

From the DSC thermograms reported in Figures 3.2.1 (c) and 3.2.1 (d) it is possible to observe that the freezing temperature of the water is higher for the most hydrated samples, in accordance with previous results by Lee et al.[56]. In the case of cg19, the melting peak was observed neither in the cooling nor in the heating thermograms, in agreement with previous works on pHEMA hydrogels[56] and commercial contact lenses[57], while in pg20 a small amount of free water (<0.05) is still present.

Figure 3.2.1 (e) shows the fractions of free water with respect to the total water content for pg and cg hydrogels, to evidence how the water is distributed in the two different states. Bound water fraction increases with the water content and reaches a plateau after 20 %wt, as a consequence of the limited binding capacity of the hydroxyl group that can strongly coordinate about two water molecules. In fact, when the two water molecules threshold is reached additional water can not bind to the polymer network and behaves like free water maintaining its ability to freeze (see Figure 3.2.1 (e)). In the pg the plateau values are lower than in the cg, confirming that the hydroxyl groups are involved in the hydrogel network formation and they are not completely available to interact with water. Such results are consistent with the presence of different fractions of water with various mobilities, more similar to the bulk water or more associated with the polymer matrix, as demonstrated by Quasi Elastic Neutron Scattering experiments performed on these gels[58]. In fact, the diffusion coefficients of the water molecules increase, while their residence times decrease with

increasing the hydration level. At 20 %wt hydration, the water mobility is considerably higher in the physical gels, whereas at 30 %wt the water mobilities in the physical and chemical gels are more similar.

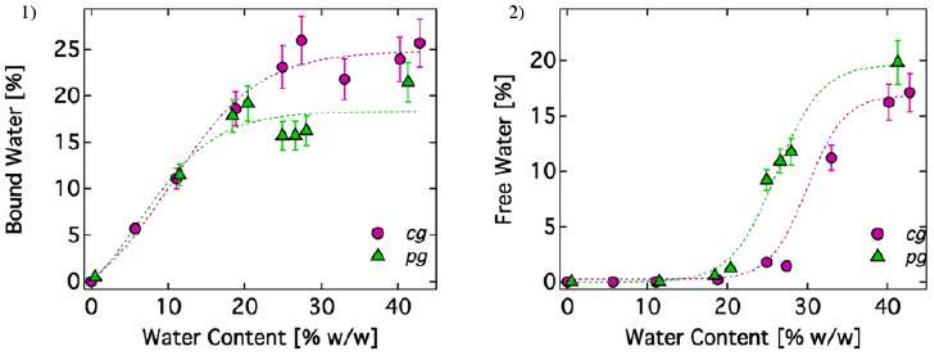

Figure 3.2.1 (e). Bound (1) and free (2) water in pg and cg pHEMA hydrogels. Dashed lines are only a guide for the eye. Copyright © 2019 American Chemical Society[58].

	FWI (±0.01)	free water % (±0.1)	boundwater % (±0.1)
pg11	0	0	11.5
pg18	0.03	0.6	17.8
pg20	0.06	1.2	19.2
pg25	0.37	9.2	15.7
pg27	0.41	10.9	15.7
pg28	0.42	11.8	16.2
pg41	0.48	19.8	21.5
cg6	0	0	5.7
cg11	0	0	11.1
cg19	0.01	0.2	18.6
cg25	0.07	1.79	23.1

cg27	0.05	1.4	26.0
cg33	0.34	11.2	21.8
cg40	0.40	16.2	24.0
cg43	0.40	17.1	25.7

Table 3.2.1 (c). Free water and bound water index derived from thermal analysis for pg and cg hydrogels with water content up to about 40%w/w. Bound and water content %wt are reported as well to show the distribution of the total water content in the two states.

Further investigations on the hydration properties were carried out, first on pHEMA classical hydrogels (40% wt of water) to evaluate the effect of different percentage of cross-linker on water confinement, then on pHEMA/PAA semi-IPNs with various amount of PAA and water. Considering pHEMA classical hydrogels, the equilibrium water content decreases increasing the percentage of cross-linking agent according to an exponential decay (see Figure 3.2.1 (f)).

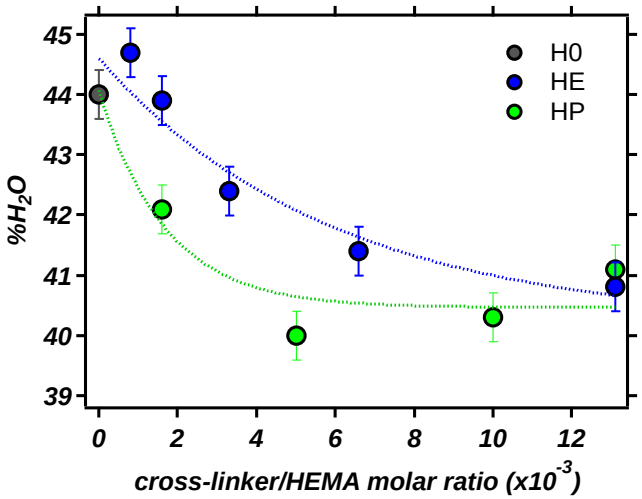

Figure 3.2.1 (f). Equilibrium water content as a function of the amount of cross-linking agent in classical pHEMA hydrogels.

This behaviour can be explained calculating the water/n-octanol partition coefficients cLogP[59] of the different components of the polymer network. These data were obtained from DataWarrior[60], a software that is able to calculate the chemical-physical properties of a compound through its molecular structure. The most polar components are HEMA fragments (cLogP: 0.48), while the water affinity decreases for the cross-linker molecules (cLogP PGD: 1.10; cLogP EGDMA: 1.84). Thus, the EWC% decreases moving from the hydrogel H0, containing just HEMA monomers, to the other hydrogels containing increasing amounts of cross-linker. Despite the higher water affinity, the hydrogel with PGD shows lower EWC% than with EGDMA. In fact, considering the dimension of the cross-linker molecules, PGD fragments occupy a bigger amount of the polymer network than EGDMA fragments (n=9 vs n=1), leading to a lower relative amount of HEMA fragments, the most polar components, in the PGD hydrogels.

For the semi-IPN pHEMA/PAA hydrogels, the water content is almost the same in pHEMA/PAA 38 %wt series and it corresponds to the amount of water used during the synthesis. On the contrary, considering pHEMA/PAA 8:1 series, the water content shows small discrepancies from the water amount used for the synthesis. In particular, in s-IPN50 and s-IPN60 the EWC are about 8 %wt and 5 %wt less than the amount used during the synthesis (see table 3.2.1 (d)).

	EWC %wt

s-IPN60 8:1	54.5 ± 0.5
s-IPN50 8:1	42.4 ± 0.4
s-IPN38 8:1	38.8 ± 0.4
s-IPN38 4:1	37.7 ± 0.4
s-IPN38 2:1	37.5 ± 0.4

Table 3.2.1 (d). Equilibrium water content %wt of semi-IPN pHEMA/PAA hydrogels.

The state of water in the hydrogels is determined from the analysis of DSC curves. In particular, C_{free}, related to the bulk-like water and the loosely bound water present in the hydrogels, is an important parameter that accounts for the retention and diffusive properties of a hydrogel[61].
Figure 3.2.1 (g) shows DSC thermograms of the classical pHEMA hydrogels, while Table 3.2.1 (e) reports the details about the melting enthalpy and the calculated values of C_{free} and C_{bound}.

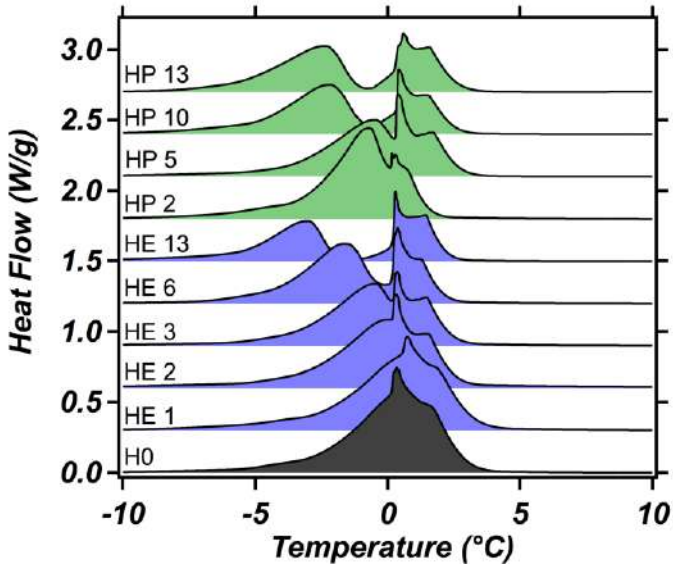

Figure 3.2.1 (g). DSC thermograms of classical pHEMA hydrogels. The reported curves are offset along y-axis for clarity (y-offset: 0.6 W/g).

	ΔH_{tr} (J/g)	C_{free} (±0.01)	C_{bound} (±0.01)	C_{free}/C_{bound}
HE 13	53.2 ± 0.7	0.16	0.26	0.61 ± 0.01
HE 6	63.7 ± 0.8	0.19	0.22	0.86 ± 0.02
HE 3	64.4 ± 0.8	0.19	0.24	0.79 ± 0.02
HE 2	67.6 ± 0.9	0.20	0.20	1.00 ± 0.02
HE 1	75.9 ± 1.0	0.23	0.22	1.04 ± 0.02
H0	78.9 ± 1.0	0.24	0.20	1.20 ± 0.03
HP 13	62.0 ± 0.8	0.19	0.23	0.83 ± 0.02
HP 10	62.1 ± 0.8	0.19	0.21	0.90 ± 0.02
HP 5	65.4 ± 0.8	0.20	0.20	0.96 ± 0.02
HP 2	69.5 ± 0.9	0.21	0.21	1.00 ± 0.02

Table 3.2.1 (e). Data obtained from DSC analysis of classical pHEMA hydrogels.

In HE and HP hydrogels, the ratio between free water and bound water decreases increasing the percentage of cross-linker, as a result of a higher number of hydrogen bond acceptor groups that can interact and bind water molecules (Figure 3.2.1 (h)). Comparing pHEMA/PGD and pHEMA/EGDMA networks with the same amount of cross-linking agent, the C_{free}/C_{bound} ratio is higher in HP hydrogels than in HE, probably because PGD is a much longer cross-linking molecule. This leads to a higher mobility of the polymeric network and, consequently, to less friction between water molecules and polymer chains. Finally, DSC thermograms reported in Figure 3.2.1 (g) show that, increasing the percentage of the cross-linker, the freezing peak broadens until two distinct peaks appear in the hydrogel when the cross-linker/molar ratio is 13.1. The peak at lower temperature can be related to loosely bound water, usually refers to water molecules that interact with the polar groups of the network only through hydrogen bonds. This contribution becomes more important for samples containing high percentage of cross-linker, because of the formation of a compact network and/or because of an increase of the polar groups in the network that can interact with water.

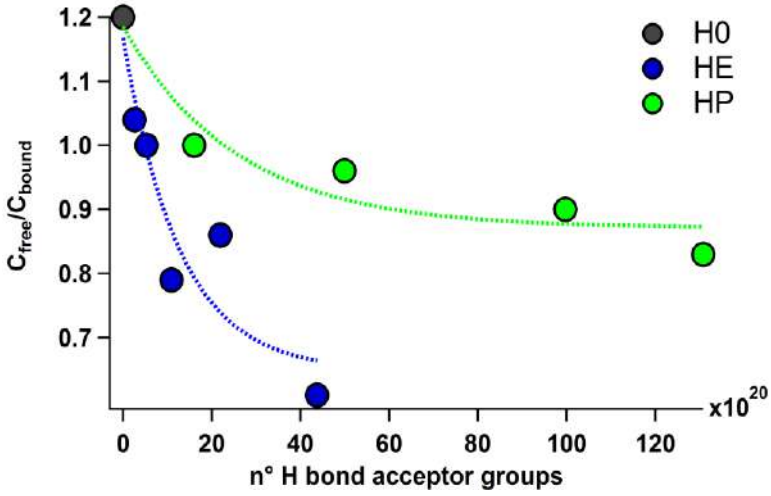

3.2.1 (h). FWI/BWI in pHEMA hydrogels with EGDMA (blue) and PGD (green) as a function of hydrogen bond acceptor groups.

Regarding semi-IPN pHEMA/PAA hydrogels, the DSC thermograms and the calculated values of C_{free} and C_{bound} are reported in Figure 3.2.1 (i) and Table 3.2.1 (f), respectively.

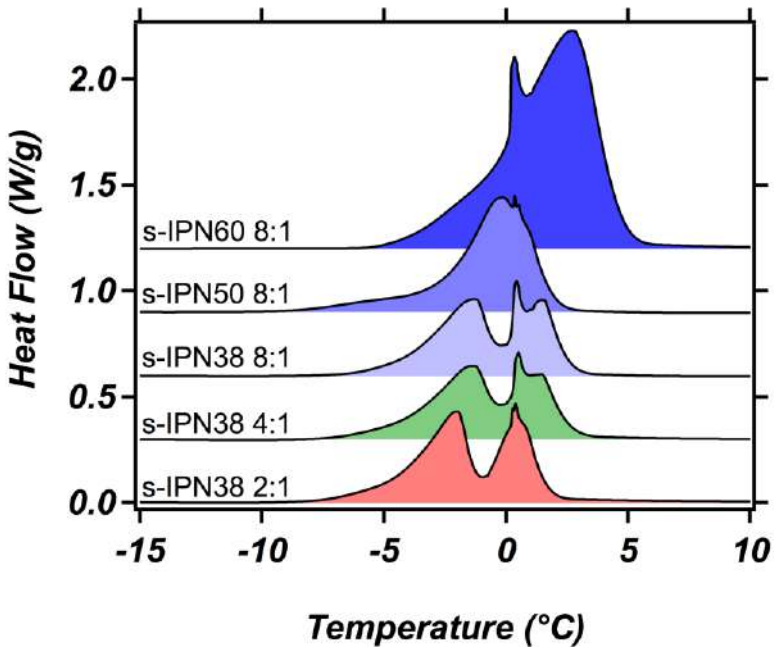

Figure 3.2.1 (i). DSC thermograms of semi-IPN pHEMA/PAA hydrogels. The reported curves are offset along y-axis for clarity.

	ΔH_{tr} (J/g)	C_{free} (±0.01)	C_{bound} (±0.01)	C_{free}/C_{bound}
s-IPN60 8:1	141.6 ± 1.8	0.42	0.12	3.52 ± 0.08
s-IPN50 8:1	62.0 ± 0.8	0.19	0.24	0.79 ± 0.02
s-IPN38 8:1	57.8 ± 0.8	0.17	0.22	0.77 ± 0.02
s-IPN38 4:1	56.2 ± 0.7	0.17	0.21	0.81 ± 0.02

s-IPN38 2:1	57.3 ± 0.7	0.17	0.20	0.85

Table 3.2.1 (f). Data obtained from DSC analysis of semi-IPN pHEMA/PAA hydrogels.

s-IPN60 8:1 and s-IPN50 8:1 curves (Figure 3.2.1 (i)) show only one broad peak, while in pHEMA/PAA 38% series, it is possible to distinguish two different peaks, one related to bulk like water and the other, at lower temperature, to the loosely bound water. Considering pHEMA/PAA 8:1 series, the network with 60 %wt of water has the higher C_{free}/C_{bound} ratio since a larger amount of water was used during the synthesis. On the contrary, in pHEMA/PAA 38% series, there are no appreciable differences of the C_{free}/C_{bound} ratio. Moreover, the C_{free}/C_{bound} value is similar to that obtained for HE 6, the classical pHEMA hydrogel with the same composition of the semi-IPNs except for the absence of PAA. Thus, the presence of PAA trapped into the gel matrix does not influence the free water fraction. It is possible to conclude that the percentage of cross-linking agent is the only parameter that can be changed to modify the retention properties of the hydrogels.

Diffusional properties of hydrophilic molecules

pHEMA hydrogels, incubated with FITC, FITC-dextran 4 kDa, and FITC-dextran 40 kDa, were analysed with confocal laser scanning microscopy to evaluate the diffusion coefficients and the possible interactions of these hydrophilic probes with the networks.

Thus, FRAP experiments were performed on classical pHEMA and semi-IPN pHEMA/PAA hydrogels in order to determine the self-diffusion coefficients of these hydrophilic solutes. As an example, the FRAP curve of HE 2 hydrogel, loaded with FITC, is reported in Figure 3.2.1 (j).

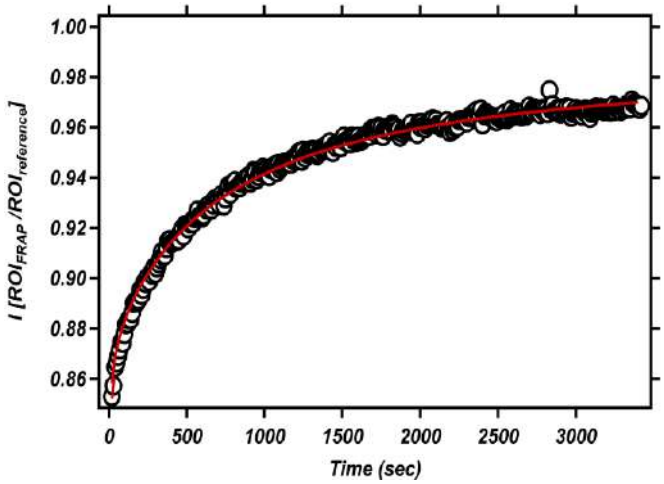

Figure 3.2.1 (j). FRAP curve (markers) of HE 2 hydrogel loaded with FITC and its respective fitting (continuous line).

The diffusion coefficients values in pHEMA classical hydrogels, obtained from the fitting of the FRAP curves with Soumpasis model[27], range from 0.392 to 0.091 $\mu m^2/s$ and decrease increasing the percentage of the cross-linking agent (see Table 3.2.1 (g)). These values are about three orders of magnitude lower than the FITC in water. In particular, the diffusion coefficient of FITC decreases of about 5% from H0 to HE 1 and 64% from H0 to HE 2. The lowest diffusion coefficient value is measured in HE 13, that contains the highest amount of cross-linker. The same trend was observed in the HP series, but the motion of the probe is faster in HP

networks than in HE networks. This can be explained considering that the longer chain of PGD leads to a higher mobility of the polymeric network.

	cross-linker/HEMA molar ratio (*10^{-3})	FITC - D ($\mu m^2/s$)
Water solution	-	397[a]
H0	0	0.392 ± 0.032
HE 13	13.1	0.060 ± 0.005
HP 13	13.1	0.091 ± 0.007
HE 2	1.6	0.142 ± 0.011
HP 2	1.6	0.286 ± 0.023
HE 1	0.8	0.373 ± 0.030

Table 3.2.1 (g). Diffusion coefficients of FITC in classical pHEMA hydrogels. [a]Diffusion coefficient of FITC in water solution was calculated from the Stokes-Einstein equation at 20 °C $\left(D = \frac{kT}{6\pi\eta R_h}\right)$, where η is the viscosity of the solvent (i.e 1 cP) and R_h hydrodynamic of the fluorophore (i.e 0.54 nm for FITC).

The FITC diffusion coefficients can be related to the ratio between free and bound water: the probe mobility increases with C_{free}/C_{bound} ratio, with a sigmoidal trend (Figure 3.2.1 (k)). In this regard, the diffusion process, mediated by the free water fraction, seems to be completely activated only when the C_{free}/C_{bound} ratio reaches the unity.

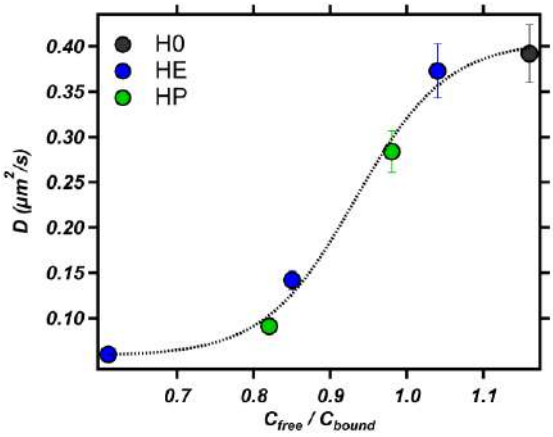

Figure 3.2.1 (k). Trend of FITC diffusion coefficients as a function of the ratio between free and bound water in classical pHEMA hydrogels.

In the case of the other hydrophilic probes with greater molecular weight, i.e. FITC-dextrans, confocal microscopy reveals that, differently from FITC, they do not enter into any of classical pHEMA hydrogels. In particular, in the case of FITC, the green fluorescence of the probe is evident both in solution and in the polymeric network (Figure 3.2.1 (l) A), while, in the case of FITC-dextran 4 kDa, the green fluorophore is confined only in solution (Figure 3.2.1 (l) B).

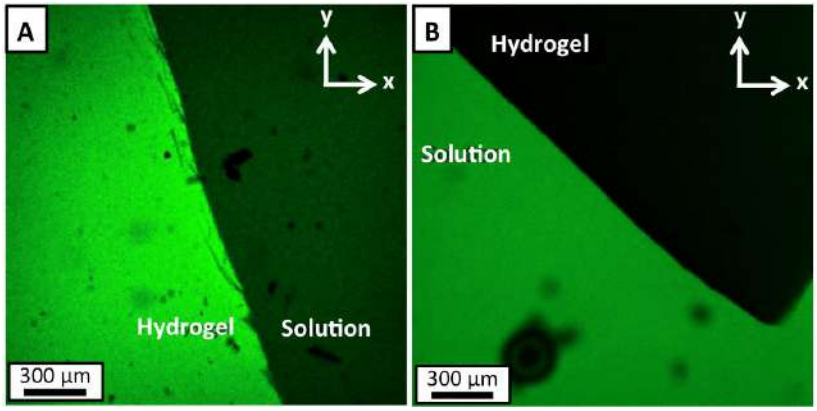

Figure 3.2.1 (l). Laser confocal scanning microscopy horizontal sections of HE D hydrogels loaded with aqueous solutions of FITC (A) and FITC-dextran 4 kDa (B).

The incomplete recovery of the photobleaching in FRAP experiment means that a portion of molecules cannot freely diffuse in the polymer network. Therefore, fluorescence measurements were performed to investigate the possible interactions between the fluorophore and the polymeric network. The protolytic constants of FITC, relating the chemical activities of the cation, neutral, anion and dianion forms, are pK_1= 2.08, pK_2= 4.31 and pK_3=6.43, respectively[62].

Figure 3.2.1 (m) shows the fluorescence spectra of FITC measured in the solution in equilibrium with the hydrogels and inside classical pHEMA hydrogels.

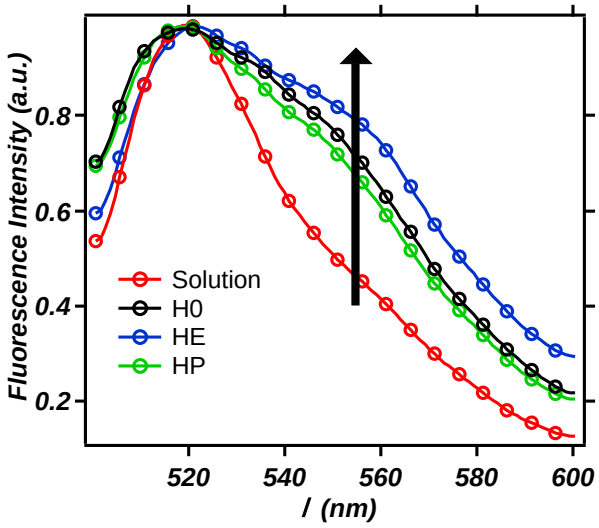

Figure 3.2.1 (m). Fluorescence spectra of FITC in solution and in H0, HE D and HP D hydrogels. All data are normalized at 520 nm.

Since the pH value of the solution in equilibrium with the hydrogels is around 6.7, the fluorescence spectrum of FITC in solution presents one peak with a maximum at 520 nm, ascribable to the presence of the dianionic form of the FITC as reported by Sjoback et al.[63]. On the contrary, FITC spectra in H0, HE and HP networks show one additional broad peak around 550 nm, ascribable to the presence of FITC molecules in the mono-anionic form[63], due to the formation of hydrogen bonds between hydroxyl and carboxyl groups of fluorescein and hydroxyl groups of HEMA.
Also the mobility of the probes in the semi-IPN pHEMA/PAA hydrogels was evaluated by means of FRAP experiment (see Table 3.2.1 (h)).

	FITC **D ($\mu m^2/s$)**	**FITC-dextran 4 kDa D ($\mu m^2/s$)**	**FITC-dextran 40 kDa D ($\mu m^2/s$)**
Water	397[a]	153[a]	48[a]
s-IPN60 8:1	0.242 ± 0.019	0.028 ± 0.002	0.003 ± 0.001
s-IPN50 8:1	0.107 ± 0.009	0.038 ± 0.003	-
s-IPN38 8:1	0.067 ± 0.005	0.021 ± 0.002	-
s-IPN38 4:1	0.041 ± 0.003	0.015 ± 0.001	-
s-IPN38 2:1	0.034 ± 0.003	0.013 ± 0.001	-

Table 3.2.1 (h). Diffusion coefficients of the different probes in the semi-IPN pHEMA/PAA hydrogels. [a]Diffusion coefficient of probes in solution are obtained from Stokes-Einstein equation.

The diffusion coefficients of the fluorescent molecules, obtained from the fitting of the FRAP curves performed on pHEMA/PAA networks, are about four orders of magnitude slower than those measured in water. This is a clear evidence of the confinement of the liquid phase inside the polymeric network. Comparing the diffusion coefficients of the different probes in the same hydrogel, it is possible to observe that they decrease of about one order of magnitude from FITC to FITC-dextran 4 kDa and FITC-dextran 40 kDa, according to an increase of the molecular dimension. In particular, FITC-dextran 40 kDa can penetrate only into the s-IPN60 8:1 network since its mean mesh size is higher than the others, as seen by SAXS experiments. Examining the mobility of the same probe into the different

networks, the diffusion coefficients decrease with increasing the water content of the hydrogels (Figure 3.2.1 (n)).

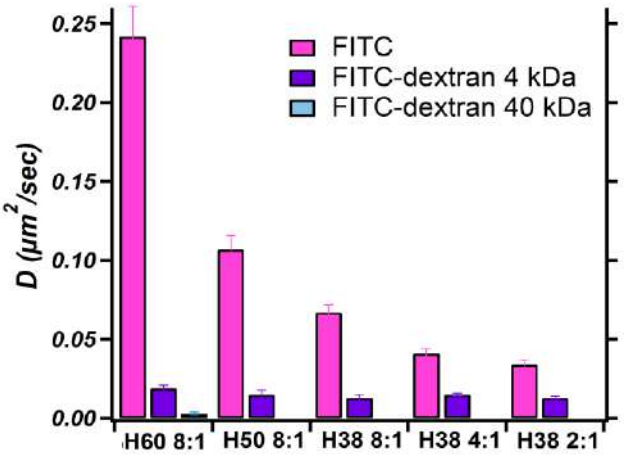

Figure 3.2.1 (n). Diffusion coefficients of FITC (pink column), FITC-dextran 4 kDa (violet column) and FITC-dextran 40 kDa (light blue column) in semi-IPN pHEMA/PAA hydrogels.

As in the case of classical pHEMA hydrogels, the fluorescence spectra of FITC were measured in the solution in equilibrium with the hydrogels and inside the polymeric network to evaluate possible interactions between the probe and the gel structure (Figure 3.2.1 (o)).

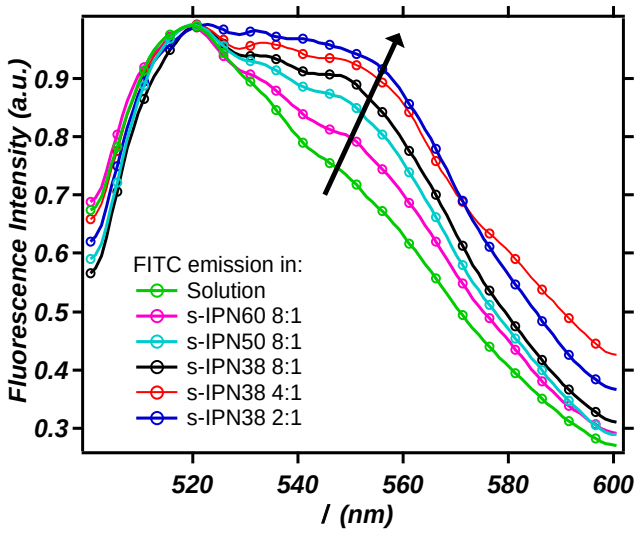

Figure 3.2.1 (o): Fluorescence spectra of FITC in solution and in semi-IPN pHEMA/PAA hydrogels. All data are normalized at 520 nm.

The fluorescence spectrum of FITC in the solution in equilibrium with the gel (pH=5.4) shows two peaks, one with a maximum at 520 nm, and the other, less intense, around 550 nm, meaning that FITC is mainly present as anion. The fluorescence spectra acquired on FITC loaded in pHEMA/PAA networks shows the same two peaks. In particular, considering pHEMA/PAA 8:1 series, the peak centred at 550 nm becomes more intense decreasing the water content of the gel, as a consequence of a stronger interaction between hydroxyl and carboxyl groups of fluorescein and hydroxyl and carboxyl groups of pHEMA and PAA, that shifts the equilibrium to the anionic form of FITC. The same trend is observed increasing the amount of PAA, keeping constant the water content (from s-IPN38 8:1 to s-IPN38 2:1).

3.2.2 Conclusions

Understanding the correlation between the hydrogel structure and hydration level with the diffusion processes of small molecules and macromolecules is interesting for several applications, spanning from biomedical field as drug delivery systems, to art restoration for the confinement of complex cleaning fluids.

For this purpose, two different systems have been investigated: pHEMA classical hydrogels, widely used for soft contact lenses technology, and semi-IPN pHEMA/PAA polymer networks, novel hydrogels formulated to understand the influence of a polyelectrolyte (polyacrylic acid) on the network structure and on the diffusion through the hydrogel. Classical pHEMA networks were synthesized with various cross-linker/HEMA ratio and with two cross-linking agents of different length, while the semi-IPNs were formulated with different water content (i.e. 38%, 50%, 60), but the same ratio between HEMA and PAA monomers (i.e. 8:1) or with a constant water content of 38%, but diverse HEMA/PAA ratio (i.e. 8:1, 4:1, 2:1).

First of all, the hydration properties of classic pHEMA hydrogels were compared with physical pHEMA hydrogels at various water content to figure out the influence of the cross-linking process on the interaction of the polymer chains among themselves and with water molecules. Then, considering classical pHEMA hydrogels, it was demonstrated that the water content and the free/bound water ratio decreases with increasing the amount of cross-linker. The latter value is higher in HP networks, as a consequence of a longer chain of PGD than EGDMA leading to a higher mobility of the gel matrix. SAXS experiments reveal a local correlation length below 1 nm in all the pHEMA systems, suggesting that the length

and concentration of the cross-linking agent does not influence their nanostructure. Due to the small mesh size of all classical pHEMA hydrogels, only FITC can diffuse inside them for size exclusion phenomena. FRAP curves do not show a complete recovery of the photobleaching, meaning that an interaction between the probe and the network occurs, as confirmed from fluorescence spectra, where it was possible to qualitatively follow the hydrogen bond interactions between the probe and the network. FRAP curves reveal also an increase of the FITC diffusion inside the hydrogels decreasing the cross-linker density and increasing the ratio between free and bound water. In particular, a sigmoidal trend of D vs C_{free}/C_{bound} seems to indicate that the diffusion becomes completely activated only when the hydrogel reaches a water-percolated state as a result of a cooperative process.

In the case of semi-IPN pHEMA/PAA hydrogels, the C_{free}/C_{bound} is almost the same for all the samples, since PAA has almost the same capability of pHEMA to interact with water molecules. SAXS analysis reveals the existence of solid-like inhomogeneities, that increase in size with the increasing of the water content in the gels, and an average mesh dimension similar to that of classical pHEMA, except in the case of s-IPN60 8:1. FITC and FITC-dextran 4 kDa can diffuse into all these hydrogels, while FITC-dextran 40 kDa can penetrate only in s-IPN60 8:1, thanks to its bigger mesh size. From FRAP experiments it was possible to assess that the diffusion coefficient increases with the water content and with the decrease of the amount of PAA, as the result of a lower interaction between the probes and the polymeric network.

All these results provide a complete picture of the link between the structure, water state and transport properties in pHEMA based classical

and semi-IPN hydrogels, giving valuable information for the development of improved formulation specific for new applications.

3.3 Semi-IPN hydrogels for the removal of Cu(II) alteration products from bronze

Metallic artifacts represent a wide part of the artistic and architectural production spanning over millennia, however they usually suffer from degradation processes that can alter their appearance and integrity. In particular, copper-based artifacts are affected by corrosion phenomena that lead to the formation of a patina on their surface, also characterized by the presence of copper oxychlorides (atacamite and its polymorphs, $Cu_2(OH)_3Cl$). These compounds are responsible of the so called "bronze disease", a cyclic degradative process able to consume the objects up to their complete disintegration (see reaction below).

$$4CuCl + O_2 + 4H_2O \rightarrow 2Cu_2(OH)_3Cl + 2H^+ + 2Cl^-$$

Traditionally, the removal of copper oxychlorides is performed by mechanical (vibrating or abrasive tools, ultra-high-pressure water)[64], optical (laser ablation), or chemical methods (bases, acids and complexing agents)[65], however these approaches involve several risks for the artifacts, because they are invasive and scarcely selective. Therefore, the confinement of cleaning fluids is a necessary step to allow a controlled removal of the patina without affecting the original objects. Traditional

thickeners used in restoration are not enough retentive and exhibit poor mechanical properties, leaving residues on the treated surfaces[66]. In the last decade, chemical hydrogels have been proposed as optimal matrices to confine fluids for the safe cleaning of works of art[67,68,69,70]. In particular, in this work a semi-IPN pHEMA/PVP hydrogel was chosen as confining matrices for cleaning solutions, based on its ideal mechanical properties and retentivness and on the ability of PVP to form complexes with metal ions[1]. Moreover, a pHEMA/PAA network, previously studied, was selected, due to its ability to give strong coordination bonds with Cu(II) at alkaline pH, thanks to the presence of carboxylate groups[72]. The cleaning fluid upload in the semi-IPNs, owing to its high complexing selectivity to Cu(II) ions, was tetraethylenpentamine (TEPA). In fact, the complex formed with Cu(II) has a stability constant $\log K_f = 22.8$ at 25°C[73], four orders of magnitude higher than that of the complex with tetrasodium salt of ethylenediaminetetraacetic acid (EDTA, Y^{4-}) ($\log K_f = 18.8$ at 25°C and 1 M)[74], the chelating agent traditionally used for the removal of copper corrosion products[64,75].

To understand the influence of structural and chemical changes of pHEMA/PVP and pHEMA/PAA hydrogels and the role of TEPA in the coordination of Cu(II) ions, the semi-IPNs were swollen in water at different pH values (6, 8, 12), and in a water solution of TEPA (pH 12), and analyzed by means of SAXS, SEM, DSC, TGA, and FTIR-FPA. Finally, the semi-IPNs were applied on an ‘’archaeological’’ bronze coin, to investigate, by FTIR-FPA chemical mapping, their ability to solubilize and remove copper oxychlorides.

3.3.1 Results and discussion

Changes in the hydrogels structure at the microscale level, caused by pH variations, were investigated through SEM analysis. At pH 6, pHEMA/PAA semi-IPN shows a compact structure without micron-scale porosity (Figure 3.3.1 (a-1)), while at pH 8 it has a quite homogeneous porosity in the 7-10 μm range (Figure 3.3.1 (a-2)). A heterogeneous structure with pores that have an irregular shape and a broad size distribution (from 1 to 15 μm) are noted at pH=12 (Figure 3.3.1 (a-3)). In the case of pHEMA/PVP semi-IPNs, a micron-scale porous structure is present at all pH: pores with a fairly regular shape that have dimensions of 5-12 μm are observable at pH=12 (Figure 3.3.1(a-4)), while at pH 8 (Figure 3.3.1 (a-5)), it is possible to note three different size distributions (i.e. < 1 μm, 4-5 μm, and 14-20 μm); at pH 12 pores with an elongated shapes, whose dimensions range from 2 to 8 μm, are arranged in rows in a ordered pattern, (Figure 3.3.1 (a-6)). When the gels are loaded with TEPA, the free-drying process results in a collapse of the porosity, and a plain smooth surface is observed, with no relevant features.

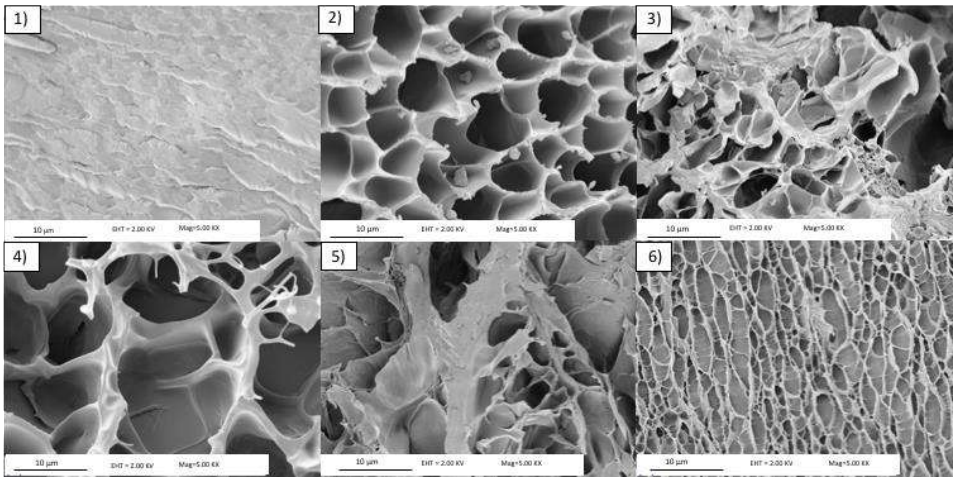

Figure 3.3.1 (a). SEM images of pHEMA/PAA and pHEMA/PVP xerogels obtained from the corresponding hydrogels swollen in water at pH 6 (left, top and bottom), 8 (center, top and bottom), and 12 (right, top and bottom). Bar is 10 μm.

SAXS experiments were performed to investigate changes in the nanostructure of the semi-IPN hydrogels due to pH variations, the presence of TEPA, and TEPA with Cu(II) ions (following the application of the gels onto corroded bronze coins). Figure 3.3.1 (b) and 3.3.1 (c) show respectively the SAXS curves of pHEMA/PAA and pHEMA/PVP hydrogels at pH 6, 8 and 12 (3.3.1 (b) and 3.3.1 (c)), and loaded with TEPA 3.3.1 or with TEPA and Cu(II) ions (3.3.1 (b) and 3.3.1 (c)), after subtraction of cell contribution. All the SAXS curves were modelled using a generalized version of the Debye-Bueche approach[76], with two q-dependent contributions and an instrumental flat background, as described in Chapter II.

Table 3.3.1 (a) and Figure 3.3.1 (b) report respectively the fitting parameters and the SAXS curves of pHEMA/PAA semi-IPNs swollen in

water. The average mesh size increases moving from pH 6 to pH 12, due to the electrostatic repulsion between PAA chains when the carboxyl groups are ionized, leading to the stretching of the polymer chains[77]. In fact, increasing the pH values, also an increase of EWC is observed, in agreement with other studies where the mesh dimension is associated to the equilibrium water content[55]. The hydrogel at pH 6 has a Porod exponent of ca. 3.8, indicating that the polymer network is collapsed, while at pH 8 and 12 this value is around 2.3 for both systems, suggesting that the semi-IPNs are in a theta solvent[78]. The increase in water content (higher EWC) leads to a less homogeneous semi-IPN at the nanoscale, as previously reported in another study[34]. In particular the dimension of spatial inhomogeneities increases from 1.7 nm at pH 6 to 7.3 nm at pH 8, and ca. 5 at pH 12.

When pHEMA/PAA is loaded with a water solution of TEPA (20%, pH=12) the mesh size and the dimension of solid-like inhomogeneities are smaller than those of the gel swollen in water at the same pH, while the Porod exponent is slightly higher. These changes are probably related to interactions among TEPA and the carboxyl groups in PAA. TEPA molecules might interpose between PAA chains, screening the repulsion between the ionized carboxyl groups, and making the semi-IPN tighter. In the presence of copper II ions, a further decrease of the mesh and inhomogeneities size is detected. In a study of Cheng et al. a decrease of the radius of gyration (R_g) was reported for a poly(N-isopropylacrylamide) copolymer hydrogel that adsorbed Cu(II). This change was attributed to the formation of complexes between the ions and chelating groups in the polymer chains[79]. In our case, the lower mesh size can be ascribable to the formation of complexes between Cu(II), ionized carboxyl groups of PAA and amine groups of TEPA[80]. Moreover, also a small decrease in the EWC

(about 6%) is observed after the uptake of ions, in agreement with a lower mesh size value[55]. Finally, the increase in the Porod exponent (see Table 3.3.1 (a)) indicates a transition to a denser aggregate structure.

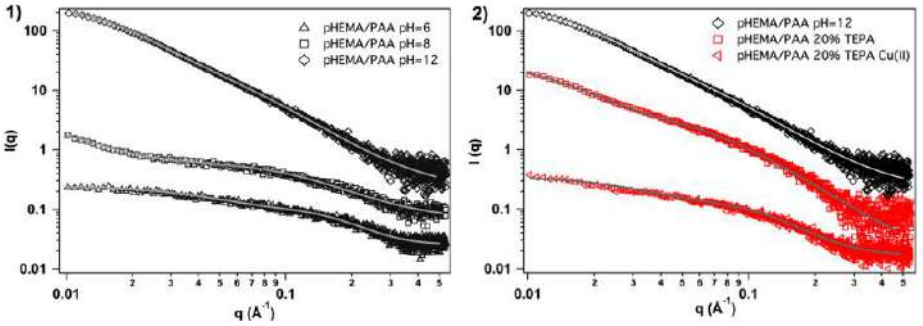

Figure 3.3.1 (b). SAXS curves and fitting (grey lines) of pHEMA/PAA semi-IPNs swollen in water: 1) at pH 6 (triangles), 8 (squares), and 12 (diamonds), and 2) loaded with TEPA (red squares) or TEPA and copper II ions (red triangles).

	pH=6	pH=8	pH=12	20%TEPA	20%TEPA Cu(II)
I_{sol}	1.37 ± 0.05	2.77 ± 0.05	11.15 ± 0.58	9.48 ± 0.19	3.36 ± 0.09
ξ (nm)	0.60 ± 0.01	0.83 ± 0.01	1.82 ± 0.06	1.14 ± 0.02	0.78 ± 0.01
m	3.75 ± 0.16	2.29 ± 0.05	2.34 ± 0.04	2.43 ±0.03	3.33 ± 0.07
I_{ex}	2.67 ± 0.05	13.35 ± 0.96	144.33 ± 0.99	79.30 ± 0.89	7.86 ± 0.17
a (nm)	1.67 ± 0.06	7.28 ± 0.03	4.96 ± 0.05	5.54 ± 0.05	2.52 ± 0.07
bkg	0.44 ± 0.01	0.34 ± 0.01	0.11 ± 0.01	0.03 ± 0.01	0.54 ± 0.01

Table 3.3.1 (a). Fitting parameters obtained from SAXS curves of pHEMA/PAA hydrogels.

Regarding pHEMA/PVP hydrogels (see Table 3.3.1(b), and Figure 3.3.1(c)), the average mesh size at pH=6 is in agreement with previous studies[34], and remains unchanged at pH=8, while at pH 12 it decreases of about 1 nm. This can be explained considering that the enol tautomer of PVP can lose a proton to form an enolate at alkaline pH values (>> 10)[81]. Thus, the partial deprotonation might result in an increase of inter and intramolecular hydrogen bonds between enol and enolate groups in the PVP chains, leading to a smaller mesh size and to a more compact structure, as also suggested by the slight increase of the Porod exponent. The smallest value of ξ (ca. 2 nm) and the highest value of m (2.7) are obtained for the gel swollen in the water solution of TEPA (pH=12) (see Table 3.3.1 (b)). Similarly low values are found after Cu(II) uptake, likely because the enolate groups are able to interact with TEPA molecules and Cu(II) ions, closing together in the formation of complex structures.

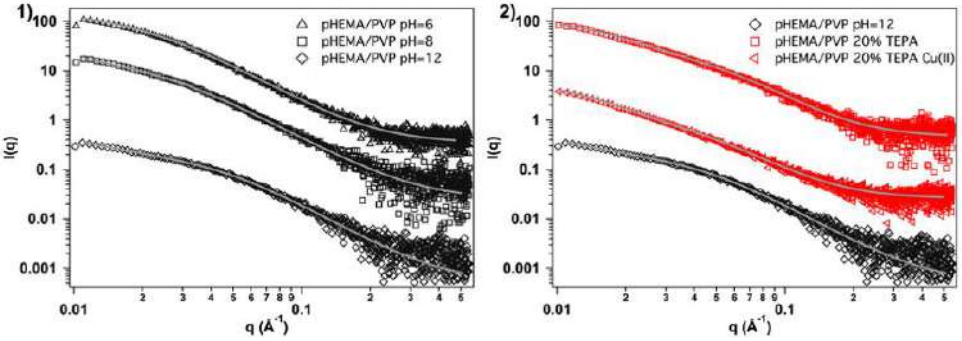

Figure 3.3.1 (c) SAXS curves and fitting (grey lines) of pHEMA/PVP hydrogels swollen in water: 1) at pH 6 (triangles), 8 (squares), and 12 (diamonds), and 2) loaded with TEPA (red squares) or TEPA and copper II ions (red triangles).

	pH=6	pH=8	pH=12	20%TEPA	20%TEPA Cu(II)
I_{sol}	25.26 ± 11.3	37.70 ± 5.39	15.46 ± 0.63	7.31 ± 0.41	10.78 ± 0.54
ξ (nm)	3.43 ± 0.54	3.81 ± 0.23	2.34 ± 0.06	1.94 ± 0.06	2.28 ± 0.07
m	2.49 ± 0.03	2.44 ± 0.02	2.58 ± 0.03	2.69 ±0.05	2.61 ± 0.05
I_{ex}	68.48 ± 8.84	62.19 ± 2.92	34.90 ± 2.03	46.35 ± 0.62	89.08 ± 0.98
a (nm)	4.93 ± 0.57	6.85 ± 0.83	6.50 ± 0.37	5.05 ± 0.10	6.15 ± 0.09
bkg	0.20 ± 0.01	0.09 ± 0.01	0.04 ± 0.01	0.20 ± 0.01	0.38 ± 0.01

Table 3.3.1 (b). Fitting parameters obtained from SAXS curves of pHEMA/PVP hydrogels.

The study of the water content and state in the hydrogels gives information on the absorption and permeation properties of these systems. The DSC curves of all the gels are reported in Figure 3.3.1 (d).

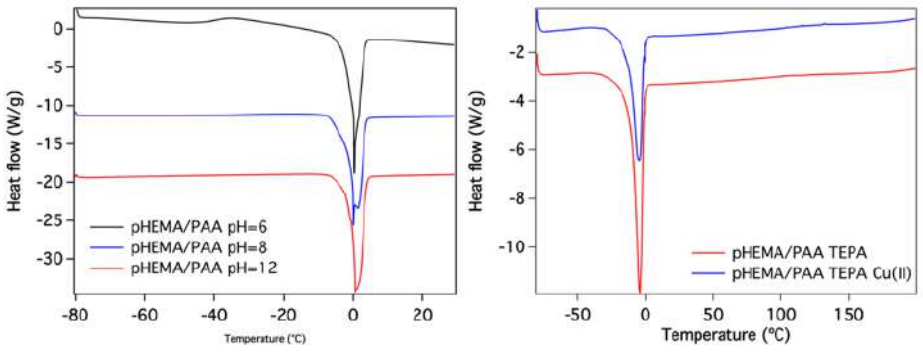

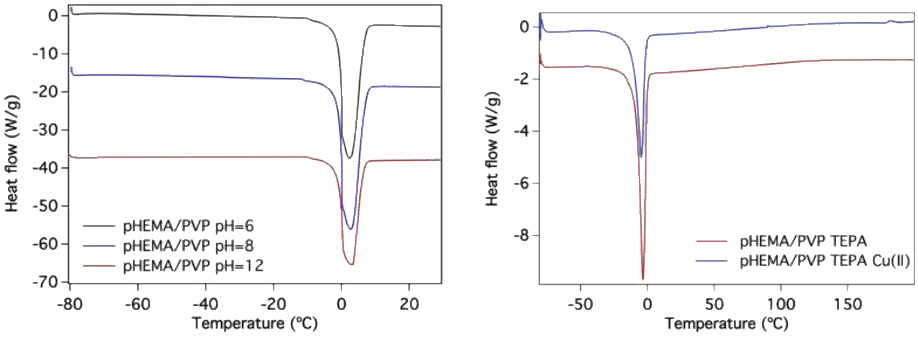

Figure 3.3.1 (d). DSC curves of pHEMA/PAA and pHEMA/PVP hydrogels swollen in water (left panel top and bottom respectively) and in the water solution of TEPA (right panel top and bottom respectively). The reported curves are offset along y-axis for clarity.

The equilibrium water content in pHEMA/PAA semi-IPNs, swollen at different pH, is strongly related to the porosity of the gels and to the hydrophilic character of PAA. The EWC is similar to the values obtained for the classical pHEMA chemical gels[58,82]at pH 6, when the carboxyl group are completely protonated (see Table 3.3.1 (c)), and it increases up to 57 and 79% at pH 8 and 12, due to the ionization of the carboxyl groups. When the hydrogel is loaded with TEPA (pH 12), the solvent content is c.a. 76% and passing to 71% after the absorption of Cu(II). This indicates that some free water and TEPA are lost through evaporation during the application of the gel on the bronze coin, even if the gel was covered with parafilm. Moreover, the free water index increases passing from pH 6 to 12 (see Table 3.3.1(c)), according to the presence of more hydrophilic moieties in the network (carboxylate groups in PAA), and a higher meso- and microporosity, as shown by SAXS and SEM experiments.

	pH 6	pH 8	pH 12	TEPA	TEPA Cu
ΔH_{tr} (J/g)	76.5 ± 1.7	154.3 ± 1.27	293.2 ± 6.1	127.4 ± 4.1	109.0 ± 3.1
EWC %	42.9 ± 0.9	56.8 ± 1.1	79.1 ± 3.7	76.3 ± 1.6	71.3 ± 1.4
FWI	0.53 ± 0.02	0.81 ± 0.02	1.11 ± 0.07	0.50 ± 0.03	0.46 ± 0.02

Table 3.3.1 (c). Data obtained from DSC and TGA analysis of pHEMA/PAA semi-IPNs swollen in water at pH 6, 8, and 12 and in TEPA water solution before and after Cu(II) uptake.

Both the EWC and FWI of the pHEMA/PVP hydrogels do not change when the semi-IPNs are swollen in water at different pH (Table 3.3.1(d)). The values of these parameters are higher than those of pHEMA/PAA gels, due to the high relative content of PVP, a very hydrophilic polymer. The equilibrium solvent content does not change significantly in the presence of TEPA and Cu(II) ions, indicating the high hydrophilicity of these systems.

It must be pointed out that, for both systems, there is a significant decrease in the heat of the ice melting transition and, consequently, in the FWI (ΔH_{tr}, see Table 3.3.1 (c) and 3.3.1 (d)), when Cu(II) ions are absorbed in the gels. In fact, part of the bulk water molecules can coordinate with the metal ions, participating in the formation of complexes.

	pH 6	pH 8	pH 12	TEPA	TEPA Cu
ΔH_{tr} (J/g)	296.1 ± 3.9	317.2 ± 1.1	299.5 ± 5.26	154.6 ± 2.5	133.5 ± 4.1
EWC %	88.3 ± 0.5	89.1 ± 1.3	89.0 ± 2.1	86.5 ± 0.01	85.6 ± 0.8
FWI	1.01 ± 0.02	1.07 ± 0.02	1.01 ± 0.04	0.54 ± 0.01	0.47 ± 0.02

Table 3.3.1 (d). Data obtained from DSC and TGA analysis of pHEMA/PVP semi-IPNs swollen in water at pH 6, 8, and 12 and in TEPA water solution before and after Cu(II) uptake.

FTIR 2D imaging performed on the pHEMA/PAA hydrogel at pH 6 provides spectra that exhibit derivative-shaped peaks and distortions typical of reflective surfaces (see Figure 3.3.1 (e)). The OH and CH stretching bands are not present, and the main peaks are those of C=O stretching (derivative shape, maximum at 1745 cm^{-1}), CH_2 bending (1496 cm^{-1}), C-O stretching (1294 cm^{-1}), and C-O-C stretching (derivative shape, maximum at 1197 cm^{-1}, and 1092 cm^{-1})[83,84]. At alkaline pH values the shape of the spectra are more similar to that of standard transmission spectra, due to a change in the refractive index of the gel, following the neutralization of the carboxyl groups in PAA and the rearrangement of the polymer chains. Both the OH and CH stretching bands are clearly observable, and the C=O stretching peak shows two components around 1740 cm^{-1} (pHEMA) and 1715 (PAA) cm^{-1} [83,84]. Moreover, the spectra show a new band at 1578 cm^{-1}, related to the antisymmetric stretching of the carboxylate in PAA, whose intensity increases moving from pH 8 to pH 12 (see Figure 3.3.1(e)). Besides, at pH 8 the carboxylate groups are concentrated in domains from tens to hundreds of microns, while at pH 12 all the gel matrix exhibits the presence of $–COO^-$ groups.

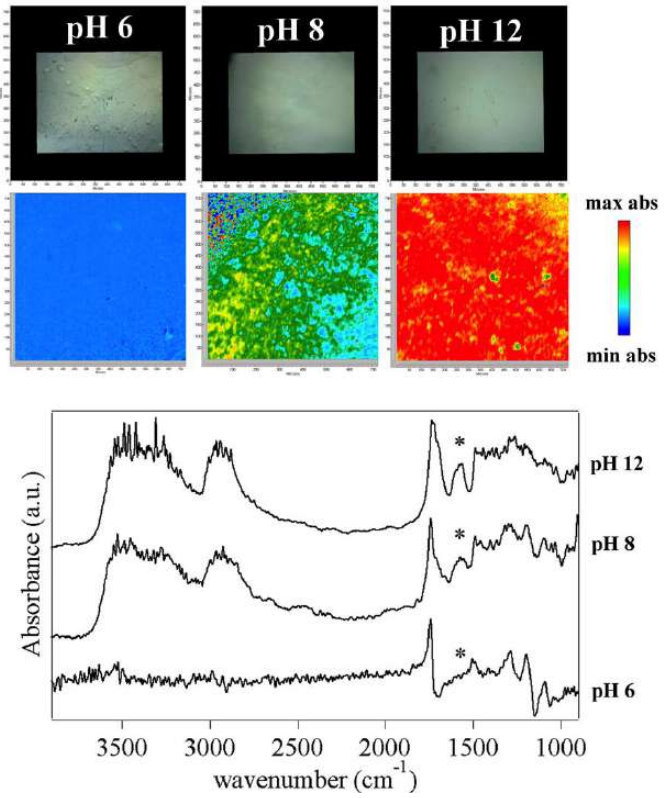

Figure 3.3.1 (e). FTIR 2D Imaging of pHEMA/PAA xerogels obtained from hydrogels swollen in water at different pH values. Below each visible image, the corresponding 2D FTIR Imaging map shows the intensity of the band at 1578 cm^{-1} ($-COO^-$ antisymmetric stretching of carboxylate groups in PAA). All maps have dimensions of 700 x 700 μm^2, each axis tick being 50 µm. The bottom panel shows spectra of representative pixels (5.5 x 5.5 μm^2) in the corresponding 2D Imaging map.

The FTIR 2D imaging of pHEMA/PAA xerogels, obtained from semi-IPNs loaded with TEPA, is shown in Figure 3.3.1 (f). The polyethylene amine loaded in the gels changes their refractive index, leading to strongly

derivative-shaped C=O and C-O-C stretching peaks. The most relevant band has two maxima at 1660 and 1610 cm^{-1}. The latter is assigned to the NH deformation of primary amine in TEPA[85], while the first component can be ascribed to the stretching of the carboxyl groups in PAA neutralized by a polyethylene amine[86]. The interaction occurs between the amine group of TEPA and the acid moieties of PAA, interfering with the interchain hydrogen bonds. Thus, the H atom of the carboxyl group protonates the amine groups, shifting the carboxylate vibration to a higher wavenumber with respect to the gels swollen in water at the same pH. In the presence of Cu(II) ions, the peak is no longer clearly observable across all the gel's surface, as shown by the 2D Imaging maps. Our hypothesis is that the carboxylate vibration peak might be either shifted back to lower wavenumbers (convoluting with the TEPA NH deformation band), or decreased in intensity, due to the formation of a ternary polymer-metal complex by both PAA and TEPA with the copper ions. In fact, the formation of mixed Cu(II) complexes with PAA and polyethylene imines (PEI) has been already reported by Kabanov *et al.*[87], where two coordination sites are occupied by PAA carboxylates, and two by amine groups. Similar complexes can be formed in the case of the PAA-Cu-TEPA.

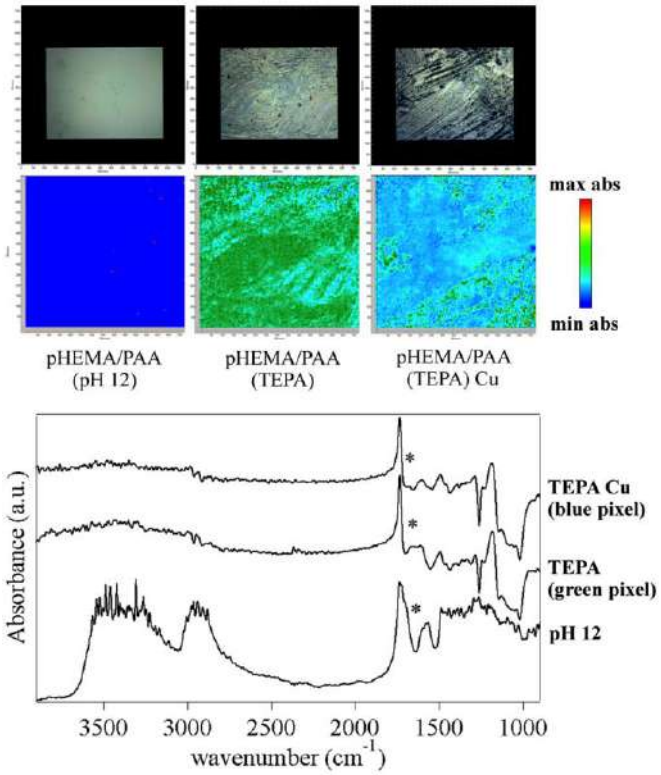

Figure 3.3.1 (f). (Top) FTIR 2D Imaging of xerogels obtained from pHEMA/PAA hydrogels: (top left) swollen with water at pH 12; (top center) xerogels obtained from gels swollen with a TEPA solution (20 wt%); (top right) xerogels obtained from gels that were swollen with the TEPA solution and then placed on a bronze coin mock-up containing Cu(II) corrosion products. Below each visible image, the corresponding 2D FTIR Imaging map shows the intensity of the band at 1660 cm^{-1} (assigned to the $-COO^-$ antisymmetric stretching of carboxylate groups in PAA). All maps have dimensions of 700 x 700 μm^2, each axis tick being 50 µm. The bottom panel shows spectra of representative pixels (5.5 x 5.5 μm^2) in the corresponding 2D imaging map.

The FTIR 2D imaging of pHEMA/PVP xerogels, obtained from the gels swollen in water at different pH values, is reported in Figure 3.3.1 (g). All the main vibrational bands of the two polymers are clearly observable[88,83] , however a band at 1578 cm^{-1} progressively emerges at alkaline pH and increases passing from pH 8 to pH 12, as shown in the 2D Imaging maps. This band could be assigned either to a combination of O-H and C-H bending[89], or to the presence of an enolate ion, even if the latter would be expected at slightly higher wavenumbers[90]. In fact, as previously reported by Nikiforova T. *et al.* [81], the hydroxyl group of the enol structure of PVP loses a proton at pH >> 10, converting the polymer to its enolate form. It must be noticed that the carbonyl band of the lactam form of PVP is also observable at 1655 cm^{-1}.

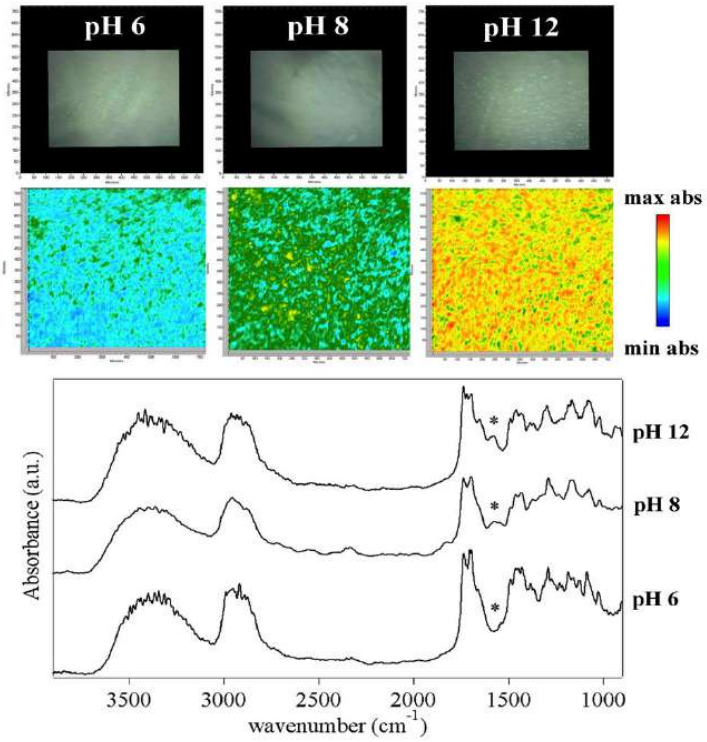

Figure 3.3.1 (g). FTIR 2D Imaging of pHEMA/PVP xerogels obtained from hydrogels swollen in water at different pH values. Below each visible image, the corresponding 2D FTIR Imaging map shows the intensity of the band at 1578 cm^{-1} (assigned to the stretching of enolate ions in PVP). All maps have dimensions of 700 x 700 μm^2, each axis tick being 50 µm. The bottom panel shows spectra of representative pixels (5.5 x 5.5 μm^2) in the corresponding 2D Imaging map.

In the pHEMA/PVP gels, loaded with TEPA, an inhomogeneous pattern of the absorbance intensity in the 1615-1535 cm^{-1} region is detected in the FTIR 2D Imaging maps (see Figure 3.3.1(h)). In the main portion of the maps (yellow-red pixels), the band at 1600 cm^{-1}, related of NH deformation

of TEPA, is clearly observable, as part of a derivative peak whose flexus falls at ca. 1580 cm^{-1}. This band might include the contribution from enolate groups in PVP. In some portions (green pixels), there is no band around 1600 cm^{-1}, but a shoulder of the PVP carbonyl peak is detected at ca. 1620 cm^{-1}, along with a derivative band with a maximum at 1500 cm^{-1} and a flexus at ca. 1485 cm^{-1}. The first peak is assigned to the NH deformation of TEPA (shifted upwards), while the latter to the enolate (shifted downwards) and CH_2 vibrations. The bands shifts were ascribed to interactions between the amine groups in TEPA and polar or charged CO groups in PVP. In fact, after the uptake of Cu(II) ions in the gel, the shifts are observed in a larger portion of the maps (i.e. majority of green pixels in FT-IR imaging map). Since PVP is able to coordinate with copper through the O atom rather than N[91], the interactions between PVP and TEPA might be favored by the coordination of Cu(II) with CO groups and amines, which come close together while binding to the ions.

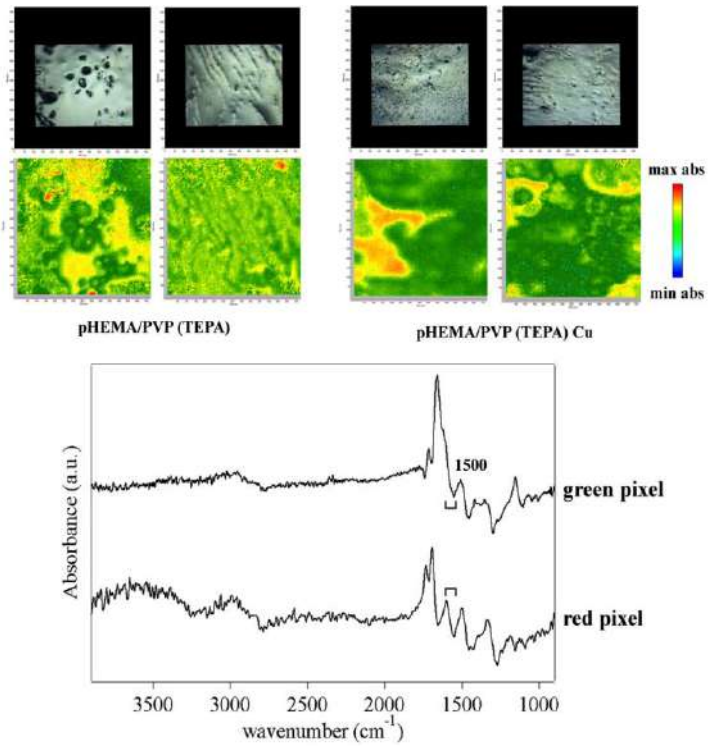

Figure 3.3.1 (h). (Top, left panels) FTIR 2D Imaging of xerogels obtained from pHEMA/PVP hydrogels swollen with a water solution of TEPA (20 wt%); (Top, right panels) xerogels obtained from gels that were swollen with the TEPA solution and then placed on a bronze coin mock-up containing Cu(II) corrosion products. Below each visible image, the corresponding 2D FTIR Imaging map shows the intensity of the 1615-1535 cm^{-1} region. All maps have dimensions of 700 x 700 μm^2, each axis tick being 50 μm. The bottom panel shows spectra of high (red) or low (green) intensity representative pixels (5.5 x 5.5 μm^2) in the corresponding 2D Imaging map.

The semi-IPN hydrogels, loaded with TEPA, were applied on the surface of a bronze coin that was artificially aged to mimic archaeological bronze

artifacts (see Figures 3.3.1 (i and j)). After aging, the coin surface was covered with a thick and heterogeneous green patina of copper oxychlorides, which shows characteristic IR bands between 3550 and 3300 cm^{-1} (OH stretching[92]) and at 950 cm^{-1} [93]. The application of the gels resulted in a progressive removal of the oxychlorides, preserving the inner red layer (whose color is indicative of cuprite, Cu_2O[93] inhomogeneously present over the surface). Since cuprite is considered a protective layer against further corrosion, as it passivates the surface, the use of these retentive semi-IPNs, that can control the cleaning action, is advantageous from an applicative standpoint resulting in a strong control of the cleaning action. Where cuprite was not present, the cleaning intervention brought back the bronze surface and the whitish patinas of calcium carbonate (with characteristic IR bands at 2512, 1793 and 1463 cm^{-1} [94]) that can eventually be removed through the use of complexing agent selective for calcium. As shown in Figure 3.3.1 (j), the removal of copper oxychlorides at the micron scale was confirmed by 2D FTIR imaging, with a detection limit < 1 pg/pixel (1 pixel = 5.5 x 5.5 μm^2). It must be noticed that pHEMA/PVP and pHEMA/PAA gels, loaded with TEPA, were equally effective in terms of cleaning power and duration of the intervention. In theory, pHEMA/PAA semi-IPN should be more efficient in the removal of copper corrosion products, thanks to the stronger complexing strength of carboxylate groups in PAA as compared to carbonyls in PVP. However, pHEMA/PVP gels have higher equilibrium solvent content, thanks to the superior hydrophilicity of PVP. Both formulations work better than semi-IPNs loaded with EDTA (see Figure 3.3.1 (i)), as expected from the higher stability constant of TEPA-Cu(II) than of EDTA-Cu(II).

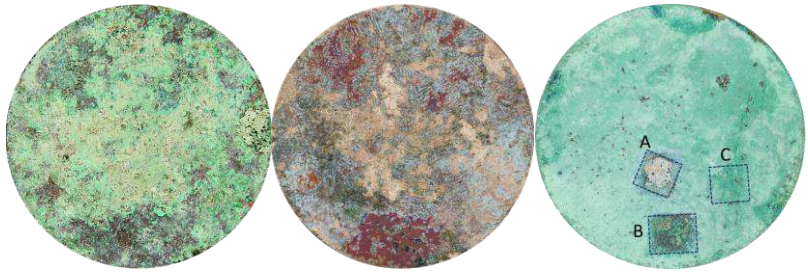

Figure 3.3.1 (i). Artificially aged bronze coin before (left) and after (center) cleaning with semi-IPNs loaded with TEPA. The application of the gels (two cleaning rounds, 45 minutes each) led to the removal of the green corrosion products (copper oxychlorides), preserving the red cuprite layer that is inhomogeneously present on the coin surface. (Right) Preliminary cleaning tests show the progressive removal of corrosion products after the application of semi-IPNs loaded with TEPA for 1 hour (A) or 20 minutes (B). The application of a gel loaded with EDTA for 1 hour (C) did not remove the copper oxychlorides.

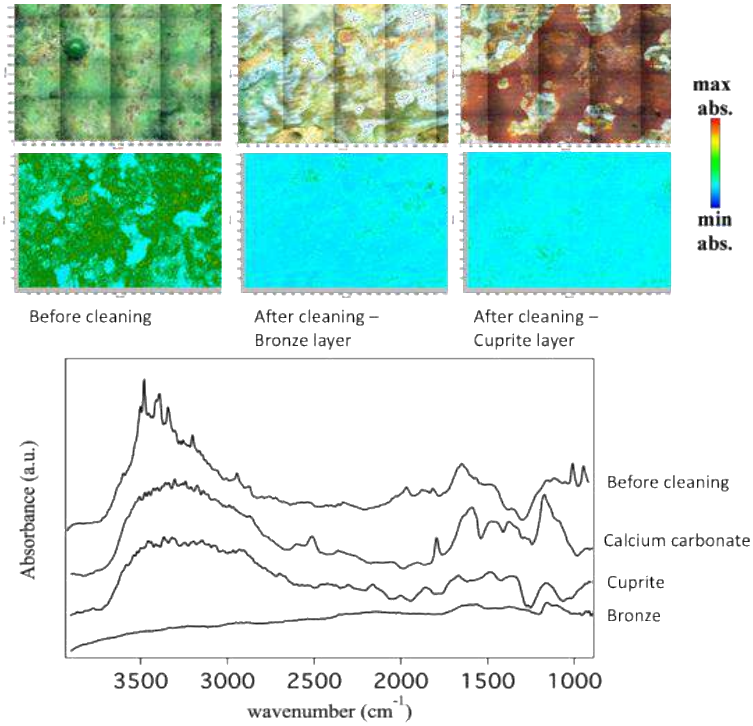

Figure 3.3.1 (j). FTIR 2D Imaging of an artificially aged bronze coin before (top, left panel) and after (top, center and right panel) the application of a pHEMA/PVP gel loaded with TEPA. Below each visible image, the corresponding 2D FTIR Imaging map shows the intensity of the band between 3550 and 3300 cm^{-1} (stretching of OH groups in Cu(II) oxychlorides). All maps have dimensions of 1400 x 2000 μm^2, each axis tick being 50 µm. The bottom panel shows representative spectra of pixels (5.5 x 5.5 μm^2) in the corresponding 2D Imaging maps.

3.3.2 Conclusions

The pHEMA/PAA hydrogel s-IPN50 8:1, previously studied, was chosen among the others thanks to its good mechanical and optical properties, and compared with a pHEMA/PVP semi-IPN, after uploading both systems with aqueous solutions at different pH values (i.e. 6, 8, and 12). These two gels were selected due to the capability of both polymers (PAA and PVP) to strongly coordinate Cu(II) ions. To remove corrosion products from aged bronze coins, these semi-IPNs were also swollen in aqueous solutions of TEPA (pH=12), a strong complexing agent for Cu (II) able to dissolve the copper oxychlorides.

Increasing the pH induces changes in the nano- and micro-structure of the gels. In the case of pHEMA/PAA, the carboxyl group in PAA chains are progressively ionized, as confirmed by 2D FTIR imaging, leading to the swelling of the polymer network, that results in an increase in the meso- and macroporosity, and in the amount of free water uploaded in the gels. In presence of TEPA molecules, the amines interact with carboxyl groups in PAA, making the semi-IPN tighter (lower mesh size) by screening the repulsion between carboxylate groups. The absorption of Cu(II) ions in the TEPA-loaded network, leads probably to the formation of ternary PAA-Cu-TEPA complexes, where two sites of coordination are occupied by PAA carboxylates, and two by amine groups. In the case of pHEMA/PVP semi-IPNs, increasing the pH causes the partial deprotonation of the alcohol group in the enol form of PVP (pH >> 10). Change in the microstructure are observed at each pH variation, while the mean mesh size decreases at high pH values, as the result of inter and intramolecular

hydrogen bonds between enol and enolate groups in the PVP chains. From FTIR 2D Imaging it was possible to hypothesize that the interactions between polar or charged CO groups of PVP and TEPA are favored by the formation of ternary complexes with Cu(II) ions, where CO and amine groups come close together while binding to the metal.

When the gels loaded with TEPA are applied onto corroded bronze coins, the controlled release of the polyamine solution on the surface allows the solubilization and removal of the Cu(II) oxychlorides in the corrosion layers. The dissolved copper ions migrate into the gel matrix and form complexes, which give the gels a blue color. Both pHEMA/PAA and pHEMA/PVP led to an efficient and controlled removal of corrosion products, preserving the inner red corrosion layer (cuprite) that acts as a passivation layer against recurring corrosion. Compared to EDTA, the loading with TEPA enhanced the cleaning power of the gels and decreased the time needed for the intervention.

Therefore, pHEMA/PAA and pHEMA/PVP semi-IPNs loaded with TEPA results promising tools for the preservation of archaeological and historical bronze artifacts, overcoming the limitations of traditional restoration practice.

Chapter 4

Microgels

Hydrophilic and hydrophobic microgels

Microgels are soft colloidal particles constituted by a cross-linked three dimensional polymer network. The presence and the amount of cross-links and the swelling degree determine their character, more "colloidal" (i.e. rigid) or "macromolecular" (i.e. flexible). In fact, when collapsed, microgels behave as hard colloids, even if they still contain solvent, while they are soft and deformable when they are completely swollen[95]. The swelling leads to an open structure with high mobility of the solvent and solute molecules, and of the entire particle, that maintains anyway its structural integrity. In fact, microgels can combine different modes of mass transport, from the diffusion inside their structure to the diffusive or field driven displacement of the microgels themselves. For these reasons, it results important to plan the synthetic design selecting the building blocks, the reaction sequence and conditions to define parameters as size, shape, swelling degree, chemical and topological composition.

Moreover, since the rate of volume change scales as l^{-2}, with l the relevant length scale of the gel, microgels respond much faster than bulk gel to external stimuli, such as change of temperature, pH, ionic strength and electric field[96]. The consequent adjustment of their shape and volume gives the opportunity to reversibly tune their physicochemical properties.

All these features lead very versatile systems to be used in a wide variety of applications, including drug delivery, sensing, catalysis, enzyme immobilization and also as model systems in fundamental research[97].

Within this framework, my studies have been focused on finding an easy and versatile approach to synthesize hydrophilic and hydrophobic monodisperse micron-sized microgels to use them as model systems for two different aspect: the investigation of diffusional properties of soft spheres inside bulk gels, and the development a macroscopic gel with a dual nature (hydrophilic and hydrophobic). In fact, since microgels are not easy to handle, it is interesting to create macroscopic systems (i.e. macrogels), that preserve all the properties of microscopic gels, combining the characteristic of different microgels. Thus, these hydrophilic-hydrophobic macrogels should swell in both organic solvent and water, absorbing and releasing hydrophilic and hydrophobic drugs. They are constituted by two structural levels: a primary network, consists of cross-linked polymer chains of each particle, and a secondary one, composed by crosslinked microparticles, giving the possibility to tune, in a controlled way, both their micro and nanostructure. The morphology of the obtained gels was investigated through Confocal Microscopy and SEM, while Thermogravimetric Analysis was performed to evaluate the solvent content.

To synthesized hydrophilic microgels, N-isopropylacrylamide (NIPAM) was chosen as monomer, whose most important property is its thermosensitivity[98]. In fact, at room temperature, PNIPAM (see Figure 4 (a)) is a relatively hydrophilic polymer and the microgels are widely swollen in water, while above its volume phase transition temperature (VPTT) (i.e. 32 °C), which corresponds to the lower critical solution temperature (LCST) for the polymer, PNIPAM becomes relatively hydrophobic, and the particles shrink sharply. The VPTT can be tuned by copolymerization with other comonomers and, from a rational design, it

was possible also to obtain PNIPAM microgels sensitive to other stimuli, such as pH[99], light[100], glucose[99] and metal cation[101]. Thanks to their versatility, these systems have found numerous applications particularly in the biomedical areas, for drug delivery and biosensing.

In this study PNIPAM microgels were labelled with Oregon Green 488, a fluorescent dye with a good photostability, and loaded in macroscopic poly(vinyl alcohol) (PVA) cryogels, to investigate the anomalous diffusion of the microparticles confined into the polymeric network.

Methyl methacrylate (MMA) was chosen as hydrophobic monomer, since PMMA (see Figure 4 (a)) is a widely investigated polymer that has been the subject of numerous nanocomposite studies focused on the improvement of its strength and durability[102,103]. PMMA organogels recently have been also used in the field of conservation of cultural heritage to remove unwanted hydrophobic layers from canvas painting[104]. Also PMMA microparticles, thanks to their stability, have been extensively used, for example as model systems to study phase behavior[105,106], or as scaffold to incorporate liquid crystal[107]. Thus, a simple surfactant free polymerization method was developed to obtain monodisperse micron-sized microgels, marked with Nile Red, a non ionic dye with high photostability.

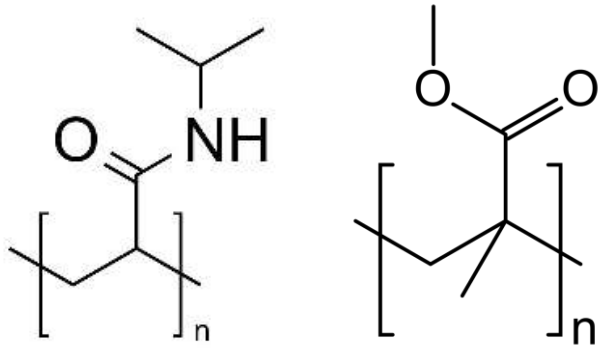

Figure 4 (a). Molecular structure of PNIPAM (left) and PMMA (right).

4.1 Microgels synthesis

Materials

N-isopropylacrylamide (NIPAM, purity 99%), N,N'-Methylenebis(acrylamide) (MBA, purity 99%), Ammonium persulfate (APS, purity ≥98%), Methanol (purity 99.8%) , Methyl methacrylate (MMA, purity 99%), Ethylene glycol dimethacrylate (EGDMA, purity 98%), Rhodamine 110 chloride (purity ≥88%) , Fluorescein isothiocyanate (FITC, purity ≥90%), Fluorescein o-acrylate (FLA, purity 95%), Nile red ((purity ≥95%), and Rhodamine B (purity ≥95%) were purchased from Sigma Aldrich and used as received.

Oregon Green 488 (purity ≥95%) was purchased from ThermoFisher Scientific and used as received.

Water was purified by using a MilliRO-6 Milli-Q gradient system (Milli-pore, resistance >18 MΩ cm).

PNIPAM microgels synthesis

To obtain micron-sized PNIPAM microgels, a surfactant free emulsion polymerization method was adopted to carry out the reaction. The synthesis was performed in a 250 mL three-neck flask placed in a heating oil bath. The flask was equipped with a nitrogen inlet tube, a water-cooled reflux condenser, and a rubber septum for adding the initiator via a syringe. The top of the condenser was connected to a water bubbler to prevent diffusion of oxygen into the system. 1.00g of NIPAM and 0.03g MBA were placed in 110 mL of MilliQ water in the flask and stirred at 200 rpm until they were dissolved. The temperature was then raised at 43 °C and the solution

was purged with nitrogen for 15 min. The polymerization was initiated by the addition, through the syringe, of 5 mL of an APS solution (see Table 4.1 (a)). After about 10 minutes the solution started to become turbid. In fact, when the PNIPAM chain grows beyond a critical length, phase separation occurs because of the polymer's insolubility in water at the reaction temperature.

Then, the temperature was raised again until 60 °C and the reaction ended after 3 hours. The colloidal suspension was cooled down rapidly below room temperature with an ice bath. It was transferred in 4 falcon and centrifugated twice to remove the unreacted monomers.

	PNIPAM microgel
Water	6.4 mol
NIPAM	$8.8 \cdot 10^{-3}$ mol
MBA	$1.9 \cdot 10^{-4}$ mol
APS	$4.4 \cdot 10^{-4}$ mol
MBA/NIPAM molar ratio %	2.2 %

Table 4.1 (a). reagents for PNIPAM microgels synthesis.

To label the microgels with a fluorescent dye, 4 different synthesis were made with different probes. The first trial consisted in the addition of 0.01g of FLA, a fluorescent monomer, to obtained copolymer fluorescent microgels. However, during the reaction, FLA lost almost all its property to emit light, probably as a result of temperature degradation. Therefore, we tried to include other probes inside the microparticles without any chemical reaction with the polymeric network. 0.002g of Rhodamine 110

chloride, a cationic molecule, were added to the water solution of NIPAM. The obtained Rh110/NIPAM microgels were polydispersed with ellipsoidal shapes, mreover the dye was localized predominantly on the external part (see left panel of Figure 4.1(a)). On the contrary, using FITC (i.e. a negatively charged dye) the particles were monodisperse and the probe was equally distributed in all the volume, as it is shown in the right panel of Figure 4.1 (a). In this last case the microgels were tested for particle tracking analysis with scares results due to photobleaching problems associated to the laser, thus Oregon Green 488, a more stable derivative of fluorescein, was used.

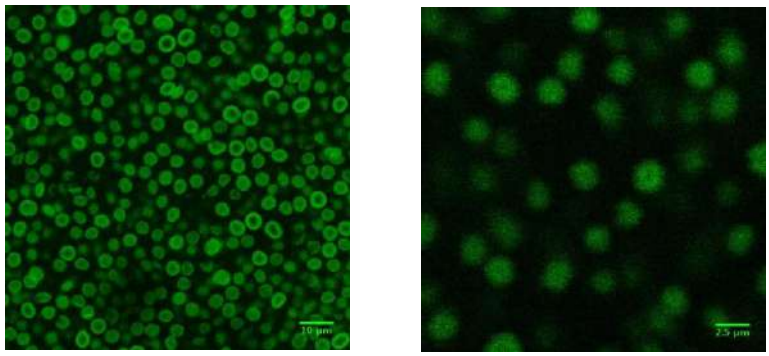

Figure 4.1 (a). Microgels labelled with Rhodamine Chloride 110 (left) and FITC (right).

The steps and the parameters involve in the microgels synthesis are here reported. First of all, the polymerization starts when APS is added to reaction solution, leading to the formation of PNIPAM chains. As these chains grow, they become more and more hydrophobic and, at a critical chain length, they precipitate and agglomerate to form primary seeds, that agglomerate until they become stable colloids[108]. The charge on the colloidal surface, derived from the sulfonate groups of the initiator,

stabilize the microgels. In fact, the primary seeds continue to agglomerate until the resulting particles have accumulated enough charges to avoid further coagulation[109]. In this condition, the number of stable seeds is determined and it remains constant, leading to a homogeneously growth of the particles (equilibrium phase) (see Figure 4.1 (b)).

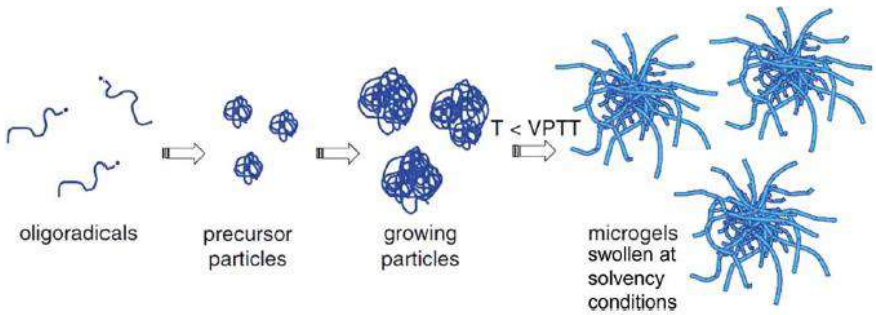

Figure 4.1 (b). Schematic representation of microgels formation and growth. (Pich and Richtering, 2010, Copyright, Springer-Verlag Berlin Heidelberg) [110].

The microgels size and polydispersity is influenced by various parameters including initial monomer concentration, temperature, monomer-to-crosslinker ratio, the rate of stirring, and the presence of surfactants.
In fact, higher crosslinking degree should result in a smaller mean diameter of the microgels, but with more uniform and regular spherical shape. In contrast, a lower amount of crosslinker induces the co-presence of agglomerates, composed of irregular and few regular spherical microparticles[111].
Higher temperature of reaction has been empirically found to deliver more uniform particles compared to particles synthesized at lower temperatures[112], while high stirring rate brings to a less controlled

microgels growth, leading usually to more polydisperse and smaller particles.

The addition of a surfactant to the reaction, such as sodium dodecyl sulfate, brings to a decrease of the microgel diameter compared to a surfactant-free polymerization method, applied in this work[113]. As the electrostatic repulsion is the only factor that leads to the stabilization of the particles, the positively charged dyes, interacting with the sulfonate groups, induce the destabilization of the microgels, resulting in a not uniformly growth. On the contrary, FITC and Oregon Green 488 increase the net negative charge on the particles surface, giving them more stability.

Optical microscopy (Figure 4.1 (c)), and confocal microscopy images (Figure 4.1 (a)) show the obtained microgels, that present a spherical shape and dimension of about 2 μm. This last result is confirmed also by laser granulometry analysis, where it is found that the mean diameter of the microgels in water is (2.09 ± 0.47) μm.

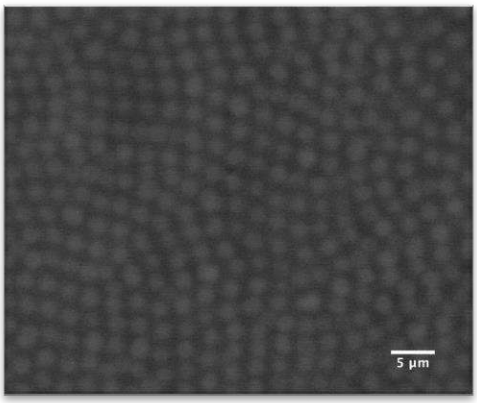

Figure 4.1 (c). Optical microscopy image of PNIPAM microgels synthesized without fluorescent probe. The diameter in the dry state is d = (1.82 ± 0.15) μm.

PMMA microgels synthesis

PMMA microgels, in the micron-size range, were also synthesized using a surfactant free emulsion polymerization method. The same setup of the previous synthesis was adopted to prevent diffusion of oxygen into the three-neck flask. 100 g of methanol and 40g of MilliQ water were placed in the flask and, under magnetic stirring at 200 rpm, 5g of MMA and 0.217g of EGDMA were added to the solution (see Table 4.1(b)). The temperature was raised up to 70 °C under nitrogen flux, then 0.060g of APS, dissolved in 10 mL of milliQ water was placed in the flask through a syringe. After about 10 minutes the solution started to become opalescent due to the growth of PMMA chains that lead to a phase separation caused by the polymer insolubility of the continuous medium. The reaction ended after 24 hours. The colloidal suspension was cooled down rapidly below room temperature with an ice bath, and centrifuged twice at 6000 rpm for 10 minutes.

	PMMA microgel
Methanol	6.2 mol
Water	2.7 mol
MMA	$5.0 \cdot 10^{-2}$ mol
EGDMA	$1.1 \cdot 10^{-3}$ mol
APS	$2.6 \cdot 10^{-4}$ mol
EGDMA/MMA molar ratio %	2.2 %

Table 4.1 (b). reagents for PMMA microgels synthesis.

To label the microgels with a fluorescent dye that absorbs and emits light at higher wavelength than 488 nm (i.e. emission of FITC and Oregon Green 488), 2 different synthesis were carried out with 2 different probes. The first trial consisted in the addition of 0.003g of Rhodamine B, a cationic fluorescent dye, together with the monomer and the cross-linker. However, no microgels were obtained, but only PMMA aggregated on the flask wall. On the contrary, using Nile Red, a non ionic probe, the particles were spherical and monodisperse with a mean diameter of about 1.5 μm (Figure 4.1 (d)). In fact, also these particles were stabilized only by the electrostatic repulsion, thus positively charged dyes, interacting with the sulfonate groups, induce the aggregation of the microgels. On the contrary, non ionic probes does not influence the stability of the particles.

The agitation speed and the temperature of the reaction affects both the dimension and the polydispersity of the PMMA microgels. As reported in a study of S. E. Shim et al. [114], the highest monodispersity can be obtained with low rate of stirring (i.e. about 100 rpm) and keeping the reaction around 70 °C, while the average size increases with the increasing of the temperature. Thus, the more appropriate temperature to synthesized monodisperse PMMA microspheres, with dimension between 1.4 to 1.6 μm, in a relatively short period of polymerization, was 70 °C.

The increasing of monomer concentration results in larger particle size with improved uniformity[115], considering that the amounts of the initiator should correspondingly augment when the monomer content is increased. In surfactant free emulsion polymerization the particle size and concentration of initiator are usually correlated by an inverse relationship, since higher amount of initiator leads to the formation of a greater number of

micelles[116]. On the contrary, in this case, the microgels size increases with the initiator concentration. In fact, as all the reagents are soluble in the methanol/water mixture, the polymerization starts in solution to give surface active oligomers, originated from the decomposition of APS. These oligomers grow until they reach a critical chain length, then they precipitate to form primary particles. The increase of the initiator concentration gives oligomers with lower average molecular weight that prefer to stay in the methanol/water medium, thus the number of the precipitating primary particles decrease leading to the formation of larger microgels.

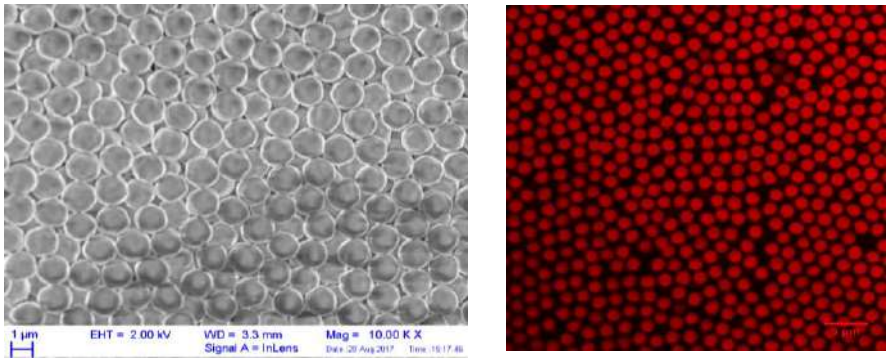

Figure 4.1 (d). SEM (left) and CLSM (right) images of PMMA microgels dry and swollen in water. Bars are 1 µm and 5 µm respectively.

4.2 Microgels for "macrogels" preparation

PNIPAM have been already covalently or physically crosslinked to form 3D networks, namely macroscopic gels (or shortly macrogels). Various cross-linker can be used to obtain covalent networks hierarchically structured, with high surface area and uniform, tunable mesh size. Therefore, they may represent a potential multifunctional drug carriers, as in the case of P(NIPAM-allylamine) microgel network, where dextran was used as a macromolecular model drug entrapped in these gels. The drug can be released with a rate regulated by its molecular weight and the cavity size of the macrogel, as well by the temperature. On the contrary, no release it was observed from a the corresponding conventional bulk PNIPAM gel[117]. In another approach, poly(acrylic acid) was added to the dispersion of the P(NIPAM-allyl-amine) microgels leading to the formation of microgel clusters due to a polymer-mediated bridging process. Then glutaraldehyde was added to covalently link these microgel clusters together, obtaining a stable system[118]. Recently it was found that PNIPAM microgel dispersions are thermogelable under proper conditions, making these materials very useful for a wide range of biomedical applications, such as injectable drug carriers and cell scaffolds. In fact, Xia *et al.*[14] synthesized IPN PNIPAM/PAA microgels, whose concentrated dispersion underwent to an inverse thermoreversible gelation at about 33 °C. Drug loading was achieved by mixing the drug with the microgels dispersion at room temperature and the solution can be implanted by subcutaneous injection, where the liquid quickly gelled. The control of drug release

occurs through the mesh size of the network, that can be tuned by the particle size and concentration[1]. Previously, thermogelling injectable scaffolds were prepared through linear or branched thermosensitive polymers. The potential advantages of the microgels comparing to linear macromolecules include reduced viscosity and better mechanical properties at the same concentration, as well as the possibility to encapsulate bioactive molecules inside the particles and release them in proper time. In addition to the heating method, the in situ gelation of concentrated PNIPAM microgels can occur also by cooling the dispersion of the particles, that swell to a larger degree and close-pack into a 3D network[120], or by changing the pH for pH-sensitive PNIPAM microgels[121]. Within this framework it is interesting to find a simple method to prepare chemically cross-linked hydrophilic and hydrophobic macrogels that are mechanical resistant and easy to handle. In fact, until now no studies have been reported on the synthesis of this kind of macroscopic gels, that could be useful for many applications, spanning from drug delivery to cleaning of cultural heritage artifacts, thanks to their potential ability to absorb and release both hydrophilic and hydrophobic molecules.

Materials

Poly(ethylene glycol) dimethacrylate (PGD (Mw=550 g/mol), purity 98%), Azobisisobutyronitrile (AIBN, purity 99%), and Methyl ethyl ketone (purity ≥99%) were purchased from Sigma Aldrich and used as received.
Ethanol (purity 99%), Acetone (purity 99%), were purchased from Carlo Erba and used as received.
Water was purified by using a MilliRO-6 Milli-Q gradient system (Milli-pore, resistance >18 MΩ cm).

Choice of solvent and synthesis

For the preparation of the hydrophilic/hydrophobic macrogels, the first important step is to find a solvent where all the reagents are soluble (i.e. microgels, initiator and cross-linker) at the reaction temperature. In particular it should swell at the same time the PNIPAM and PMMA microparticles. Water and methyl ethyl ketone (MEK) are not good solvents since the first one can swell only PNIPAM microgels until their VTTP, while the second only PMMA. Therefore, it was necessary to study the co-nonsolvency behavior of these two systems, a rather rare phenomenon, where a polymer perfectly soluble in two different solvents becomes insoluble in mixtures of both. The solubility in alcohol-water solvent mixtures was studied, but since PMMA is soluble in methanol/water solutions only at high temperature and high alcohol concentration, the investigation was focused on ethanol/water mixtures. From a study of I. Bishofberger *et al.*[122] on PNIPAM polymers and microgels, it was demonstrated that, considering ethanol/water solutions, the phase behavior of PNIPAM in water-rich environments is controlled by hydrophobic hydration, due to the difference of the enthalpy between bulk water and the water that creates a hydration shell around the hydrophobic groups of the polymer. The addition of alcohol to water leads to a decrease in the enthalpy difference between bulk and shell water, that can vanish at the solvent composition where the bulk water enthalpy is minimal. In the alcohol-rich environments classical mixing contributions were considered, where the interactions between PNIPAM and the solvent were nonspecific. Thus, the addition of water to ethanol, a good solvent for PNIPAM,

worsens the solvent quality of ethanol. This can give a phase separation when the water content is exceeded. Therefore, when the molar fraction of ethanol is higher than 0.4, water/ethanol mixtures result good solvents for PNIPAM microgels, that should maintain the same diameter than in water (see Figure 4.2(a)).

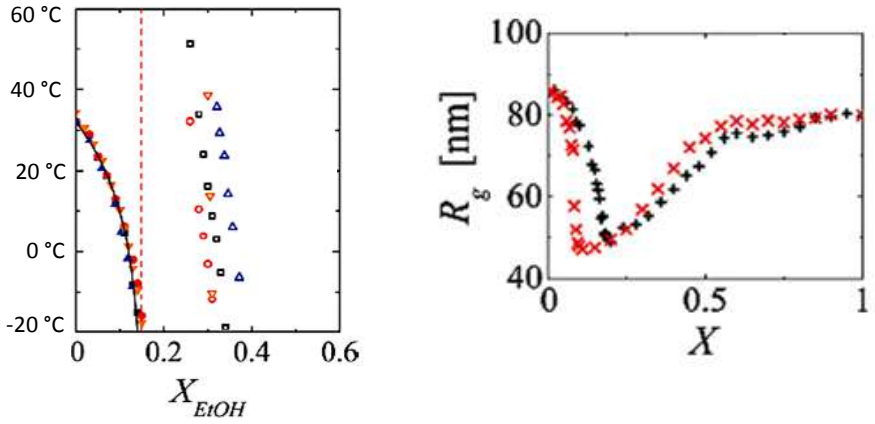

Figure 4.2 (a). Water–ethanol mixtures as a function of the alcohol molar fraction X. Full and open symbols denote respectively the lower critical solution temperature (LCST) and the upper critical solution temperature (UCST) of PNIPAM at different molecular weight and concentration (left). Dependence of radius of gyration of PNIPAM microgels on the alcohol molar fraction X at a fixed temperature of T=12.5°C for water–methanol mixtures (black pluses) and water–ethanol mixtures (red crosses). (I. Bischofberger et al., 2014, Copyright, Royal Society of Chemistry)[122].

A study of R. Hoogenboom *et al.*[123] investigated the solubility of PMMA polymers with different molecular weight in water/ethanol solutions upon heating and cooling (see Figure 4.2 (b)). The PMMA phase transition

temperature in ethanol/water increases with increasing molar mass and polymer concentration, due to an enhanced entropy loss upon unfolding of a larger polymer globule. Anyway, the best range of solubility for PMMA results when the ethanol content is about 80-90 wt%.

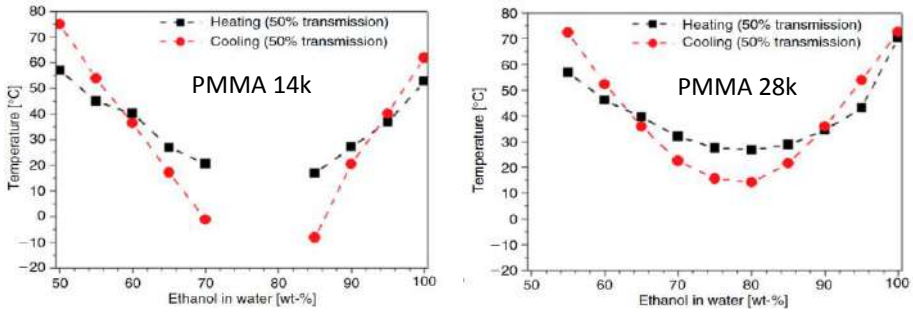

Figure 4.2 (b). Water–ethanol mixtures as a function of the alcohol content (wt%). Black squares represent clearance points upon heating, while red circles cloud points upon cooling (red circles) of PMMA polymer of 13.8 kDa (left) and 27.4 kDa (right). Reproduced from Hoogenboom et al. [123], (2010) with permission from CSIRO Publishing.

As a consequence of these studies, PMMA and PNIPAM microgels were swollen in EtOH/water mixtures at a concentration of 80 and 90 wt% of ethanol to synthesize the macrogels. The diameter of the microparticles, measured from the analysis of confocal laser scanning microscopy images, results (1.38 ± 0.06) μm and (1.82 ± 0.15) μm for PMMA and PNIPM respectively, that are almost the same values obtained for the systems swollen in pure water.

Two reactions were carried out with the same procedure using the particles swollen in the two ethanol/water solutions. The microgels were mixed in a vial in the presence of the initiator (i.e. AIBN dissolved in the minimum

amount of EtOH/water), then they were put in the oven at 70 °C for 10 minutes before adding the cross-linker (i.e. PGD). The solutions were kept at 70 °C for 4 hours, checking every half an hour the reaction progresses. The obtained systems showed a non-homogeneous structures with gel-like aggregates and excess of solvent on the top (see Figure 4.2 (c)).

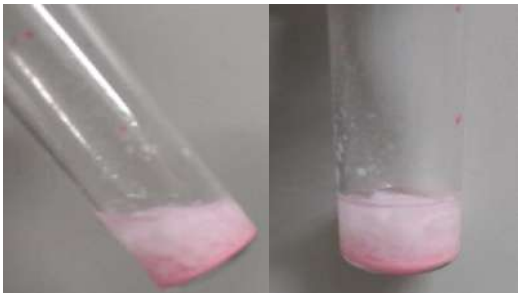

Figure 4.2 (c). Systems obtained from the reaction between PNIPAM and PMMA microgels swollen in EtOH/water mixtures after 4 hours.

Therefore, there was the need to find another solvent that could swell better both the microgels. Acetone is well-known to be a good solvent for PMMA, in fact the diameter of the particles, as measured from CLSM, is bigger than those in water and EtOH/water mixtures (i.e. d=1.57 ± 0.09 μm). Moreover, a study of T. Munk *et. al.*[124], reveals that no phase separation occurs for different PNIPAM polymers when the acetone content in a acetone/water mixtures exceeds 50 vol%. Thus, also PNIPAM microgels were swollen in pure acetone, reaching a diameter of (2.17 ± 0.19) μm.
Macrogels with different cross-linking concentration (i.e. 10, 5, and 2.5 wt%) and different PNIPAM/PMMA ratio (i.e. 25/75 and 75/25 wt%) were synthesized. First of all, the microgels solutions were concentrated through

centrifugation, then the right amount of PNIPAM and PMMA was placed in a glass vial with different quantity of an acetone solution of AIBN (25 wt%), and put in the oven at 70 °C. After 10 minutes, PGD was added to the mixture, that was gently shaken and kept at this temperature for 2.5 hours. The solid gel system obtained was put in water and washed changing the solvent every day for 5 days (see Figure 4.2 (d-e)).

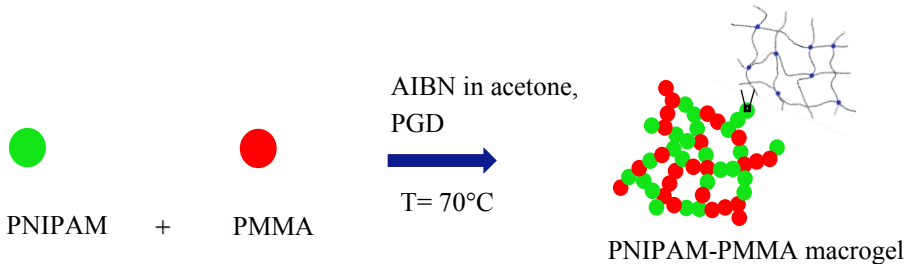

Figure 4.2 (d). Scheme of macrogel synthesis.

Figure 4.2 (e). Photography of the macrogel obtained immediately after synthesis.

The microstructure of the macrogels was investigated through CLSM irradiating the samples with two different wavelengths, one at 488 nm, to see PNIPAM microgels labelled with Oregon Green 488, and the other at 563 nm to excite Nile Red labelled PMMA particles. As it shown in Figure 4.2 (e), the black spots on the right image represent the PNIPAM microgels,

while the red ones are PMMA microgels, all interconnected each other through PGD strands, as it is shown in SEM micrographs.

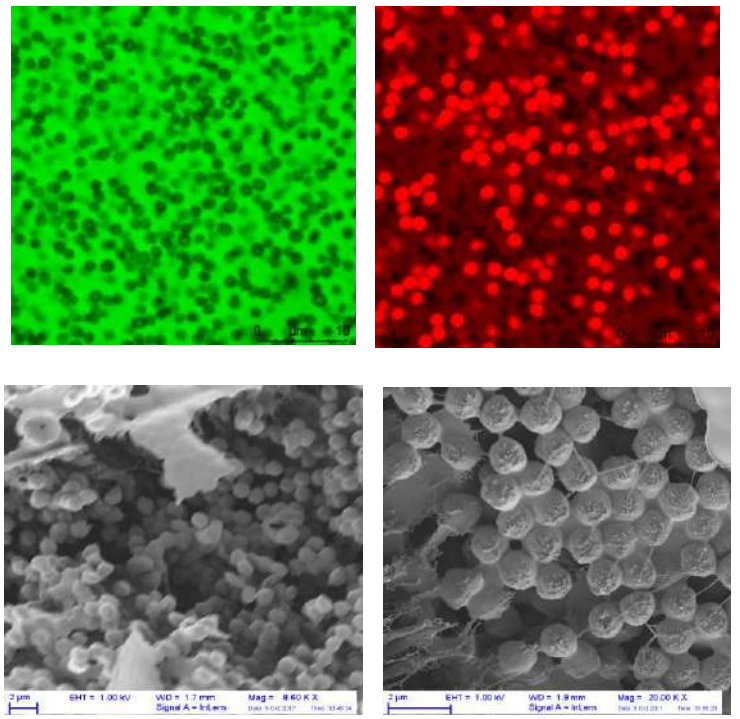

Figure 4.2 (e). (Top) CLSM image of a macrogel obtained irradiating the sample with a wavelength at 488 nm (left) and at 563 nm (right). Bar is 10 µm. (Bottom) SEM micrographs of the same macrogel at two different magnifications. (left, 8.6 and right 20 kX). Bar is 2 µm.

Thermogravimetric analysis was performed on the macrogels swollen in water to understand the influence of different PNIPAM/PMMA ratio and cross-linker concentration on the solvent content. Considering PNIPAM/PMMA 75/25 wt%, a decrease of the cross-linking percentage

leads to an increase of the solvent content, as a consequence of a less compact and more flexible structure (see Table 4.2(a)). Keeping constant the cross-linking concentration (i.e. 10% wt) but varying the PNIPAM/PMMA ratio to 25/75 wt%, the water content decreases of about 5%, while the acetone content increases of the same percentage, due to the more hydrophobic nature of this system (see Table 4.2 (b)).

	Water (wt%)	Acetone (wt%)
10% cross-linker	50.0 ± 0.5	31.1 ± 0.3
5% cross-linker	59.4 ± 0.6	34.3 ± 0.3
2,5 % cross-linker	70.2 ± 0.7	46.3 ± 0.5

Table 4.2 (a). Water and acetone content obtained from TGA analysis performed on PNIPAM/PMMA 75/25 wt% macrogels with different cross-linking percentage.

	Water (wt%)	Acetone (wt%)
PNIPAM/PMMA 75/ 25 wt%	50.0 ± 0.5	31.1 ± 0.3
PNIPAM/PMMA 25/ 75 wt%	45.1 ± 0.5	36.2 ± 0.4

Table 4.2 (b). Water and acetone content obtained from TGA analysis performed on macrogels with 10 wt% of cross-linker with different PNIPAM/PMMA ratio.

Due to time constrains, it was not possible to perform a more detailed investigation. Thus, further studies should be carried out swelling the systems in solvents with growing polarity. In particular, we should analyze

the change of the rheological and mechanical properties, and the swelling degree through TGA measurements and CLSM analysis to visualize the change of microgels dimension, even at different temperature. Unlike macroscopic gel systems, the macrogels have two distinct regions, one hydrophilic and one hydrophobic. This feature results in the ability of absorbing and releasing simultaneously hydrophilic and hydrophobic drugs, leading the macrogels useful candidates for many applications especially in biomedical field and for the conservation of cultural heritage.

Diffusion properties of PNIPAM microgels in macroscopic gels

Diffusion through crowded environments is related to many natural and industrial processes, such as proteins moving through cells, and particles confined in nanocomposite materials or gels. In the presence of a confining medium, the motion of objects can assume anomalous behavior of diffusion, usually manifested by the presence of sub-diffusivity[125,126].

Hydrogels have an important role in regulating the diffusive transport of molecules in a wide variety of biological systems, from cartilage to mucus and extracellular matrix[127], allowing the passage of certain molecules while rejecting other. In general, particles are retained when they are larger than the characteristic pore dimension of the gel, while smaller particles are able to pass through the gel, diffusing with a diffusion constant limited by the local viscosity. On the time scale of structural reorganization within the gel, even particles with a dimension that approaches the pore size of the gel network can slowly diffuse leading to processes of anomalous diffusion.

Anyway, the slow movement of the host matrix has been largely ignored, even if it represents real situations of biological[128,129] and industrial interest[130,131,132]. Thus, to address confined transport in slowly rearranging hydrogels matrices, constrained transport of dilute micron-sized PNIPAM microgels was investigated using polymeric network of simple and semi-IPN poly(vinyl) alcohol (PVA) cryogels.

These systems combine the confinement of a dilute fluid of mobile intruders with the slow dynamics of the gel matrix, providing simple model for the investigation of motion in crowded soft and biological matter. Thus, using confocal laser scanning microscopy with particle tracking analysis, it was possible evaluate the mean square displacement (MSD) of the particles in different conditions of temperature and sample preparation, understanding the diffusional behavior of the microgels in systems with a porosity similar to their size dimension.

Sample preparation

To synthesized simple PVA and semi-IPN PVA/PVA cryogels, using a procedure developed by R. Mastrangelo et.al.[133], PVA 87-124 kDa 88% of hydrolysis and PVA 146-186 kDa 99% of hydrolysis were purchased from Sigma Aldrich and used as received.

Simple PVA cryogels, named PVA0.13 and PVA 1.2, loaded with PNIPAM fluorescent microgels, were prepared dissolving 9g of PVA 146-186 kDa in 100 mL of water at 100 °C under stirring for 4 hours. Then, two concentrations of PNIPAM microgels (i.e. 0.13 or 1.2 g/L) were added to two different solutions, that were mixed for other 15 minutes and subjected to a freeze-thaw cycle. The samples were put in water and washed changing the solvent every day for five days.

The semi-IPNs, loaded with the two different concentrations of the microgels (named PVA/PVA 0.13 and PVA/PVA 1.2), were synthesized using the same procedure, but adding also 3g of PVA 87-124 kDa together with PVA 146-186 kDa.

Moreover, other samples were prepared lyophilizing the semi-IPN cryogels and then loading them with PNIPAM and PNIPAM-poly(ethylene glycol) (PEG) microparticles, swelling pieces of 1x1 cm^2 of the PVA/PVA in 4 mL of the microgels solutions.

The scheme of the PNIPAM-PEG microparticles synthesis is shown in Figure 4.3 (a). 50 mL of PNIPAM microgels solution (containing 0.455g of microgels), loaded with Oregon Green 488, were placed in a flask with 0.023g of poly(ethylene glycol) methacrylate (PEG-MA, Mn=950 Da) and 3 mg of MBA. The solution was heated in an oil bath at 60 °C for 1 hour and half under nitrogen flux. 10 mg of APS were added to the reaction that was kept for other 5 hours at the same temperature. The solution was then cooled down under room temperature and centrifuged twice at 7000 rpm for 30 minutes to remove the unreacted monomers. TGA and CLSM measurements were performed to confirm the presence of PEG and the micron-size dimensions of the PNIPAM-PEG microgels.

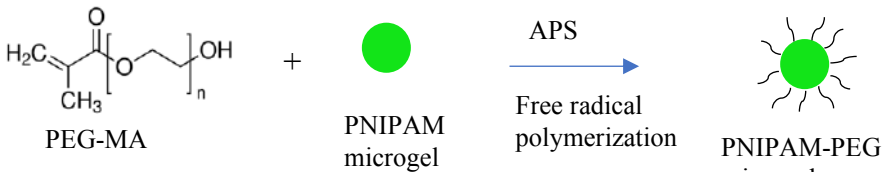

Figure 4.3 (a). Scheme of PNIPAM-PEG microgels synthesis.

Summary of results

To perform measurements in hydrated conditions and at different temperatures, the samples were placed between a microscope slide and a cover glass, sealed tight with UV glue, connected to a channel filled with water.

2D movies of PVA0.12 and PVA/PVA1.2 systems were recorded to monitor the dynamics of the particles in the samples, through the use of particle tracking to determine the mean squared displacements of the microgels. For each sample three different regions were investigated. The results evidence an arrested dynamics of the PNIPAM particles at T = 22 °C in both samples see Figure 4.3 (b) red filled squares), with the repeated experiments that are comparable within statistical fluctuations. Measurements from different regions gave comparable results. Thus, at this temperature the particles are trapped in the gel matrix. At 35 °C on average the dynamics is also arrested, even if the localization is generally less than at 22 °C (i.e. higher values of MSD), due to the shrinking of PNIPAM microgels at 35 °C. Analyzing more in detail the data at 35 °C, it was found that there are some subregions where particles move. As an example, the MSD of two of these regions is reported in Figure 4.3 (b), showing a clearly diffusive behavior for region 1 (r1), and a higher mobility for region 2 (r2). Anyway, the average dimension of the pores (i.e. 1 μm) in the gel are still very tight also for the smaller particle size at T= 35 °C, thus particle cannot freely diffuse.

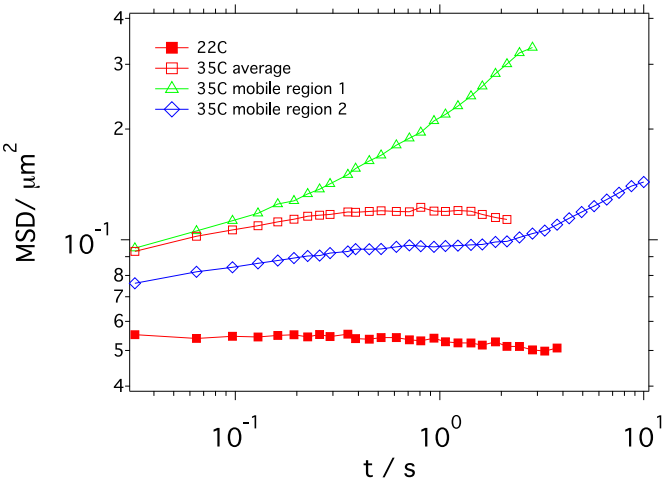

Figure 4.3 (b). Mean square displacement (MSD) of PNIPAM microgels in PVA1.2 at 22 °C (red filled squared), and at 35 °C (green triangles, red empty squares and blue diamonds).

For this reason, PVA/PVA 0.3, PVA/PVA1.2 and lyophilized cryogels loaded with PNIPAM and PNIPAM-PEG microgels were investigated, as they are hydrogels with a bigger average pores dimension (i.e. 3-4 μm). The first two samples presented not perfectly spherical particles, thus only the diffusion properties of lyophilized samples were analyzed.

At 25 °C most of the regions show pronounced dynamics of PNIPAM microgels, except that in region r2 (see Figure 4.3 (c), top left, red triangles), where the particles show slow dynamics that starts to deviate from diffusive behavior, probably due to the effect of the broad size distribution of the pores in the hydrogel matrix. Similar results were obtained at 30 °C, where again the dynamic is similar and, on average, diffusive for most of the regions, except for region r4, where the dynamics

is substantially slower indicatig sub-diffusive behavior (see Figure 4.3 (c), top right, green triangles). At 40 °C, when the PNIPAM microgels are shrunk, the difference between regions r1, r2 and r3 is significantly more pronounced. The dynamics in regions 1 and 2 is very fast, while in region r3 (Figure 4.3 (c), bottom, blue triangles) is almost stuck. PNIPAM-PEG microgels led almost to the same results, meaning that the more hydrophilic character of PNIPAM-PEG particles does not influence the interaction with the PVA matrix, that is absent when the dynamic is diffusive.

Comparing three mobile regions at the different temperature, it is possible to conclude that the MSD at 40 °C is about 2 to 2.5 times larger than at 25 °C and, giving a diffusive motion, with a diffusion coefficient D about 2 to 2.5 larger. Assuming the Stokes-Einstein relation for D, this is the factor expected for a reduction of the particle radius of a factor 2 to 2.5, which is reasonable for PNIPAM considering a temperature change from 25 °C to 40 °C. Therefore, in regions where confinement induced by the hydrogel is weak, the dynamic change can be essentially attributed to the size variation.

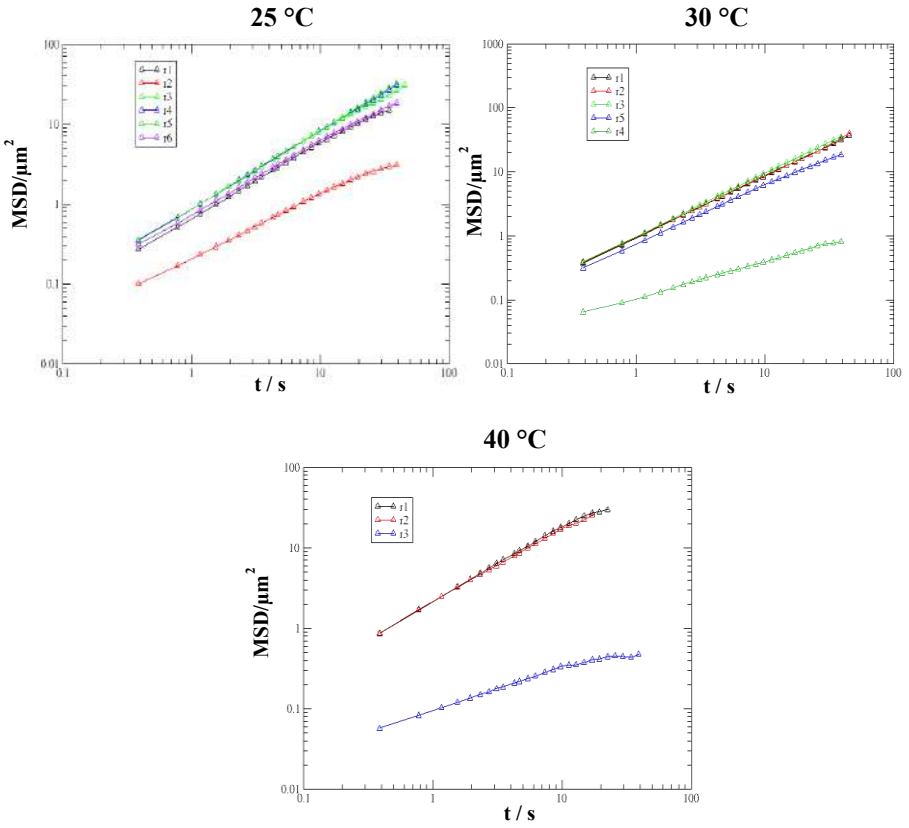

Figure 4.3 (c). MSD of PNIPAM microgels loaded in PVA/PVA liophylized cryogels at 25 °C (top left), 30 °C (top right), and 40 °C (bottom).

4.3 Conclusions

Since microgels respond quickly to external stimuli, compressing and deforming to higher degree than bulk gels, they are widely used as model systems in fundamental research and also in a lot of biomedical applications, spanning from drug delivery to sensing, catalysis, and enzyme immobilization. Therefore, in this study simple methods, based on surfactant free emulsion polymerization, were developed to synthesized spherical, monodisperse, micron-sized particles, adjusting existent experimental conditions. Varying the rate of stirring, the temperature of reaction, the cross-linker/monomer ratio and the quantity of solvent, it was possible to tune the size of the microgels and reduce their polydispersity.

Moreover, since only the electrostatic stabilization, attributed to the sulfate groups of the initiator, acts on the particles, it was found that positively charged fluorescent dyes destabilized PNIPAM microgels, that resulted polydisperse with various shape, and did not allow the formation of PMMA particles. Thus, PNIPAM labelled with negatively charged probes (i.e. FITC and Oregon Green 488) and PMMA synthesized with a neutral probe (i.e. Nile Red) were prepared.

Starting from these two different microgels, an easy way to prepare chemically cross-linked hydrophilic and hydrophobic macrogels was developed, in order to obtain systems that are mechanical resistant and easy to handle. For this purpose, it was necessary to find a solvent able to swell both PNIPAM and PMMA particles. Acetone turned out to be a good candidate. A radical polymerization method activated by the temperature was used to synthesize the macrogels, mixing together the microgels swollen in acetone, the initiator and the cross-linker and keeping the

mixture at 60°C for two hours and half. Macroscopic gels with various cross-linker concentration (i.e. 10, 5, 2.5 %wt) and PNIPAM/PMMA ratio (i.e. 75/25 %wt and 25/75 %wt) were obtained. A decrease of the cross-linker percentage brings to an increase of the solvent content due to the formation of a less compact structure, while the decrease of PNIPAM content leads to a more hydrophobic system that can absorb more acetone at the equilibrium.

More detailed investigations are needed on these macrogels to have a better picture of their structural, mechanical and physical behavior, after swelling them in solvent with increasing polarity. These systems could be useful candidates for many applications especially in biomedical field and for the preservation and restoration of cultural heritage, as a consequence of their potential ability of absorbing and releasing simultaneously hydrophilic and hydrophobic molecules and macromolecules.

PNIPAM and the more hydrophilic PNIPAM-PEG microgels, were also employed as model systems to study the diffusion inside PVA and semi-IPN PVA/PVA macroscopic cryogels with pore dimensions similar to the size of the microparticles. It was found that in PVA hydrogels the dynamics is arrested at 22°C and even at 35°C, the temperature at which the microgels are shrunk, as a consequence of a too small average pore size (i.e. 1 μm). Measurements on the semi-IPNs PVA/PVA, with an average pore dimension of 3-4 μm, revealed diffusive dynamics at both 25 °C and 30 °C, except in some regions, where it is slower, indicating sub-diffusive behavior, probably due to broad size pore distribution. At 40 °C, when the particles are completely shrunk, the MSD, and also the diffusion coefficient, are about 2 to 2.5 times higher than at 25 °C, values that are in accordance with a reduction of the PNIPAM particles radius of a factor 2

to 2.5. Thus, it is possible to assess that, where the confinement induced by the polymer network is weak, the variation of the microgels motion is related to their size change.

As a future prospective, in order to obtain information on the anomalous diffusion of the microgels almost arrested by the hydrogels matrix, instead of particle tracking, Differential Dynamic Microscopy (DDM) will be employed. This technique is based on the time correlation, in Fourier space, of the difference between images separated by a time delay Δt. The decay of the density autocorrelation function f(q, Δt), corresponds to the loss of correlation of the particle density on a length scale determined by q^{-1}, that is related to the characteristic time of the particle motions on the length scale q^{-1}.

All these results could provide important information to understand the diffusional properties of many natural and industrial processes, such as biomolecules and macromolecules that moves through cells or other biological fluids, and drugs confined in nanocomposite materials.

Bibliography

(1) Alemán, J.; Chadwick, A. V.; He, J.; Hess, M.; Horie, K.; Jones, R. G.; Kratochvíl, P.; Meisel, I.; Mita, I.; Moad, G.; et al. *SUBCOMMITTEE ON POLYMER TERMINOLOGY DEFINITIONS OF TERMS RELATING TO THE STRUCTURE AND PROCESSING OF SOLS, GELS, NETWORKS, AND INORGANIC–ORGANIC HYBRID MATERIALS (IUPAC Recommendations 2007) Prepared by a Working Group Consisting Of*; 1801.

(2) Woo, H.-S.; Moon, Y.-B.; Seo, S.; Lee, H.-T.; Kim, D.-W. Semi-Interpenetrating Polymer Network Composite Gel Electrolytes Employing Vinyl-Functionalized Silica for Lithium-Oxygen Batteries with Enhanced Cycling Stability. *ACS Appl. Mater. Interfaces* **2018**, *10* (1), 687–695. https://doi.org/10.1021/acsami.7b15573.

(3) Tong, X.; Yang, F. Recent Progress in Developing Injectable Matrices for Enhancing Cell Delivery and Tissue Regeneration. *Adv. Healthc. Mater.* **2018**, *7* (7), e1701065. https://doi.org/10.1002/adhm.201701065.

(4) Hoffman, A. S. Hydrogels for Biomedical Applications. *Adv. Drug Deliv. Rev.* **2002**, *54* (1), 3–12. https://doi.org/10.1016/S0169-409X(01)00239-3.

(5) Chelazzi, D.; Fratini, E.; Giorgi, R.; Mastrangelo, R.; Rossi, M.; Baglioni, P. Gels for the Cleaning of Works of Art. In *Gels and Other Soft Amorphous Solids*; ACS Symposium Series; American Chemical Society, 2018; Vol. 1296, pp 291–314. https://doi.org/10.1021/bk-2018-1296.ch015.

(6) Flory, P. J. *Principles of Polymer Chemistry*; Cornell University Press, 1953.

(7) Stauffer, D.; Coniglio, A.; Adam, M. Gelation and Critical Phenomena. In *Polymer Networks, Advances in Polymer Science*; Springer Berlin Heidelberg, 1982; pp 103–158.

(8) Flory, P. J. Molecular Size Distribution in Three Dimensional Polymers. I. Gelation1. *J. Am. Chem. Soc.* **1941**, *63* (11), 3083–3090. https://doi.org/10.1021/ja01856a061.

(9) Coniglio, A.; Stanley, H. E.; Klein, W. Site-Bond Correlated-Percolation Problem: A Statistical Mechanical Model of Polymer Gelation. *Phys. Rev. Lett.* **1979**, *42* (8), 518–522. https://doi.org/10.1103/PhysRevLett.42.518.

(10) Kawanishi, K.; Komatsu, M.; Inoue, T. Thermodynamic Consideration of the Sol-Gel Transition in Polymer Solutions. *Polymer* **1987**, *28* (6), 980–984. https://doi.org/10.1016/0032-3861(87)90173-X.

(11) Coniglio, A. Some Cluster-Size and Percolation Problems for Interacting Spins. *Phys. Rev. B* **1976**, *13*, 2194–2207. https://doi.org/10.1103/PhysRevB.13.2194.

(12) Varaprasad, K.; Raghavendra, G. M.; Jayaramudu, T.; Yallapu, M. M.; Sadiku, R. A Mini Review on Hydrogels Classification and Recent Developments in Miscellaneous Applications. *Mater. Sci. Eng. C* **2017**, *79*, 958–971. https://doi.org/10.1016/j.msec.2017.05.096.

(13) Bonelli, N.; Chelazzi, D.; Baglioni, M.; Giorgi, R.; Baglioni, P. Confined Aqueous Media for the Cleaning of Cultural Heritage: Innovative Gels and Amphiphile-Based Nanofluids. In *Nanoscience and Cultural Heritage*; Dillmann, P., Bellot-Gurlet, L., Nenner, I., Eds.; Atlantis Press: Paris, 2016; pp 283–311. https://doi.org/10.2991/978-94-6239-198-7_10.

(14) Sing, K. S. W.; Everett, D. H.; Haul, R. A. W.; Moscou, L.; Pierotti, R. A.; Rouquérol, J.; Siemieniewska, T. Reporting Physisorption Data for Gas/Solid Systems With Special Reference to the Determination of Surface Area and Porosity.

(15) Tarun, G.; Ajay, B.; Bhawana, K.; Sunil, K.; Ravi, J. ORGANOGELS: ADVANCED AND NOVEL DRUG DELIVERY SYSTEM. *Int. Res. J. Pharm.* **2011**, 7.

(16) Mujawar, N. K.; Ghatage, S. L.; Yeligar, V. C. ORGANOGEL: FACTORS AND ITS IMPORTANCE. **2014**, 16.

(17) Ahmed, E. M. Hydrogel: Preparation, Characterization, and Applications: A Review. *J. Adv. Res.* **2015**, *6* (2), 105–121. https://doi.org/10.1016/j.jare.2013.07.006.

(18) Oh, J. K.; Drumright, R.; Siegwart, D. J.; Matyjaszewski, K. The Development of Microgels/Nanogels for Drug Delivery Applications. *Prog. Polym. Sci.* **2008**, *33* (4), 448–477. https://doi.org/10.1016/j.progpolymsci.2008.01.002.

(19) Yamauchi, A. Section 1 - Gels: Introduction. In *Gels Handbook*; Osada, Y., Kajiwara, K., Fushimi, T., Irasa, O., Hirokawa, Y., Matsunaga, T., Shimomura, T., Wang, L., Ishida, H., Eds.; Academic Press: Burlington, 2001; pp 4–12. https://doi.org/10.1016/B978-012394690-4/50075-X.

(20) Müller-Plathe, F. Different States of Water in Hydrogels? *Macromolecules* **1998**, *31* (19), 6721–6723. https://doi.org/10.1021/ma980685b.

(21) Bhagwan, P. *A Handbook Of Thermodynamics*; Mittal Publications.

(22) Horkay, F.; Hammouda, B. Small-Angle Neutron Scattering from Typical Synthetic and Biopolymer Solutions INVITED REVIEW; 2008.

(23) Kamide, K.; Dobashi, T. Physical Chemistry of Polymer Solutions. 11.

(24) Shibayama, M. Inhomogeneous Structure and Dynamics of Condensed Soft Matter. In *Neutrons in Soft Matter*; Imae, T., Kanaya, T., Furusaka, M., Torikai, N., Eds.; John Wiley & Sons, Inc.: Hoboken, NJ, USA, 2011; pp 493–516. https://doi.org/10.1002/9780470933886.ch18.

(25) Shibayama, M.; Norisuye, T. Gel Formation Analyses by Dynamic Light Scattering. *Bull. Chem. Soc. Jpn.* **2002**, *75* (4), 641–659. https://doi.org/10.1246/bcsj.75.641.

(26) Braeckmans, K.; Peeters, L.; Sanders, N. N.; De Smedt, S. C.; Demeester, J. Three-Dimensional Fluorescence Recovery after Photobleaching with the Confocal Scanning Laser Microscope. *Biophys. J.* **2003**, *85* (4), 2240–2252. https://doi.org/10.1016/S0006-3495(03)74649-9.

(27) Soumpasis, D. M. Theoretical Analysis of Fluorescence Photobleaching Recovery Experiments. *Biophys. J.* **1983**, *41* (1), 95–97.

(28) Crocker, J. C.; Grier, D. G. Methods of Digital Video Microscopy for Colloidal Studies. *J. Colloid Interface Sci.* **1996**, *179* (1), 298–310. https://doi.org/10.1006/jcis.1996.0217.

(29) Frenkel, D.; Smit, B. Chapter 4 - Molecular Dynamics Simulations. In *Understanding Molecular Simulation (Second Edition)*; Frenkel,

D., Smit, B., Eds.; Academic Press: San Diego, 2002; pp 63–107. https://doi.org/10.1016/B978-012267351-1/50006-7.

(30) Wichterle, O.; Lím, D. Hydrophilic Gels for Biological Use. *Nature* **1960**, *185* (4706), 117. https://doi.org/10.1038/185117a0.

(31) Peppas, N. A.; Moynihan, H. J.; Lucht, L. M. The Structure of Highly Crosslinked Poly(2-Hydroxyethyl Methacrylate) Hydrogels. *J. Biomed. Mater. Res.* **1985**, *19* (4), 397–411. https://doi.org/10.1002/jbm.820190405.

(32) Meakin, J. R.; Hukins, D. W. L.; Aspden, R. M.; Imrie, C. T. Rheological Properties of Poly(2-Hydroxyethyl Methacrylate) (PHEMA) as a Function of Water Content and Deformation Frequency. *J. Mater. Sci. Mater. Med.* **2003**, *14* (9), 783–787. https://doi.org/10.1023/A:1025088405674.

(33) Jeyanthi, R.; Rao, K. P. In Vivo Biocompatibility of Collagen-Poly(Hydroxyethyl Methacrylate) Hydrogels. *Biomaterials* **1990**, *11* (4), 238–243. https://doi.org/10.1016/0142-9612(90)90004-a.

(34) Domingues, J. A. L.; Bonelli, N.; Giorgi, R.; Fratini, E.; Gorel, F.; Baglioni, P. Innovative Hydrogels Based on Semi-Interpenetrating p(HEMA)/PVP Networks for the Cleaning of Water-Sensitive Cultural Heritage Artifacts. *Langmuir* **2013**, *29* (8), 2746–2755. https://doi.org/10.1021/la3048664.

(35) Fowlkes, J. D.; Hullander, E. D.; Fletcher, B. L.; Retterer, S. T.; Melechko, A. V.; Hensley, D. K.; Simpson, M. L.; Doktycz, M. J. Molecular Transport in a Crowded Volume Created from Vertically Aligned Carbon Nanofibres: A Fluorescence Recovery after Photobleaching Study. *Nanotechnology* **2006**, *17* (22), 5659–5668. https://doi.org/10.1088/0957-4484/17/22/021.

(36) Watson, P. M. D.; Paterson, J. C.; Thom, G.; Ginman, U.; Lundquist, S.; Webster, C. I. Modelling the Endothelial Blood-CNS Barriers: A Method for the Production of Robust in Vitro Models of the Rat Blood-Brain Barrier and Blood-Spinal Cord Barrier. *BMC Neurosci.* **2013**, *14* (1), 59. https://doi.org/10.1186/1471-2202-14-59.

(37) Braeckmans, K.; Peeters, L.; Sanders, N. N.; De Smedt, S. C.; Demeester, J. Three-Dimensional Fluorescence Recovery after Photobleaching with the Confocal Scanning Laser Microscope. *Biophys. J.* **2003**, *85* (4), 2240–2252. https://doi.org/10.1016/S0006-3495(03)74649-9.

(38) Ingo, G. M.; Riccucci, C.; Guida, G.; Albini, M.; Giuliani, C.; Di Carlo, G. Rebuilding of the Burial Environment from the Chemical Biography of Archeological Copper-Based Artifacts. *ACS Omega*

2019, *4* (6), 11103–11111. https://doi.org/10.1021/acsomega.9b00569.

(39) Boschetti, E. Preparative Chromatography Including 10th International Symposium on Preparative ChromatographyAdvanced Sorbents for Preparative Protein Separation Purposes. *J. Chromatogr. A* **1994**, *658* (2), 207–236. https://doi.org/10.1016/0021-9673(94)80017-0.

(40) Peppas, N. A.; Bures, P.; Leobandung, W.; Ichikawa, H. Hydrogels in Pharmaceutical Formulations. *Eur. J. Pharm. Biopharm. Off. J. Arbeitsgemeinschaft Für Pharm. Verfahrenstechnik EV* **2000**, *50* (1), 27–46.

(41) Amsden, B. Solute Diffusion within Hydrogels. Mechanisms and Models. *Macromolecules* **1998**, *31* (23), 8382–8395. https://doi.org/10.1021/ma980765f.

(42) Jones, D. S.; Lorimer, C. J.; Andrews, G. P.; McCoy, C. P.; Gorman, S. P. An Examination of the Thermorheological and Drug Release Properties of Zinc Tetraphenylporphyrin-Containing Thermoresponsive Hydrogels, Designed as Light Activated Antimicrobial Implants. *Chem. Eng. Sci.* **2007**, *62* (4), 990–999. https://doi.org/10.1016/j.ces.2006.10.017.

(43) Tanaka, H.; Matsumura, M.; Veliky, I. A. Diffusion Characteristics of Substrates in Ca-Alginate Gel Beads. *Biotechnol. Bioeng.* **1984**, *26* (1), 53–58. https://doi.org/10.1002/bit.260260111.

(44) Zustiak, S. P.; Boukari, H.; Leach, J. B. Solute Diffusion and Interactions in Cross-Linked Poly(Ethylene Glycol) Hydrogels Studied by Fluorescence Correlation Spectroscopy. *Soft Matter* **2010**, *6* (15). https://doi.org/10.1039/C0SM00111B.

(45) Wu, Y.; Joseph, S.; Aluru, N. R. Effect of Cross-Linking on the Diffusion of Water, Ions, and Small Molecules in Hydrogels. *J. Phys. Chem. B* **2009**, *113* (11), 3512–3520. https://doi.org/10.1021/jp808145x.

(46) Liu, D. E.; Kotsmar, C.; Nguyen, F.; Sells, T.; Taylor, N. O.; Prausnitz, J. M.; Radke, C. J. Macromolecule Sorption and Diffusion in HEMA/MAA Hydrogels. *Ind. Eng. Chem. Res.* **2013**, *52* (50), 18109–18120. https://doi.org/10.1021/ie402148u.

(47) Johansson, L.; Elvingson, C.; Lofroth, J. Diffusion and Interaction in Gels and Solutions .3. Theoretical Results. *Macromolecules* **1991**, *24* (22), 6024–6029. https://doi.org/10.1021/ma00022a019.

(48) Masaro, L.; Zhu, X. X. Physical Models of Diffusion for Polymer Solutions, Gels and Solids. *Prog. Polym. Sci.* **1999**, *24* (5), 731–775. https://doi.org/10.1016/S0079-6700(99)00016-7.

(49) Fujita, H. Diffusion in Polymer-Diluent Systems. In *Fortschritte Der Hochpolymeren-Forschung*; Advances in Polymer Science; Springer Berlin Heidelberg, 1961; pp 1–47. https://doi.org/10.1007/BFb0050514.

(50) Griffiths, P. C.; Stilbs, P.; Chowdhry, B. Z.; Snowden, M. J. PGSE-NMR Studies of Solvent Diffusion in Poly(N. *Colloid Polym. Sci. 273* (4), 405–411. https://doi.org/10.1007/BF00652357.

(51) Han, Y. A.; Lee, E. M.; Ji, B. C. Mechanical Properties of Semi-Interpenetrating Polymer Network Hydrogels Based on Poly(2-Hydroxyethyl Methacrylate) Copolymer and Chitosan. *Fibers Polym.* **2008**, *9* (4), 393–399. https://doi.org/10.1007/s12221-008-0063-8.

(52) Ahmed, E. M. Hydrogel: Preparation, Characterization, and Applications: A Review. *J. Adv. Res.* **2015**, *6* (2), 105–121. https://doi.org/10.1016/j.jare.2013.07.006.

(53) Domingues, J. A. L.; Bonelli, N.; Giorgi, R.; Fratini, E.; Gorel, F.; Baglioni, P. Innovative Hydrogels Based on Semi-Interpenetrating p(HEMA)/PVP Networks for the Cleaning of Water-Sensitive Cultural Heritage Artifacts. *Langmuir* **2013**, *29* (8), 2746–2755. https://doi.org/10.1021/la3048664.

(54) Kanaya, T.; Takahashi, N.; Nishida, K.; Seto, H.; Nagao, M.; Takeba, Y. Dynamic and Static Fluctuations in Polymer Gels Studied by Neutron Spin-Echo. *Phys. B Condens. Matter* **2006**, *385*, 676–681.

(55) Canal, T.; Peppas, N. A. Correlation between Mesh Size and Equilibrium Degree of Swelling of Polymeric Networks. *J. Biomed. Mater. Res.* **1989**, *23* (10), 1183–1193. https://doi.org/10.1002/jbm.820231007.

(56) Lee, H. B.; Mu Shik Jhon; Andrade, J. D. Nature of Water in Synthetic Hydrogels. I. Dilatometry, Specific Conductivity, and Differential Scanning Calorimetry of Polyhydroxyethyl Methacrylate. *J. Colloid Interface Sci.* **1975**, *51* (2), 225–231. http://dx.doi.org/10.1016/0021-9797(75)90107-1.

(57) Tranoudis, I.; Efron, N. Water Properties of Soft Contact Lens Materials. *Contact Lens Anterior Eye J. Br. Contact Lens Assoc.* **2004**, *27* (4), 193–208. https://doi.org/10.1016/j.clae.2004.08.003.

(58) Noferini, D.; Faraone, A.; Rossi, M.; Mamontov, E.; Fratini, E.; Baglioni, P. Disentangling Polymer Network and Hydration Water Dynamics in Polyhydroxyethyl Methacrylate Physical and Chemical Hydrogels. *J. Phys. Chem. C* **2019**. https://doi.org/10.1021/acs.jpcc.9b04212.

(59) Mannhold, R.; Poda, G. I.; Ostermann, C.; Tetko, I. V. Calculation of Molecular Lipophilicity: State-of-the-Art and Comparison of Log P Methods on More than 96,000 Compounds. *J. Pharm. Sci.* **2009**, *98* (3), 861–893.

(60) Sander, T.; Freyss, J.; von Korff, M.; Rufener, C. DataWarrior: An Open-Source Program for Chemistry Aware Data Visualization and Analysis. *J. Chem. Inf. Model.* **2015**, *55* (2), 460–473.

(61) Wang, Y.; Tan, G.; Zhang, S.; Guang, Y. Influence of Water States in Hydrogels on the Transmissibility and Permeability of Oxygen in Contact Lens Materials. *Appl. Surf. Sci.* **2008**, *255* (2), 604–606.

(62) Mchedlov-petrossyan, N. O.; Isaenko, Y. V.; Vodolazkaya, N. A.; Goga, S. T. *Acid-Base Behavior of Fluorescein Isothiocyanate in Aqueous Media and in Micellar Surfactant Solutions*.

(63) Sjoback, R.; Nygren, J.; Kubista, M. Absorption and Fluorescence Properties of Fluorescein. *Spectrochim. Acta Part -Mol. Biomol. Spectrosc.* **1995**, *51* (6), L7–L21. https://doi.org/10.1016/0584-8539(95)01421-P.

(64) Degrigny, C. *Survey of European Experience on Cleaning Procedures*; Nardini Editore, 2004.

(65) Scott, D. A. *Copper and Bronze in Art*; The Getty Conservation Institute, 2002.

(66) Baglioni, P.; Chelazzi, D.; Giorgi, R. *Nanotechnologies in the Conservation of Cultural Heritage: A Compendium of Materials and Techniques*; Springer, 2014.

(67) Chelazzi, D.; Giorgi, R.; Baglioni, P. Microemulsions, Micelles, and Functional Gels: How Colloids and Soft Matter Preserve Works of Art. *Angew. Chem. Int. Ed Engl.* **2018**, *57* (25), 7296–7303. https://doi.org/10.1002/anie.201710711.

(68) Baglioni, P.; Chelazzi, D.; Giorgi, R.; Poggi, G. Colloid and Materials Science for the Conservation of Cultural Heritage: Cleaning, Consolidation, and Deacidification. *Langmuir* **2013**, *29* (17), 5110–5122. https://doi.org/10.1021/la304456n.

(69) Baglioni, P.; Carretti, E.; Chelazzi, D. Nanomaterials in Art Conservation. *Nat. Nanotechnol.* **2015**, *10* (4), 287–290. https://doi.org/10.1038/nnano.2015.38.

(70) Carretti, E.; Bonini, M.; Dei, L.; Berrie, B. H.; Angelova, L. V.; Baglioni, P.; Weiss, R. G. New Frontiers in Materials Science for Art Conservation: Responsive Gels and Beyond. *Acc. Chem. Res.* **2010**, *43* (6), 751–760. https://doi.org/10.1021/ar900282h.

(71) Díaz, E.; Valenciano, R. B.; Katime, I. A. Study of Complexes of Poly(Vinyl Pyrrolidone) with Copper and Cobalt on Solid State. *J.*

Appl. Polym. Sci. **2004**, *93* (4), 1512–1518. https://doi.org/10.1002/app.20620.

(72) Sebastian, N.; George, B.; Mathew, B. Metal Complexes of Poly(Acrylic Acid): Synthesis, Characterization and Thermogravimetric Studies. *Polym. Degrad. Stab.* **1998**, *60* (2), 371–375. https://doi.org/10.1016/S0141-3910(97)00095-5.

(73) Critical Stability Constants - Volume 2: Amines | Arthur Martell | Springer https://www.springer.com/gp/book/9781461344544 (accessed Jul 17, 2019).

(74) Comyns, A. E. Handbook of Copper Compounds and Applications. H.W. Richardson (Ed.) Marcel Dekker, New York, 1997 Viii + 432 Pages $175 ISBN 0-8247-8998-9. *Appl. Organomet. Chem.* **2000**, *14* (3), 174–175. https://doi.org/10.1002/(SICI)1099-0739(200003)14:3<174::AID-AOC940>3.0.CO;2-G.

(75) *Ancient & Historic Metals: Conservation and Scientific Research: Proceedings of a Symposium Organized by the J. Paul Getty Museum and the Getty Conservation Institute, November 1991*; Scott, D. A., Podany, J., Considine, B. B., J. Paul Getty Museum, Getty Conservation Institute, Eds.; Getty Conservation Institute: Marina del Rey, CA, 1994.

(76) Debye, P.; Bueche, A. M. Scattering by an Inhomogeneous Solid. *J. Appl. Phys.* **1949**, *20*, 518–525. https://doi.org/10.1063/1.1698419.

(77) Wang, W.; Chu, F.; Li, L.; Han, H.; Tian, Y.; Wang, Y.; Yuan, Z.; Zhou, Z.; Guo, X. Interactions among spherical poly(acrylic acid) brushes: Observation by rheology and small angle X-ray scattering https://onlinelibrary.wiley.com/doi/abs/10.1002/polb.23901 (accessed Jul 4, 2019). https://doi.org/10.1002/polb.23901.

(78) Hammouda, B.; Ho, D. L. Insight into Chain Dimensions in PEO/Water Solutions. *J. Polym. Sci. Part B Polym. Phys.* **2007**, *45* (16), 2196–2200. https://doi.org/10.1002/polb.21221.

(79) Cheng, J.; Shan, G.; Pan, P. Temperature and PH-Dependent Swelling and Copper(II) Adsorption of Poly(N-Isopropylacrylamide) Copolymer Hydrogel. *RSC Adv.* **2015**, *5* (76), 62091–62100. https://doi.org/10.1039/C5RA09965J.

(80) Hara, K.; Sugiyama, M.; Annaka, M.; Soejima, Y. Nanostructural Characterization of the Dehydrated (NIPA/SA+additive Ion) Gels. *Colloids Surf. B Biointerfaces* **2004**, *38* (3–4), 197–200. https://doi.org/10.1016/j.colsurfb.2004.04.012.

(81) Nikiforova, T. E.; Kozlov, V. A.; Islyaikin, M. K. Acid-Base Interactions and Complex Formation While Recovering Copper(II)

Ions from Aqueous Solutions Using Cellulose Adsorbent in the Presence of Polyvinylpyrrolidone. *Russ. J. Phys. Chem. A* **2012**, *86* (12), 1836–1846. https://doi.org/10.1134/S0036024412120199.

(82) Okay, O. Macroporous Copolymer Networks. *Prog. Polym. Sci.* **2000**, *25* (6), 711–779.

(83) Perova, T. S.; Vij, J. K.; Xu, H. Fourier Transform Infrared Study of Poly (2-Hydroxyethyl Methacrylate) PHEMA. *Colloid Polym. Sci.* **1997**, *275* (4), 323–332. https://doi.org/10.1007/s003960050089.

(84) Dong, J.; Ozaki, Y.; Nakashima, K. FTIR Studies of Conformational Energies of Poly(Acrylic Acid) in Cast Films. *J. Polym. Sci. Part B Polym. Phys.* **1997**, *35* (3), 507–515. https://doi.org/10.1002/(SICI)1099-0488(199702)35:3<507::AID-POLB9>3.0.CO;2-O.

(85) Srikanth, C. S.; Chuang, S. S. C. Spectroscopic Investigation into Oxidative Degradation of Silica-Supported Amine Sorbents for CO2 Capture. *ChemSusChem* **2012**, *5* (8), 1435–1442. https://doi.org/10.1002/cssc.201100662.

(86) Todica, M.; Stefan, R.; Pop, C. V.; Olar, L. IR and Raman Investigation of Some Poly(Acrylic) Acid Gels in Aqueous and Neutralized State. *Acta Phys. Pol. A* **2015**, *128* (1), 128–135. https://doi.org/10.12693/APhysPolA.128.128.

(87) Kabanov, N. M.; Kokorin, A. I.; Rogacheva, V. B.; Zezin, A. B. Study of the Structure of a Polyacrylic Acid-Polyethyleneimine-Copper (II) Ternary Polymer-Metal Complex. *Polym. Sci. USSR* **1979**, *21* (1), 230–240. https://doi.org/10.1016/0032-3950(79)90338-1.

(88) M. Koczkur, K.; Mourdikoudis, S.; Polavarapu, L.; E. Skrabalak, S. Polyvinylpyrrolidone (PVP) in Nanoparticle Synthesis. *Dalton Trans.* **2015**, *44* (41), 17883–17905. https://doi.org/10.1039/C5DT02964C.

(89) Mondal, A.; Mandal, B. CO2 Separation Using Thermally Stable Crosslinked Poly(Vinyl Alcohol) Membrane Blended with Polyvinylpyrrolidone/Polyethyleneimine/Tetraethylenepentamine. *J. Membr. Sci.* **2014**, *Complete* (460), 126–138. https://doi.org/10.1016/j.memsci.2014.02.040.

(90) Bender, M. L.; Figueras, J. The Infrared Spectra of Enolate Ions. *J. Am. Chem. Soc.* **1953**, *75* (24), 6304–6304. https://doi.org/10.1021/ja01120a505.

(91) Shahmiri, M.; Ibrahim, N. A.; Shayesteh, F.; Asim, N.; Motallebi, N. Preparation of PVP-Coated Copper Oxide Nanosheets as

Antibacterial and Antifungal Agents. *J. Mater. Res.* **2013**, *28* (22), 3109–3118. https://doi.org/10.1557/jmr.2013.316.

(92) Martens, W.; Frost, R. L.; Williams, P. A. Raman and Infrared Spectroscopic Study of the Basic Copper Chloride Minerals – Implications for the Study of the Copper and Brass Corrosion and "Bronze Disease." *Neues Jahrb. Für Mineral. - Abh.* **2003**, *178* (2), 197–215. https://doi.org/10.1127/0077-7757/2003/0178-0197.

(93) Di Carlo, G.; Giuliani, C.; Riccucci, C.; Pascucci, M.; Messina, E.; Fierro, G.; Lavorgna, M.; Ingo, G. M. Artificial Patina Formation onto Copper-Based Alloys: Chloride and Sulphate Induced Corrosion Processes. *Appl. Surf. Sci.* **2017**, *421*, 120–127. https://doi.org/10.1016/j.apsusc.2017.01.080.

(94) Ricci, C.; Miliani, C.; Brunetti, B. G.; Sgamellotti, A. Non-Invasive Identification of Surface Materials on Marble Artifacts with Fiber Optic Mid-FTIR Reflectance Spectroscopy. *Talanta* **2006**, *69* (5), 1221–1226. https://doi.org/10.1016/j.talanta.2005.12.054.

(95) Mourran, A.; Wu, Y.; Gumerov, R. A.; Rudov, A. A.; Potemkin, I. I.; Pich, A.; Möller, M. When Colloidal Particles Become Polymer Coils. *Langmuir ACS J. Surf. Colloids* **2016**, *32* (3), 723–730. https://doi.org/10.1021/acs.langmuir.5b03931.

(96) Tanaka, T.; Fillmore, D. J. Kinetics of Swelling of Gels. *J. Chem. Phys.* **1979**, *70* (3), 1214–1218. https://doi.org/10.1063/1.437602.

(97) Seiffert, S. Sensitive Microgels as Model Colloids and Microcapsules. *J. Polym. Sci. Part Polym. Chem.* **2014**, *52* (4), 435–449. https://doi.org/10.1002/pola.27024.

(98) Pelton, R. Temperature-Sensitive Aqueous Microgels. *Adv. Colloid Interface Sci.* **2000**, *85* (1), 1–33.

(99) Zhou, S.; Chu, B. Synthesis and Volume Phase Transition of Poly(Methacrylic Acid-Co-N-Isopropylacrylamide) Microgel Particles in Water. *J. Phys. Chem. B* **1998**, *102* (8), 1364–1371. https://doi.org/10.1021/jp972990p.

(100) Gorelikov, I.; Field, L. M.; Kumacheva, E. Hybrid Microgels Photoresponsive in the Near-Infrared Spectral Range. *J. Am. Chem. Soc.* **2004**, *126* (49), 15938–15939. https://doi.org/10.1021/ja0448869.

(101) Luo, Q.; Guan, Y.; Zhang, Y.; Siddiq, M. Lead-Sensitive PNIPAM Microgels Modified with Crown Ether Groups. *J. Polym. Sci. Part Polym. Chem.* **2010**, *48* (18), 4120–4127. https://doi.org/10.1002/pola.24205.

(102) Jin, Z.; Pramoda, K. P.; Xu, G.; Goh, S. H. Dynamic Mechanical Behavior of Melt-Processed Multi-Walled Carbon

Nanotube/Poly(Methyl Methacrylate) Composites. *Chem. Phys. Lett.* **2001**, *337* (1), 43–47. https://doi.org/10.1016/S0009-2614(01)00186-5.

(103) Coleman, J. N.; Khan, U.; Gun'ko, Y. K. Mechanical Reinforcement of Polymers Using Carbon Nanotubes. *Adv. Mater.* **2006**, *18* (6), 689–706. https://doi.org/10.1002/adma.200501851.

(104) Baglioni, P.; Bonelli, N.; Chelazzi, D.; Chevalier, A.; Dei, L.; Domingues, J.; Fratini, E.; Giorgi, R.; Martin, M. Organogel Formulations for the Cleaning of Easel Paintings. *Appl. Phys. A* **2015**, *121* (3), 857–868. https://doi.org/10.1007/s00339-015-9364-0.

(105) Kodger, T. E.; Lu, P. J.; Wiseman, G. R.; Weitz, D. A. Stable, Fluorescent Polymethylmethacrylate Particles for the Long-Term Observation of Slow Colloidal Dynamics. *Langmuir ACS J. Surf. Colloids* **2017**, *33* (25), 6382–6389. https://doi.org/10.1021/acs.langmuir.7b00852.

(106) van der Linden, M. N.; Stiefelhagen, J. C. P.; Heessels-Gürboğa, G.; van der Hoeven, J. E. S.; Elbers, N. A.; Dijkstra, M.; van Blaaderen, A. Charging of Poly(Methyl Methacrylate) (PMMA) Colloids in Cyclohexyl Bromide: Locking, Size Dependence, and Particle Mixtures. *Langmuir* **2015**, *31* (1), 65–75. https://doi.org/10.1021/la503665e.

(107) Park, N.-H.; Park, S.-I.; Suh, K.-D. A Novel Method for Encapsulation of a Liquid Crystal in Monodisperse Micron-Sized Polymer Particles. *Colloid Polym. Sci.* **2001**, *279* (11), 1082–1089. https://doi.org/10.1007/s003960100524.

(108) Shimizu, H.; Wada, R.; Okabe, M. Preparation and Characterization of Micrometer-Sized Poly(N-Isopropylacrylamide) Hydrogel Particles. *Polym. J.* **2009**, *41* (9), 771–777. https://doi.org/10.1295/polymj.PJ2009039.

(109) Routh, A. F.; Vincent, B. Salt-Induced Homoaggregation of Poly(N-Isopropylacrylamide) Microgels. *Langmuir* **2002**, *18* (14), 5366–5369. https://doi.org/10.1021/la011869d.

(110) Pich, A.; Richtering, W. Microgels by Precipitation Polymerization: Synthesis, Characterization, and Functionalization. In *Chemical Design of Responsive Microgels*; Pich, A., Richtering, W., Eds.; Springer Berlin Heidelberg: Berlin, Heidelberg, 2010; Vol. 234, pp 1–37. https://doi.org/10.1007/12_2010_70.

(111) Petrusic, S.; Jovancic, P.; Lewandowski, M.; Giraud, S.; Bugarski, B.; Djonlagic, J.; Koncar, V. Synthesis, Characterization and Drug

Release Properties of Thermosensitive Poly(N-Isopropylacrylamide) Microgels. *J. Polym. Res.* **2012**, *19* (10), 9979. https://doi.org/10.1007/s10965-012-9979-1.

(112) Alsayed, A. M.; Han, Y.; Yodh, A. G. Melting and Geometric Frustration in Temperature-Sensitive Colloids. In *Microgel Suspensions*; Fernandez-Nieves, A., Wyss, H. M., Mattsson, J., Weitz, D. A., Eds.; Wiley-VCH Verlag GmbH & Co. KGaA: Weinheim, Germany, 2011; pp 229–281. https://doi.org/10.1002/9783527632992.ch10.

(113) Wu, X.; Pelton, R. H.; Hamielec, A. E.; Woods, D. R.; McPhee, W. The Kinetics of Poly(N-Isopropylacrylamide) Microgel Latex Formation. *Colloid Polym. Sci.* **1994**, *272* (4), 467–477. https://doi.org/10.1007/BF00659460.

(114) Shim, S. E.; Kim, K.; Oh, S.; Choe, S. Preparation of Ultra Fine Poly(Methyl Methacrylate) Microspheres in Methanol-Enriched Aqueous Medium. *Macromol. Res.* **2004**, *12* (2), 240–245. https://doi.org/10.1007/BF03218394.

(115) Zhang, J.; Chen, Z.; Wang, Z.; Zhang, W.; Ming, N. Preparation of Monodisperse Polystyrene Spheres in Aqueous Alcohol System. *Mater. Lett.* **2003**, *57* (28), 4466–4470. https://doi.org/10.1016/S0167-577X(03)00344-6.

(116) Prescott, S. W.; Fellows, C. M.; Gilbert, R. G. Maximum Achievable Particle Size in Emulsion Polymerization: Modeling of Large Particle Sizes. *Macromol. Theory Simul.* **2002**, *11* (2), 163–170. https://doi.org/10.1002/1521-3919(20020201)11:2<163::AID-MATS163>3.0.CO;2-6.

(117) Huang, G.; Gao, J.; Hu, Z.; St. John, J. V.; Ponder, B. C.; Moro, D. Controlled Drug Release from Hydrogel Nanoparticle Networks. *J. Controlled Release* **2004**, *94* (2), 303–311. https://doi.org/10.1016/j.jconrel.2003.10.007.

(118) Cho, E. C.; Kim, J.-W.; Fernández-Nieves, A.; Weitz, D. A. Highly Responsive Hydrogel Scaffolds Formed by Three-Dimensional Organization of Microgel Nanoparticles. *Nano Lett.* **2008**, *8* (1), 168–172. https://doi.org/10.1021/nl072346e.

(119) Hu, Z.; Xia, X. Hydrogel Nanoparticle Dispersions with Inverse Thermoreversible Gelation. *Adv. Mater.* **2004**, *16* (4), 305–309. https://doi.org/10.1002/adma.200305560.

(120) Zhao, Y.; Cao, Y.; Yang, Y.; Wu, C. Rheological Study of the Sol−Gel Transition of Hybrid Gels. *Macromolecules* **2003**, *36* (3), 855–859. https://doi.org/10.1021/ma020919y.

(121) Saunders, J. M.; Tong, T.; Le Maitre, C. L.; Freemont, T. J.; Saunders, B. R. A Study of PH-Responsive Microgel Dispersions: From Fluid-to-Gel Transitions to Mechanical Property Restoration for Load-Bearing Tissue. *Soft Matter* **2007**, *3* (4), 486. https://doi.org/10.1039/b613943d.

(122) Bischofberger, I.; Calzolari, D. C. E.; Trappe, V. Co-Nonsolvency of PNiPAM at the Transition between Solvation Mechanisms. *Soft Matter* **2014**, *10* (41), 8288–8295. https://doi.org/10.1039/C4SM01345J.

(123) Hoogenboom, R.; Becer, C. R.; Guerrero-Sanchez, C.; Hoeppener, S.; Schubert, U. S. Solubility and Thermoresponsiveness of PMMA in Alcohol-Water Solvent Mixtures; 2010. https://doi.org/10.1071/ch10083.

(124) Munk, T.; Hietala, S.; Kalliomäki, K.; Nuopponen, M.; Tenhu, H.; Tian, F.; Rantanen, J.; Baldursdóttir, S. Behaviour of Stereoblock Poly(N-Isopropyl Acrylamide) in Acetone–Water Mixtures. *Polym. Bull.* **2011**, *67* (4), 677–692. https://doi.org/10.1007/s00289-011-0458-3.

(125) Klafter, J.; Sokolov, I. M. Anomalous Diffusion Spreads Its Wings. *Phys. World* **2005**, *18* (8), 29–32. https://doi.org/10.1088/2058-7058/18/8/33.

(126) Höfling, F.; Franosch, T. Anomalous Transport in the Crowded World of Biological Cells. *Rep. Prog. Phys.* **2013**, *76* (4), 046602. https://doi.org/10.1088/0034-4885/76/4/046602.

(127) Lieleg, O.; Ribbeck, K. Biological Hydrogels as Selective Diffusion Barriers. *Trends Cell Biol.* **2011**, *21* (9), 543–551. https://doi.org/10.1016/j.tcb.2011.06.002.

(128) Ellis, R. J.; Minton, A. P. Cell Biology: Join the Crowd. *Nature* **2003**, *425* (6953), 27–28. https://doi.org/10.1038/425027a.

(129) Trimble, W. S.; Grinstein, S. Barriers to the Free Diffusion of Proteins and Lipids in the Plasma Membrane. *J. Cell Biol.* **2015**, *208* (3), 259–271. https://doi.org/10.1083/jcb.201410071.

(130) Cherdhirankorn, T.; Harmandaris, V.; Juhari, A.; Voudouris, P.; Fytas, G.; Kremer, K.; Koynov, K. Fluorescence Correlation Spectroscopy Study of Molecular Probe Diffusion in Polymer Melts. *Macromolecules* **2009**, *42* (13), 4858–4866. https://doi.org/10.1021/ma900605z.

(131) Grabowski, C. A.; Mukhopadhyay, A. Size Effect of Nanoparticle Diffusion in a Polymer Melt. *Macromolecules* **2014**, *47* (20), 7238–7242. https://doi.org/10.1021/ma501670u.

(132) Babu, S.; Gimel, J. C.; Nicolai, T. Tracer Diffusion in Colloidal Gels. *J. Phys. Chem. B* **2008**, *112* (3), 743–748. https://doi.org/10.1021/jp076342+.

(133) Mastrangelo, R.; Montis, C.; Bonelli, N.; Tempesti, P.; Baglioni, P. Surface Cleaning of Artworks: Structure and Dynamics of Nanostructured Fluids Confined in Polymeric Hydrogel Networks. *Phys. Chem. Chem. Phys.* **2017**, *19* (35), 23762–23772. https://doi.org/10.1039/C7CP02662E.

Chapter 5

List of papers

Paper I

P. Baglioni, D. Chelazzi, E. Fratini, R. Giorgi, R. Mastrangelo, M. Rossi. ACS Symposium Series, vol. 1296, Chapter 15, pp 291-314,

List of papers

Gels for the cleaning of works of art

P. Baglioni, D. Chelazzi, E. Fratini, R. Giorgi, R. Mastrangelo, M. Rossi

Department of Chemistry Ugo Schiff and CSGI, University of Florence, Via della Lastruccia 3, Sesto Fiorentino, 50019 Florence, Italy

Corresponding author: Piero Baglioni: baglioni@csgi.unifi.it

Abstract

Works of art must be readable and well preserved in order to be accessible. Therefore, the removal of unwanted layers (dirt, soil, aged adhesives and varnishes) is fundamental in conservation practice, to maintain the readability of artworks and prevent their degradation. Because most artworks' surfaces are sensitive to aqueous solutions or organic solvents, the cleaning fluids must be confined in retentive networks able to grant a controlled release and the non-invasive removal of the unwanted layers, without affecting the original components of the artifacts. This contribution reports on the most promising classes of polymer networks that have been specifically developed and applied for the cleaning of artworks, namely: chemical hydrogels based on poly(2-hydroxyethyl methacrylate) (pHEMA), chemical organogels based on Poly(methyl methacrylate) (PMMA), peelable hydrogels based on poly(vinyl alcohol) (PVA), and physical cryogels based on PVA. The physico-chemical properties and

applicative aspects of these materials are discussed. Key characteristics include high viscoelasticity (to grant the feasible handling and removal of the gels from the treated surfaces) and retentiveness. Some representative conservation cases are shown, regarding the cleaning of metal objects and easel paintings. Overall, a large palette of innovative formulations has been provided to the conservation community, to improve on the limitations of traditional solvent thickeners.

Introduction

The surface of an artwork conveys the aesthetic values and the message of the artist. Any alteration of the surface directly affects the readability and enjoyability of the work, with potential impact on the social and economic aspects related to the accessibility and exhibition of the artwork. The surface of the work of art is continuously subjected to degradation induced by weathering (for exterior facades, murals, statutes, stone, etc.), light, temperature and relative humidity, pollution gases and volatile organic compounds (VOCs), dust and soil, microorganisms, and even materials applied in previous restoration interventions that may prove detrimental [1-4]. Not surprisingly, the removal of unwanted materials (e.g. dust, soil, patinas, aged adhesives) from the surfaces of artworks is one of the most frequent operations in the restoration practice that requires great care and attention to avoid the removal or alter the original components of the work.

Traditionally, conservators have used both wet and dry methods to clean works of art. Dry cleaning with conventional tools such as scalpels, swabs and brushes, is difficult to control, with the risk of unselective removal or physical damage to the artwork; recently, the potential of laser cleaning for easel paintings has been explored [5]. Wet cleaning is commonly adopted as a standard procedure, and the main approach is to select solvents whose solubility parameters (e.g. as indicated in a Teas chart [6]) match those of the unwanted layers that need to be removed. This allows to swell (and mechanically remove) or directly solubilize the layers, which are then absorbed into cotton swabs, blotting paper, or other absorbents. However, the use of solvents involves several risks to the artwork and the operator. Once the solvents are applied onto the artwork's surface they are difficult to control, and are able to penetrate through porous substrates, unselectively affecting original components along with unwanted materials. This can lead to swelling, leaching or solubilization of

dyes, binders, and other components of the work of art. Moreover once the unwanted layers are solubilized, they can be transported within the pores of the artwork, making their effective removal difficult. Finally, the use of solvents involves health risks that must be taken into account.

The ecotoxicological impact can be greatly reduced using aqueous solutions of surfactants, chelating agents, enzymes, acids or bases. By tuning the conductivity and ionic strength of the solutions, it is also possible to limit the extraction of water-soluble original components from painted layers [7]. A significant improvement that emerged in the last decade is the use of oil-in-water (o/w) microemulsions, where limited amounts of solvents are stably dispersed as nano-sized droplets in a continuous water phase, using surfactants; these aqueous systems interact with aged adhesives and varnishes through different mechanisms mainly belonging to classic detergency, and in some cases dewetting the unwanted layers from the surface. o/w microemulsions have proven a valid alternative to solvent blends in the removal of aged adhesives, varnishes, soil, and other unwanted materials from the surface of artefacts [8,9]. The main drawback is due to the fact that the use of free (non confined) aqueous systems can be risky on highly water-sensitive surfaces; this is the case, for instance, of paper artworks featuring water-soluble inks or dyes, or some formulations of acrylic or oil paintings.

To overcome these limitations, solvents and aqueous systems can be confined in retentive networks, able to upload the fluids and release them at controlled rate. The gradual release of fluids favors the selective removal of unwanted layers, preserving the original surface. Besides, when solvents are confined, their evaporation rate is reduced, hence the toxicity of the whole cleaning system consistenly is reduced.

Thickeners have been used for decades in the restoration practice to increase the viscosity of cleaning fluids, so as to limit their spreading and penetration. Several products have been derived from cosmetics, food science and pharmaceutics, e.g. cellulose derivatives (hydroxypropylcellulose, methyl 2-hydroxyethyl cellulose, hydroxypropyl methylcellulose) and polysaccharides (agar, gellan, xanthan gum). These polymers have been used to thicken aqeuous solutions of enzymes, chelating agents and surfactants, or blends of water and polar solvents (e.g. alcohols and glycols). While the thickened solutions are relatively easy to prepare and use, the main concern involves the possibility of leaving polymer residues on the treated surface [10]. At the concentration values typically used for cleaning purposes, cellulose ethers solutions display the mechanical dynamic response of viscoelastic liquids: once applied on a surface, the thickened solutions are still able to flow, granting only limited control of the cleaning intervention; moreover, their removal from the treated surface is difficult, owing to the fact that the weak cohesive forces within the polymer solution are comparable to the adhesive forces between the polymer chains and the surface. Gellan and agar are often prepared as “rigid” sheets [11], which

behave rheologically as strong gel networks, and as such can be removed from surfaces leaving only minimal or no polymer residues. However, in several cases artworks have surface roughness on the order of millimiters or centimeters, and rigid sheets can not grant homogeneous adhesion and removal of dirt.

Polyacrylic acid (PAA) was introduced in the restoration practice by Richard Wolbers in the late 1980s [12]. PAA chains unfold at alkaline pH, forming extended 3D networks that increase the viscosity of the solution. When alkaline surfactants are used to deprotonate PAA, the thickened solution acquires emulsifying and detergent properties. Typically, tertiary amine ethoxylates (Ethomeen®) are used to prepare these systems, named "solvent gels", which have been widely adopted by conservators. One of their main advantages relies in their versatility: using Ethomeen® surfactants with different HLB (hydrophilic-lipophilic balance), it is possible to thicken a wide range of solvents, from low-polarity (aliphatic and aromatic hydrocarbons), to average- or high-polarity (alcohols, ketones, esters), and even enzyme solutions. Short application times are needed, typically few minutes. Similarly to cellulose ethers, the main drawback regards the presence of polymer residues and other non-volatile compounds left on the artwork's surface. Because the cross-links between the PAA chains are not permanent, the thickened solutions display a prevalently viscous behavior, and once applied (e.g. with spatulas or swabs) they must be removed coupling mechanical action with the use of clearing solvents. However, it has been shown that residues of PAA and Ethomeen can be found on the surface of paintings even after clearance with solvents [13], and clearing solvents can induce changes to the surface. Moreover, some concerns have been raised regarding the possible long-term synergistic effect of amine N-oxides (formed by the degradation of Ethomeen) on the degradation of terpenoid resins and oils used in paints [14].

To improve on traditional thickeners, several systems have been developed in the last decades in the framework of colloids science and soft matter. The fundamental idea is to formulate polymer networks with tunable properties, so as to adapt the vast range of conservation issues found in the cleaning of artworks. The formulations must exhibit optimal mechanical behavior and retentiveness of the uploaded fluids. High viscoelasticity is fundamental to grant the feasible handling of the systems and their removal in a single step from the surface (e.g. by peeling) after the application, without rinsing. Both chemical gels (i.e. held by covalent crosslinks) and physical gels (held by secondary bonds) have been explored, monitoring the rheological properties, the micro- and mesoporosity, and the macroscopic behavior of the formulations [15,16]. By changing the nature of the polymer and adjusting the pore size distribution of the network, it is possible to obtain highly retentive gels that are usable even on sensitive layers. The desired viscoelasticity for practical applications can be obtained tuning the amount of crosslinks between the polymer chains. In the

case of physical gels, strong networks can be obtained without using crosslinkers, for instance via freeze-thaw cycles that form highly ordered regions (crystallites) where the polymer chains are held by secondary bonds.

A particularly interesting aspect regards the possibility of loading the gels with nanostructured cleaning fluids, i.e. o/w microeulsions. Recently, the structure of an o/w microemulsion, confined in a poly(vinyl alcohol) (PVA) gel, have been investigated; only minimal alteration of the structure of both the fluid and gel occurs, thus the functionality of the cleaning system is maintained [17]. Besides hydrogels (loaded with aqueous systems or polar solvents), organogels (loaded with average- or low-polarity solvents) have been proposed as complementary tools for surfaces that can not tolerate any contact with water [18,19]. Overall, a palette of tools and solutions has been provided to conservators, who can select, together with formulators, the best candidate for each cleaning case study.

In the following sections, an overview of the most promising classes of hydro- and organogels is presented, namely: chemical hydrogels based on poly(2-hydroxyethyl methacrylate) (pHEMA); chemical organogels based on Poly(methyl methacrylate) (PMMA); peelable hydrogels based on PVA; physical cryogels based on PVA. The physico-chemical properties of these systems will be discussed, and the main applicative aspects regarding their use for the cleaning of artworks will be highlighted. These formulations have been selected as they represent some of the most advanced tools currently available for the cleaning of works of art, and have been successfully used on artifacts belonging to the classic, modern, and contemporary Cultural Heritage, from inked manuscripts to stone, wall paintings, and easel paintings by artists such as Pablo Picasso and Jackson Pollock [20-23].

Polyvinilalcohol-based formulations for cleaning

The great variety of artistic substrates to be cleaned, and the complex surface morphology that some of them present, may require cleaning tools with mechanical and rheological properties that vary depending on the case study. This means that in some cases highly viscous systems are preferred, while in others it is more advisable to work with strong gels with high elastic modulus.

Polyvinylalcohol (PVA) with different hydrolysis degrees, even combined with other components, is a versatile macromolecule that allows obtaining gels with characteristics that fulfill most of the conservators' requirements.

Condensation of alcohol groups with borates originates a network of chains that provides high viscosity to the system [24,25] The first formulation investigated for art conservation was based on an aqueous dispersion of highly hydrolyzed PVA. Depending on the average molecular weight of PVA, its concentration, the concentration of borate ions, the pH of the aqueous solution [26], and the temperature, the system can be very stiff or quite malleable [27].

Rheological characterization provided a quantitative description of the obtained systems. The frequency sweep curves obtained for all the formulations investigated are typical of Highly Viscous Polymeric Dispersions (HVPD): at low frequency, the loss modulus G'' is greater than the storage modulus G' (i.e. the elastic character), but at high frequency, G' exceeds G'' [28].

Successively, an aqueous dispersion of poly(vinyl alcohol-co-vinyl acetate) random copolymer (PVAc), cross-linked through the addition of borates, was developed. While the presence of the hydroxyl groups grants the cross-linking reactions, the vinyl acetate groups (about 27% w/w) allow the inclusion of relevant amounts of the organic solvents normally used by conservators for cleaning purposes (e.g. acetone, ethanol, propanol, ethyl acetate, etc.) [28]. The high shear elastic modulus of PVAc-borate HVPDs accounts for their peeling from the cleaned surfaces. This allows minimizing the amount of residues left onto the paint surface, which is the biggest limitation of thickened solvents (i.e. solvent gels).

Particularly relevant is the role of solvents in structuring and reinforcing the gel network. It was demonstrated that increasing the solvent concentration, the free water index (FWI, i.e. the mole fraction of water that behaves as if it were in the neat bulk) decreases linearly down to a value of 0.45 at 25 wt % 1-propanol (i.e. the highest concentration possible without syneresis). 1-propanol acts as a water-structure maker, with a consequent reinforcement of the gel network (e.g. the elasticity is enhanced, see figure 1), and the same behaviour was observed with methylethylketone, MEK [28].

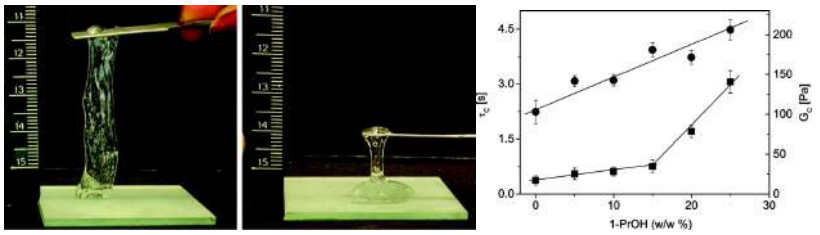

Figure 1. Removal of hydrogels by peeling them off of a glass surface by means of a spatula. (Left): 3 wt % PVA/0.6 wt % borax/20 wt % 1-propanol; (middle) 2 wt % PVA/0.4 wt % borax/20 wt % 1-propanol; (right) Crossover parameters G_c (crossover modulus) (black circles) and τ_c (i.e. $1/\omega_c$, where ω_c is the crossover frequency) (black squares) as a function of 1-propanol (1- PrOH) content. The vertical bars are standard deviations of six measurements. Adapted with permission from ref. 28. Copyright 2009 American Chemical Society."

PVA- and PVAc-borate HVPDs loaded with solvents of medium polarity possess good adaptability to rough surfaces thanks to their viscous character, but at the same time, their elasticity allows a gentle peeling off of the gel network,

without residues left on the cleaned area. These systems were successfully used for the cleaning of different artwork surfaces. Water/MEK blends loaded into PVAc-borate systems were used to remove aged protective varnish layers from wood paintings and contemporary oil on canvas paintings [29]. In both cases, few minutes are required for an almost complete swelling of the undesired layer, which is then fully removed with gentle mechanical action performed with a wet cotton swab. FTIR measurements performed on the cleaned areas, demonstrated that no residues of the cleaning systems could be detected on the surface after the application and removal of the HVPDs. Besides, laboratory tests performed on model films of shellac, showed that the PVAc-borate systems used during the cleaning tests exhibited fluorescence. This led to the conclusion that the shellac resin had partially migrated inside the HVPD during the cleaning [30].

Recently, partially hydrolyzed poly(vinyl acetate) was combined with benzene-1,4-diboronic acid (BDBA), that forms covalent cross-links, to obtain a soft and peelable organogel, able to load a set of solvents largely used by conservators (e.g. dimethylsulfoxide, 2-ethoxyethanol, tetrahydrofuran). Some formulations were successfully used for the removal of aged varnish from a 16th century reliquary and from valuable oil paintings, without leaving any residue on the surface, and respecting the delicate paint layer [31].

Aqueous dispersions of PVA exhibit peculiar film forming properties [32], besides excellent chemical stability, high biocompatibility, low toxicity and low costs. This makes PVA dispersions highly attractive as film forming systems, which can be loaded with chelating agents for the selective surface cleaning of copper-based artifacts. In particular, partially hydrolyzed semi-crystalline PVA shows high water solubility and the ability to form films with good mechanical properties, thanks to the presence of ordered (crystalline) and amorphous domains [33].

The film forming PVA-based dispersion used in association with a complexing agent, such as EDTA that is effective in the removal of copper ions [34], yields a cleaning system with enhanced performances in terms of applicability and efficacy on corroded metal artifacts. This system is particularly relevant for bronze artworks affected by the “bronze disease”, an irreversible process originated by the contact of chlorides with copper alloys, which brings to the formation of tenacious and undesired patinas [35].

For conservation purposes, the system must fulfil the following requirements: i) its softness and adhesiveness should permit its application on both horizontal and non-horizontal surfaces; ii) the evaporation rate of the liquid phase should be slow enough (but not longer than ca. four hours for a single application) to allow the reaction of the chelating agent with the patina; iii) the formed film should be strong, elastic, and easy to remove in one piece, by means of a gentle peeling action; iv) polymer dispersions should be able to load an appreciable amount of ligand.

During the evaporation process, the formation of two distinct regions occurs [36]. A glassy region forms at the polymer-air interface, where the solvent evaporation proceeds faster, and the progressive immobilization of the chains hinders the formation of crystalline domains. The formation of this glassy barrier decreases the solvent evaporation rates, favouring the formation of crystalline domains in the underlying rubbery region, which is characterized by residual mobility of the entangled polymer chains throughout the whole drying process. The glassy-rubbery interface moves inward as the drying process proceeds until a glassy film, containing crystalline domains, is formed.
At the interface between the rubbery region and the corrosion patina, the ligands solution is free to diffuse and interact with the corrosion products, and the formed complexes are confined within the film.
This innovative system represents an enhancement with respect to the commonly used cleaning procedures since it permits to i) achieve complete patina removal thanks to the simultaneous chemical and mechanical action (provided by the gentle peeling of the film); ii) adjust the physical and mechanical properties of the viscous paste (texture, adhesiveness, transparency, etc.) to adapt to different substrates (non-horizontal, rough and irregular surfaces).
Different plasticizers, mainly polyglycols, can be added to the formulation in order to improve specific properties, e.g. the softness of the final dry film that permits its easier peeling.
Frequency sweep tests on the investigated systems show a prevalent viscous behavior with G' < G" over almost the entire range of explored frequencies in a 0-300 minutes time range. A cross-over between G' and G" is observed at high frequencies, typical of polymer dispersions with low cross-linking density. As the volatile fraction evaporates, the progressive increase of G' values indicates an increase in entanglement density of the polymer chains due to the formation of inter- and intra-molecular hydrogen bonds. The frequency sweep curves of an already dried film are characterized by the absence of a crossover between G' and G" curves: G' is higher than G" over the whole range of investigated frequencies, indicating that after drying the system is characterized by a solid-like behavior.
A significant difference can be observed between films obtained from dispersions containing or not EDTA. The storage modulus (G') of a dry film obtained from an EDTA solution is almost double (7000 Pa) than that of a system without EDTA (4500 Pa), as a consequence of enhanced chain entanglement promoted by the presence of EDTA, which results in a stronger network. It is worth noting that the magnitude of G' accounts for the easy peeling of the final film in a single piece (as shown in figure 2 (c)).
Preliminary cleaning tests were performed on artificially aged samples in order to observe the cleaning performances of the selected formulations. These mock-up samples were originally attacked with an acidic solution, and then submitted

to natural aging (burial for several months) producing samples with a highly adherent and inhomogeneous patina. A preliminary characterization, performed by XRD, indicated the presence of copper oxychlorides (atacamite, clinoatamite) on the surface, and of an underlying cuprite layer. After a first cleaning test, performed with a dispersion loaded with 3% w/w EDTA (pH 10), a partial removal of the corrosion products was obtained. The EDS analysis revealed a reduction of 59 % w/w of the typical elements coming from the burial soil (Na, Si, P, Cl). An additional application of gel loaded with 4% w/w EDTA (pH 10) resulted in the complete observable removal of the surface corrosion products, and in a 92% w/w reduction of the extraneous elements [37].

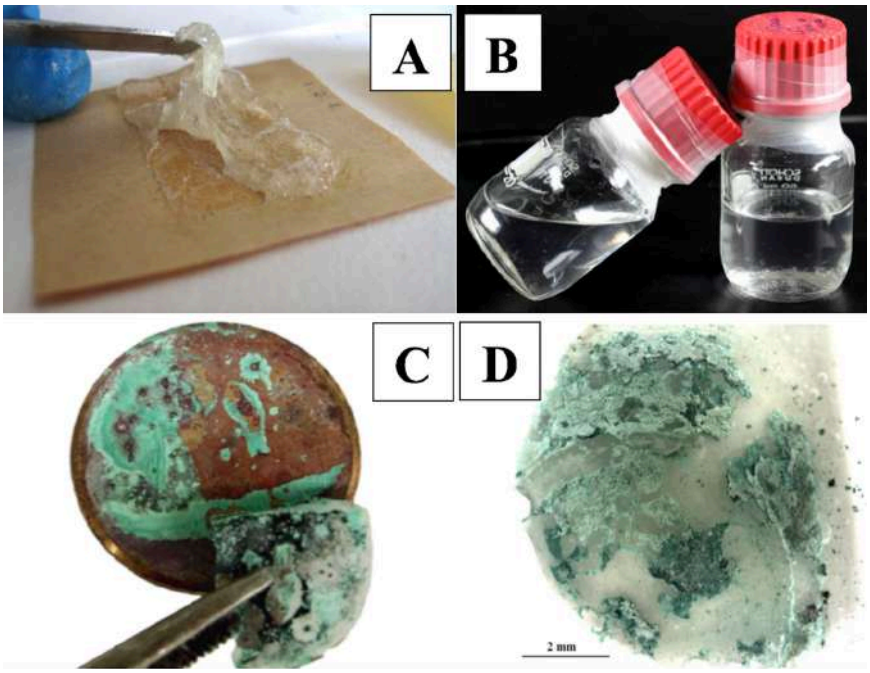

Figure 2. (A) Weak gel of hydroxypropyl cellulose (Klucel) used as reference; (B) vial containing a 3% w/w EDTA (pH 10) loaded PVA70 formulation; (C) easy removal of the dry film by peeling; (D) film containing the removed corrosion patina.

The first cleaning test on real artworks was performed on a bronze fountain (17^{th} century) made by Pietro Tacca in Florence [37]. Corrosion patinas were composed by copper carbonates (malachite $CuCO_3(OH)_2$), sulphates (antlerite $Cu_3(SO_4)(OH)_4$, brochantite $Cu_4(SO_4)(OH)_6$), nitrates and chlorides (atacamite $Cu_2Cl(OH)_3$ and its polymorph clinoatacamite). The cleaning test was performed by applying a 3.5% w/w EDTA solution (pH 7) loaded in a PVA-based

formulation. After a single application, both white calcium carbonate/sulphate and copper corrosion layers were removed. In fact, EDTA is an effective complexing agent also for Ca^{2+} ions, thus performing a double cleaning action. High control of the cleaning process was also ensured, since the complexing reaction cannot further occur after loss of the volatile fraction and the formation of the polymeric film.

As previously mentioned, chemically cross-linked hydrogels possess a highly cohesive structure, which is able to prevent the release of gel residues on the surface of a painting. Nevertheless, a chemical network is not the only option to ensure the physical integrity of the final system. A cyclic freeze-thawing (FT) procedure has been applied to PVA solutions in order to obtain solid-like gels [38]. The low temperature in the freezing step causes a phase separation [39]. Water starts to freeze, and the ice crystals squeeze the PVA chains in a polymer-rich phase: hydrogen bonding among the hydroxyl groups eventually leads to the formation of polymer crystallites, i.e. the tie-points in the newly formed physical gel [40,41].

The term "physical gel" is usually taken to mean a structure whose cross-links are both physical and transient. It behaves as a liquid on long time scales [42]. Gels obtained through freeze-thawing (FT) are physical gels (because PVA chains interact through hydrogen bonds), but they mostly behave as solids, showing mechanical properties close to those of a chemical gel.

In this context is thus more appropriate to further distinguish between 'strong' and 'weak' physical gels [43]:

- strong gels, like cryogels, have a network that is permanent under certain conditions [44], even in the absence of chemical cross-links.
- weak gels fall under the general description of physical gels given above.

Due to their high biocompatibility, PVA hydrogels have been broadly investigated for medical applications, such as substitution of damaged articular cartilage [45], wound dressing [46], and controlled release of drugs [47,48].

In addition to high cohesion and low chemical reactivity, PVA cryogels show other salient characteristics that made them ideal for the cleaning of artworks: high porosity [41], high water content [49] and retention [17], and a pronounced adaptability to irregular surfaces.

When a painting requires cleaning, a key aspect to select the cleaning system is the morphology of the painted surface. For instance, in modern art canvases, the relief of the brushstrokes often creates an uneven and fragile background. In this case, mechanical removal of soil is not advisable.

PVA FT hydrogels, produced as thin films (figure 3-C), easily adapt this type of surface.

The flexibility of the system is strongly related to its rheological characteristics, and can be tailored varying the polymer concentration, the duration of the freezing steps, and the number of FT cycles. All these aspects influence the degree of crystallinity of the resulting gel [50].

Recently [17], the physico-chemical properties of PVA cryogels prepared by one or three FT cycles (starting from polymer solutions at the same concentration) were investigated.
Rheological measurements on the gels showed that G' is higher than G'' in the entire range of frequencies: the gels are solid-like. Moreover, the values of G' and G'' strongly increase with FT cycles (figure 3-A); the number of tie-points is higher in the FT3 gel, causing the structure to be more dense and elastic.
An evidence that the FT3 hydrogel contains a higher concentration of polymer in its structure is also provided by measuring the gel content G(%) [51], i.e. the residual fraction of polymer after storage in water, and the crystallinity X_C [52], see figure 3-B.

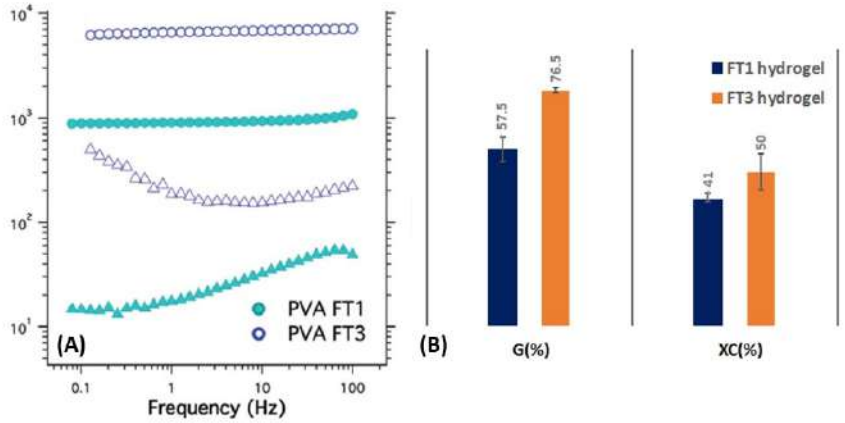

Figure 3. (A) Storage (G', circles) and loss (G'', triangles) moduli measured for PVA FT1 (filled markers) and PVA FT3 (empty markers) gels; (B) Gel content (G(%)) and crystallinity (X_C(%)) for PVA FT1(blue bars) and PVA FT3 (orange bars). Adapted from ref. 17. Copyright (2017) Royal Society of Chemistry.

Indirect consequences of these properties are the higher ability to swell and the larger volumetric capacity of the FT1 gel.
In order to achieve effective cleaning, fluids should be able to freely diffuse inside the polymer matrix and reach the surface on which the gel is lying: high porosity and interconnected channels are required. The porosity of the cryogels is caused by the formation and growth of ice crystals during the freezing steps: they act as templates for the final spongy structure, while packing the polymer chains together [53]. Therefore, the higher the number of FT cycles, the larger the pores, the thicker the polymer walls of the gels (figure 4-A,B). The transmittance of light also changes (figure 4-C).

While water-loaded gels are suitable for the removal of dust, o/w microemulsions embedded in the network are needed to remove hydrophobic dirt from a surface, capturing and holding it inside the gel matrix (figure 5-A).
The diffusion in the gel of a labelled o/w microemulsion can be studied through Fluorescence Correlation Spectroscopy (FCS). The implemented model [54,55] (figure 5-B) confirms that the diffusion of the microemulsion droplets is free in both FT1 and FT3 gels, albeit showing some boundaries in the FT1 sample: as a matter of fact, water-polymer phase separation is less distinct after only one FT cycle, and free polymer chains can occlude some gel channels, and then entrap few droplets.

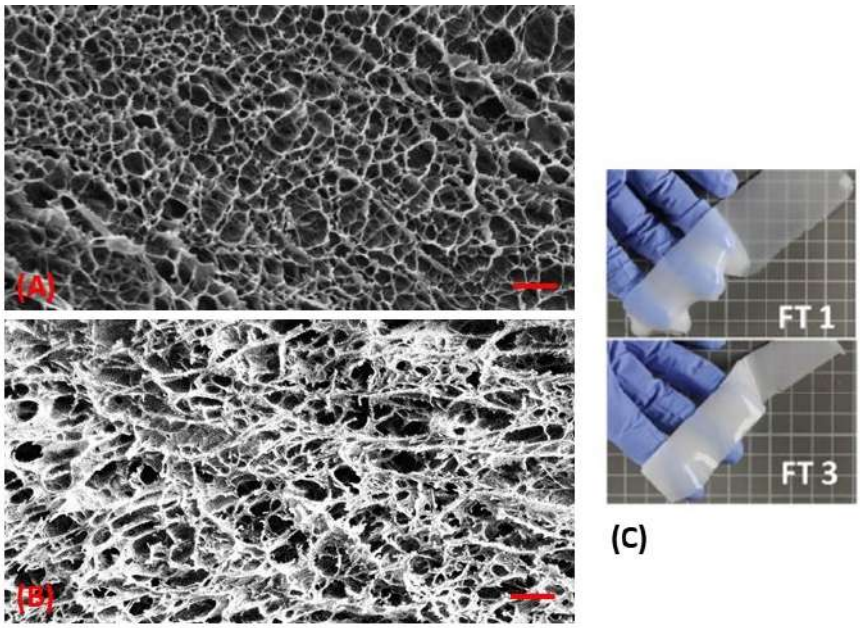

Figure 4. (A-B) SEM images of PVA FT1 (A) and PVA FT3 (B) gels (bar is 1 micron); (C) Appearance of the two gels. Adapted from ref. 17. Copyright (2017) Royal Society of Chemistry.

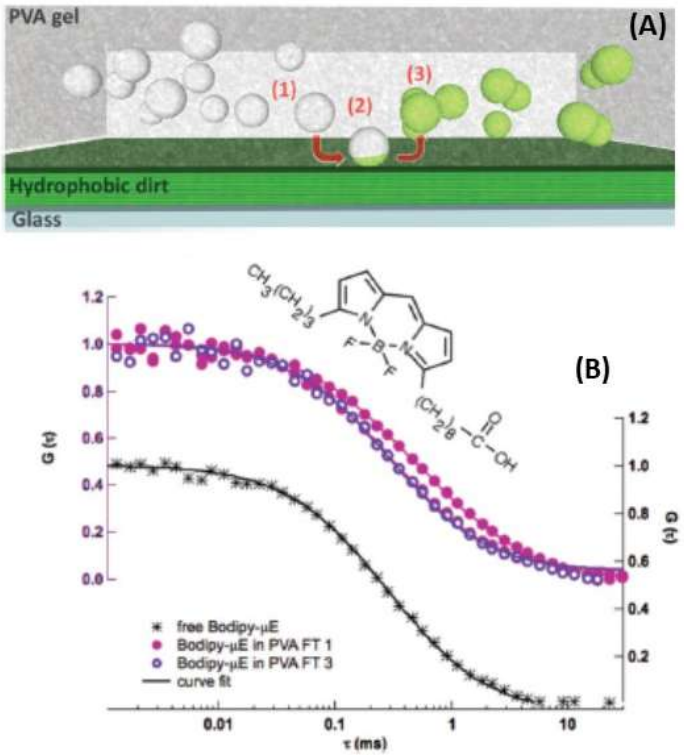

Figure 5. (A) Microemulsion droplets diffusing in the gel (1), interacting with a dirty model substrate and entrapping the dirt (2), and then carrying it into the gel (3); (B) Correlation curves for a microemulsion marked with a fluorescent amphiphilic dye: diffusion in FT1 gel (full marker), in FT3 gel (empty marker) and free diffusion (*stars); solid lines show the fit.* Adapted from ref. 17. Copyright (2017) Royal Society of Chemistry.

Acrylate/methacrylate-based chemical gels

Poly(methyl methacrylate) (PMMA) is a transparent and durable polymer that has been used in a wide range of fields and applications, spanning from technological elements to medical and aesthetic uses [56-59].

Due to its hydrophobicity, PMMA based organogels can be obtained by free radical copolymerization of methyl methacrylate (MMA) and diacrylate monomers in several organic solvents. These organogels have been reported in the literature to study the diffusion of polymer chains in gels [60] and control the swelling of polymeric network through measurments of fast transient fluorescence [61], but only recently their use in the field of conservation of

cultural heritage has been considered [18]. Traditionally, unwanted hydrophobic layers were often removed applying organic solvents directly onto the artifacts surface, even if this method caused some issues [10], as discussed in the previous sections. Therefore, the development of chemical gels, where the confined liquid phase is a low-polarity solvent (as complementary tools to hydrogels), expands the applicability of chemical networks for the cleaning of cultural heritage.

PMMA organogels have been recently synthesized tuning the amount of cross-linker, the type of solvent (i.e. methyl ethyl ketone (MEK), cyclohexanone (cyclo), ethyl acetate (EA) and butyl acetate(BA)), and the monomer/solvent ratio [18,19]. A decrase of the cross-linker density usually leads to an increase in the mesh size, even if the gel porosity is mainly influenced by the equilibrium solvent content (Q), that has the highest value in the systems with MEK. The evaporation kinetics of free and confined solvents were evaluated comparing the loss of weight of swollen PMMA gels to that of a petri dish containing the solvent. Due to its retention power, the evaporation rate is reduced in the polymeric network (Figure 6), allowing the control of the cleaning action and decreasing the impact of the solvents on operators. All the obtained organogels exhibit good optical transparency, useful to directly observe the treated surface during the cleaning action, and good mechanical stability. No gel residues are left on the treated surface, as confirmed by ATR-FTIR analysis.

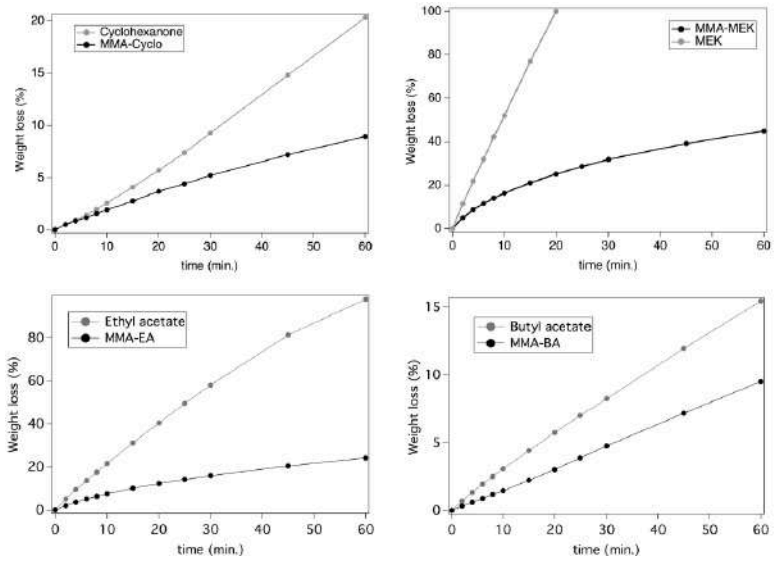

Figure 6. Evaporation kinetics of free and confined solvents in PMMA gels. Reprinted with permission from ref. 18. Copyright 2015 Springer Nature.

A PMMA gel, synthesized with EA, was applied on a canvas painting (early 20th century) and, after 5 minutes, it swelled and softened the unwanted varnish layer, which was then mechanically removed. Part of the varnish was also solubilized, and migrated into the polymeric network (Figure 7) [18].
PMMA-MEK organogels, with different amounts of cross-linker, were applied on a 19th century printed missal book to remove paraffin wax. Two successive applications of 15 minutes were performed in order to obtain a gradual and controlled removal. In fact, only after the second application, the swollen wax that did not adhere to the gel was easly removed with a cotton swab. [19]
Only the polymeric network with the highest cross-linker density has enough retentiveness to avoid uncontrolled diffusion of MEK across the paper surface. Therefore, these results confirmed that it is possible to tune the synthetic procedure to change the retentiveness of the PMMA organogel, in order to extend their use to several substrates with different porosity, hydrophilicity and surface roughness.

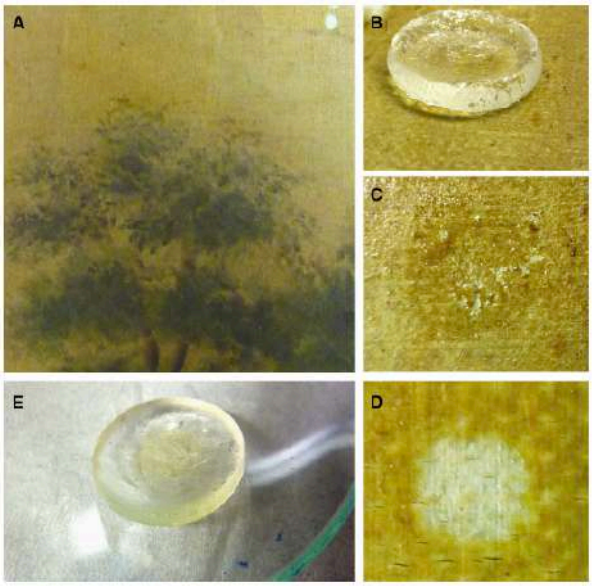

Figure 7. Application of a PMMA-EA organogel on an early 20th century oil canvas painting. Images before (A), during (B) and after (C) the application of the organogels. Spot after the mechanical removal of the swollen varnish (D) and PMMA-EA gel after the application (E). Reprinted with permission from ref. 18. Copyright 2015 Springer Nature.

Poly(2-hydroxyethyl methacrylate) (pHEMA) hydrogels were first prepared and described for biological use by Wichterle and Lim [62]. Thanks to their high water content, soft and rubbery consistence, and low interfacial tension, these hydrogels have physical properties similar to those of living tissue. Therefore, they have been applied or proposed as biomaterials for synthetic prostheses [63], artificial skin [64] and corneal replacement [65], in addition to being used as contact lenses [66] and drug delivery [67] systems.

pHEMA hydrogels are obtained by free radical copolymerization of 2-hydroxyethyl methacrylate (HEMA) and a cross-linker, usually a diacrylate monomer, in water solution. To ensure the production of optically transparent and homogeneous gels, the solvent content in the monomer mixture must not exceed 40-45 wt% [68,69]; in fact, larger amounts of water lead to phase separation during polymerization [70]. When a salt, such as NaCl, is added during the synthesis, a heterogeneous hydrogel with a water content less than 40 wt% is obtained. The salt addition also influences the structure of the polymeric network, which is inverted from a pore interconnetted microstructure to an

irregular macroporosity consisting of interconnected spheres. This effect is due to a decrease of pHEMA compatibility with the solvent that becomes more polar, leading to the so called salting out effect.
It is also possible to vary the water content and mechanical strength of the polymeric network using different types and amounts of cross-linkers during the hydrogel synthesis.
Anyway, classical pHEMA hydrogels does not swell enough to get the required softness for many applications, especially in the field of conservation of cultural heritage. For this reason, a wide range of co-monomers can be incorporated into the pHEMA network, to improve its chemical, physical and mechanical properties. For example, introducing different amounts of N-vinyl-1-pyrrolidone (VP), it is possible to increase the equilibrium water content and change the porosity (Figure 8) and optical transparency, but these gels usually do not have good mechanical stability.

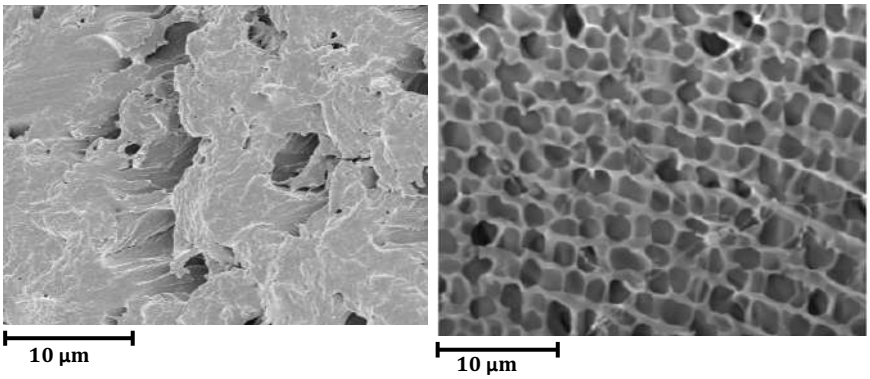

Figure 8. SEM micrographs of classical pHEMA (left) and pHEMA/VP hydrogels (right).

Semi-interpenetrating (semi-IPN) hydrogels, constituted by linear or branched polymers embedded into one or more polymeric network during the polymerization reaction, can overcome this problem, since the obtained hydrogel has features similar to the average of the single homopolymer properties. Domingues et al.[71] developed a new class of semi-IPN polymeric networks, pHEMA/PVP hydrogels, consisting of a pHEMA network, which provides mechanical strength to the hydrogel, and an interpenetrated polymer polyvinylpyrrolidone (PVP), which increases the hydrophilicity and porosity of the system. Hydrogels with various water contents and PVP/HEMA ratio were synthesized to evaluate how these parameters affect the gels' structure, mechanical behaviour (i.e. softness, elasticity and resistance to tensile strength) and affinity to water. In particular, three different hydrogels were obtained with

water contents of 50, 58, and 65 wt% and with HEMA/PVP ratios of 50/50, 40/60, and 30/70 respectively. It was found that the addition of higher amounts of PVP into the reaction mixture leads to an increase of the network hydrophilicity and equilibrium water content (EWC), causing an increment of the average micro and nano porosity. Moreover, also the free water index is affected by the PVP and water content. In fact, the free water index increases of about two times from the hydrogel with 50 wt% of water to that with 65 wt% of water, as a consequence of a lower number of water molecules in contact with the pore walls due to larger pore dimensions.
Rheological characterization showed that these systems are rigid [72], thus they can be applied and removed in one step without leaving residues on the treated surfaces, as confirmed by ATR-FTIR analysis (Figure 9)[71]. Due to the tunable retentiveness, water-loaded pHEMA/PVP hydrogels can be used to clean water-sensitive artefacts. In particular, a pHEMA/PVP hydrogel with a water content of 58 wt% and a HEMA/PVP ratio of 30/70 was tested on a very delicate Thang-Ka (a Tibetan votive artefact made with a '*tempera magra*' on canvas; the pigments are only poorly cohered and adhered to the surface) mock-up. The chosen hydrogel grants the homogeneous and confined cleaning of the grime layer without causing any colour leaching (Figure 10), as instead occurs using traditional agar-agar hydrogels [71].

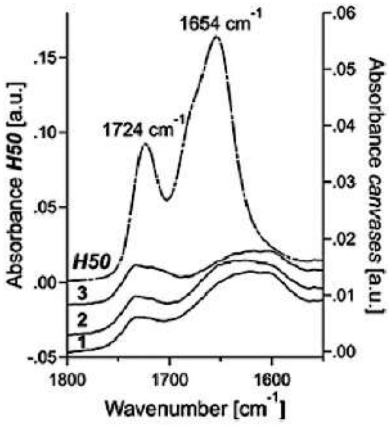

Figure 9. ATR-FTIR spectra of: pHEMA/PVP hydrogels (slash-dotted line); canvases in contact with hydrogels (1) and (2); canvas as is (3). Adapted with permission from ref. 71. Copyright 2013 American Chemical Society.

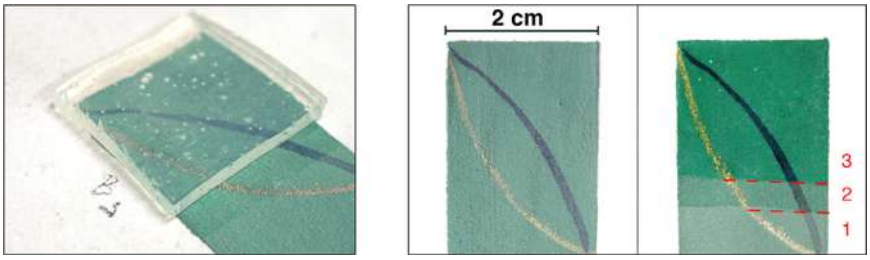

Figure 10. Thang-Ka mock-up with different level of soil removal: not cleaned (1); after 20 minutes of pHEMA/PVP hydrogel application (2); after further 20 minutes of application (3). Adapted with permission from ref. 71. Copyright 2013 American Chemical Society.

pHEMA/PVP hydrogels loaded with a water-ethanol solution (50%) were also successfully used for the removal of aged dammar varnish from oil paintings on canvas (see figure 11) [73].

In order to remove hydrophobic layers from surfaces and limit the cleaning action at the interface, microemulsions can be loaded into pHEMA/PVP hydrogels. In particular, ethyl acetate/propylene carbonate-based o/w microemulsions (μEAPC) were confined into pHEMA/PVP polymeric networks and applied onto a canvas painting, to swell and partially solubilize artificially aged polymer adhesives. In this way, the swollen hydrophobic coating cloud be easily removed by gentle mechanical action [74] (see figure 12). Moreover, from confocal microscopy measurements, Mazzuca *et al.* showed that these hydrogels can be loaded with hydrolytic enzymes that can digest selectively aged pastes and glues, usually found in old paper artworks. The diffusional properties and the pore size of the gels allow the absorption of the product, detached from the paper during the cleaning process, into the polymeric network [72].

Figure 11. Removal of aged varnish from an 18th-century canvas painting. (a) Photographs of the painting and of the poly(2–hydroxyethyl methacrylate)/poly(vinylpyrrolidone) hydrogel application. From left to right: the painting before cleaning (visible light); the painting before cleaning (ultraviolet light); the application of the hydrogel (visible light); the painting after cleaning (visible light); and the painting after cleaning (ultraviolet light). (b) Ultraviolet photographs of the painting showing the feasibility of using chemical gels over a large area. Ultraviolet light fluorescence highlights the efficacy of the cleaning process (left image, not cleaned; right image, cleaned). (c) Visible light photographs of the painting showing the feasibility of using chemical gels over a large area (left image, not cleaned;

right image, cleaned). Reprinted with permission from ref. 73. Copyright 2015 Springer Nature.

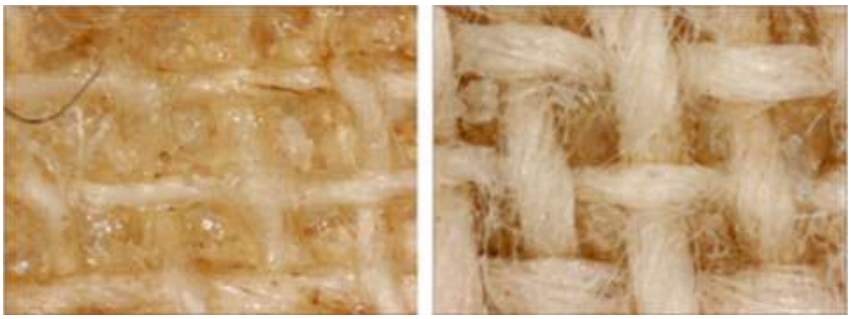

Figure12. Optical microscopy images (x100 magnification) of canvas before (left) and after (right) the removal of aged adhesive using microemulsions confined in the pHEMA/PVP hydrogel with 65 wt% of water. Reprinted with permission from ref. 74. Copyright 2014 Springer Nature.

Conclusions

A wide palette of formulations has been developed in the framework of colloids science and soft matter, specifically designed to allow the controlled removal of unwanted layers from the surface of artworks. The formulation of hydrogels and organogels enables to confine, and gradually release, a wide range of cleaning fluids, from aqueous solutions (of enzymes, chelators, acids/bases, surfactants) to oil-in-water microemulsions, and average- and low-polarity solvents. It is thus possible to remove surface dirt, hydrophilic or hydrophobic soil, overpaints, and aged coatings, adhesives and varnishes. Networks of polymers such as poly(2-hydroxyethyl methacrylate) (pHEMA), Poly(methyl methacrylate) (PMMA), and poly(vinyl alcohol) (PVA) have been formulated. By changing the type of polymer and the synthetic process, it is possible to tune the physico-chemical properties of gels, polymer viscous dispersions, and films. Highly viscoelastic materials can be easily handled, applied, and removed from the surface of artworks without leaving observable polymer residues (e.g. by ATR-FTIR), as opposed to traditional thickeners (e.g. cellulose ethers or "solvent gels" of polyacrylic acid).

Highly viscous polymer dispersions (HVPDs) of PVA can be loaded with water or polar solvents, applied on artworks (e.g. to remove yellowed varnishes), and removed from the surface in a single step. Films of PVA can be cast from polymer dispersions (for instance, loaded with chelators) directly on the surface of metallic artifacts; then, the films are peeled off the surface,

selectively removing corrosion patinas. Organogels of PMMA, loaded with average-polarity solvents, allow the quick removal of adhesives or wax from solvent-sensitive inked manuscripts. Finally, highly retentive semi-IPN hydrogels based on pHEMA and PVP allow the controlled removal of surface dirt from highly water-sensitive surfaces, where the colors are poorly cohered and adhered.

These systems have been validated on numerous case studies, regarding the cleaning of objects and masterpieces from the classic, modern, and contemporary art productions. Overall, a new generation of cleaning tools has been provided to the conservation community, to improve on traditional solvent thickeners.

Acknowledgments

CSGI and the European Union (NANORESTART project, Horizon 2020 research and innovation programme under grant agreement No 646063) are gratefully acknowledged for financial support.

References

1. Keune, K.; Pigment degradation in oil paint induced by indoor climate: comparison of visual and computational backscattered electron images. *Microsc. Microanal.* 2016, *22*, 448-457.
2. Ciferri, O.; Microbial degradation of paintings. *Appl. Environ. Microbiol.* 1999, *65*, 879-885.
3. Favaro, M.; Mendichi, R.; Ossola, F.; Russo, U.; Simon, S.; Tomasin, P.; Vigato, P.A. evaluation of polymers for conservation treatments of outdoor exposed stone monuments. Part I: photo-oxidative weathering. *Polym. Degrad. Stab.* 2006, *91*, 3083-3096.
4. Chelazzi, D.; Chevalier, A.; Pizzorusso, G.; Giorgi, R.; Menu, M.; Baglioni, P. Characterization and degradation of poly(vinyl acetate)-based adhesives for canvas. *Polym. Degrad. Stab.* 2014, *107*, 314-320.
5. Siano, S.; Osticioli, I.; Pavia, A.; Ciofini, D. Overpaint removal from easel paintings using an LQS Nd:YAG laser: The first validation study. *Stud. Conserv.* 2017, *60*, S49-S57.
6. Teas, J.P. Graphic analysis of resin solubilities. *J. Paint Technol.* 1968, *40*, 19-25.
7. Dillon, C.E.; Lagalante, A.F.; Wolbers, R.C. Acrylic emulsion paint films: The effect of solution pH, conductivity, and ionic strength on film swelling and surfactant removal. *Stud. Conserv.* 2014, *59*, 52-62.
8. Baglioni, M.; Montis, C.; Chelazzi, D.; Giorgi, R.; Berti, D.; Baglioni, P. Polymer Film Dewetting by Water/Surfactant/Good-Solvent Mixtures: A Mechanistic Insight and Its Implications for the Conservation of Cultural Heritage. *Angew. Chem. Int. Ed. Engl.* 2018, 130, 1-6.

9. Chelazzi, D.; Giorgi, R.; Baglioni, P. Microemulsions, Micelles and Functional Gels. How Colloid and Soft Matter Preserve Works of Art. *Angew. Chem. Int. Ed. Engl.* 2017, doi: 10.1002/anie.201710711. [Epub ahead of print]
10. Casoli, A.; Di Diego, Z.; Isca, C. Cleaning painted surfaces: evaluation of leaching phenomenon induced by solvents applied for the removal of gel residues. *Environ. Sci. Pollut. Res.* 2014, *23*, 13252-13263.
11. Iannuccelli, S.; Sotgiu, S. Wet treatments of works of art on paper with rigid gellan gels. *The Book and Paper Group Annual*, 2010, *29*, 25-39.
12. Wolbers, R.; Sterman, N.; Stavroudis, C. *Notes for the Workshop on New Methods in Cleaning of Paintings*; The Getty Conservation Institute: Marina del Rey, CA, 1988.
13. Burnstock, A.; Kieslish, T. A study of the clearance of solvent gels used for varnish removal from paintings. *Proceedings of ICOM committee for conservation, 11th Triennal meeting in Edimburgh, Scotland, September 1-6, 1996*; James & James, London, UK, 253-262.
14. Burnstock, A.; White, R. In *Tradition and innovation: advances in conservation, contributions the Melbourne Congress, 10-14 Oct 2000 (IIC)*; Roy, A., Smith, P., Ed.; London, UK, 2000; pp 34-38.
15. Baglioni, P.; Berti, D.; Bonini, M.; Carretti, E.; Perez, M.D.C.C.; Chelazzi, D.; Dei, L.; Fratini, E.; Giorgi, R.; Natali, I.; Arroyo, M.C. Gels for the conservation of cultural heritage. *Materials Research Society Symposium Proceedings.* 2012, *1418*, 17-26.
16. Bonelli, N.; Chelazzi, D.; Baglioni, M.; Giorgi, R.; Baglioni, P. In *Nanoscience and Cultural Heritage*; Dillmann, P., Bellot-Gurlet, L., Ed.; Atlantis Press: Paris, FR, 2016; Vol. 3, pp 283-311.
17. Mastrangelo, R.; Montis, C.; Bonelli, N.; Tempesti, P.; Baglioni, P. Surface Cleaning of Artworks: Structure and Dynamics of Nanostructured Fluids Confined in Polymeric Hydrogel Networks. *Phys. Chem. Chem. Phys.* 2017, *19*, 23762-23772.
18. Baglioni, P.; Bonelli, N.; Chelazzi, D.; Chevalier, A.; Dei, L.; Domingues, J.; Fratini, E.; Giorgi, R.; Martin, M. Organogel formulations for the cleaning of easel paintings. *Appl. Phys. A.* 2015, *121*, 857-868.
19. Pianorsi, M.D.; Raudino, M.; Bonelli, N.; Chelazzi, D.; Giorgi, R.; Fratini, E.; Baglioni, P. Organogels for the cleaning of artifacts. *Pure Appl. Chem.* 2017, 89, 3-17.
20. Baglioni, M.; Bartoletti, A., Bozec, L., Chelazzi, D., Giorgi, R., Odlyha, M., Pianorsi, D., Poggi, G.; Baglioni, P. Nanomaterials for the cleaning and pH adjustment of vegetable-tanned leather. *Appl. Phys. A.* 2016, *114*, 1-11.
21. Berlangieri, C.; Andrina, E.; Matarrese, C.; Carretti, E.; Traversi, R.; Severi, M.; Chelazzi, D.; Dei, L.; Baglioni, P. Chelators confined into 80pvac-borax highly viscous dispersions for the removal of gypsum degradation layers. *Pure Appl. Chem.* 2017, *89*, 97-109.

22. Giorgi, R.; Baglioni, M.; Baglioni, P. Nanofluids and chemical highly retentive hydrogels for controlled and selective removal of overpaintings and undesired graffiti from street art. *Anal. Bioanal. Chem.* 2017, *409*, 3707-3712.
23. PEGGY GUGGENHEIM COLLECTION - Restoration project with NANORESTART - 2015-2016". http://www.guggenheim-venice.it/inglese/conservation/pollock-project.html; Accessed on January 26, 2018.
24. Shibayama, M.; Yoshizawa, H.; Kurokawa, H.; Fujiwara, H.; Nomura, S. Rheological properties of poly(vinyl alcohol)/sodium borate aqueous solutions. *Polymer* 1988, *29*, 2066– 2071
25. Shibayama, M.; Takeushi, T.; Nomura, S. Swelling shrinking and dynamic light-scattering-studies on chemically cross-linked poly(vinyl alcohol) gels in the presence of borate ions. *Macromolecules* 1994, *27*, 5350– 5358.
26. Wu, W.; Shibayama, M.; Roy, S.; Kurokawa, H.; Coyne, L. D.; Nomura, S.; Stein, R. S. Physical gels of aqueous poly(vinyl alcohol) solutions: a small-angle neutron-scattering study. *Macromolecules* 1990, *23*, 2245– 22515.
27. Lin, H.-L.; Liu, Y.-F.; Yu, T. L.; Liu, W.-H.; Rwei, S.-P. Light scattering and viscoelasticity study of poly(vinyl alcohol)-borax aqueous solutions and gels. *Polymer* 2005, *46*, 5541– 55496.
28. Carretti, E.; Grassi, S.; Cossalter, M.; Natali, I.; Caminati, G.; Weiss, R. G.; Baglioni, P.; Dei, L. Poly(vinyl alcohol)−Borate Hydro/Cosolvent Gels: Viscoelastic Properties, Solubilizing Power, and Application to Art Conservation. *Langmuir* 2009, *25*, 8656-8662.
29. Natali, I.; Carretti, E.; Angelova, L.; Baglioni, P.; Weiss, R.G.; Dei, L. Structural and Mechanical Properties of "Peelable" Organoaqueous Dispersions with Partially Hydrolyzed Poly(vinyl acetate)-Borate Networks: Applications to Cleaning Painted Surfaces. *Langmuir*, 2011, *27*, 13226–13235.
30. Carretti, E.; Bonini, M.; Dei, L.; Berrie, B.H.; Angelova, L.V.; Baglioni, P.; Weiss, R.G. New Frontiers in Materials Science for Art Conservation: Responsive Gels and Beyond. *Acc. Chem. Res.*, 2010, *43*, 751–760.
31. Duncan, TT.; Berrie, B.H.; Weiss, R.G. Soft, Peelable Organogels from Partially Hydrolyzed Poly(vinyl acetate) and Benzene-1,4-diboronic Acid: Applications to Clean Works of Art. ACS Appl Mater Interfaces, 2017 9, 28069-28078.
32. Hassan, C.M.; Peppas, N.A. Structure and Applications of Poly(vinyl alcohol) Hydrogels Produced by Conventional Crosslinking or by Freezing/Thawing Methods. *Adv. Polym. Sci*. 2000, *153*, 37-65.
33. Carraher, C.E. *Polymer Chemistry*; CRC Press: Boca Raton, FL, 2014.
34. Scott, D.A.; Podany, J.; Considine, B.B. *Ancient & Historic Metals*; The Getty Conservation Institute: Marina del Rey, CA, 1991.

35. Scott, D.A. *Copper and Bronze in Art*; The Getty Conservation Institute: Los Angeles, CA, 2002.
36. Mallapragada, S. K.; Peppas, N. A. Dissolution mechanism of semicrystalline poly(vinyl alcohol) in water. *J. Polym. Sci. Pol. Phys.*, 1996, *34,* 1339-1346.
37. Parisi, E.I.; Bonelli, N.; Carretti, E.; Giorgi, R.; Ingo, G.M.; Baglioni, P. Film forming PVA-based cleaning systems for the removal of corrosion products from historical bronzes, *Pure Appl. Chem.* 2017; 90, 507-522.
38. Peppas, N. A. Turbidimetric studies of aqueous poly(vinyl alcohol) solutions, *Makromol. Chem.* 1975, 176, 11, 3433–3440.
39. Lozinsky, V. I.; Solodova, E. V.; Zubov, A. L.; Simenel, I. A. Study of cryostructuration of polymer systems. XI. The formation of PVA cryogels by freezing–thawing the polymer aqueous solutions containing additives of some polyols, *J. Appl. Polym. Sci.* 1995, 58, 171–177.
40. Peppas, N. A.; Stauffer, S. R. Reinforced uncrosslinked poly (vinyl alcohol) gels produced by cyclic freezing-thawing processes: a short review, *J. Controlled Release* 1991,16, 305–3101.
41. Lozinsky, V. I.; Plieva, F. M. Poly(vinyl alcohol) cryogels employed as matrices for cell immobilization. 3. Overview of recent research and developments, *Enzyme Microb. Technol.* 1998, 23, 227–242.
42. An, Y.; Solis, F. J.; Jiang, H. A thermodynamic model of physical gels, *J. Mech. Phys. Solids* 2010, 58, 2083–2099.
43. Okay, O. *Polymeric Cryogels: Macroporous Gels with Remarkable Properties*. Springer, 2014.
44. Ross-Murphy, S. B.; Shatwell, K. P. Polysaccharide strong and weak gels, *Biorheology* 1993, 30, 217–227.
45. Stammen, J. A.; Williams, S.; Ku, D. N.; Guldberg, R. E. Mechanical properties of a novel PVA hydrogel in shear and unconfined compression, *Biomaterials* 2001, 22, 799–806.
46. Yang, X.; Liu, Q.; Chen, X.; Yu, F.; Zhu, Z. Investigation of PVA/ws-chitosan hydrogels prepared by combined γ-irradiation and freeze-thawing, *Carbohydr. Polym.* 2008, 73, 401–408.
47. Peppas, N. A.; Scott, J. E. Controlled release from poly(vinylalcohol) gels prepared by freezing-thawing processes, *J. Controlled Release* 1992, 18, 95–100.
48. Li, J. K.; Wang, N.; Wu, X. S. Poly(vinyl alcohol) nanoparticles prepared by freezing–thawing process for protein/peptide drug delivery, *J. Controlled Release* 1998, 56, 117–126.
49. Cha, W.-I.; Hyon, S.-H.; Ikada, Y. Microstructure of poly(vinyl alcohol) hydrogels investigated with differential scanning calorimetry, *Macromol. Chem. Phys.* 1993, 194, 2433–2441.
50. Ricciardi, R.; Auriemma, F.; Gaillet, C.; De Rosa, C.; Lauprêtre, F. Investigation of the Crystallinity of Freeze/Thaw Poly(vinyl alcohol)

Hydrogels by Different Techniques, *Macromolecules* 2004, 37, 9510–9516.
51. Kuo, S. M.; Chang, S. J.; Wang, Y. J. Properties of PVA-AA cross-linked HEMA-based hydrogels, *J. Polym. Res.*1999, 6, 191–196.
52. Peppas, N. A.; Merrill, E. W. Differential scanning calorimetry of crystallized PVA hydrogels, *J. Appl. Polym. Sci.*1976, 20, 1457–1465.
53. Willcox, P. J. *et al.*, Microstructure of poly(vinyl alcohol) hydrogels produced by freeze/thaw cycling, *J. Polym. Sci. Part B Polym. Phys.* 1999, 37, 3438–3454.
54. Ries, J.; Schwille, P. Fluorescence correlation spectroscopy, *BioEssays* 2012, 34, 361–368.
55. Koynov, K.; Butt, H.-J. Fluorescence correlation spectroscopy in colloid and interface science, *Curr. Opin. Colloid Interface Sci.* 2012, 17, 377–387.
56. Hacker, M. C.; Mikos, A. G. *Principles of Regenerative Medicine (Second edition)*; Academic Press, San Diego, 2011.
57. Frazer, R. Q.; Byron, R. T.; Osborne, P. B.; West, K. P. PMMA: an essential material in medicine and dentistry. *J. Long. Term Eff. Med. Implants* 2005, 15, 629–639.
58. Lloud, A.W.; Faragher, R.G.; Denyer, S.P. Ocular biomaterials and implants. *Biomaterials* 2001, 22, 769-785.
59. Naghash, H. J. Formation and structure of poly(methyl methacrylate) gels containing triphenyl vinyl silane. *J. Appl. Polym. Sci.* 2010, 116, 2465–2472.
60. Pajevic, S.; Bansil, R.; Konak, C. Diffusion of linear polymer chains in methyl methacrylate gels. *Macromolecules* 1993, 26, 305–312.
61. Pekcan, Ö.; Kaya, D.; Erdoğan, M. Fast transient fluorescence technique for monitoring swelling of poly(methyl methacrylate) gels. *Polymer* 2000, 41, 4915–4921.
62. Wichterle, O.; Lím, D. Hydrophilic Gels for Biological Use. *Nature* 1960, 185, 117-118.
63. Bhatia, S.; Bergethon, P.R.; Blease, S.; Kemper, T.; Rosiello, A.; Zimbardi, G.P.; Franzblau, C.; Spatz, E. L. A synthetic dural prosthesis constructed from hydroxyethylmethacrylate hydrogels. *J. Neurosurg.* 1995, 83, 897–902.
64. Young, C. D.; Wu, J. R.; Tsou, T. L. High-strenght, ultra-thin and fiber-reinforced pHEMA artificial skin. *Biomaterials* 1998, 19, 1745–1752.
65. Zellander, A.; Wardlow, M.; Djalilian, A.; Zhao, C.; Abiade, J.; Chi, M. Engineering copolymeric artificial cornea with salt porogen. *J. Biomed. Mater. Res. A* 2014, 102, 1799–1808.
66. Opdahl, A.; Kim S.H.; Koffas, T.S.; Marmo, C.; Somorjai G.A. Surface mechanical properties of pHEMA contact lenses: viscoelastic and adhesive property changes on exposure to controlled humidity. *J. Biomed. Mater. Res. A* 2003, 67, 350–356.

67. Meakin, J. R.; Hukins, D. W. L.; Aspden, R. M.; Imrie, C. T. Rheological properties of poly(2-hydroxyethyl methacrylate) (pHEMA) as a function of water content and deformation frequency *J. Mater. Sci. Mater. Med.* 2003, 14, 783–787.
68. Okay, O. Macroporous copolymer networks. *Prog. Polym. Sci.* 2000, 25, 711–779.
69. Gouda, J. H.; Povodator, K.; Warren, T. C.; Prins, W. Evidence for a micro-mesomorphic structure in poly (2-hydroxyethyl methacrylate) hydrogels. *J. Polym. Sci. B* 1970, 8, 225–229.
70. Lou, X.; Munro, S.; Wang, S. Drug release characteristics of phase separation pHEMA sponge materials. *Biomaterials* 2004, 25, 5071–5080.
71. Domingues, J.; Bonelli, N.; Giorgi, R.; Fratini, E.; Gorel, F.; Baglioni P. Innovative hydrogels based on semi-interpenetrating p(HEMA)/PVP networks for the cleaning of water-sensitive cultural heritage artifacts. *Langmuir* 2013, 29, 2746–2755.
72. Mazzuca, C.; Poggi, G.; Bonelli, N.; Micheli, L.; Baglioni, P.; Palleschi, A. Innovative chemical gels meet enzymes: a smart combination for cleaning paper artworks. *J. Colloid Interface Sci.* 2017**,** 502, 153–164.
73. Baglioni, P.; Chelazzi, D.; Carretti, E. Nanomaterials in art conservation, *Nature Nanotechnology*, 2015, 10, 287-290
74. Domingues, J.; Bonelli, N.; Giorgi, R.; Baglioni, P. Chemical semi-IPN hydrogels for the removal of adhesives from canvas paintings. *Appl. Phys. A* 2014, 114, 705–710.

Paper II

Daria Noferini, Antonio Faraone, Marta Rossi, Eugene Mamontov, Emiliano Fratini, and Piero Baglioni.

Reprinted with permission from The Journal of Physical Chemistry C, 2019, 123, pp 19183-19194,

List of papers

THE JOURNAL OF PHYSICAL CHEMISTRY C

Article

Cite This: J. Phys. Chem. C 2019, 123, 19183−19194

pubs.acs.org/JPCC

Disentangling Polymer Network and Hydration Water Dynamics in Polyhydroxyethyl Methacrylate Physical and Chemical Hydrogels

Daria Noferini,[§,▽] Antonio Faraone,[‡] Marta Rossi,[§] Eugene Mamontov,[⊥] Emiliano Fratini,[*,§] and Piero Baglioni[§]

[§]Department of Chemistry "Ugo Schiff" and CSGI, University of Florence, Via della Lastruccia 3, 50019 Sesto Fiorentino, Florence, Italy

[‡]NIST Center for Neutron Research, National Institute of Standards and Technology, Gaithersburg, Maryland 20899-6100, United States

[⊥]Neutron Scattering Division, Oak Ridge National Laboratory, Oak Ridge, Tennessee 37831, United States

Supporting Information

ABSTRACT: The cross-linker nature and water content may impact the microscopic dynamics of hydrogels components and thus their properties in applications such as drug delivery and water confinement. To investigate these aspects, we used quasi-elastic neutron scattering with contrast variation to distinctly study the polymer and water dynamics in polyhydroxyethyl methacrylate (pHEMA) chemical (*cg*) and physical (*pg*) hydrogels with various water contents. For the polymer network, a distribution of relaxation processes was observed, mainly related to the side chains. Water dynamics was found to occur as a H-bond governed process with a jump-diffusion mechanism. The interaction with the polymer matrix considerably slows the water dynamics with respect to bulk water and other confined systems and leads to a fraction of water molecules appearing as immobile. With a higher hydration level, the mobility of both the water and the polymer network increases. For the same water content, *pg* presents slower relaxation processes and a smaller explored space than their *cg* equivalents as a result of side chains involvement in the formation of the three-dimensional network typical of hydrogels. In the less hydrated gels, water mobility is sensibly reduced in the *cg* compared with *pg*, whereas at higher hydration the mobilities are similar but with shorter residence times in *cg*.

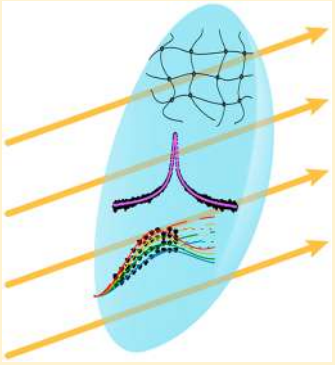

INTRODUCTION

Hydrogels are mainly cross-linked polymeric three-dimensional (3D) networks where a continuous water phase is "confined".[1] They can be classified as physical or chemical depending on the nature of the cross-linker. In the first case, the polymeric chains are held together by physical interactions such as hydrophobic forces, hydrogen bonds, electrostatic interactions, and entanglements, whereas if the chains are connected by real chemical bonds the hydrogel is a continuous polymeric network falling in the second class by definition. 2-Hydroxyethyl methacrylate (HEMA) based chemical hydrogels are one of the very first examples of synthetic hydrogels. They were developed in the 1960s by O. Wichterle and D. Lim.[2,3] Since their synthesis, they have been extensively employed in many biomedical fields (orthopedics, surgery, burned skin treatments, artificial tissues, contact lenses, etc.),[3−9] due to their excellent biocompatibility, permeability, and tunable mechanical properties. At equilibrium, they reach a water content (EWC) of about 40% w/w. The attention to these systems, even in the presence of comonomers, has been particularly focused onto soft contact lenses and drug delivery applications, mainly for transdermal and ophthalmic delivery.[10−14] Very recently, various hydrogels and, in particular, polyhydroxyethyl methacrylate (pHEMA) semi-interpenetrated with linear polyvinylpyrrolidone (PVP) have also been used in exotic applications such as cultural heritage conservation of water sensitive artifacts,[15−18] due to the possibility to load water-based nanofluids (i.e., micellar systems and microemulsions) and tune the transport properties of the continuous aqueous phase by simply changing the HEMA/PVP ratio.[19,20] Intimate knowledge of the transport properties in these materials is of fundamental importance when the final application needs to be optimized,[14] and a better understanding of the dynamics at the molecular scale has often been proven beneficial.[21−25]

To this aim, quasi-elastic neutron scattering (QENS) represents a very powerful technique to study the dynamics of hydrogenated systems thanks to the peculiarities of neutrons as a probe such as the high incoherent cross section for hydrogen and the time window associated with the exchanged energy.[26] QENS was successfully exploited for the investigation of the dynamic behavior of hydrogel components at the molecular level and in the nano-/picosecond time scale in similar systems.[27−30] Very interestingly, in the case of a

Received: May 3, 2019
Revised: June 21, 2019
Published: July 8, 2019

DOI: 10.1021/acs.jpcc.9b04212
J. Phys. Chem. C 2019, 123, 19183−19194

thermoresponsive hydrogel (i.e., poly(vinyl alcohol)/poly(methacrylate-*co*-*N*-isopropylacrylamide) network), a distinctive change in the values of the diffusion coefficient of bound water was observed at the transition temperature as a consequence of the structural collapse induced by temperature,[31] as well as at a lower temperature, around 250 K, in connection with a dynamical transition of the polymer.[32]

In this paper, we present a systematic study on pHEMA hydrogels, both chemical and physical, with different weight fractions of water (hereafter indicated as w/w). The proposed systems, even if rather simple, allow us to investigate the effect of the water content and the nature of the cross-linker on the final transport properties of the hydrogel. QENS and thermal analysis were used to depict the confining effect of the polymer network on the water molecules in fully hydrogenated systems, while gels loaded with deuterated water were used to study the dynamics of the 3D polymeric network.

MATERIALS AND METHODS

Preparation of the Hydrogels. Water was purified by using a MilliRO-6 Milli-Q gradient system (Milli-pore, resistance >18 MΩ cm). Deuterium oxide (D_2O, 99.90% D) was purchased from Eurisotop, France, and all the other reagents were purchased from Sigma-Aldrich, Milan, Italy, and used as received.

Physical gels (***pg***) with 10% to 41% w/w hydration levels were prepared by adding the corresponding amount of H_2O (or D_2O) to poly(2-hydroxyethyl methacrylate) with an average molecular weight of 20000 Da (CAS: 529265). The so-obtained dispersions were centrifuged at 500 r.p.m. until a homogeneous transparent gel was obtained.

Chemical gels (***cg***) with an equilibrium water content of 40% w/w were prepared through radical copolymerization of HEMA monomer, 2-hydroxyethyl methacrylate (CAS: 128635, assay ≥97%), and EGDMA cross-linker, ethylene glycol dimethacrylate (CAS: 335681, assay ≥98%), which was added as 2% w/w with respect to the monomer. The obtained product, water (or D_2O), and the radical initiator ammonium persulfate (APS), (purity >98%) added as 2.5 mg per each gram of HEMA, were mixed under a flux of N_2 for about 10 min to remove O_2. To promote the homolysis of APS, 80 μL of TEMED, *N*,*N*,*N*′,*N*′-tetramethylethylene-diamine (purity ≥99%), were added as a catalyst. The polymerization was thermally initiated at 40 °C in a 0.25−0.5 mm thin flat demountable and gastight container, to obtain gels already shaped for the neutron scattering experiment. The matrix was polymerized for at least 4 h. So-obtained gels were washed five times with water (or D_2O) to remove unreacted reagents (and totally exchange the labile H with D). Finally, 10%, 20%, and 30% w/w hydration levels were reached by dehydrating the 40% w/w gel in a controlled humidity chamber with a relative humidity of about 50% (i.e., $MgNO_3$ saturated solution).

The pHEMA/H_2O samples are hereafter indicated as ***pg*** for physical gels and ***cg*** for chemical gels, followed by the hydration percentage (e.g., ***pg20*** for physical gel with 20% w/w hydration level). Samples hydrated with heavy water, pHEMA/D_2O systems, are marked by adding the suffix ***_D*** (e.g., ***pg20_D*** for a physical gel hydrated at 20% w/w with D_2O).

Thermal Analysis Experiments. Differential scanning calorimetry (DSC) measurements were carried out with a Q2000 calorimeter (TA Instruments) at a constant nitrogen flow rate of 50 mL/min on about 10−20 mg of hydrogel. Samples were loaded in a closed aluminum pan, and an empty pan was used as a reference. The thermograms were recorded with the following cycle: equilibrate at 278 K, ramp 0.50 K/min to 193 K, ramp 0.50 K/min to 350 K.

Thermogravimetric analysis (TGA) measurements were performed by SDT Q600 (TA Instruments) in a N_2 atmosphere with a purge flow rate of 100 mL/min. The balance sensitivity is 0.1 μg with respect to the weight change in the sample. The samples (10−15 mg) were placed in open aluminum pans and dehydrated by heating 10 K/min from room temperature up to 523 K.

Quasi-Elastic Neutron Scattering Experiments. QENS spectra were acquired for ***cg20***, ***cg30***, ***pg20***, and ***pg30***, and for ***cg20_D***, ***cg30_D***, ***pg20_D***, and ***pg30_D*** with the high-resolution near-backscattering crystal-analyzer spectrometer BASIS at the Spallation Neutron Source (SNS) of the Oak Ridge National Laboratory (ORNL) in Tennessee, USA. The energy of the neutrons scattered by a sample, Bragg-selected by Si(111) crystal analyzers at 88° scattering angle, is 2.082 meV, giving an accessible scattering vector *Q* range of about 0.25−2 $Å^{-1}$.[33] The maximum accessible neutron energy transfer window was ±0.1 meV.

The samples were arranged as to take an annular shape with a thickness of ∼0.25 mm, to obtain a transmission of about 90%. Data were collected at 10 K (or 20 K), 270 K, 280 K, 290 K, and 300 K. The temperature was controlled within ±0.5 K by a closed cycle refrigerator. Because of the available beam-time constraint, ***cg20*** and ***cg20_D*** were measured only at 270 and 300 K. The low-temperature measurements (10 or 20 K) were used to determine the instrumental resolution function. This approach is well justified as the recorded signal is dominated by incoherent scattering from hydrogen atoms, and nonvibrational dynamics measurable at BASIS are frozen out at such low temperatures. An average full width at half-maximum (FWHM) of (4.0 ± 0.5) μeV was derived, in agreement with the specifications of the BASIS[33] spectrometer for the used experimental setup. Raw data were reduced to a dynamic structure factor $S(Q, E)$ using software available at SNS. For each sample, 16 spectra in a Q range from 0.35 $Å^{-1}$ to 1.85 $Å^{-1}$ (step = 0.1 $Å^{-1}$) were obtained and analyzed.

The difference in the hydrogen and deuterium incoherent cross sections[34] allows us to isolate the dynamics of the polymer network in the hydrogel by replacing the hydration water with D_2O. The incoherent contribution of the heavy water is negligible, being about 1.2% (20% w/w hydrated samples) and 1.8% (30% w/w hydrated samples) with respect to the total signal. Furthermore, the signal from the hydration water, $S_w(Q, E)$, was obtained by subtracting the spectra of the pHEMA/D_2O hydrogel out of the correspondent pHEMA/H_2O spectra, using standard routines provided at SNS as part of the raw data reduction package. The so-obtained data are labeled with the suffix ***_w*** (e.g., ***pg20_w*** for the signal obtained by subtracting the spectra obtained for ***pg20_D*** from those obtained for ***pg20***). The fitting procedures were carried out with routines and χ^2 minimization algorithms of the software DAVE,[35] Matlab, and IgorPro.

POLYMER NETWORK

QENS Data Analysis. To derive a model for the description of the $S(Q, E)$, considerations on the composition and structure of the polymer were taken into account. Figure 1 shows the HEMA monomer chemical formula. For the pHEMA/D_2O systems, only nine H atoms have to be considered after the H−D exchange: three from the methyl

DOI: 10.1021/acs.jpcc.9b04212
J. Phys. Chem. C 2019, 123, 19183−19194

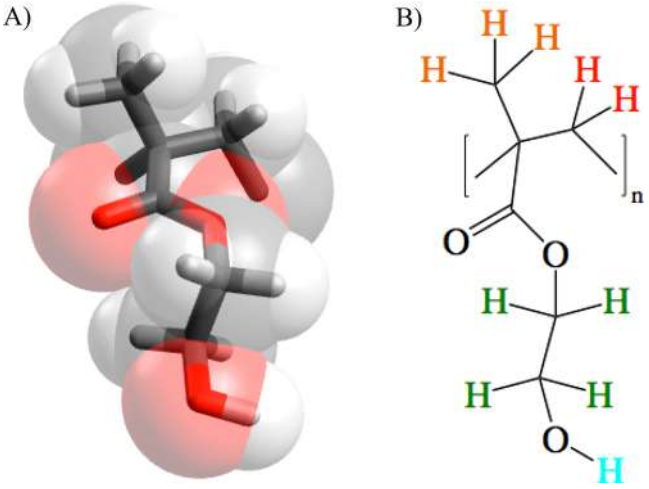

Figure 1. Structure of the main repetition unit present in both physical and chemical pHEMA hydrogels. (A) Stick/space-filling mixed model with standard color-codes for elements (C = gray, O = red and H = white). (B) Structural formula. The different colors for H indicate the different parts in which the monomer unit has been ideally divided: orange for the methyl group, red for the backbone, green for the side chain and light blue for the hydroxyl group.

moiety (in orange), two from the ethylene groups present in the backbone (in red), and four from the ethylene group constituting the side chain (in green) attached to the backbone; the hydrogen on the hydroxyl group (in light blue) is totally exchanged with deuterium and washed away during sample preparation. Moreover, in the case of the chemical gels, the cross-linker contribution has been neglected since it accounts only for 2% w/w with respect to the HEMA monomer constituting a small contribution to the backbone dynamics.

We define $S_B(Q, E)$ as the dynamic structure factor of the backbone hydrogen atoms. The dynamic structure factors of the methyl group and the side chain, with respect to the backbone, are indicated as $S_M(Q, E)$ and $S_{SC}(Q, E)$, respectively. The methyl group and the side chain move together with the backbone; hence, to describe the dynamics of their H atoms, $S_M(Q, E)$ and $S_{SC}(Q, E)$ have to be convoluted with $S_B(Q, E)$. Within these approximations, the following expression can be used to analyze the data:

$$S(Q, E) = A'(Q)\left\{S_B(Q, E) \otimes \left[\frac{2}{9}\delta(E) + \frac{1}{3}S_M(Q, E) + \frac{4}{9}S_{SC}(Q, E)\right]\right\} \otimes \mathrm{Res}(Q, E) + \mathrm{bkg}(Q, E) \quad (1)$$

where $A'(Q)$ is a normalization constant, $\otimes$ indicates the convolution product, $\mathrm{Res}(Q, E)$ is the experimental resolution function, and $\mathrm{bkg}(Q, E)$ is a linear background which takes into account dynamical processes too fast to fall within the instrumental window and instrumental noise.

A segmental backbone dynamics characterized by a relaxation distribution and a Q dependence from Q^2 and Q^4 was identified in previous studies, for example, on poly(vinyl methyl ether) solutions.[28] The presence of a delta function in all our fits, in agreement with many studies on the polymer network dynamics in various hydrogels,[27,29,31,36−38] points toward the assumption that the long-range backbone dynamics is too slow to be resolved with our experimental setup. However, some localized dynamics might be still appreciable in the probed length and time window. For this reason, assuming localized motions, the backbone dynamics can be modeled as

$$S_B(Q, E) = \mathrm{EISF}_B(Q)\delta(E) + (1 - \mathrm{EISF}_B(Q))Y_B(Q, E) \quad (2)$$

$\mathrm{EISF}_B(Q)$ and $Y_B(Q, E)$ provide information on the explored volume of the dynamics and its time scale, respectively. Assuming that the backbone explores uniformly a region of space with dimension R_B, its elastic incoherent structure factor $\mathrm{EISF}_B(Q)$ can be modeled as

$$\mathrm{EISF}_B(Q) = \exp\left(-\frac{1}{3}Q^2R_B^2\right) \quad (3)$$

where R_B is assumed to be small on the order of 1 Å. The functional form of $Y_B(Q, E)$ will be discussed in the following.

Under the assumption that the methyl carbon atom is rigidly attached to the backbone (i.e., no dynamics), the motion of the hydrogen atoms of the methyl can be modeled simply as a 3-fold rotation:

$$S_M(Q, E) = \mathrm{EISF}_M(Q)\delta(E) + [1 - \mathrm{EISF}_M(Q)]L_M(E) \quad (4)$$

with the elastic incoherent structure factor proper of the methyl group rotation, $\mathrm{EISF}_M(Q)$, taking the form:

$$\mathrm{EISF}_M(Q) = \frac{1}{3}[1 + 2j_0(\sqrt{3}QR_M)] \quad (5)$$

where j_0 is the first-order spherical Bessel function and R_M is the radius of the methyl group (i.e., about 1 Å).[34,39] At the measurement temperatures we used, the half-width at half-maximum (HWHM) of the Lorentzian function L_M is expected to be around 1 meV,[34,39] which is much broader than our experimental energy window, suggesting no contributions to the observed QENS signal. Even considering a distribution of jumping rates for the methyl rotation in polymers,[40] the contribution to the observed signal in the current dynamical window at the measured temperatures is expected to be marginal.

The motions of the side chain with respect to the backbone can be considered as localized, with no long-range diffusion. An acceptable approximation is therefore

$$S_{SC}(Q, E) = \mathrm{EISF}_{SC}(Q)\delta(E) + [1 - \mathrm{EISF}_{SC}(Q)]Y_{SC}(Q, E) \quad (6)$$

The elastic incoherent structure factor $\mathrm{EISF}_{SC}(Q)$ can also be modeled as

$$\mathrm{EISF}_{SC}(Q) = \exp\left(-\frac{1}{3}Q^2R_{SC}^2\right) \quad (7)$$

where R_{SC} is expected to be about 5 Å, from a rough estimation of the bond distances. Therefore, its contribution is mostly limited at low Q. The quality of the data does not warrant the use of a more detailed approach.

The functional form of $Y_B(Q, E)$ and $Y_{SC}(Q, E)$ needs to be determined. For a simple, i.e., exponential, relaxational process it would be a Lorentzian; for more complex processes and, as often is the case with polymers, when there is a distribution of relaxation times, the Fourier transform of a stretched exponential is a suitable model.

DOI: 10.1021/acs.jpcc.9b04212
J. Phys. Chem. C 2019, 123, 19183−19194

With the above-mentioned considerations, the expression for the observed $S(Q, E)$ is

$$S(Q,E) = A'(Q)\left\{\left[\frac{2}{9}\mathrm{EISF_B}(Q) + \frac{1}{3}\mathrm{EISF_B}(Q)\mathrm{EISF_M}(Q) + \frac{4}{9}\mathrm{EISF_B}(Q)\mathrm{EISF_{SC}}(Q)\right]\delta(E) + [1 - \mathrm{EISF_B}(Q)]\left[\frac{2}{9} + \frac{1}{3}\mathrm{EISF_M}(Q) + \frac{4}{9}\mathrm{EISF_{SC}}(Q)\right]Y_B(Q,E) + \frac{1}{3}[1 - \mathrm{EISF_M}(Q)][\mathrm{EISF_B}(Q)L_M(Q,E) + [1 - \mathrm{EISF_B}(Q)]Y_B(Q,E) \otimes L_M(Q,E)] + \frac{4}{9}[1 - \mathrm{EISF_{SC}}(Q)][\mathrm{EISF_B}(Q)Y_{SC}(Q,E) + [1 - \mathrm{EISF_B}(Q)]Y_B(Q,E) \otimes Y_{SC}(Q,E)]\right\} \otimes \mathrm{Res}(Q,E) + \mathrm{bkg}(Q,E) \quad (8)$$

The dynamics of the methyl group is much faster than the backbone motion, and therefore we can approximate $Y_B(Q, E) \otimes L_M(Q, E) \approx L_M(Q, E)$. Under the above introduced assumption that the methyl group dynamics is much faster than the investigated time scale, the above equation can be simplified:

$$S(Q,E) = A'(Q)\left\{\left[\frac{2}{9}\mathrm{EISF_B}(Q) + \frac{1}{3}\mathrm{EISF_B}(Q)\mathrm{EISF_M}(Q) + \frac{4}{9}\mathrm{EISF_B}(Q)\mathrm{EISF_{SC}}(Q)\right]\delta(E) + [1 - \mathrm{EISF_B}(Q)]\left[\frac{2}{9} + \frac{1}{3}\mathrm{EISF_M}(Q) + \frac{4}{9}\mathrm{EISF_{SC}}(Q)\right]Y_B(Q,E) + \frac{4}{9}[1 - \mathrm{EISF_{SC}}(Q)][\mathrm{EISF_B}(Q)Y_{SC}(Q,E) + [1 - \mathrm{EISF_B}(Q)]Y_B(Q,E) \otimes Y_{SC}(Q,E)]\right\} \otimes \mathrm{Res}(Q,E) + \mathrm{bkg}'(Q,E) \quad (9)$$

The backbone and side chain dynamics are expected to have similar time scales so that the experimental separation of $Y_B(Q, E)$, $Y_{SC}(Q, E)$, and $Y_B(Q, E) \otimes Y_{SC}(Q, E)$ is beyond current experimental capabilities, especially because each of these functions is already likely representing a distribution of relaxation times, and the instrumental resolution function further smears the signal. Therefore, the data have been analyzed in terms of the simplified scattering law:

$$S(Q,E) = [A_{EL}(Q)\delta(E) + A_{QE}(Q)Y_{polymer}(Q,E)] \otimes \mathrm{Res}(Q,E) + \mathrm{bkg}(Q,E) \quad (10)$$

The analysis of $Y_{polymer}(Q, E)$ yields insights into the time scale of the polymer motions, whereas the a posteriori analysis of the EISF(Q):

$$\mathrm{EISF}(Q) = \frac{A_{EL}(Q)}{A_{EL}(Q) + A_{QE}(Q)} \quad (11)$$

will provide information on the dynamics of the different hydrogen groups in the polymer.

Results and Discussion. As anticipated, the functional form of $Y_{polymer}$ was determined during the fitting procedure as the Fourier transform (FT) of a stretched exponential (or Kohlrausch–Williams–Watts, KWW, function):

$$\mathrm{FT\_KWW} = \mathrm{FT}\left[\exp\left(-\frac{t}{\tau'}\right)^{\beta}\right] \quad (12)$$

where τ' is the relaxation time and β is the stretching exponent, which can take values between 0 and 1. In polymer dynamics, the exponent is usually on the order of 0.5.[28] This functional form can be the result of a distribution of relaxation processes in the system. It is well established that polymer networks in general can be characterized by heterogeneous environments at the molecular scale, which give rise to nonexponential relaxation functions.[41] In this respect, β indicates the extent of the heterogeneity. For all the samples, β was found to be almost Q independent. Figure 2a shows the Q dependence of β in ***pg30_D*** at 280 K, taken as an example. To reduce the number of free parameters in the fitting routines, final fits were thus carried out fixing β on the calculated average for each sample and temperatures. The averaged stretching exponents $\langle\beta\rangle_Q$, Figure 2b, are in the range from 0.45 to 0.56 and do not vary significantly among different temperatures and samples. In Figure 3, we report the dynamic structure factors of the hydrogels loaded with D_2O at 300 K and Q = 0.95 A^{-1} and their fits. The good agreement between fits and experimental data supports the approximation of the use of $\langle\beta\rangle_Q$.

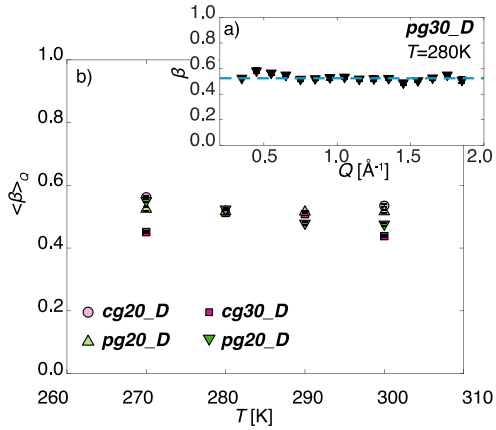

Figure 2. (a) Example of the stretching exponent as a function of Q. The dashed blue line represents the average value. In (b), the stretching exponent averaged in the whole Q range for the different samples and temperatures is reported.

The average relaxation time,[42] $\overline{\tau'}$, can be derived as

$$\overline{\tau'} = \frac{\tau'}{\beta}\Gamma\left(\frac{1}{\beta}\right) \quad (13)$$

where Γ is the Gamma function. The obtained values (comprised between 0.073 and 0.312 ns) do not show a significant trend with Q, validating the assumption that the dynamics of the side chain is localized. In the following, their Q-averaged values $\langle\overline{\tau'}\rangle_Q$ are discussed. Increasing the temperature, $\langle\overline{\tau'}\rangle_Q$ generally decreases, showing that the relaxation dynamics is activated by thermal fluctuations. Moreover, ***pg*** samples present slower relaxation processes than their ***cg*** equivalents, of about 40% (***pg20***) or 10% (***pg30***)

DOI: 10.1021/acs.jpcc.9b04212
J. Phys. Chem. C 2019, 123, 19183−19194

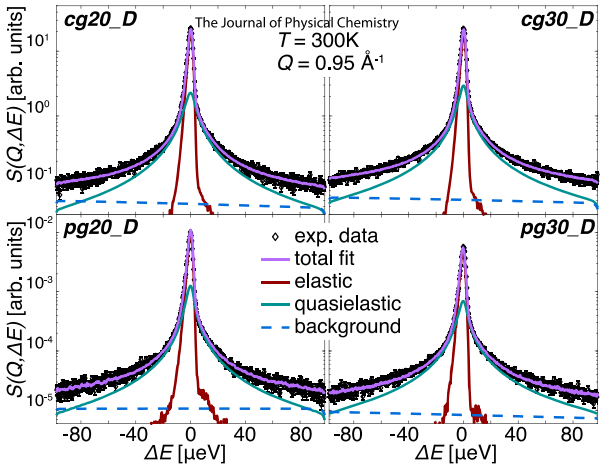

Figure 3. Dynamic structure factor for the pHEMA/D_2O samples at 300 K and $Q = 0.95$ Å^{-1} and relative fit. The different components of the fit, i.e., elastic (delta function convoluted for the experimental resolution), quasi-elastic (FT_KWW convoluted with instrumental resolution), and background, are shown for completeness. Throughout the paper, error bars represent one standard deviation.

on average, depending on T. This reduced mobility of the side chain for the physical hydrogels of pHEMA is a clear evidence of the hydroxyl group involvement in the network formation. Figure 4 shows the Arrhenius plots of the relaxation times.

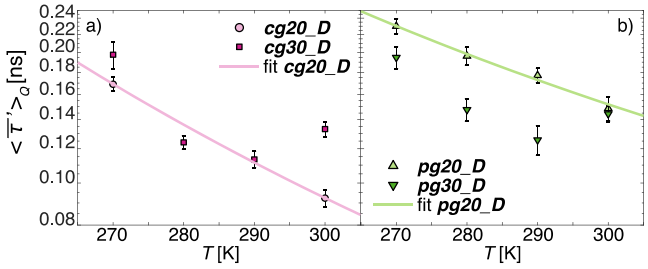

Figure 4. Arrhenius plots for pHEMA (a) ***cg*** and (b) ***pg***. Dashed lines show the fits for the low hydrated samples. With only two temperatures, the Arrhenius behavior for ***cg20_D*** is assumed and expected in analogy with ***pg20_D***.

Although the probed temperature range is quite limited, it seems that hydrogels with 20% w/w of water content follow an Arrhenius law much better than 30% w/w samples. Such a difference with hydration could be due to the plasticizer role of the solvent, which allows a higher mobility and thus several local minima in the energy landscape.[43,44] In the scheme proposed by Angell,[45] this would correspond to a more fragile behavior. As a matter of fact, considering the composition of the samples, we expect to have about one water molecule per −OH group (side chain) in the 10% w/w sample, two in the case of the 20% w/w, four in the 30% w/w hydrogels, and six when the water content is 40% w/w. Going from two water molecules per hydroxyl group to four changes the response to the temperature from Arrhenius to super-Arrhenius and the hydrogel from strong to fragile-like. For ***pg20_D***, an activation energy of −0.10(2) eV (or −10(2) kJ/mol) was found. Assuming an Arrhenius behavior for ***cg20_D***, a similar, slightly higher, value is obtained (−0.14 eV).

The analysis of the EISF(Q), Figure 5, can provide insights into the geometry of the motion of the different hydrogen

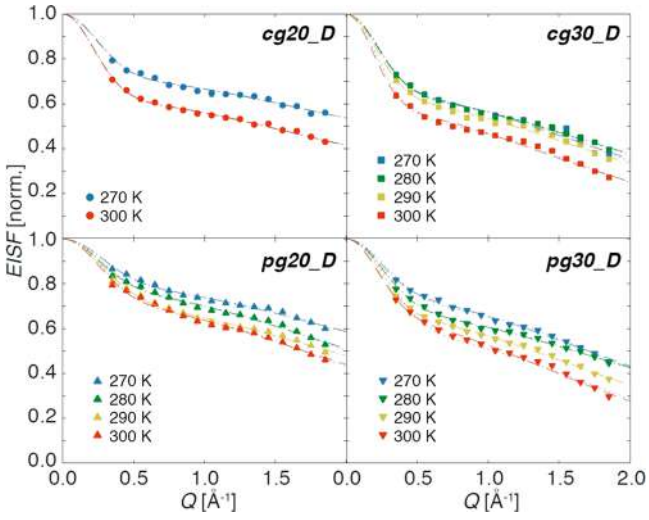

Figure 5. Elastic incoherent structure factor EISF(Q). Lines are fit according to eq 14 (dashed lines) and eq 15 (dotted lines), with the color code referring to the different temperatures, as in the legend.

groups in the polymer. It can be noted that the profile is fairly similar for all the samples and temperatures, suggesting that the same dynamical processes are observed. The decay is slightly more pronounced at increasing the temperature and hydration, evidencing an increased mobility. In deriving an expression for the EISF, it is assumed that the methyl group dynamics is fast, so that it contributes to the background only, therefore being counted out of the total spectral area. Support for this idea comes from the analysis of the normalized total integrated intensities, calculated as the ratio between the sum of the integrated intensity of the delta function and the FT_KWW function ($A_{EL} + A_{QE} = A_{tot}$) and the integrated intensity of the measurements below 50 K (A_{res}). Its Q-dependence shows that the mean squared displacements obtained by considering simply a Debye−Waller factor, in the range from 0.16 Å^2 to 0.4 Å^2, are much higher than those expected for pure atomic vibrations[46] (about 0.01 Å^2), suggesting that the background indeed comprises also other kinds of fast motions. The EISF fits were carried out in accordance with two different hypotheses: (i) the backbone dynamics is too slow and constrained to be appreciated, $S_B(Q, E) \approx \delta(E)$, $R_B \approx 0$; (ii) the backbone explores a region of space of radius R_B. The dashed lines in Figure 5 are fits using an expression derived from eq 9 under the first scenario:

$$\mathrm{EISF}(Q) = \frac{A + B(1-A)\mathrm{EISF}_M(Q) + (1-A)(1-B)\mathrm{EISF}_{SC}(Q)}{A + B(1-A)\mathrm{EISF}_M(Q) + (1-A)(1-B)} \quad (14)$$

where $\mathrm{EISF}_M(Q)$ and $\mathrm{EISF}_{SC}(Q)$ are the contributions of methyl groups and side chains to the total EISF(Q), as defined in eq 5 and eq 7, respectively.

Conversely, the fits represented by the dotted lines are in accordance with the second scenario and thus to the equation:

$$\begin{aligned}\mathrm{EISF}(Q) = {} & [A\ \mathrm{EISF}_B(Q) + B(1-A)\mathrm{EISF}_B(Q)\mathrm{EISF}_M(Q) \\ & + (1-A)(1-B)\mathrm{EISF}_B(Q)\mathrm{EISF}_{SC}(Q)] \\ & /[A + B(1-A)\mathrm{EISF}_B(Q)\mathrm{EISF}_M(Q) \\ & + (1-A)(1-B)] \end{aligned} \quad (15)$$

DOI: 10.1021/acs.jpcc.9b04212
J. Phys. Chem. C 2019, 123, 19183−19194

For both eq 14 and eq 15 and according to stoichiometry of the polymer (see Figure 1), A and B are supposed to take the values of 2/9 and 3/7, respectively. However, in the fitting according to eq 14 A, B, R_{SC} were all free fitting parameters, whereas in the fitting according to eq 15 $B(1 - A)$ was fixed to 1/3, the fraction of hydrogen atoms in the methyl groups, to maintain the number of fitting parameters as three, i.e., A, R_B, and R_{SC}, manageable considering the experimental uncertainties.

Both models give similar results and well approximate the data. In this context, we note that a small contribution from the methyl rotation to the observed signal would be compatible with the EISF data in the accessible Q range. Fit parameters are reported in Figure S1 in the Supporting Information, SI. R_B values range from 0.36(2) Å to 0.72(2) Å, increasing with both water content and temperature. For the ***cg20_D*** sample, $R_B \approx$ 0.4 Å, for ***pg20_D*** $R_B \approx$ 0.5 Å, and for both ***cg30_D*** and ***pg30_D*** $R_B \approx$ 0.6 Å. These values are consistent with a strongly constrained dynamic. The radius of the region explored by the side chains, R_{SC}, takes physically reasonable values in the range of 4.4−5.8 Å (4.5−6.5 Å for eq 15), with uncertainties on the order of 2−10%. The values moderately increase with increasing temperature and are higher in ***cg*** with respect to ***pg***. Similar to the results obtained for the relaxation time, the involvement of the side chain in the network formation might be the reason for the reduced mobility in the physical gels compared with the cross-linked equivalents. The obtained weights of the different parts of the polymer are slightly different from the expected values. In the fits using eq 14, A is smaller than 2/9 and $B(1 - A)$ is larger than 1/3, which is indicative of some mobility of the backbone. On the other hand, the fact that A takes values larger than 2/9 for eq 15 indicates that some of the side chain hydrogens explore a region smaller than 1 Å. In summary, the data indicate that the hydrogens in the system explore the surrounding space with a distribution of accessible volumes. The model underlying eq 15 simplifies this picture considering only two possible sizes. However, the limited number of data points do not warrant the analysis in terms of a distribution of R_B and R_{SC}. Moreover, the analysis employed provides us with the relevant information on the size of the space explored by the backbone and side chain, at least as an average.

HYDRATION WATER

The analysis of the dynamic structure factor of the hydration water $S_w(Q, E)$, obtained as described in the Materials and Methods, was carried out for $Q < 1.4$ Å^{-1}, i.e., in the region where the contribution from the center of mass dynamics is the major component of the scattering, thus allowing the rotational motions to be ignored.[47] Referring to the Sears expansion,[48] the translational dynamics of water dominates the spectra up to ∼1 Å^{-1}. However, simulation results[49] indicate that, because of translational-rotational coupling,[50] the translational intermediate scattering function (ISF) approximates the ISF of the hydrogen atoms. Furthermore, within this Q range and in the probed time scale, the short-time vibrational motion of the water molecules can be considered as equal to 1.[42,49] It is therefore justified to consider the scattering function as approximated by its translational part only.

During a first, model-free analysis, we tried to assess the best functional form for the fit of the $S_w(Q, E)$. Very good agreement with the data was reached already using a simple combination of a delta function, $\delta_w(E)$, a Lorentzian function, $L_w(Q, E)$, and a linear background, $bkg_w(Q, E)$:

$$S_w(Q, E) = C(Q)\{\delta_w(E)\mathrm{EISF}_w(Q) + L_w(Q, E)(1 - \mathrm{EISF}_w(Q))\} \otimes \mathrm{Res}_w(Q, E) + \mathrm{bkg}_w(Q, E) \quad (16)$$

where $\mathrm{Res}_w(Q, E)$ is the experimental resolution function, $C(Q)$ is a normalization constant, and $\mathrm{EISF}_w(Q)$ is the elastic incoherent structure factor of the water. Such a model has been previously used, for example, for water confined in Vycor.[51]

This approach is also justified by DSC measurements (see Figures S2 and S3 in the Supporting Information, SI), which clearly evidence two fractions of water in pHEMA hydrogels with up to 40% w/w of water content according to their diverse response to freezing/melting cycles: one fraction is bound (i.e., interacting with the polar groups of the polymer), and thus it does not freeze and melt, and one is free (i.e., in a bulk-like state). In particular, DSC detects the amount of water that is still freezable in the sample, and, if combined with TGA determining the total amount of water in the hydrogel, the free water index, FWI, can be calculated as[52]

$$\mathrm{FWI} = \frac{\Delta H_{exp}}{W \Delta H_{th}} \quad (17)$$

where ΔH_{exp} is the enthalpy associated with the water melting determined by the peak integral in the DSC heating scan, W is the water weight fraction in the sample, and ΔH_{th} is the theoretical value of the melting enthalpy for pure water (333.55 J/g).[23] Results, summarized in Table 1, show a consistent fraction of water, BWI (i.e., bound water index), still not frozen at −80 °C in all samples.

From the DSC thermograms reported in Figures S2 and S3 in the Supporting Information, it is possible to observe that the freezing temperature of the water is higher for the most hydrated samples, in accordance with previous results by Lee et al.[22] For ***cg20***, transition peaks were observed neither in the

Table 1. Free Water and Bound Water Index Derived from Thermal Analysis for *pg* and *cg* Hydrogels with Water Content up to about 40% w/w[a]

	hydration, % (±0.1)	FWI (±0.01)	BWI (±0.01)	free water, % (±0.1)	bound water, % (±0.1)
pg11	11.5	0	1	0	11.5
pg18	18.4	0.03	0.97	0.6	17.8
pg20	20.4	0.06	0.94	1.2	19.2
pg25	24.9	0.37	0.63	9.2	15.7
pg27	26.6	0.41	0.59	10.9	15.7
pg28	28.0	0.42	0.58	11.8	16.2
pg41	41.3	0.48	0.52	19.8	21.5
cg6	5.7	0	1	0	5.7
cg11	11.1	0	1	0	11.1
cg19	18.8	0.01	0.99	0.2	18.6
cg25	24.9	0.07	0.93	1.79	23.1
cg27	27.4	0.05	0.95	1.4	26.0
cg33	33	0.34	0.66	11.2	21.8
cg40	40.2	0.40	0.60	16.2	24.0
cg43	42.8	0.40	0.60	17.1	25.7

[a]Bound and water content % are reported as well to show the distribution of the total water content in the two states.

DOI: 10.1021/acs.jpcc.9b04212
J. Phys. Chem. C 2019, 123, 19183−19194

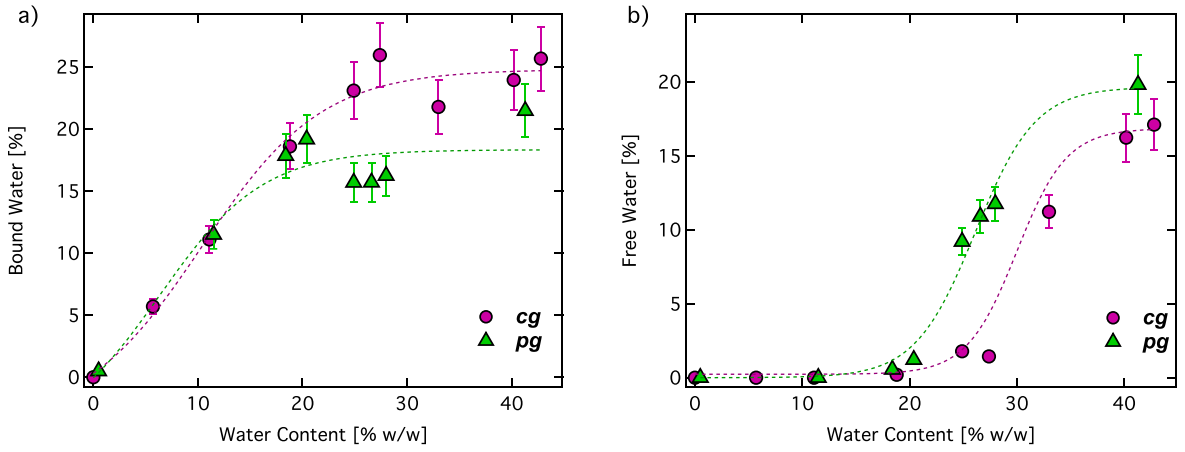

Figure 6. (a, b) Bound and free water in ***pg*** and ***cg*** pHEMA hydrogels. Dashed lines are only a guide for the eye.

cooling nor in the heating thermograms, in agreement with previous works on pHEMA hydrogels[22] and commercial contact lenses.[21] In the case of ***pg20***, a small amount of free water (<0.05) is still detectable.

Figure 6 shows the fractions of bound and free water with respect to the total water content for both ***pg*** and ***cg***, to better emphasize how the water is distributed in the two different states. Bound water fraction increases with the water content and gets to a plateau after 20% w/w (see Figure 6a) as a consequence of the limited binding capacity of the hydroxyl group that can strongly coordinate about two water molecules. The plateau value results are lower in the ***pg*** case, thus confirming that the hydroxyl groups are not completely available but also involved in the hydrogel network formation. When the two water molecules threshold is reached, additional water behaves like bulk water maintaining its ability to freeze; see Figure 6b.

Such findings are consistent with the presence of diverse fractions of water with different mobilities, either more similar to the bulk water or more associated with the polymer matrix, thus justifying the use of a delta plus a Lorentzian function in the fitting of the QENS data relative to the total hydration water signal. The addition of a second Lorentzian, following the approach of several studies on analogous systems,[27,31,36−38,53,54] could not be justified in our experimental window, as the broader component was mainly a background, as similarly reported for PVA hydrogels.[27] The use of a FT_KWW function was also considered, according to the study of Zanotti et al.[51] for water confined in Vycor glass. The agreement with the data slightly improved, but being yet comparable to the single Lorentzian model, the use of a higher degree of complexity was beyond the aims of the present paper. Indeed, the FT_KWW can easily superimpose with the elastic fraction and/or with the background, making it more difficult to distinguish among different populations with different dynamical behavior and to determine possible trends as a function of T, hydration, and type of gel.

A preliminary fit was also used to investigate a possible effect of the confinement imposed by the gel on the probed dynamics. For a mesh size of ca. 7 Å, or below, characteristic of these gels,[19] a signature of confined diffusion would be a Q-independent value of the HWHM of the Lorentzian function, $\Gamma/2(Q)$, up to ca. 1 Å^{-1}.[55,56] Conversely, we observed an increasing $\Gamma/2(Q)$, following roughly a Q^2 dependence up to 0.6−0.8 Å^{-1} and then plateauing at higher Q-values. We thus concluded that the elastic part of the spectra does not originate from a confinement effect, as for example in refs 51 and 57, but it is rather primarily related to the existence of a hydrogen atoms population whose dynamics is too slow to be appreciated within the experimental resolution. This population is related to the bound water fraction evidenced by DSC. The slight Q-dependence observed in $EISF_w(Q)$ is likely reminiscent of the water molecule rotation.[34] In order to reduce the number of free parameters during the fit, we thus fixed $EISF_w(Q)$ to its averaged value in Q for each sample and temperature, $\langle EISF_w \rangle_Q$. Figure 7 shows the fits of the $S_w(Q, E)$

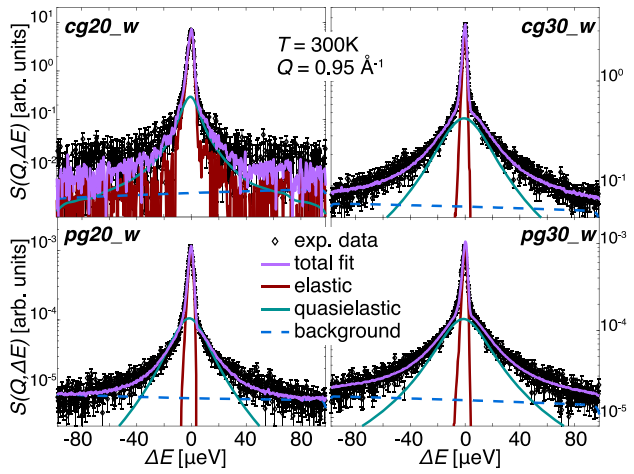

Figure 7. Dynamic structure factor of hydration water in pHEMA gels and relative fit according to eq 16. The different components of the fit, i.e., elastic (delta function convoluted for the experimental resolution), quasi-elastic (Lorentzian function convoluted with instrumental resolution), and background, are shown for completeness.

for the different hydrogels at 300 K and Q = 0.95 Å^{-1} taken as examples. It can be noted that the good agreement with the experimental data is maintained when introducing such an approximation.

The relative weight of the elastic part $\langle EISF_w \rangle_Q$ can be therefore regarded as the fraction of water that strongly interacts with the polymer network, motionless in our time scale, and $(1 - \langle EISF_w \rangle_Q)$ as the fraction of water that is free to diffuse. The observation of several populations with distinct dynamic behavior is quite common in liquids under confine-

DOI: 10.1021/acs.jpcc.9b04212
J. Phys. Chem. C 2019, 123, 19183−19194

ment, as evidenced by neutron scattering studies on other hydrogels[27,31,37,53] and studies conducted with ^{1}H NMR and DSC on pHEMA hydrogels.[23,58] Figure 8 shows <EISF$_w$>$_Q$ as a

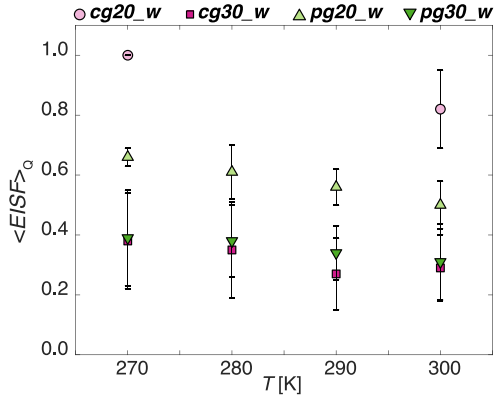

Figure 8. <EISF$_w$>$_Q$ as a function of T for the different investigated pHEMA hydrogels.

function of temperature. In all the samples, part of the immobile water fraction converts into mobile water as the temperature increases. Moreover, the relative amount of immobile water is higher in the less hydrated gels, in agreement to results obtained with other techniques as reported in literature[22,58] and to the DSC analysis of the present study (see Figure 6).

The results of Figure 8 indicate that in the 20% w/w chemical gel, the vast majority of the water molecules are tightly bound to the polymer chains at the investigated temperatures. At the same hydration, the physical gel is less effective in binding the water in agreement with DSC results. At higher water contents, i.e., 33% w/w, the ***cg*** and ***pg*** present almost the same distribution of immobile/mobile water.

The Q-dependence of $\Gamma/2$ are shown in Figure 9. A clear slowing down of the dynamics with respect to bulk water at the same temperature, induced by the confinement, can be identified, for example, by comparison with the work of Teixeira et al. on translational diffusion of bulk water.[59,60] Indeed, it was proposed that dynamics of the interfacial water, confined within nanocavities or on the surface of biological materials, resembles the dynamic behavior of bulk water at temperatures lower by 20 K.[61]

The typical shape of the jump-diffusion can be observed: a Q^2 profile at low Q-values and a leveling off toward a plateau at high Q's. In this respect, it should be also noted that the spectrum at the lowest Q-value in the ***pg20_w*** is extremely noisy, and the derived fit parameters are not reliable. In ***cg20_w***, a large part of the water is immobile at the time scale of the experiment. As a consequence, the visibility of the quasi-elastic broadening with respect to the elastic line is very reduced. Furthermore, QENS widths are found to be extremely narrow, at the edge or below the resolution limit of the instrument. At 270 K, almost exclusively elastic scattering is observed. Although with a prominent contribution from the elastic line, for the same sample at 300 K the mobile water fraction is increased and the dynamics is faster, and it is possible to recognize the jump-diffusion behavior.

Some general differences among the investigated systems can be noted. The less hydrated hydrogels show a narrower Lorentzian component, i.e., slower dynamics, for both ***cg*** and ***pg***. In the 30% w/w hydrated samples, the widths are overall slightly larger for ***cg30_w***. However, while at low temperatures the differences among the samples are quite constant in the entire Q range, at high temperatures the values are almost identical at low Q and become larger for increasing Q, as highlighted in Figure 10. Considering a jump-diffusion

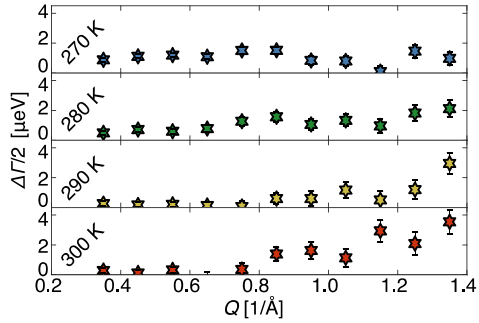

Figure 10. Difference of quasi-elastic widths between chemical and physical gels at 30% w/w of hydration. $\Delta\Gamma/2 = \Gamma/2_{cg30\_w} - \Gamma/2_{pg30\_w}$.

mechanism, this suggests shorter residence times, τ, for the chemical gel and different T-dependence of the residence time and jump length, l, within the two systems. As opposed to the higher hydrated samples, the widths of ***pg20_w*** are much larger than those of ***cg20_w***, both at low and high temperatures.

In Figure 9, the lines are fits according to the well-established jump-diffusion models of Singwi and Sjölander[62] (SSM), Hall and Ross[63] (HRM), and Chudley and Elliot[64] (CEM), which are all parametrized in terms of τ and l.

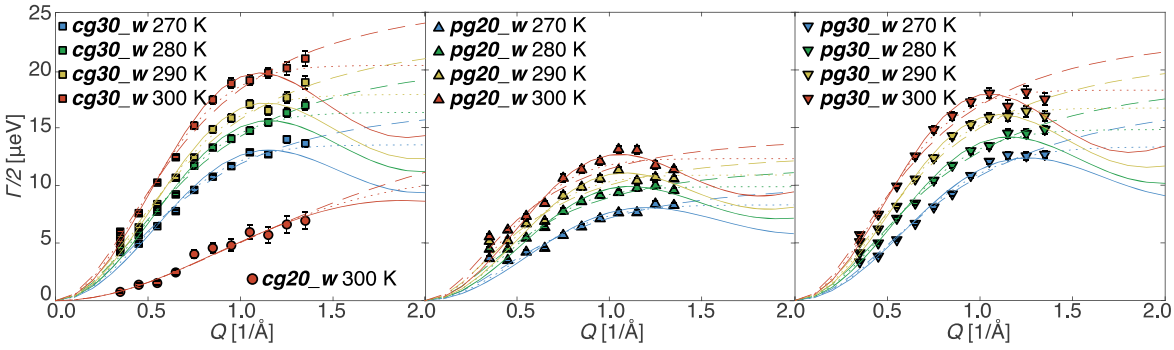

Figure 9. Q-dependence of $\Gamma/2$. Lines refer to jump-diffusion models (see text): CEM (sold line), SSM (dashed line), HRM (dotted line); color code for temperature follows that of symbols.

DOI: 10.1021/acs.jpcc.9b04212
J. Phys. Chem. C 2019, 123, 19183−19194

However, whereas the CEM refers to a jump process with a well-defined jump length, the SSM and HRM take a jump length uncertainty into consideration, following exponential and Gaussian distributions, respectively. More details on the models are given in the Supporting Information. For both ***cg30_w*** and ***pg30_w***, the use of a distribution of jump lengths seems to be needed, as SSM and HRM better approximate the experimental data compared with the CEM. Conversely, the CEM seems to be the most consistent to approximate the experimental points for the 20% w/w hydrated systems. In the following, we will therefore refer to values from the HRM and SSM for the 30% w/w samples and CEM for the 20% w/w samples. For completeness, the fit parameters obtained for the different models and samples are reported in Tables S1 and S2 of the Supporting Information. A distribution of jump lengths is usually employed to describe the diffusion of bulk water.[59,60] In this respect, it is perhaps not surprising to observe an analogous behavior in the higher hydrated materials. The better agreement with a model based on a well-defined jump length for the less hydrated materials conversely points toward a higher degree of order when the number of water molecules per hydroxyl group is about 2, likely due to the strong interactions with the polymer. Such observations are in agreement with the different fragility behavior for the different hydrations, as previously discussed in the case of the polymer mobility. The values of the (averaged) jump length l are overall similar, around 3−4 Å (see Supporting Information for exact values and uncertainties), with a slight increase at higher temperature. In the ***cg30_w*** the T-dependence is less pronounced than in the physical gels, possibly because a real mesh, created by the cross-linker, is present only in the former systems, whereas the structure of the physical gel likely evolves more drastically with the temperature changes.

Figure 11 shows the values for the residence time, τ, (a) and the diffusion coefficient, D, (b), calculated as $D = \frac{l^2}{6\tau}$. The lines represent fits according to an Arrhenius law: $\tau = \tau_0 \exp\left(\frac{-E_\tau}{k_B T}\right)$ in (a), and $D = D_0 \exp\left(\frac{-E_D}{k_B T}\right)$ in (b), where E_τ and E_D are activation energies for residence time and diffusion coefficient, respectively, k_B is the Boltzmann constant, and τ_0 and D_0 are the high temperature limits for residence time and diffusion coefficient. In general, diffusion coefficients become larger as the temperature increases, whereas residence times become smaller, as expected and in agreement with previous studies on bulk[59,60] and confined water.[27,38,51,65,66] We note here that diffusion in bulk water is not an Arrhenius process,[53] but in the limited temperature range investigated here, the Arrhenius fit provides for water hydrating pHEMA gels a reasonable approximation useful for comparison with other systems. As already pointed out, at 30% w/w of hydration the chemical gels show shorter residence times than the physical gels. The difference between the τ values obtained using the SSM or HRM model provides an estimate of the experimental uncertainty. However, E_τ is the same, within error bars, for both models, indicating the robustness of this insight. The temperature dependence is steeper (larger absolute values of E_τ) in ***cg30_w*** than in ***pg30_w*** and τ_0 is much smaller (see Table S3 in Supporting Information); i.e., the attempt frequency for the jump, τ_0^{-1}, is higher for the chemical gels. Within the same type of gel, a higher water concentration corresponds to shorter residence times, closer to those of bulk water. The values of E_D, ranging

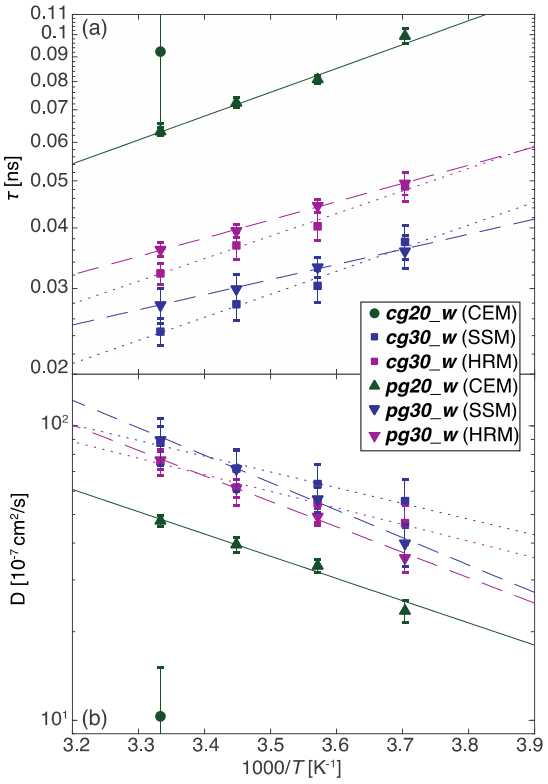

Figure 11. Residence times (a) and diffusion coefficients (b). Lines are fits according to Arrhenius law (solid lines for ***pg20_w***, dashed lines for ***pg30_w***, dotted lines for ***cg30_w***; color code according to the different models used to derived $\tau[D]$ for the different samples, as in the legend).

from 0.11(1) eV [11(1) kJ/mol] to 0.18(1) eV [17(1) kJ/mol], are similar to those obtained in other confined media such as Vycor glass (0.12 eV [12 kJ/mol])[66] or PVA hydrogels (0.16(2) eV [15(2) kJ/mol]),[27] and anyway comparable to those of bulk water (~0.2−0.26 eV [19−25 kJ/mol]),[59,67] showing that water diffusion in pHEMA hydrogels remains an H-bonding governed mechanism. Nevertheless, considering for example the values at 300 K, where the signal is clearer (because of a higher quasi-elastic to elastic ratio), the diffusion coefficients are smaller and residence times are larger than the values for water in confinement in both hard and soft media, such as Vycor and PVA hydrogels,[66,27] underlining a severely reduced water mobility and strong interactions with the pHEMA matrix.

CONCLUSIONS

Hydrogels with optimal release and confining properties, such as HEMA based systems, are highly relevant for medical and cultural heritage applications. The intimate comprehension of transport phenomena in these systems constitutes a basis in the fine-tuning of their delivery properties from a molecular point of view. Quasi-elastic neutron scattering with contrast variation was used to selectively investigate the dynamics of the polymer network and the transport properties of the water confined into the hydrogel matrix, and how such dynamics are affected by temperature, cross-linker nature, and water content.

A distribution of relaxation processes was observed for the polymer network, mainly associated with the side chain dynamics. The dynamics is faster with increasing temperature and hydration, the latter underlining the plasticizer role of the

DOI: 10.1021/acs.jpcc.9b04212
J. Phys. Chem. C 2019, 123, 19183−19194

solvent, which also leads to a more fragile behavior. In physical gels, the relaxation is slower with a smaller portion of the space explored than in the chemical equivalents, likely because of the involvement of the side chains in the network formation. In order to better discriminate the motions of the different part of the polymer chain, further investigation could be extended to selectively deuterated polymer segments, also combining different dynamical ranges.

Regarding the hydration water, a very strong confining effect imposed by the gel matrix was observed. The presence of a fraction of water strongly associated with the polymer matrix and immobile in the experimental time scale (up to few nanoseconds), and a mobile fraction, was detected. The ratio of the two fractions depends on T, hydration, and cross-linker nature. The dynamics of the mobile fraction well agrees with an H-bond governed process with activation energies on the order of 0.11−0.18 eV and jump-diffusion mechanism. The jumps lengths are on the order of 3−4 Å, and well-defined for the less hydrated gels. For the 30% w/w hydrated gels a distribution of jump lengths needs to be considered, consistently with the plasticizer effect observed in the polymer network dynamics. The diffusion coefficients increase and residence times decrease with increasing temperature and hydration. At 20% w/w hydration, the water mobility is considerably higher in the physical gels, whereas at 30% w/w the water mobilities are more similar between the physical and chemical gels, although with slightly shorter residence times in the second case.

Our approach represents a useful starting point for the investigation of more sophisticated hydrogel systems.

■ ASSOCIATED CONTENT

Supporting Information

The Supporting Information is available free of charge on the ACS Publications website at DOI: 10.1021/acs.jpcc.9b04212.

Polymer network EISF fitting parameters, jump-diffusion models, DSC thermograms for chemical and physical gels, tables with residence times, jump lengths, diffusion coefficients and activation energies (PDF)

■ AUTHOR INFORMATION

Corresponding Author

*Phone: +39 055 457 3037. E-mail: emiliano.fratini@unifi.it. Web: www.csgi.unifi.it.

ORCID

Daria Noferini: 0000-0002-7680-8415
Antonio Faraone: 0000-0002-3783-5816
Eugene Mamontov: 0000-0002-5684-2675
Emiliano Fratini: 0000-0001-7104-6530
Piero Baglioni: 0000-0003-1312-8700

Present Address

[▽](D.N.) Forschungszentrum Jülich GmbH, JCNS at Heinz Maier-Leibnitz Zentrum, Lichtenberstraße 1, 85747, Garching, Germany.

Notes

The full description of the procedures used in this paper requires the identification of certain commercial products and their suppliers. The inclusion of such information should in no way be construed as indicating that such products or suppliers are endorsed by NIST or are recommended by NIST or that they are necessarily the best materials, instruments, software or suppliers for the purposes described.

The authors declare no competing financial interest.

■ ACKNOWLEDGMENTS

D.N., M.R., E.F., and P.B. thank MIUR and CSGI for partial financial support. A.F. acknowledges support from the Center for High Resolution Neutron Scattering, a partnership between the National Institute of Standards and Technology and the National Science Foundation under Agreement No. DMR-1508249. The neutron scattering experiments at Oak Ridge National Laboratory's (ORNL) Spallation Neutron Source were supported by the Scientific User Facilities Division, Office of Basic Energy Sciences.

■ REFERENCES

(1) Donnelly, R. F.; Laverty, G..; Singh, T. R. R. *Hydrogels: Design, Synthesis and Application in Drug Delivery and Regenerative Medicine*; CRC Press/Taylor & Francis Group, 2017.

(2) Wichterle, O.; Lím, D. Hydrophilic Gels for Biological Use. *Nature* **1960**, *185* (4706), 117−118.

(3) Kopeček, J. Hydrogels From Soft Contact Lenses And Implants To Self-Assembled Nanomaterials. *J. Polym. Sci., Part A: Polym. Chem.* **2009**, *47* (22), 5929−5946.

(4) Montheard, J.-P.; Chatzopoulos, M.; Chappard, D. 2-Hydroxyethyl Methacrylate (HEMA): Chemical Properties and Applications in Biomedical Fields. *J. Macromol. Sci., Polym. Rev.* **1992**, *32* (1), 1−34.

(5) Dvorankova, B.; Holikova, Z.; Vacik, J.; Konigova, R.; Kapounkova, Z.; Michalek, J.; Pradn, M.; Smetana, K. Reconstruction of Epidermis by Grafting of Keratinocytes Cultured on Polymer Support - Clinical Study. *Int. J. Dermatol.* **2003**, *42* (3), 219−223.

(6) Bhatia, S.; Bergethon, P. R.; Blease, S.; Kemper, T.; Rosiello, A.; Zimbardi, G. P.; Franzblau, C.; Spatz, E. L. A Synthetic Dural Prosthesis Constructed from Hydroxyethylmethacrylate Hydrogels. *J. Neurosurg.* **1995**, *83* (5), 897−902.

(7) Bavaresco, V. P.; de Carvalho Zavaglia, C. A.; de Carvalho Reis, M.; Malmonge, S. M. Devices for Use as an Artificial Articular Surface in Joint Prostheses or in the Repair of Osteochondral Defects. *Artif. Organs* **2000**, *24* (3), 202−205.

(8) Ronel, S. H.; D'Andrea, M. J.; Hashiguchi, H.; Klomp, G. F.; Dobelle, W. H. Macroporous Hydrogel Membranes for a Hybrid Artificial Pancreas. I. Synthesis and Chamber Fabrication. *J. Biomed. Mater. Res.* **1983**, *17* (5), 855−864.

(9) Studenovská, H.; Slouf, M.; Rypácek, F. Poly(HEMA) Hydrogels with Controlled Pore Architecture for Tissue Regeneration Applications. *J. Mater. Sci.: Mater. Med.* **2008**, *19* (2), 615−621.

(10) Peppas, N. A.; Bures, P.; Leobandung, W.; Ichikawa, H. Hydrogels in Pharmaceutical Formulations. *Eur. J. Pharm. Biopharm.* **2000**, *50* (1), 27−46.

(11) Ferreira, L.; Vidal, M. M.; Gil, M. H. Evaluation of Poly(2-Hydroxyethyl Methacrylate) Gels as Drug Delivery Systems at Different pH Values. *Int. J. Pharm.* **2000**, *194* (2), 169−180.

(12) He, H.; Cao, X.; Lee, L. J. Design of a Novel Hydrogel-Based Intelligent System for Controlled Drug Release. *J. Controlled Release* **2004**, *95* (3), 391−402.

(13) Lu, S.; Anseth, K. S. Photopolymerization of Multilaminated Poly(HEMA) Hydrogels for Controlled Release. *J. Controlled Release* **1999**, *57* (3), 291−300.

(14) Gulsen, D.; Chauhan, A. Dispersion of Microemulsion Drops in HEMA Hydrogel: A Potential Ophthalmic Drug Delivery Vehicle. *Int. J. Pharm.* **2005**, *292* (1−2), 95−117.

(15) Baglioni, P.; Carretti, E.; Chelazzi, D. Nanomaterials in Art Conservation. *Nat. Nanotechnol.* **2015**, *10* (4), 287−290.

(16) Bonelli, N.; Montis, C.; Mirabile, A.; Berti, D.; Baglioni, P. Restoration of Paper Artworks with Microemulsions Confined in

DOI: 10.1021/acs.jpcc.9b04212
J. Phys. Chem. C 2019, 123, 19183−19194

Hydrogels for Safe and Efficient Removal of Adhesive Tapes. *Proc. Natl. Acad. Sci. U. S. A.* **2018**, *115* (23), 5932−5937.
(17) Chelazzi, D.; Giorgi, R.; Baglioni, P. Microemulsions, Micelles, and Functional Gels: How Colloids and Soft Matter Preserve Works of Art. *Angew. Chem., Int. Ed.* **2018**, *57* (25), 7296−7303.
(18) Baglioni, P.; Berti, D.; Bonini, M.; Carretti, E.; Dei, L.; Fratini, E.; Giorgi, R. Micelle, Microemulsions, and Gels for the Conservation of Cultural Heritage. *Adv. Colloid Interface Sci.* **2014**, *205*, 361−371.
(19) Domingues, J. A. L.; Bonelli, N.; Giorgi, R.; Fratini, E.; Gorel, F.; Baglioni, P. Innovative Hydrogels Based on Semi-Interpenetrating p(HEMA)/PVP Networks for the Cleaning of Water-Sensitive Cultural Heritage Artifacts. *Langmuir* **2013**, *29* (8), 2746−2755.
(20) Baglioni, M.; Domingues, J. A. L.; Carretti, E.; Fratini, E.; Chelazzi, D.; Giorgi, R.; Baglioni, P. Complex Fluids Confined into Semi-Interpenetrated Chemical Hydrogels for the Cleaning of Classic Art: A Rheological and SAXS Study. *ACS Appl. Mater. Interfaces* **2018**, *10* (22), 19162−19172.
(21) Tranoudis, I.; Efron, N. Water Properties of Soft Contact Lens Materials. *Cont. Lens Anterior Eye* **2004**, *27* (4), 193−208.
(22) Lee, H. B.; Jhon, M. S.; Andrade, J. D Nature of Water in Synthetic Hydrogels. I. Dilatometry, Specific Conductivity, and Differential Scanning Calorimetry of Polyhydroxyethyl Methacrylate. *J. Colloid Interface Sci.* **1975**, *51* (2), 225−231.
(23) Roorda, W.; Bouwstra, J.; de Vries, M. A.; Junginger, H. Thermal Analysis of Water in p(HEMA) Hydrogels. *Biomaterials* **1988**, *9* (6), 494−499.
(24) Peschier, L.J.C.; Bouwstra, J.A.; de Bleyser, J.; Junginger, H.E.; Leyte, J.C. Water Mobility and Structure in Poly[2-Hydroxyethylmethacrylate] Hydrogels by Means of the Pulsed Field Gradient NMR Technique. *Biomaterials* **1993**, *14* (12), 945−952.
(25) Manetti, C.; Casciani, L.; Pescosolido, N. Diffusive Contribution to Permeation of Hydrogel Contact Lenses: Theoretical Model and Experimental Evaluation by Nuclear Magnetic Resonance Techniques. *Polymer* **2002**, *43* (1), 87−92.
(26) Sears, V. F. Neutron Scattering Lengths and Cross Sections. *Neutron News* **1992**, *3* (3), 26−37.
(27) Paradossi, G.; Cavalieri, F.; Chiessi, E.; Telling, M. T. F. Supercooled Water in PVA Matrixes: I. An Incoherent Quasi-Elastic Neutron Scattering (QENS) Study. *J. Phys. Chem. B* **2003**, *107* (33), 8363−8371.
(28) Capponi, S.; Arbe, A.; Cerveny, S.; Busselez, R.; Frick, B.; Embs, J. P.; Colmenero, J. Quasielastic Neutron Scattering Study of Hydrogen Motions in an Aqueous Poly(Vinyl Methyl Ether) Solution. *J. Chem. Phys.* **2011**, *134* (20), 204906.
(29) Rubio Retama, J.; Frick, B.; Seydel, T.; Stamm, M.; Fernandez Barbero, A.; López Cabarcos, E. Polymer Chain Dynamics of Core−Shell Thermosensitive Microgels. *Macromolecules* **2008**, *41* (13), 4739−4745.
(30) Rubio-Retama, J.; Frick, B.; Seydel, T.; López-Ruiz, B.; Fernandez-Barbero, A.; López-Cabarcos, E. Molecular Motions in Low Cross-Linked Poly(N-Isopropylacrylamide) Microgels. *Colloids Surf., A* **2008**, *319* (1−3), 149−153.
(31) Ghugare, S. V.; Chiessi, E.; Telling, M. T. F.; Deriu, A.; Gerelli, Y.; Wuttke, J.; Paradossi, G. Structure and Dynamics of a Thermoresponsive Microgel around Its Volume Phase Transition Temperature. *J. Phys. Chem. B* **2010**, *114* (32), 10285−10293.
(32) Zanatta, M.; Tavagnacco, L.; Buratti, E.; Bertoldo, M.; Natali, F.; Chiessi, E.; Orecchini, A.; Zaccarelli, E. Evidence of a Low-Temperature Dynamical Transition in Concentrated Microgels. *Sci. Adv.* **2018**, *4* (9), eaat5895.
(33) Mamontov, E.; Herwig, K. W. A Time-of-Flight Backscattering Spectrometer at the Spallation Neutron Source, BASIS. *Rev. Sci. Instrum.* **2011**, *82* (8), 085109.
(34) Bée, M. *Quasielastic Neutron Scattering: Principles and Applications in Solid State Chemistry, Biology and Materials Science*; Adam Hilger: Bristol and Philadelphia, 1988.
(35) Azuah, R.; Kneller, L.; Qiu, Y.; Tregenna-Piggott, P. L. W.; Brown, C. M.; Dimeo, R. M.; Copley, J. R. D. DAVE: A Comprehensive Software Suite for the Reduction, Visualization, and Analysis of Low Energy Neutron Spectroscopic Data. *J. Res. Natl. Inst. Stand. Technol.* **2009**, *114* (6), 341−358.
(36) Paradossi, G.; Cavalieri, F.; Chiessi, E.; Mondelli, C.; Telling, M. T. F. Structural Fluctuations in Cross-Linked Matrices with Narrow Pore Size Distribution. *Chem. Phys.* **2004**, *302* (1−3), 143−148.
(37) Paradossi, G.; Cavalieri, F.; Chiessi, E. Proton Fluctuations and Water Diffusion in Dextran Chemical Hydrogels Studied by Incoherent Elastic and Quasielastic Neutron Scattering. *Carbohydr. Res.* **2005**, *340* (5), 921−927.
(38) Paradossi, G.; Di Bari, M. T.; Telling, M. T. F.; Turtu', A.; Cavalieri, F. Incoherent Quasi-Elastic Neutron Scattering Study of Chemical Hydrogels Based on Poly(Vinyl Alcohol). *Phys. B* **2001**, *301* (1−2), 150−156.
(39) Roh, J. H.; Curtis, J. E.; Azzam, S.; Novikov, V. N.; Peral, I.; Chowdhuri, Z.; Gregory, R. B.; Sokolov, A. P. Influence of Hydration on the Dynamics of Lysozyme. *Biophys. J.* **2006**, *91* (7), 2573−2588.
(40) Chahid, A.; Alegria, A.; Colmenero, J. Methyl Group Dynamics in Poly(Vinyl Methyl Ether). A Rotation Rate Distribution Model. *Macromolecules* **1994**, *27* (12), 3282−3288.
(41) Colmenero, J.; Arbe, A.; Alegría, A.; Monkenbusch, M.; Richter, D. On the Origin of the Non-Exponential Behaviour of the α-Relaxation in Glass-Forming Polymers: Incoherent Neutron Scattering and Dielectric Relaxation Results. *J. Phys.: Condens. Matter* **1999**, *11* (10A), A363−A370.
(42) Zhang, Y.; Lagi, M.; Ridi, F.; Fratini, E.; Baglioni, P.; Mamontov, E.; Chen, S. H. Observation of Dynamic Crossover and Dynamic Heterogeneity in Hydration Water Confined in Aged Cement Paste. *J. Phys.: Condens. Matter* **2008**, *20* (50), 502101.
(43) Bizzarri, A.; Cannistraro, S. Molecular Dynamics of Water at the Protein-Solvent Interface. *J. Phys. Chem. B* **2002**, *106*, 6617−6633.
(44) Katava, M.; Stirnemann, G.; Zanatta, M.; Capaccioli, S.; Pachetti, M.; Ngai, K. L.; Sterpone, F.; Paciaroni, A. Critical Structural Fluctuations of Proteins upon Thermal Unfolding Challenge the Lindemann Criterion. *Proc. Natl. Acad. Sci. U. S. A.* **2017**, *114* (35), 9361−9366.
(45) Ito, K.; Moynihan, C. T.; Angell, C. A. Thermodynamic Determination of Fragility in Liquids and a Fragile-to-Strong Liquid Transition in Water. *Nature* **1999**, *398* (6727), 492−495.
(46) Thiessen, W. E.; Narten, A. H. Neutron Diffraction Study of Light and Heavy Water Mixtures at 25 °C. *J. Chem. Phys.* **1982**, *77* (5), 2656.
(47) Gallo, P.; Sciortino, F.; Tartaglia, P.; Chen, S. Slow Dynamics of Water Molecules in Supercooled States. *Phys. Rev. Lett.* **1996**, *76* (15), 2730−2733.
(48) Sears, V. F. Cold Neutron Scattering by Molecular Liquids: III. Methane. *Can. J. Phys.* **1967**, *45* (2), 237−254.
(49) Chen, S.-H.; Gallo, P.; Sciortino, F.; Tartaglia, P. Molecular-Dynamics Study of Incoherent Quasielastic Neutron-Scattering Spectra of Supercooled Water. *Phys. Rev. E: Stat. Phys., Plasmas, Fluids, Relat. Interdiscip. Top.* **1997**, *56* (4), 4231−4243.
(50) Faraone, A.; Liu, L.; Chen, S.-H. Model for the Translation−Rotation Coupling of Molecular Motion in Water. *J. Chem. Phys.* **2003**, *119* (12), 6302−6313.
(51) Zanotti, J.-M.; Bellissent-Funel, M.-C.; Chen, S.-H. Relaxational Dynamics of Supercooled Water in Porous Glass. *Phys. Rev. E: Stat. Phys., Plasmas, Fluids, Relat. Interdiscip. Top.* **1999**, *59* (3), 3084−3093.
(52) Carretti, E.; Grassi, S.; Cossalter, M.; Natali, I.; Caminati, G.; Weiss, R. G.; Baglioni, P.; Dei, L. Poly(Vinyl Alcohol)−Borate Hydro/Cosolvent Gels: Viscoelastic Properties, Solubilizing Power, and Application to Art Conservation. *Langmuir* **2009**, *25* (15), 8656−8662.
(53) Cavalieri, F.; Chiessi, E.; Finelli, I.; Natali, F.; Paradossi, G.; Telling, M. T. F. Water, Solute, and Segmental Dynamics in Polysaccharide Hydrogels. *Macromol. Biosci.* **2006**, *6* (8), 579−589.
(54) Cavalieri, F.; Chiessi, E.; Villa, R.; Viganò, L.; Zaffaroni, N.; Telling, M. T. F.; Paradossi, G. Novel PVA-Based Hydrogel

DOI: 10.1021/acs.jpcc.9b04212
J. Phys. Chem. C 2019, 123, 19183−19194

Microparticles for Doxorubicin Delivery. *Biomacromolecules* **2008**, *9* (7), 1967−1973.
(55) Volino, F.; Dianoux, A. J. Neutron Incoherent Scattering Law for Diffusion in a Potential of Spherical Symmetry: General Formalism and Application to Diffusion inside a Sphere. *Mol. Phys.* **1980**, *41* (2), 271−279.
(56) Volino, F.; Perrin, J.-C.; Lyonnard, S. Gaussian Model for Localized Translational Motion: Application to Incoherent Neutron Scattering. *J. Phys. Chem. B* **2006**, *110* (23), 11217−11223.
(57) Faraone, A.; Fratini, E.; Garai, S.; Müller, A.; Tyagi, M.; Jenkins, T.; Mamontov, E.; Paul, R. L.; Copley, J. R. D.; Baglioni, P. Incoherent Quasielastic Neutron Scattering Study of the Relaxation Dynamics in Molybdenum-Oxide Keplerate-Type Nanocages. *J. Phys. Chem. C* **2014**, *118* (24), 13300−13312.
(58) Ghi, P. Y.; Hill, D. J. T.; Whittaker, A. K. (1)H NMR Study of the States of Water in Equilibrium Poly(HEMA-Co-THFMA) Hydrogels. *Biomacromolecules* **2002**, *3* (5), 991−997.
(59) Teixeira, J.; Bellissent-Funel, M.-C.; Chen, S.-H.; Dianoux, A. Experimental Determination of the Nature of Diffusive Motions of Water Molecules at Low Temperatures. *Phys. Rev. A: At., Mol., Opt. Phys.* **1985**, *31* (3), 1913−1917.
(60) Teixeira, J; Bellissent-Funel, M -C Dynamics of Water Studied by Neutron Scattering. *J. Phys.: Condens. Matter* **1990**, *2*, SA105−SA108.
(61) Chen, S.-H.; Gallo, P.; Bellissent-Funel, M.-C. Slow Dynamics of Interfacial Water. *Can. J. Phys.* **1995**, *73* (11−12), 703−709.
(62) Singwi, K. S.; Sjölander, A. Diffusive Motions in Water and Cold Neutron Scattering. *Phys. Rev.* **1960**, *119* (3), 863−871.
(63) Hall, P. L.; Ross, D. K. Incoherent Neutron Scattering Functions for Random Jump Diffusion in Bounded and Infinite Media. *Mol. Phys.* **1981**, *42* (3), 673−682.
(64) Chudley, C. T.; Elliott, R. J. Neutron Scattering from a Liquid on a Jump Diffusion Model. *Proc. Phys. Soc., London* **1961**, *77* (2), 353−361.
(65) Chiessi, E.; Cavalieri, F.; Paradossi, G. Supercooled Water in PVA Matrixes. II. A Molecular Dynamics Simulation Study and Comparison with QENS Results. *J. Phys. Chem. B* **2005**, *109* (16), 8091−8096.
(66) Bellissent-Funel, M.; Chen, S.; Zanotti, J.-M. Single-Particle Dynamics of Water Molecules in Confined Space. *Phys. Rev. E: Stat. Phys., Plasmas, Fluids, Relat. Interdiscip. Top.* **1995**, *51* (5), 4558−4569.
(67) Mills, R. Self-Diffision in Normal and Heavy Water in the Range 1−45°. *J. Phys. Chem.* **1973**, *77* (5), 685−688.

DOI: 10.1021/acs.jpcc.9b04212
J. Phys. Chem. C 2019, 123, 19183−19194

Supporting Information for *Disentangling Polymer Network and Hydration Water Dynamics in pHEMA Physical and Chemical Hydrogels*

Daria Noferini,[§,▽] Antonio Faraone,[‡] Marta Rossi,[§] Eugene Mamontov,[⊥] Emiliano Fratini,[*,§] and Piero Baglioni.[§]

[§]Department of Chemistry "Ugo Schiff" and CSGI, University of Florence, Via della Lastruccia 3 - 50019 Sesto Fiorentino, Florence, Italy.

[▽]Current address: Forschungszentrum Jülich GmbH, JCNS at Heinz Maier-Leibnitz Zentrum, Lichtenberstraße 1, 85747, Garching, Germany.

[‡]NIST Center for Neutron Research, Gaithersburg, MD 20899-6100, USA, USA.

[⊥]Spallation Neutron Source, Oak Ridge National Laboratory, Oak Ridge, TN, 37831, USA.

[*]Corresponding author. E-mail: emiliano.fratini@unifi.it

1 Polymer network EISF fitting parameters

The elasitc incoherent structure factor related to the H-atoms of the polymer network, $EISF(Q)$, was analysed according to Eq. 14 and Eq. 15. Such equations represent the hypothesis that the observed quasi-elastic broadening reflects only the motion of the side-chain or to both the side-chain and the methyl group, respectively (see text in the paper and Figure 5). In Figure S1, we report the weights of the different parts of the polymer chain, as obtained from the fit parameters A and B of Eq. 14 and Eq.15, and the dimension of the region of space explored by the side-chain and the backbone, R_{SC} and R_B, respectively. All the parameters are obtained from the fits shown in Figure 5. The expected values on the basis of stoichiometric or geometric considerations (dashed lines) are also reported for comparison.

2 Jump-diffusion models

For the fit of the quasi-elastic broadening, we used the models developed by Chudley and Elliot (CEM) [S1], Singwi and Sjölander (SSM) [S2], and Hall and Ross (HRM) [S3]. Such models assume a diffusive motion *via* successive jumps. In between two jumps, the particle rests on a given site for a residence time τ.

In the CEM, the jump distance l_{CEM} is a constant and the corresponding half width at half maximum of the Lorentzian quasi-elastic component is given by

$$\frac{\Gamma}{2} = \frac{\hbar}{\tau}\left(1 - \frac{\sin(Ql_{\mathrm{CEM}})}{Ql_{\mathrm{CEM}}}\right), \tag{1}$$

In the SSM, the jump distance $\rho(r)$ is exponentially distributed,

$$\rho(r) = \frac{r}{r_0^2}\exp\left(-\frac{r}{r_0}\right), \tag{2}$$

and the broadening is given by

$$\frac{\Gamma}{2} = \frac{\hbar}{6\tau}\frac{Q^2 l_{\mathrm{SSM}}^2}{1+\frac{Q^2 l_{\mathrm{SSM}}^2}{6}}, \tag{3}$$

where l_{SSM}^2 is the mean square jump length, which is equal to $\int_0^\infty r^2\rho(r)dr = 6r_0^2$.

In the HRM, the jump distance is defined by a Gaussian distribution,

$$\rho(r) = \frac{2r^2}{r_0^3(2\pi)^{1/2}\exp\left(-\frac{r^2}{2r_0^2}\right)}, \tag{4}$$

and the broadening is given by

$$\frac{\Gamma}{2} = \frac{\hbar}{\tau}\left[1 - \exp\left(-\frac{Q^2 l_{\mathrm{HRM}}^2}{6}\right)\right]. \tag{5}$$

The mean square jump length for this model, l_{HRM}^2, is equal to $\int_0^\infty r^2\rho(r)dr = 3r_0^2$.

2.1 Jump-diffusion fit parameters

The residence times and jump lengths obtained by fitting the quasi-elastic broadening using the CEM, SSM and HRM are given in Tab. S1 and Tab. S2, respectively.

The residence times and the diffusion coefficients were fitted according to an Arrhenius law (see paper, Figure 10). Table S3 lists the derived activation energies and high temperature limits.

3 DSC thermograms

Figures S2 and S3 show the most representative DSC heating scans for the pHEMA chemical and physical hydrogels.

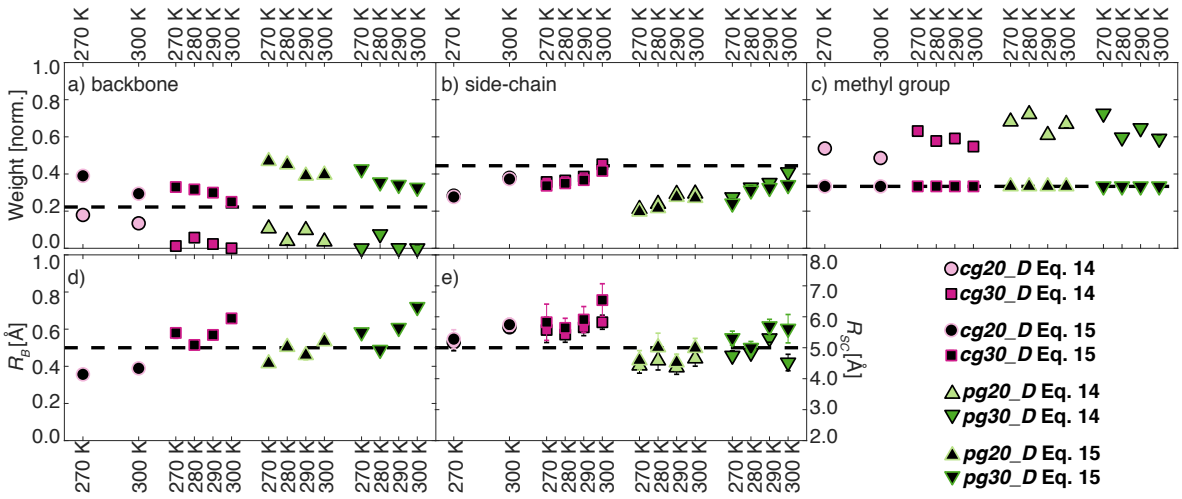

Fig. S1 Weights of the different parts of the polymer chain: a) backbone, b) side-chain, and c) methyl group. In d) and e), there are shown the regions of space explored by the backbone and the side-chain, respectively. All the parameters are obtained from the fits shown in Figure 5 in the paper and Eq. 14 and 15. Dashed lines represent the expected values on the basis of stoichiometric or geometric considerations. When not visible, error bars are within the symbols.

	CEM				SSM				HRM			
	270K	280K	290K	300K	270K	280K	290K	300K	270K	280K	290K	300K
cg20_w	-	-	-	0.09(3)	-	-	-	0.03(1)	-	-	-	0.06(2)
cg30_w	0.061(3)	0.051(3)	0.047(3)	0.041(2)	0.037(3)	0.030(2)	0.028(2)	0.024(2)	0.049(3)	0.040(3)	0.037(2)	0.032(2)
pg20_w	0.099(3)	0.081(2)	0.072(2)	0.063(1)	0.062(3)	0.055(2)	0.050(3)	0.045(3)	0.079(3)	0.067(1)	0.060(2)	0.053(2)
pg30_w	0.065(3)	0.056(2)	0.050(2)	0.045(2)	0.036(3)	0.033(1)	0.030(2)	0.028(2)	0.049(3)	0.044(1)	0.039(1)	0.036(1)

Tab. S1 Residence times τ (in ns) obtained by fitting $\frac{\Gamma}{2}$ according to Eq. (1), (3), and (5).

	l_{CEM}				l_{SSM}				l_{HRM}			
	270K	280K	290K	300K	270K	280K	290K	300K	270K	280K	290K	300K
cg20_w	-	-	-	2.4(4)	-	-	-	1.5(4)	-	-	-	1.9(4)
cg30_w	3.9(2)	3.9(2)	3.9(2)	4.1(2)	3.5(3)	3.4(2)	3.5(2)	3.6(2)	3.7(2)	3.6(2)	3.7(2)	3.8(2)
pg20_w	3.7(1)	4.0(1)	4.1(1)	4.25(9)	3.6(2)	4.1(2)	4.5(5)	4.7(6)	3.6(1)	4.0(1)	4.2(2)	4.3(3)
pg30_w	3.6(1)	3.9(1)	4.1(1)	4.3(1)	2.9(2)	3.3(1)	3.6(2)	3.9(3)	3.2(1)	3.6(1)	3.8(1)	4.1(1)

Tab. S2 Jump lengths (in Å) obtained by fitting $\frac{\Gamma}{2}$ according to Eq. (1), (3), and (5).

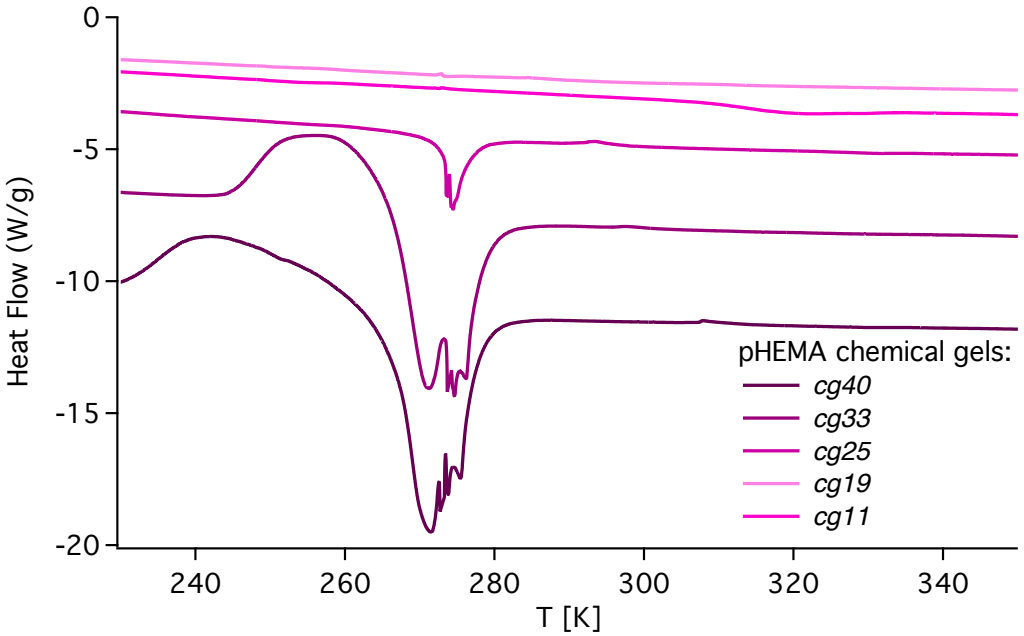

Fig. S2 DSC heating scans representative of water melting in chemical hydrogels with 10 to 40 % water content. Curves are offset along the y-axis for the sake of clarity.

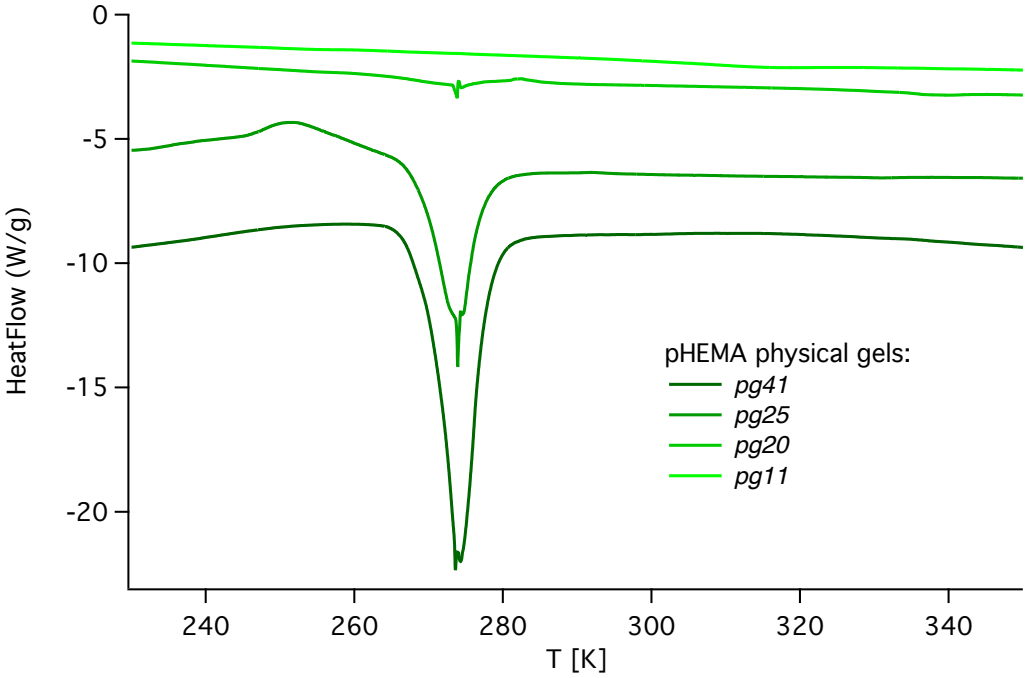

Fig. S3 DSC heating scans representative of water melting in physical hydrogels with 10 to 40 % water content. Curves are offset along the y-axis for the sake of clarity.

	τ_0 [ps]	E_τ [eV]	D_0 [10^{-3} cm^2 s^{-1}]	E_D [eV]
pg20_w (CEM)	1.5(5)	-0.097(8)	2(1)	0.15(2)
pg30_w (SSM)	2.5(4)	-0.062(4)	12(6)	0.18(1)
pg30_w(HRM)	2.0(2)	-0.075(3)	6(2)	0.17(1)
cg30_w (SSM)	0.6(2)	-0.09(1)	0.5(2)	0.11(1)
cg30_w (HRM)	0.9(3)	-0.092(7)	0.5(2)	0.11(1)

Tab. S3 Activation energies and high temperature limits for residence times and diffusion coefficients derived by Arrhenius law fits.

Note

Uncertainties and error bars represent one standard deviation.

References

S1 Chudley, C. T.; Elliott, R. J. Neutron Scattering from a Liquid on a Jump Diffusion Model. *Proc. Phys. Soc.* **1961**, *77*, 353–361.

S2 Singwi, K. S.; Sjölander, A. Diffusive Motions in Water and Cold Neutron Scattering. *Phys. Rev.*, **1960**, *119*, 863–871.

S3 Hall, P. L.; Ross, D. K. Incoherent Neutron Scattering Functions for Random Jump Diffusion in Bounded and Infinite Media. *Mol. Phys.* **1981**, *42*, 673–682.

Paper III

Marta Rossi, Giovanni Ferraro, Emiliano Fratini, and Piero Baglioni. Manuscript to be submitted.

List of papers

Classic and semi-IPN pHEMA hydrogels: structural and diffusional properties

Marta Rossi, Giovanni Ferraro, Emiliano Fratini, Piero Baglioni*

Department of Chemistry "Ugo Schiff" and CSGI, University of Florence, via della Lastruccia 3-Sesto Fiorentino, I-50019, Florence, Italy.

*email: emiliano.fratini@unifi.it

KEYWORDS: hydrogel; diffusion; FRAP; pHEMA; PAA; semi-IPN; polymeric network.

Abstract

This paper reports a detailed physico-chemical characterization of different poly(2-hydroxyethyl methacrylate) (pHEMA) hydrogels by using a combination of several techniques to provide information on the nanoscale structure of the hydrogels (small angle X-ray scattering) and their hydration (differential scanning calorimetry and thermogravimetric analysis). The diffusive properties of these hydrogels are assessed measuring the diffusion coefficients of probes with different dimension and functionalities (fluorescein isothiocyanate and fluorescein isothiocyanate-dextran) by means of confocal microscopy. In particular, we evaluate the effect of the amount of water, cross-linker percentage and composition (ethylene glycol dimethacrylates derivates) on the hydrogel properties. In addition, a new formulation of semi-interpenetrated pHEMA networks with

polyacrylic acid (PAA), referred as semi-IPN pHEMA/PAA, was developed and deeply investigated changing HEMA/PAA ratio. Our results indicate that the ratio of free to bound water in pHEMA hydrogels decreases increasing the amount of cross-linker, causing a lower mobility of the probes inside the polymeric network. In the case of semi-IPN hydrogels, the diffusion coefficients are strictly dependent on the PAA/HEMA ratio, decreasing with the increase of this ratio.

Introduction

Diffusion of solute molecules in hydrogels is of interest in a wide variety of applications, such as chromatography separation[1], membrane separation[2,3] and biomedical applications for encapsulation of cells or delivery of bioactive agents, due to the high biocompatibility of these materials[4,5]. Solute transport in hydrogels occurs mostly in the water-filled regions confined by polymer chains[6]. Thus, interactions between the solute and the gel network, due to hydrodynamic friction, physical obstruction, electro-osmosis and specific binding[4,7] cause slower diffusion than in bulk water. In particular, it is well known that solute diffusion decreases with increasing solute size[8] and decreasing the water fraction of the gel[9]. Furthermore, the cross linking process occurring during gelation brings to the formation of a 3D network with a characteristic mesh size, which plays a primary role in the diffusion process if the solute size is comparable to the mean mesh size of the gel[10]. Previous studies proved that the release of a macromolecular drug from an hydrogel can be controlled regulating the pore volume fraction and the pore size by changing the composition of the polymeric network and the amount of the cross-linker[11].

There are several theoretical models which attempt to describe diffusion processes in gels[12]. The free volume theory describes the change in the diffusion rate as a function of the average free

volume[13]; the obstruction considers the gel strands as fixed and impenetrable segments immersed in a solution[14]; the hydrodynamic assumes that the solute moves at a constant velocity in a continuum media and it is hindered by the frictional forces of the gel strands. Other approaches are developed combining these different theories[4], but the heterogeneity of the gel and the solute dimension are not considered in all of these models. To fill the gap, the aim of this work is the comprehension of the diffusion properties of different solute molecules in hydrogels with different chemical composition in order to assess a correlation between the hydrogels structure and the diffusion coefficient of the solute.

In particular, we focus on poly(2-hydroxyethyl methacrylate) (pHEMA) hydrogels, widely used as biomaterials thanks to the similarity with living tissues[15]. These materials have been used or proposed as drug delivery systems[16] and for several biomedical applications, such as contact lenses[17], corneal replacement[18], synthetic dural prosthesis[19], artificial skin[20] and articulating surface for joint prosthesis[21]. The high resistance to enzymatic digestion and their inertness is reflected in the unwillingness of normal cells to attach themselves to their surfaces and to grow on them[22], important properties that make pHEMA hydrogels suitable for medical use. Another advantage is the high hydrophilicity, even if this feature may lead to poor mechanical strength[23], limiting their use in practical applications. In order to improve the chemical and mechanical properties of these gels[24] a variety of co-monomers or polymers can be incorporated into the pHEMA network leading to formation of an interpenetrated (IPN) or a semi-interpenetrated (semi-IPN) polymeric network. There are several works that report different kinds of IPN and semi-IPN hydrogels with better capabilities of storing water and improved mechanical properties. For example, IPN pHEMA/poly(2-methacryloyloxyethyl phosphorylcholine) hydrogels exhibit enhanced tensile strength compared with the pHEMA classical hydrogel, due to the presence of a cross-linked

poly(2-methacryloyloxyethyl phosphorylcholine) network entrapped within the pHEMA, resulting in an effective transfer of stress between the two polymer networks in the IPN[25]. Another study demonstrated that p(HEMA-co-sodium methacrylate)/chitosan and pHEMA/chitosan semi-IPN hydrogels have higher tensile and compressive moduli than classical pHEMA, which increase with the molecular weight of chitosan[26]. This behaviour can be related to the increasing of the junction points between HEMA and chitosan chains.

Other studies report the use of different kinds and amounts of cross-linkers to tune the water content and the mechanical strength of the polymeric network. Han et al. [26] investigate p(HEMA-co-sodium methacrylate)/chitosan and pHEMA/chitosan semi-IPN hydrogels demonstrating that the polymeric networks with poly(ethylene glycol) diacrylate as crosslinker show much higher water content and lower tensile strength than those with ethylene glycol dimethacrylate. These properties are directly correlated to the length of cross-linker chain. Garcìa et al.[27] demonstrated that in poly(2-hydroxyethyl methacrylate-co-acrylamide) hydrogels the increase of crosslinker percentage leads to a densely crosslinked matrices that do not expand in water as much as hydrogels with lower crosslinking degree.

To the best of our knowledge, only classical "copolymer hydrogels" (pHEMA/PAA) have been synthesized, but they have usually quite different characteristics from those resulting from the sum of single homopolymer properties[28]. Thus, since semi-IPNs are based on polymer blends in which linear or branched polymers are embedded into a polymer networks during the polymerization reaction, without any chemical interaction between them, the obtained hydrogel should be present properties similar to the average of the single homopolymer properties[29].

Therefore, in this work pHEMA hydrogels with various cross-linker/HEMA ratios and two different cross-linking agents, ethylene glycol dimethacrylate (EGDMA) and poly(ethylene glycol dimethacrylate) (PGD) were prepared to evaluate the effect of the amount and the chemical nature of the cross-linker on the water content of the gel and on the diffusional behaviour of solute molecules. In addition, a new formulation of semi-IPN pHEMA/polyacrylic acid (PAA) hydrogel were synthesized and fully characterized to understand the influence of PAA on the physico-chemical properties of the gels.

The internal structure of all the prepared systems was investigated by means of small angle X-ray scattering (SAXS) in order to evaluate the mean mesh size and the inhomogeneity of the network. Differential scanning calorimetry (DSC) and thermogravimetric analysis (TGA) were employed to study the hydration level and the properties of water entrapped in the polymeric network. Finally, fluorescence recovery after photobleaching (FRAP) experiments were performed to calculate the diffusion coefficient of probes with different dimension inside the polymeric network. All these results, taken together, provide a complete description of the relationship between the structure and the hydration of the hydrogels with the diffusion properties of hydrophilic molecules.

Experimental section

Materials. 2-Hydroxyethyl methacrylate (HEMA) (purity 99%), poly(acrylic acid) (PAA) (average Mn ≈ 450 kDa), azoisobutyronitrile (AIBN) (purity 98%), ethylene glycol dimethacrylate (EGDMA) (purity 98%), poly(ethylene glycol dimethacrylate) (PGD) (average Mn ≈ 550 Da), fluorescein isothiocyanate (FITC) and fluorescein isothiocyanate-dextran (FITC-dextran) with

dextran Mw of 4, 40 and 250 kDa were obtained from Sigma-Aldrich and used as received. Water was purified by a Millipore Milli-Q gradient system (resistivity >18 MΩ·cm).

Hydrogels synthesis. Classical pHEMA hydrogels were synthesized by adding HEMA monomer to various cross-linker concentrations. The solution was bubbled with N_2, then an aqueous solution of AIBN initiator, previously degassed, was added. The mixture was transferred between two glassy covers, in which the polymerization reaction was carried out at 60°C for 4 hours. After the reaction, 1 mm thick flat transparent hydrogel films were obtained. The films were washed and placed in containers filled with water, which was renewed once a day for 7 days in order to remove unreacted monomers. The ratio HEMA/water was kept equal to 3:2 in all the prepared hydrogels, while the kind and the amount of cross-linker change. The structure of the two different cross-linking agents used in this work is reported in Figure S1 in SI (section S1). Table 1 shows the amount and the kind of cross-linker used for the different hydrogels.

sample	cross-linker	cross-linker/HEMA molar ratio ($*10^{-3}$)
H0	-	0
HE A	EGDMA	13.1
HP A	PGD	13.1
HP F	PGD	10.0
HE B	EGDMA	6.6
HP G	PGD	5.0
HE C	EGDMA	3.3
HE D	EGDMA	1.6
HP D	PGD	1.6
HE E	EGDMA	0.8

Table 1. Chemical nature and amount of cross-linker used in the preparation of classical pHEMA hydrogels.

To prepare the semi-IPN hydrogels, an aqueous solution of poly acrylic acid (PAA) was added to a solution of EGDMA/HEMA molar ratio 0.006:1, AIBN and water before polymerization. The mixture, after sonication and degassing, was transferred between two glassy covers, and polymerized at 60°C for 4 hours. After the reaction, 1 mm thick flat transparent hydrogel films were obtained. In order to remove any residue of unreacted monomers and free PAA molecules, the hydrogels were washed with water once a day for 7 days.

In particular, different semi-IPN hydrogels were obtained by varying the ratio HEMA/PAA and the amount of water. Table 2 shows the composition of the different prepared semi-IPN networks.

sample	HEMA wt%	H2O wt%	PAA wt%	OH/COOH ratio
s-IPN60 8:1	36	60	3	8:1
s-IPN50 8:1	46	50	3	8:1
s-IPN38 8:1	57	38	4	8:1
s-IPN38 4:1	53,5	38	7,5	4:1
s-IPN38 2:1	48	38	13	2:1

Table 2. Composition of semi-IPN pHEMA/PAA hydrogels. The OH/COOH ratio outlines the number of HEMA hydroxyl groups for each PAA carboxyl group.

It is noteworthy that, at macroscopic level, there are some differences between the semi-IPN hydrogels: in particular, the systems with water content higher than 38% are not transparent, as shown in Figure 1.

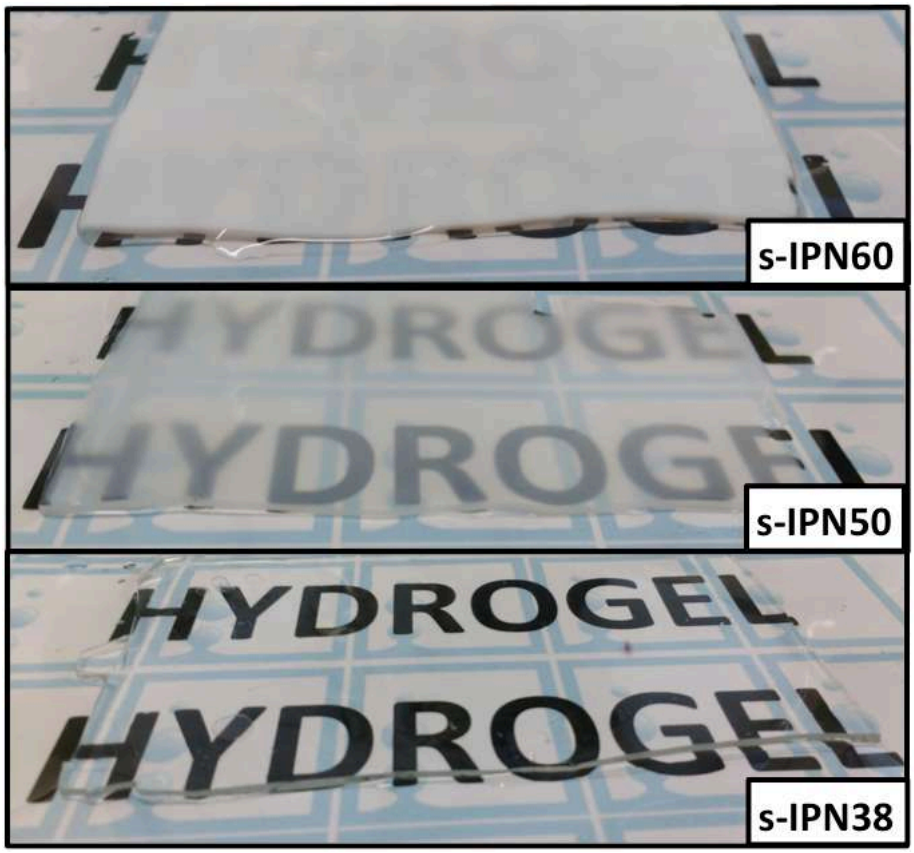

Figure 1. s-IPN 8:1 hydrogels containing different amounts of water (from top: 60 wt%, 50 wt% and 38 wt%).

Hydrogel loading with probes. Small pieces (1x1x0.1 cm^3) of the different hydrogels were loaded with fluorescent molecules of different dimension: fluoresceine isothiocyanate FITC (hydrodynamic radius = 0.54 nm[30]), FITC-dextran 4 kDa (hydrodynamic radius = 1.4 nm[31]) and FITC-dextran 40 kDa (hydrodynamic radius = 4.5 nm[31]). The samples were incubated in $1 \cdot 10^{-4}$ M water solutions of the different probes at least for two days. The concentration of FITC and FITC-dextran solutions was chosen in order to obtain a linear relationship between the fluorescence signal of the probe and its concentration, as verified by Braeckmans et al.[32].

Physicochemical characterization of hydrogels. Thermogravimetric analysis (TGA) was carried out with SDT Q600 (TA Instruments) that works in the range from room temperature to 1500 °C and the balance sensitivity is 0.1 μg with respect to the weight change in the sample. Measurements were performed in a nitrogen atmosphere with a flow rate of 100 mL/min. The samples were put into an alumina open pan and the analysis were performed with a heating rate of 10 °C/min from 25 °C to 250 °C[33]. The equilibrium water content (EWC) was calculated as followed (Eq. 1):

$$EWC = \frac{W - W_d}{W} \quad (1)$$

where W is the weight of the hydrated sample and W_d the weight of the dry sample. The values of W_d are experimentally determined from TGA analysis, considering the weight of the sample at 250 °C.

Differential scanning calorimetry analysis (DSC) was performed with a Q2000 Calorimeter (TA Instruments). The temperature range was from -60 °C to 30 °C with a scan rate of 2 °C/min; sealed stainless steel pans were used. Water in porous systems like gels can be classified as non-freezing bound water and free or bulk water[34]. The non-freezing water forms hydrogen bonds with the functional groups of the polymer, rather than with other water molecules, as would be necessary for the water to freeze; instead, the bulk water has the same properties of the pure water and for this reason can bind with other water molecules to form ice crystals when the temperature is around 0°C. From DSC curves it is possible to determine the different types of water present in the hydrogels[35].

The fraction of free water C_{free} was calculated as follow[36] (Eq. 2):

$$C_{free} = \frac{\Delta H_{tr}}{\Delta H_f} \quad (2)$$

where ΔH_{tr} (J/g) is the heat of transition obtained by the integral of DSC curves between -20°C and 10 °C and ΔH_f is the theoretical value of the specific enthalpy of fusion of water at 0 °C (333,6 J/g[37]). The fraction of bound water (C_{bound}) was calculated from the difference between the equilibrium water content (EWC), determined from TGA, and the free water fraction (C_{free}), obtained from DSC (Eq. 3).

$$C_{bound} = EWC - C_{free} \quad (3)$$

Small angle x-ray scattering analysis (SAXS) were carried out with a HECUS S3-MICRO SWAXS camera, equipped with a Hecus System3 2D-point collimator and two position-sensitive detectors (PSD-50M) containing 1024 channels with a width of 54 microns. The copper anode from the Oxford 50 W microfocus source emits radiation with the wavelength of the Kα-line given by λ= 1.542 Å. The K_β-line is removed by FOX-3D single-bounce multilayer point focussing optics (Xenocs, Grenoble). The voltage is generated by the GeniX X-ray generator (Xenocs, Grenoble). The sample-to-detector distance was 281 mm. The volume between sample and detector was kept under vacuum in order to minimize the scattering from the air. This camera was calibrated in the small angle region using silver behenate, which is known to have a well-defined lamellar structure (d = 58.38 Å)[38]. Scattering curves were acquired in the q-range between 0.01 and 0.55 $Å^{-1}$. Samples were placed into demountable cells, with kapton film used as windows. The temperature control was set to 25°C by a Peltier element, with an accuracy of ± 0.1 °C. All the scattering curves were corrected for the empty cell and water contribution considering the relative transmission factors. In the case of classical pHEMA hydrogels, the scattering curves can be analyzed using the Ornstein-Zernike model[40] while in the case semi-IPN pHEMA gels, an another

term which takes into account the solid-like inhomogeneities[42] was added. Details about these functions were reported in SI file section S1.

Fluorescence spectroscopy was performed with a laser scanning confocal microscope Leica TCS SP2 (Leica Microsystems GmbH, Wetzlar, Germany) equipped with a 10× water immersion objective. The 488 nm Ar^+ laser line was used for the excitation of the FITC and FITC-dextran fluorophores and the emitted fluorescence was acquired between 498 and 600 nm in the microscope's xyλ scan mode using a photomultiplier (PMT) detector.

Fluorescence recovery after photobleaching (FRAP) experiments were carried out using 10 serial laser pulses (Δt=1.625 sec, power = 4 mW, Ar^+ lines at 458, 476 and 488 nm) focused on a circular spot (FRAP ROI) with a diameter of 35 μm. The diameter and the shape of the spot has been chosen in order to obtain diffusion coefficients independent from the geometry of the bleach region as reported in the work of Braeckmans et al.[32]. The fluorescence intensity in the FRAP ROI was normalized with respect to the fluorescence intensity of the background measured in a circular reference ROI with the same shape and dimension. The FRAP curves can be described with a model proposed by Soumpasis[39]; all the details are reported in the SI file (Section S2).

3 RESULTS AND DISCUSSION

Structural characterization. SAXS analysis gives information about the nanostructure of pHEMA hydrogels. Figure 2 shows the SAXS curves of HE and HP hydrogels, after subtraction of water and cell contribution along with the best fit using the Ornstein-Zernike model (red lines).

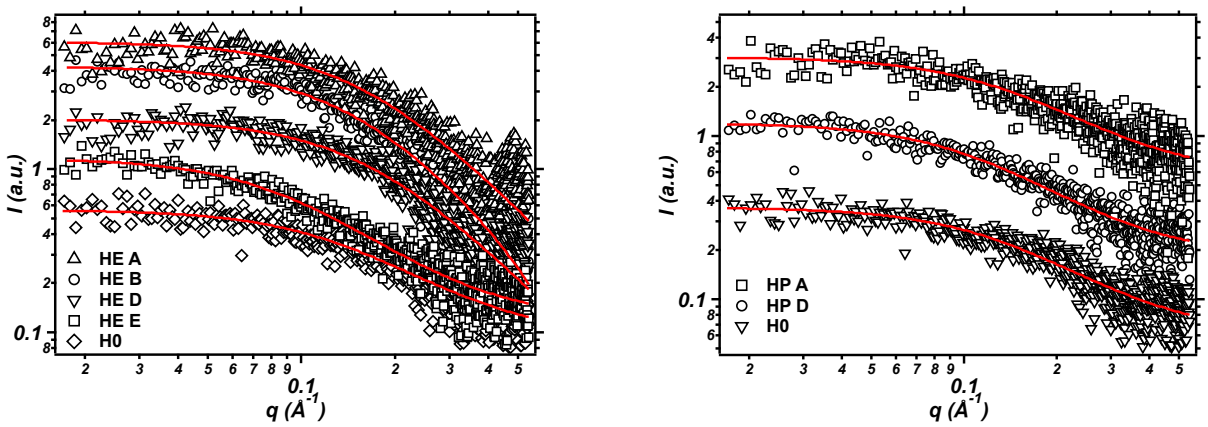

Figure 2. SAXS curves of HE (left) and HP (right) hydrogels. Fitting curves are reported as continuous lines together with the experimental data (empty markers). The reported curves are offset along y-axes for clarity.

The fitting parameters of SAXS curves for HE and HP hydrogels are reported in Table 3.

	$I_{sol}(0)$	ζ (nm)	Bkg
H0	0.74 ± 0.01	0.6 ± 0.1	0.13 ± 0.01
HE A	1.39 ± 0.01	0.6 ± 0.1	0.11 ± 0.01
HE B	1.45 ± 0.01	0.7 ± 0.1	0.11 ± 0.01
HE D	1.26 ± 0.01	0.6 ± 0.1	0.12 ± 0.01
HE E	0.86 ± 0.01	0.7 ± 0.1	0.10 ± 0.01
HP A	0.60 ± 0.01	0.7 ± 0.1	0.13 ± 0.01
HP D	0.77 ± 0.01	0.8 ± 0.1	0.13 ± 0.01

Table 3. Fitting parameters obtained from the SAXS curves of HE and HP hydrogels.

Considering that the resolution of the experiment is about 5 Å, we are not able to distinguish differences between the investigated hydrogels in terms of correlation length. Thus, an increase in the cross-linker concentration does not affect the mesh size. This is consistent with the study of T.

Kanaya et al., in which they demonstrate that in a semi-dilute solutions of polymer the cross-linking does not change the structure because the polymer chains are overlapped each other before cross-linking[41].

Figure 3 shows the SAXS curves obtained for pHEMA/PAA hydrogels, after subtraction of water and cell contribution. The fitting parameters are reported in Table 4.

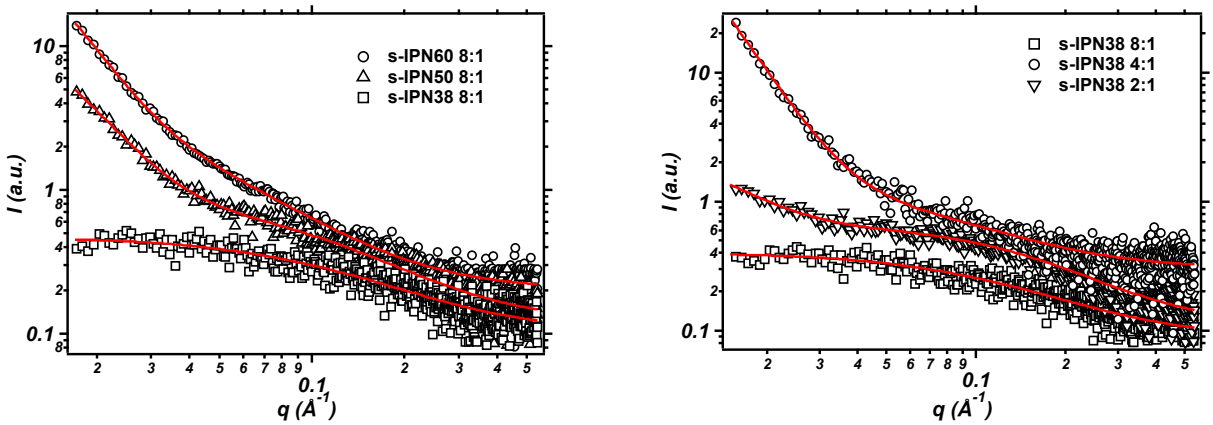

Figure 3. SAXS curves of pHEMA/PAA hydrogels. Fitting curves are reported as continuous lines together with the experimental data (empty markers). The reported curves are offset along y-axes for clarity.

	Isol(0)	ζ (nm)	a (nm)	Iex(0)	bkg
s-IPN60 8:1	0.70 ± 0.02	1.7 ± 0.1	9.6 ± 0.2	75.9 ± 4.5	0.09 ± 0.01
s-IPN50 8:1	0.90 ± 0.02	0.8 ± 0.3	6.9 ± 0.5	36.9 ± 2.1	0.18 ± 0.01
s-IPN38 8:1	0.45 ± 0.11	0.7 ± 0.1	-	-	0.18 ± 0.01
s-IPN38 4:1	0.45 ± 0.8	1.0 ± 0.1	14.5 ± 0.1	563.6 ± 0.1	0.21 ± 0.01
s-IPN38 2:1	0.80 ± 0.01	0.7 ± 0.2	6.3 ± 0.6	3.9 ± 0.8	0.16 ± 0.01

Table 4. Parameters obtained from the fitting of pHEMA/PAA semi-IPN hydrogels.

Considering s-IPN 8:1 series, samples containing 50% and 60 wt% of water show a rapid increase of the intensity at low q values, especially in the case of s-IPN60 8:1. On the contrary, the hydrogel s-IPN38 8:1 doesn't exhibit any scattering excess at low q values. As a consequence, the calculated inhomogeneity value is about 9.6 nm and 6.9 nm for s-IPN60 8:1 and s-IPN50 8:1 respectively, while the hydrogel with 38% of water does not have any appreciable inhomogeneity. The correlation length value is 1.7 nm for the s-IPN60 8:1, while in the other two systems the values are 0.8 nm (s-IPN60 8:1) and 0.7 nm (s-IPN60 8:1). A bigger average mesh size for the hydrogel with the highest water content is in agreement with other systems in which it was proved that the correlation length is inversely proportional to the water content[5].

In pHEMA/PAA 38% series, s-IPN38 4:1 shows a rapid rising of the intensity at low q values, s-IPN38 2:1 exhibits only a slightly rising in this q range, while s-IPN38 8:1 does not show any scattering excess. Concerning the average mesh size, the highest value was found for the s-IPN38 4:1 (around 1.0 nm), while s-IPN38 8:1 and s-IPN38 2:1 have comparable mesh size (0.7 nm).

Water in hydrogels. The study of the amount and the different types of water in hydrogels gives valuable information on the absorption, diffusion and permeation properties of these hydrophilic materials. The equilibrium water content (EWC %) increases decreasing the percentage of cross-linking agent in the different hydrogels according to an exponential decay (see Figure 4).

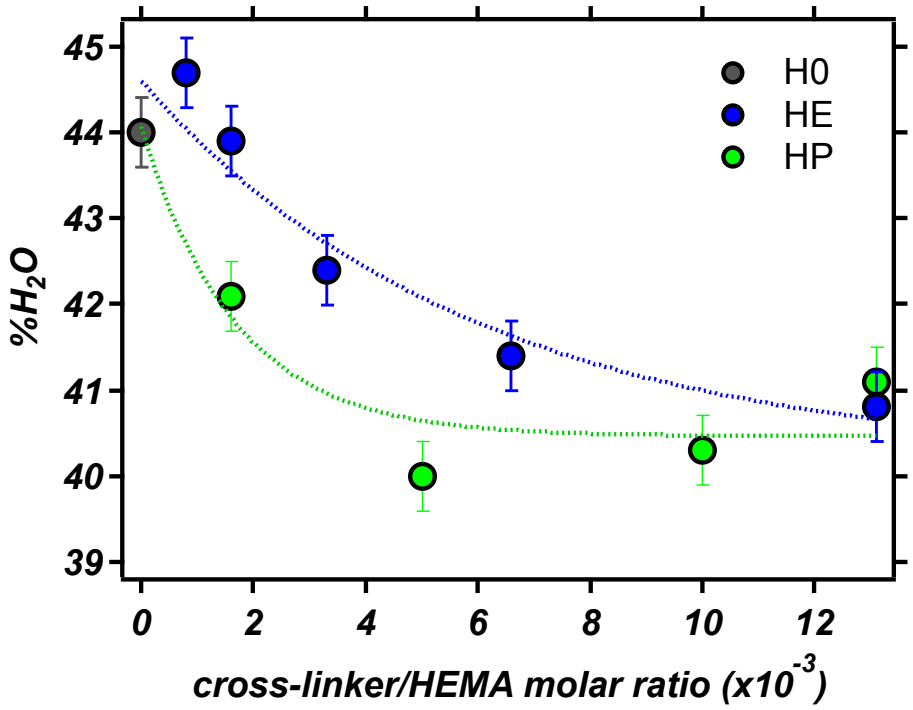

Figure 4. Equilibrium water content as a function of the amount of cross-linking agent in classical pHEMA hydrogels.

This trend can be explained considering the polar nature of the different portions of the polymer network which can be described using the water/n-octanol partition coefficients cLogP[44] (data obtained from DataWarrior software[45]). In particular, HEMA fragments are the more polar components of the polymer network (cLogP: 0.48) while the water affinity decreases for the cross-linker molecules (cLogP PGD: 1.10; cLogP EGDMA: 1.84). For this reason, the EWC% decreases moving from the hydrogel H0, containing just HEMA monomers, to the other hydrogels containing increasing amounts of cross-linker. It is worth noting that, despite the higher water affinity, the hydrogel with PGD shows the lower amount of EWC % with respect to the hydrogel with EGDMA. This can be explained considering the different dimension of these molecules (see Figure S1 in SI file): PGD fragments occupy a bigger amount of polymer network with respect to

the EGDMA fragments (n=9 vs n=1) so the relative amount of HEMA fragments, the most polar components, is lower in the PGD hydrogels.

About the semi-IPN pHEMA/PAA hydrogels, the water content is almost the same in pHEMA/PAA 38% series and it corresponds to the amount of water used during the synthesis. On the contrary, considering pHEMA/PAA 8:1 series, the water content shows small discrepancies from the water amount used for the synthesis. In particular, in s-IPN50 and s-IPN60 the EWC are about 8% and 5% less than the amount used during the synthesis. The details about the obtained EWC % are reported in the SI file Table S1.

DSC technique is employed to determine the different types of water; in particular, C_{free}, which corresponds to the bulk-like water and the loosely bound water present in the hydrogels, is an important parameter that accounts for the retention and diffusive properties of a hydrogel[46].

Figure 5 shows DSC thermograms of the classical pHEMA hydrogels. Table S2 in the SI reports details about the melting enthalpy and the calculated values of C_{free} and C_{bound}.

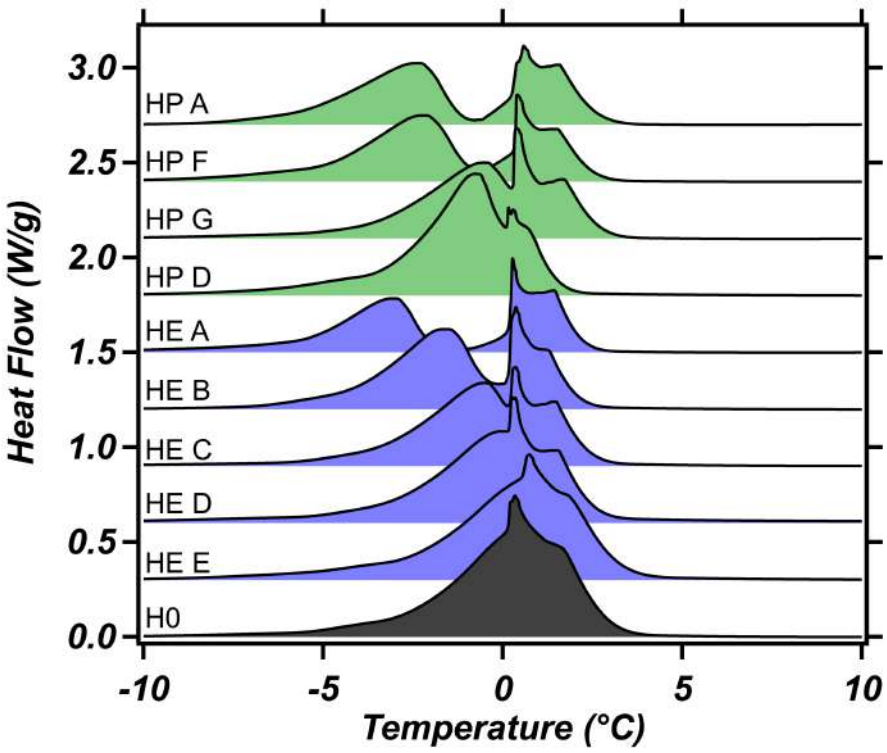

Figure 5. DSC thermograms of classical pHEMA hydrogels. The reported curves are offset along y-axis for clarity (y-offset: 0.6 W/g).

In HE and in HP hydrogels, the ratio between free water and bound water decreases substantially increasing the percentage of cross-linker, consisting with a higher number of hydrogen bond acceptor groups that can interact and bind water molecules (Figure 6). Moreover, comparing pHEMA/PGD and pHEMA/EGDMA networks with the same amount of cross-linking agent, C_{free}/C_{bound} ratio is much higher in HP than in HE: this can be probably related to the fact that PGD has a longer chain with respect to EGDMA. This leads to a higher mobility of the polymeric network and, consequently, to less friction between water molecules and polymer chains. Finally, DSC thermograms reported in Figure 5 show that, increasing the percentage of the cross-linker, the freezing peak broadens until two distinct peaks appear in the hydrogel with 2% of cross-linker. The second peak at lower temperature can be related to loosely bound water, which usually refers

to water molecules interacting with the polar groups of the network only through hydrogen bonds. This contribution becomes more important for samples containing high percentage of cross-linker because of the formation of a compact network and/or because of an increase of the polar groups in the network that can interact with water.

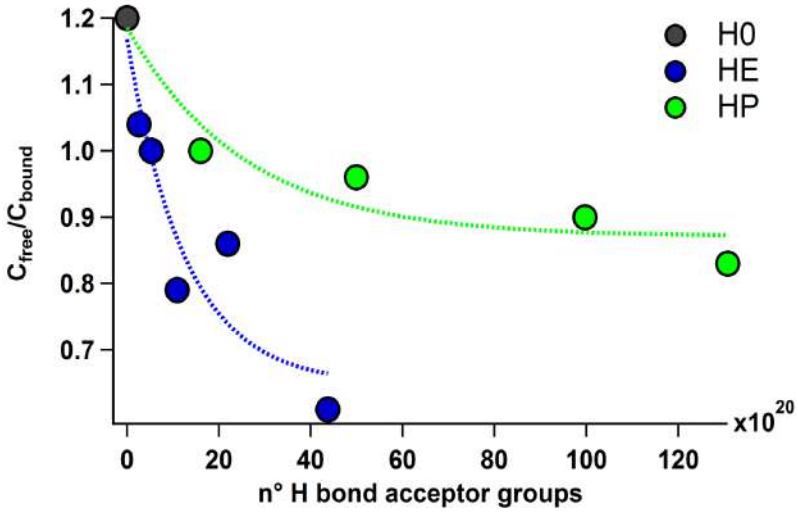

Figure 6. FWI/BWI in pHEMA hydrogels with EGDMA (blue) and PGD (green) as a function of hydrogen bond acceptor groups.

Regarding to semi-IPN pHEMA/PAA hydrogels, DSC thermograms and the calculated values of C_{free} and C_{bound} are reported in Figure 7 and Table S3 (in SI, section S4), respectively.

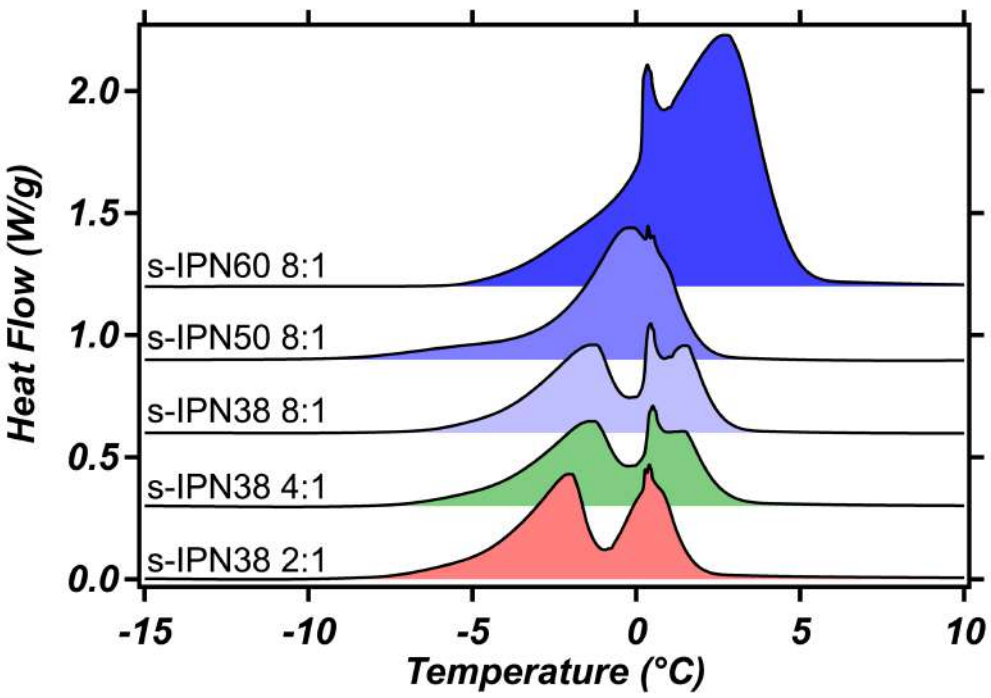

Figure 7. DSC thermograms of semi-IPN pHEMA/PAA hydrogels. The reported curves are offset along y-axis for clarity.

s-IPN60 8:1 and s-IPN50 8:1 curves (Figure 7) show only one broad peak; on the contrary, in pHEMA/PAA 38% series, it is possible to distinguish two different peaks, with the mainly of these related to bulk like water and the other one at lower temperature related to the loosely bound water. Considering pHEMA/PAA 8:1 series, the network with 60% of water has the higher C_{free}/C_{bound} ratio since a larger amount of water was used during the synthesis. On the contrary, in pHEMA/PAA 38% series, there are no appreciable differences of the C_{free}/C_{bound} ratio. Furthermore, the C_{free}/C_{bound} value is similar to that obtained for HE B, which has the same composition of the semi-IPN gels except for the absence of PAA. We can conclude that the presence of PAA trapped into the polymer network does not influence the free water fraction since PAA has almost the same capability of pHEMA to interact with water molecules. Therefore, the only parameter that can be

changed to modify the retention properties of hydrogels seems to be the percentage of cross-linking agent.

Diffusional properties of hydrophilic molecules inside hydrogels. pHEMA hydrogels, incubated with FITC (hydrodynamic radius = 0,54 nm[30]), FITC-dextran 4 kDa (hydrodynamic radius = 1,4 nm[31]) and FITC-dextran 40 kDa (hydrodynamic radius = 4,5 nm[31]), were analysed with confocal laser scanning microscopy to evaluate the diffusion coefficients and the possible interactions of these hydrophilic molecules with the networks.

In order to determine the diffusion coefficients of the hydrophilic solutes, FRAP experiments were performed. As an example, the FRAP curve of HE D hydrogel, loaded with FITC, is reported in Figure 8, while the FRAP curves of the other hydrogels and all the fitting parameters are reported in SI Section S5.

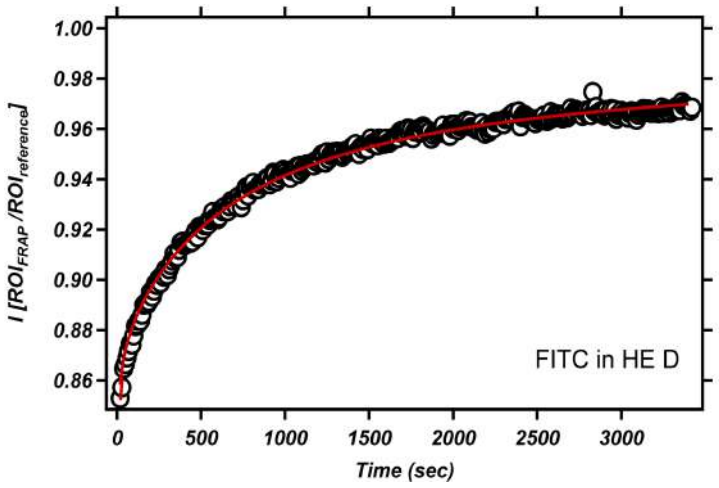

Figure 8. FRAP curve (markers) of HE D hydrogel loaded with FITC and its respective fitting (continuous line).

The obtained diffusion coefficients values, calculated from the FRAP curves performed on the hydrogels, ranging from 0.392 to 0.091 $\mu m^2/s$ (details of the values are reported in table S4 in SI)

and they decrease increasing the percentage of the cross-linking agent. These values are about three orders of magnitude lower than the FITC in water. In particular, the diffusion coefficient of FITC decreases of about 5% from H0 to HE E and 64% from H0 to HE D. The lowest diffusion coefficient value is measured in HE A containing the highest amount of cross-linker. We observe the same trend in the HP series but, comparing the values of D with those obtained for HE with the same amount of cross-linking agent, the motion of the probe is faster in HP networks. This can be explained considering that PGD has a longer chain with respect to EGDMA and this leads to a higher mobility of the polymeric network.

The FITC diffusion coefficients could be compared to the ratio between free and bound water. It is possible to note that probe mobility becomes higher increasing C_{free}/C_{bound} ratio, with a trend that seems to follow a sigmoidal function (Figure 9). In this regard, the diffusion process, which is mediated by the free water fraction, seems to be completely activated only after the C_{free}/C_{bound} ratio reaches the unity.

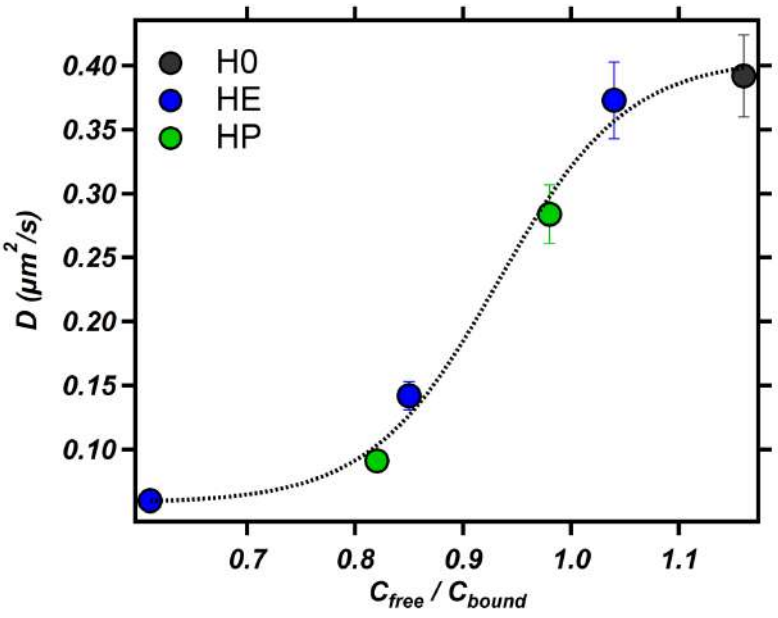

Figure 9. Trend of FITC diffusion coefficients as a function of the ratio between free and bound water in classical pHEMA hydrogels.

In the case of the other hydrophilic probes, i.e. FITC-dextran, confocal microscopy reveals that, differently from FITC, they do not enter into any of classical pHEMA hydrogels. In fact, in the case of FITC, the green fluorescence of the probe is evident both in solution and in the polymeric network (Figure 10A), while, in the case of FITC-dextran 4 kDa, the green fluorophore is confined only in solution (Figure 10B).

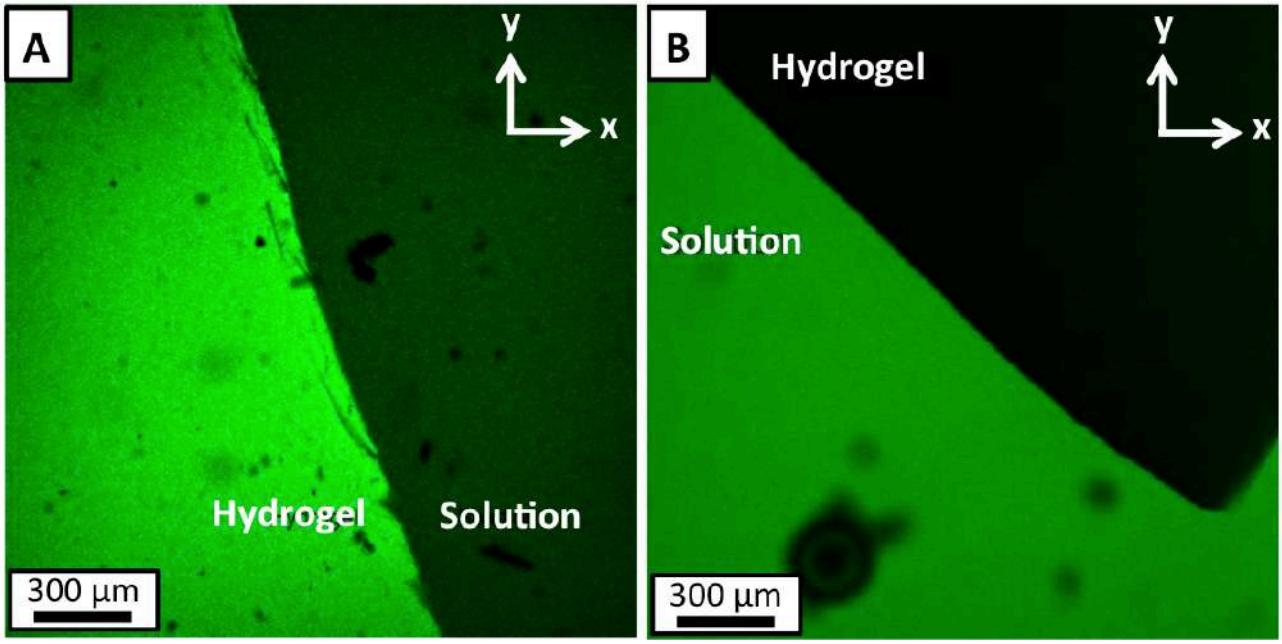

Figure 10. Confocal microscopy horizontal sections of HE D hydrogels loaded with aqueous solutions of FITC (A) and FITC-dextran 4 kDa (B).

Fluorescence measurements were performed in order to investigate the possible interactions between the fluorophore and the polymeric network. The protolytic constants of FITC relating the chemical activities of the cation, neutral, anion and dianion forms are pK_1= 2.08, pK_2= 4.31 and pK_3=6.43, respectively[47] (see Figure S5 in SI).

Figure 11 shows the fluorescence spectra of FITC measured in the solution in equilibrium with the hydrogels and inside classical pHEMA hydrogels.

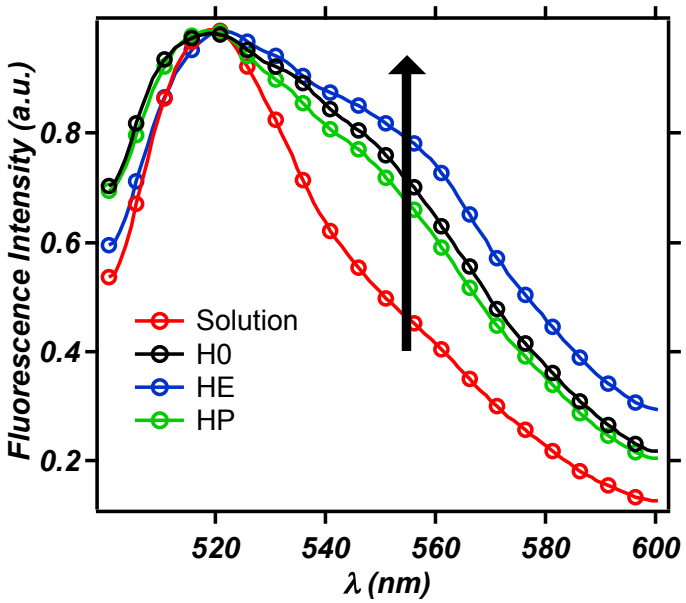

Figure 11. Fluorescence spectra of FITC in solution and in H0, HE D and HP D hydrogels. All data are normalized at 520 nm.

Since the pH value of the solution in equilibrium with the hydrogels is around 6.7, the fluorescence spectrum of FITC in solution presents an emission spectrum with one peak with a maximum at 520 nm, ascribable to the presence of the dianionic form of the FITC as reported by Sjoback et al.[48].

On the contrary, FITC spectra in H0, HE and HP networks show two broaden peaks, one centred at 520 nm, the other around 550 nm ascribable to the presence of FITC molecules in the mono-anionic form[48], due to the formation of hydrogen bonds between hydroxyl and carboxyl groups of fluorescein and hydroxyl groups of HEMA.

The mobility of the fluorescent molecules in the polymeric network of semi-IPN pHEMA/PAA hydrogels was evaluated by means of FRAP experiment (see Table S5 in the SI, section S6).

The diffusion coefficients of the probes in water are about four orders of magnitude higher than that calculated from the fitting of FRAP curves performed on pHEMA/PAA networks. This is a clear evidence of the confinement of the liquid phase inside the polymeric network. Comparing the diffusion coefficients of the different probe in the same hydrogel, we observe that it decreases of about one order of magnitude from FITC to FITC-dextran 4 kDa and FITC-dextran 40 kDa, according to an increase of the molecular dimension. In particular, FITC-dextran 40 kDa can enter only into s-IPN60 8:1 network since the mean mesh size of this network is higher than the others, as seen by SAXS experiments. Examining the diffusion of the same probe in the different networks, the calculated diffusion coefficients decrease with increasing the water content of the hydrogels, except in the case of FITC-dextran 4kDa, which diffuses faster in s-IPN50 8:1 than in s-IPN60 8:1 (Figure 13).

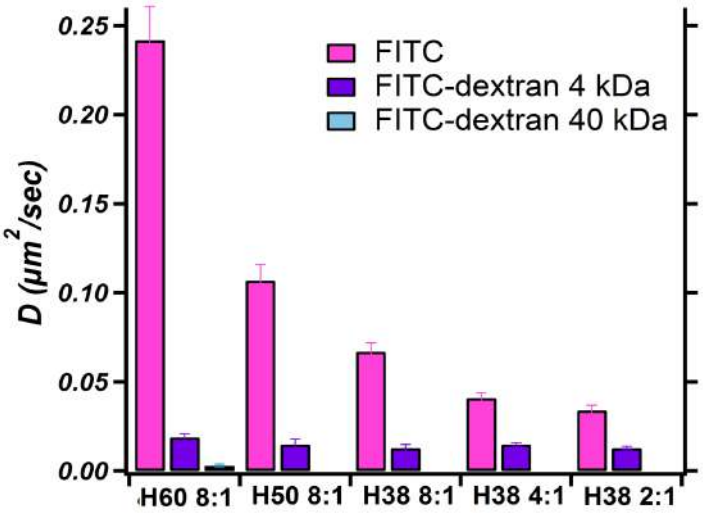

Figure 13. Diffusion coefficients of FITC (pink column), FITC-dextran 4 kDa (violet column) and FITC-dextran 40kDa (light blue column) in semi-IPN pHEMA/PAA hydrogels.

As in the case of classical pHEMA hydrogels, the fluorescence spectra of FITC were measured in the solution in equilibrium with the hydrogels and inside the polymeric network to assess possible interactions between the probe and the gel structure (Figure 14).

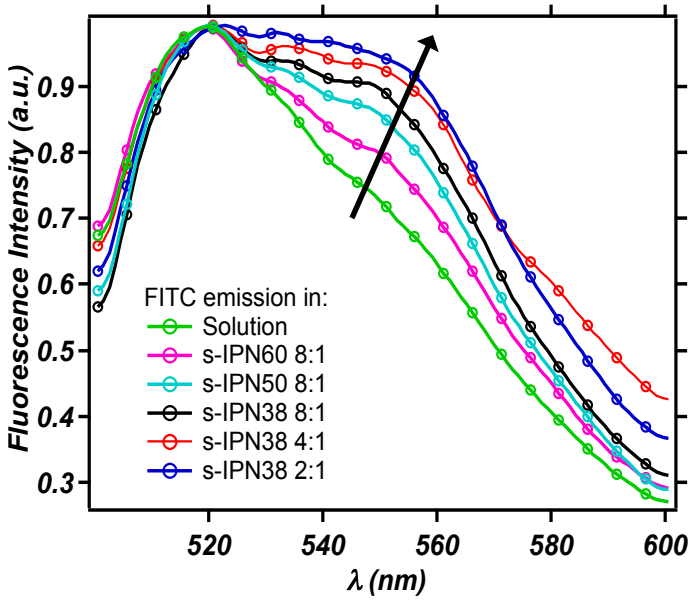

Figure 14: Fluorescence spectra of FITC in solution and in semi-IPN pHEMA/PAA hydrogels. All data are normalized at 520 nm.

As in the case of classical pHEMA networks, the fluorescence spectrum of FITC in the solution in equilibrium with the gel shows two peaks, one with a maximum at 520 nm, and the other, less intense, around 550 nm. This is consistent with the fact that the pH of the solution is about 5.2, so FITC is mainly present as anion. In the fluorescence spectra acquired on FITC loaded in pHEMA/PAA networks, we observe the same two peaks. In particular, considering pHEMA/PAA 8:1 series, the peak centred at 550 nm becomes more intense decreasing the water content of the

gel. In fact, in the hydrogels with lower water content, the probe interacts strongly with the network through hydrogen bonds between hydroxyl and carboxyl groups of fluorescein and hydroxylic and carboxylic groups of pHEMA and PAA, shifting the equilibrium to the anionic form of FITC. The same trend is observed increasing the amount of PAA, keeping constant the water content (from s-IPN38 8:1 to s-IPN38 2:1).

Conclusions

In this paper, we reported the synthesis and the characterization of classic pHEMA and semi-interpenetrating pHEMA/PAA hydrogels with different cross-linker/monomer ratio. These differences affect the network structure and the diffusional properties of the hydrogels. Considering pHEMA hydrogels, an increasing of cross-linker percentage doesn't seem to have a significant influence on the nanoscale structure of the polymeric network, but causes a decrease of the free/bound water ratio and the diffusion of FITC inside the hydrogels. A sigmoidal trend of D vs C_{free}/C_{bound} indicates that the diffusion becomes completely activated only when the hydrogel reaches a water-percolated state.

In the case of semi-IPN pHEMA/PAA hydrogels, SAXS analysis reveals the existence of solid-like inhomogeneity and, as regards pHEMA/PAA 8:1 series, FITC and FITC dextran 4 kDa can enter into all these three hydrogels, while FITC-dextran 40 kDa can penetrate only the network with 60% H_2O. In the case of s-IPN38 4:1 and s-IPN38 2:1, it was possible to establish that FITC, FITC-dextran 4 kDa and FITC-dextran 40 kDa can diffuse into both networks. The diffusion coefficients increase with the water content and with the decrease of the amount of PAA, as the result of a lower interaction between the probes and the polymeric network.

NOTES

The authors declare no competing financial interest.

ACKNOWLEDGMENT

The authors acknowledge financial support from Consorzio per lo sviluppo dei Sistemi a Grande Interfase (CSGI) and Ministero dell'Istruzione, dell'Università e della Ricerca (MiUR).

ASSOCIATED CONTENT

Supporting Information. Mathematical models, thermal analysis, FRAP experiments.

ABBREVIATIONS

Semi-IPN: semi-interpenetrating; DSC: differential scanning calorimetry; TGA: thermogravimetric analysis; FWI: free water index; BWI: bound water index; SAXS: small angle x-ray scattering; ROI: region of interest; FRAP: fluorescence recovery after photobleaching.

(1) Ozay, O.; Aktas, N.; Sahiner, N. Hydrogels as a Potential Chromatographic System: Absorption, Speciation, and Separation of Chromium Species from Aqueous Media. *Sep. Sci. Technol.* **2011**, *46* (9), 1450–1461. https://doi.org/10.1080/01496395.2011.560918.
(2) Boschetti, E. Preparative Chromatography Including 10th International Symposium on Preparative ChromatographyAdvanced Sorbents for Preparative Protein Separation Purposes. *J. Chromatogr. A* **1994**, *658* (2), 207–236. https://doi.org/10.1016/0021-9673(94)80017-0.
(3) Peppas, N. A.; Bures, P.; Leobandung, W.; Ichikawa, H. Hydrogels in Pharmaceutical Formulations. *Eur. J. Pharm. Biopharm. Off. J. Arbeitsgemeinschaft Für Pharm. Verfahrenstechnik EV* **2000**, *50* (1), 27–46.
(4) Amsden, B. Solute Diffusion within Hydrogels. Mechanisms and Models. *Macromolecules* **1998**, *31* (23), 8382–8395. https://doi.org/10.1021/ma980765f.
(5) Jones, D. S.; Lorimer, C. J.; Andrews, G. P.; McCoy, C. P.; Gorman, S. P. An Examination of the Thermorheological and Drug Release Properties of Zinc Tetraphenylporphyrin-Containing Thermoresponsive Hydrogels, Designed as Light Activated Antimicrobial Implants. *Chem. Eng. Sci.* **2007**, *62* (4), 990–999. https://doi.org/10.1016/j.ces.2006.10.017.
(6) Tanaka, H.; Matsumura, M.; Veliky, I. A. Diffusion Characteristics of Substrates in Ca-Alginate Gel Beads. *Biotechnol. Bioeng.* **1984**, *26* (1), 53–58. https://doi.org/10.1002/bit.260260111.
(7) Zustiak, S. P.; Boukari, H.; Leach, J. B. Solute Diffusion and Interactions in Cross-Linked Poly(Ethylene Glycol) Hydrogels Studied by Fluorescence Correlation Spectroscopy. *Soft Matter* **2010**, *6* (15). https://doi.org/10.1039/C0SM00111B.
(8) Wu, Y.; Joseph, S.; Aluru, N. R. Effect of Cross-Linking on the Diffusion of Water, Ions, and Small Molecules in Hydrogels. *J. Phys. Chem. B* **2009**, *113* (11), 3512–3520. https://doi.org/10.1021/jp808145x.
(9) Zaikov, G. E.; Iordanskiĭ, A. L.; Markin, V. S. *Diffusion of Electrolytes in Polymers*; VSP, 1988.

(10) Liu, D. E.; Kotsmar, C.; Nguyen, F.; Sells, T.; Taylor, N. O.; Prausnitz, J. M.; Radke, C. J. Macromolecule Sorption and Diffusion in HEMA/MAA Hydrogels. *Ind. Eng. Chem. Res.* **2013**, *52* (50), 18109–18120. https://doi.org/10.1021/ie402148u.
(11) Johansson, L.; Elvingson, C.; Lofroth, J. Diffusion and Interaction in Gels and Solutions .3. Theoretical Results. *Macromolecules* **1991**, *24* (22), 6024–6029. https://doi.org/10.1021/ma00022a019.
(12) Masaro, L.; Zhu, X. X. Physical Models of Diffusion for Polymer Solutions, Gels and Solids. *Prog. Polym. Sci.* **1999**, *24* (5), 731–775. https://doi.org/10.1016/S0079-6700(99)00016-7.
(13) Fujita, H. Diffusion in Polymer-Diluent Systems. In *Fortschritte Der Hochpolymeren-Forschung*; Advances in Polymer Science; Springer Berlin Heidelberg, 1961; pp 1–47. https://doi.org/10.1007/BFb0050514.
(14) Griffiths, P. C.; Stilbs, P.; Chowdhry, B. Z.; Snowden, M. J. PGSE-NMR Studies of Solvent Diffusion in Poly(N. *Colloid Polym. Sci. 273* (4), 405–411. https://doi.org/10.1007/BF00652357.
(15) Zhu, J.; Marchant, R. E. Design Properties of Hydrogel Tissue-Engineering Scaffolds. *Expert Rev. Med. Devices* **2011**, *8* (5), 607–626. https://doi.org/10.1586/erd.11.27.
(16) Meakin, J. R.; Hukins, D. W. L.; Aspden, R. M.; Imrie, C. T. Rheological Properties of Poly(2-Hydroxyethyl Methacrylate) (PHEMA) as a Function of Water Content and Deformation Frequency. *J. Mater. Sci. Mater. Med.* **2003**, *14* (9), 783–787.
(17) Opdahl, A.; Kim, S. H.; Koffas, T. S.; Marmo, C.; Somorjai, G. A. Surface Mechanical Properties of PHEMA Contact Lenses: Viscoelastic and Adhesive Property Changes on Exposure to Controlled Humidity. *J. Biomed. Mater. Res. A* **2003**, *67* (1), 350–356. https://doi.org/10.1002/jbm.a.10054.
(18) Zellander, A.; Wardlow, M.; Djalilian, A.; Zhao, C.; Abiade, J.; Cho, M. Engineering Copolymeric Artificial Cornea with Salt Porogen. *J. Biomed. Mater. Res. A* **2014**, *102* (6), 1799–1808. https://doi.org/10.1002/jbm.a.34852.
(19) Bhatia, S.; Bergethon, P. R.; Blease, S.; Kemper, T.; Rosiello, A.; Zimbardi, G. P.; Franzblau, C.; Spatz, E. L. A Synthetic Dural Prosthesis Constructed from Hydroxyethylmethacrylate Hydrogels. *J. Neurosurg.* **1995**, *83* (5), 897–902. https://doi.org/10.3171/jns.1995.83.5.0897.
(20) Young, C. D.; Wu, J. R.; Tsou, T. L. High-Strength, Ultra-Thin and Fiber-Reinforced PHEMA Artificial Skin. *Biomaterials* **1998**, *19* (19), 1745–1752.
(21) Bavaresco, V. P.; Zavaglia, C. a. C.; Malmonge, S. M.; Reis, M. C. Viability of PHEMA Hydrogels as Coating in Human Synovial Joint Prosthesis. *Mater. Res.* **2002**, *5* (4), 481–484. https://doi.org/10.1590/S1516-14392002000400014.
(22) Jeyanthi, R.; Rao, K. Invivo Biocompatibility of Collagen Poly(Hydroxyethyl Methacrylate) Hydrogels. *Biomaterials* **1990**, *11* (4), 238–243. https://doi.org/10.1016/0142-9612(90)90004-A.
(23) Varghese, S.; Elisseeff, J. H. Hydrogels for Musculoskeletal Tissue Engineering. In *Polymers for Regenerative Medicine*; Werner, C., Eisseeff, J. H., Fischbach, C., Freier, T., Garcia, A. J., Mooney, D. J., Pompe, T., Salchert, K., Varghese, S., Werner, C., et al., Eds.; Springer-Verlag Berlin: Berlin, 2006; pp 95–144.
(24) Peppas, N. A.; Moynihan, H. J.; Lucht, L. M. The Structure of Highly Crosslinked Poly(2-Hydroxyethyl Methacrylate) Hydrogels. *J. Biomed. Mater. Res.* **1985**, *19* (4), 397–411. https://doi.org/10.1002/jbm.820190405.

(25) Wang, J.; Li, X. Enhancing Protein Resistance of Hydrogels Based on Poly(2-Hydroxyethyl Methacrylate) and Poly(2-Methacryloyloxyethyl Phosphorylcholine) with Interpenetrating Network Structure. *J. Appl. Polym. Sci.* **2011**, *121* (6), 3347–3352. https://doi.org/10.1002/app.33960.
(26) Han, Y. A.; Lee, E. M.; Ji, B. C. Mechanical Properties of Semi-Interpenetrating Polymer Network Hydrogels Based on Poly(2-Hydroxyethyl Methacrylate) Copolymer and Chitosan. *Fibers Polym.* **2008**, *9* (4), 393–399. https://doi.org/10.1007/s12221-008-0063-8.
(27) Garcı´a, O.; Blanco, M. D.; Martı´n, J. A.; Teijón, J. M. 5-Fluorouracil Trapping in Poly (2-Hydroxyethyl Methacrylate-Co-Acrylamide) Hydrogels: In Vitro Drug Delivery Studies. *Eur. Polym. J.* **2000**, *36* (1), 111–122.
(28) Ahmed, E. M. Hydrogel: Preparation, Characterization, and Applications: A Review. *J. Adv. Res.* **2015**, *6* (2), 105–121. https://doi.org/10.1016/j.jare.2013.07.006.
(29) Domingues, J. A. L.; Bonelli, N.; Giorgi, R.; Fratini, E.; Gorel, F.; Baglioni, P. Innovative Hydrogels Based on Semi-Interpenetrating p(HEMA)/PVP Networks for the Cleaning of Water-Sensitive Cultural Heritage Artifacts. *Langmuir* **2013**, *29* (8), 2746–2755. https://doi.org/10.1021/la3048664.
(30) Fowlkes, J. D.; Hullander, E. D.; Fletcher, B. L.; Retterer, S. T.; Melechko, A. V.; Hensley, D. K.; Simpson, M. L.; Doktycz, M. J. Molecular Transport in a Crowded Volume Created from Vertically Aligned Carbon Nanofibres: A Fluorescence Recovery after Photobleaching Study. *Nanotechnology* **2006**, *17* (22), 5659–5668. https://doi.org/10.1088/0957-4484/17/22/021.
(31) Watson, P. M. D.; Paterson, J. C.; Thom, G.; Ginman, U.; Lundquist, S.; Webster, C. I. Modelling the Endothelial Blood-CNS Barriers: A Method for the Production of Robust in Vitro Models of the Rat Blood-Brain Barrier and Blood-Spinal Cord Barrier. *BMC Neurosci.* **2013**, *14* (1), 59. https://doi.org/10.1186/1471-2202-14-59.
(32) Braeckmans, K.; Peeters, L.; Sanders, N. N.; De Smedt, S. C.; Demeester, J. Three-Dimensional Fluorescence Recovery after Photobleaching with the Confocal Scanning Laser Microscope. *Biophys. J.* **2003**, *85* (4), 2240–2252. https://doi.org/10.1016/S0006-3495(03)74649-9.
(33) Fecchio, B. D.; Valandro, S. R.; Neumann, M. G.; Cavalheiro, C. C. S. Thermal Decomposition of Polymer/Montmorillonite Nanocomposites Synthesized in Situ on a Clay Surface. *J. Braz. Chem. Soc.* **2015**. https://doi.org/10.5935/0103-5053.20150216.
(34) Lele, A. K.; Hirve, M. M.; Badiger, M. V.; Mashelkar, R. A. Predictions of Bound Water Content in Poly(N-Isopropylacrylamide) Gel. *Macromolecules* **1997**, *30* (1), 157–159. https://doi.org/10.1021/ma950894l.
(35) Müller-Plathe, F. Different States of Water in Hydrogels? *Macromolecules* **1998**, *31* (19), 6721–6723.
(36) Carretti, E.; Grassi, S.; Cossalter, M.; Natali, I.; Caminati, G.; Weiss, R. G.; Baglioni, P.; Dei, L. Poly(Vinyl Alcohol)-Borate Hydro/Cosolvent Gels: Viscoelastic Properties, Solubilizing Power, and Application to Art Conservation. *Langmuir* **2009**, *25* (15), 8656–8662. https://doi.org/10.1021/la804306w.
(37) Bhagwan, P. *A Handbook Of Thermodynamics*; Mittal Publications.
(38) T. N. Blanton, T. C. H. JCPDS--International Centre for Diffraction Data Round Robin Study of Silver Behenate. A Possible Low-Angle X-Ray Diffraction Calibration Standard.

Powder Diffr. - POWDER DIFFR **1995**, *10*, 91–95. https://doi.org/10.1017/S0885715600014421.
(39) Soumpasis, D. M. Theoretical Analysis of Fluorescence Photobleaching Recovery Experiments. *Biophys. J.* **1983**, *41* (1), 95–97.
(40) P., Terech. In *Encyclopedia of Surface and Colloid Science*; Marcel Dekker: New York, 2002; pp 2299–2319.
(41) Kanaya, T.; Takahashi, N.; Nishida, K.; Seto, H.; Nagao, M.; Takeba, Y. Dynamic and Static Fluctuations in Polymer Gels Studied by Neutron Spin-Echo. *Phys. B Condens. Matter* **2006**, *385*, 676–681.
(42) Pezron, I.; Djabourov, M.; Leblond, J. Conformation of Gelatin Chains in Aqueous-Solutions .1. a Light and Small-Angle Neutron-Scattering Study. *Polymer* **1991**, *32* (17), 3201–3210. https://doi.org/10.1016/0032-3861(91)90143-7.
(43) Debye, P.; Bueche, A. M. Scattering by an Inhomogeneous Solid. *J. Appl. Phys.* **1949**, *20* (6), 518–525. https://doi.org/10.1063/1.1698419.
(44) Mannhold, R.; Poda, G. I.; Ostermann, C.; Tetko, I. V. Calculation of Molecular Lipophilicity: State-of-the-Art and Comparison of Log P Methods on More than 96,000 Compounds. *J. Pharm. Sci.* **2009**, *98* (3), 861–893.
(45) Sander, T.; Freyss, J.; von Korff, M.; Rufener, C. DataWarrior: An Open-Source Program for Chemistry Aware Data Visualization and Analysis. *J. Chem. Inf. Model.* **2015**, *55* (2), 460–473.
(46) Wang, Y.; Tan, G.; Zhang, S.; Guang, Y. Influence of Water States in Hydrogels on the Transmissibility and Permeability of Oxygen in Contact Lens Materials. *Appl. Surf. Sci.* **2008**, *255* (2), 604–606.
(47) Mchedlov-petrossyan, N. O.; Isaenko, Y. V.; Vodolazkaya, N. A.; Goga, S. T. Acid-Base Behavior of Fluorescein Isothiocyanate in Aqueous Media and in Micellar Surfactant Solutions.
(48) Sjoback, R.; Nygren, J.; Kubista, M. Absorption and Fluorescence Properties of Fluorescein. *Spectrochim. Acta Part -Mol. Biomol. Spectrosc.* **1995**, *51* (6), L7–L21. https://doi.org/10.1016/0584-8539(95)01421-P.

TOC

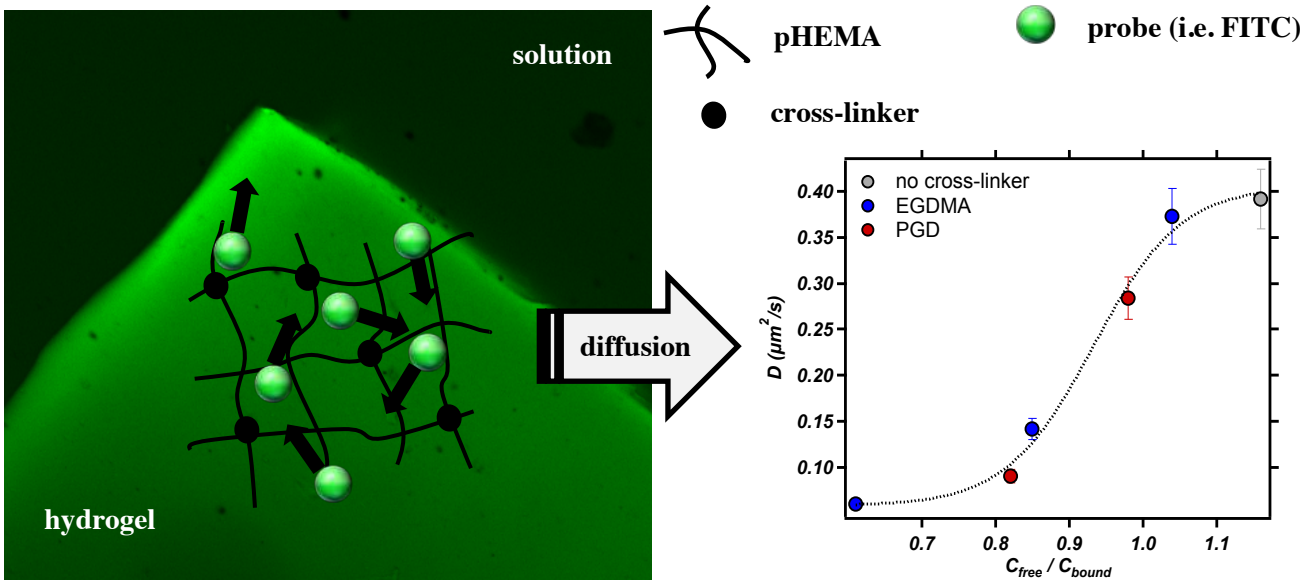
solution
hydrogel
diffusion
pHEMA
probe (i.e. FITC)
cross-linker
no cross-linker
EGDMA
PGD
D (μm²/s)
0.40
0.35
0.30
0.25
0.20
0.15
0.10
0.7
0.8
0.9
1.0
1.1
C_free / C_bound

Supporting Information

S1. Cross-linkers: molecular structure

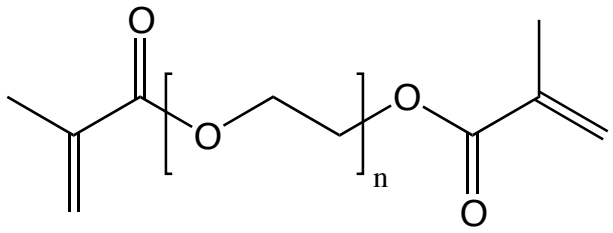

Figure S1. Molecular structure of the cross-linkers: n=1 for EGDMA molecules while n = 9 for PGD molecules (PGD M_w =550 Da).

S2. SAXS models

In the case of classical pHEMA hydrogels, the scattering curves can be analyzed using the Ornstein-Zernike equation (Eq. 1), q-dependent, plus an instrumental flat background, bkg[1].

$$I_{sol}(q) = \frac{I_{lor}(0)}{1+\zeta^2 q^2} + bkg \qquad (1)$$

where $I_{lor}(0)$ is the scattering intensity at q = 0, dependent from the contrast between the polymer and the solvent and from the volume fraction of the polymer in the gel, and ζ is the characteristic average mesh size (or correlation length) of the network.

Concerning the semi-IPN pHEMA networks, the Ornstein-Zernicke equation is not enough to describe the scattering curves, thus it is necessary to add another term (Eq. 2) in order to take into account the deviations from the ideal case, usually related to solid-like inhomogeneities[2]:

$$I_{ex}(q) = \frac{I_{ex}(0)}{(1+a^2q^2)^2} \quad (2)$$

where $I_{ex}(0)$ represents the excess intensity at q = 0 and a is the length scale that characterizes gel inhomogeneities. Therefore, the obtained SAXS profiles can be described by the Debye-Bueche equation[3] (Eq. 3):

$$I(q) = I_{sol}(q) + I_{ex}(q) + bkg \quad (3)$$

S3. FRAP analysis: Soumpasis model

The FRAP curves can be described with a model proposed by Soumpasis[4] (Eq. 4), that implies a diffusion-limited fluorescence recovery:

$$f(t) = a_0 + a_1 e^{\frac{2\tau_D}{t-t_{bleach}}}\left(I_0\left(\frac{2\tau_D}{t-t_{bleach}}\right) + I_1\left(\frac{2\tau_D}{t-t_{bleach}}\right)\right) \quad (4)$$

where a_0, a_1 are two normalizing coefficients introduced to account respectively for the non-zero intensity at the bleach moment and the incomplete recovery, t_{bleach} is the bleach time, τ_D is the characteristic timescale for diffusion, I_0, I_1 are the modified Bessel functions of the zero and first order (Eq. 5):

$$I_\alpha(x) = \frac{1}{\pi}\int_0^\pi exp(x \cdot cos\theta) \cdot cos(\alpha\theta)d\theta - \int_0^\infty exp(-x \cdot cosht - \alpha t)dt \quad (5)$$

where α is 0 for the zero order function and 1 for the first order function, while x is defined as follow (Eq.6):

$$x = \frac{2\tau_D}{(t-t_{bleach})} \quad (6)$$

The diffusion coefficient for a bleach spot of radius *w* can be calculated from τ_D according to Eq.7:

$$\tau_D = \frac{w^2}{4D} \quad (7)$$

S4. Thermal analysis

	EWC %
s-IPN60 8:1	54.5 ± 0.5
s-IPN50 8:1	42.4 ± 0.4
s-IPN38 8:1	38.8 ± 0.4
s-IPN38 4:1	37.7 ± 0.4
s-IPN38 2:1	37.5 ± 0.4

Table S1. Equilibrium water content % of semi-IPN pHEMA/PAA hydrogels.

	ΔH_{tr} (J/g)	C_{free}	C_{bound}	C_{free}/C_{bound}
HE A	53.2	0.16	0.26	0.61
HE B	63.7	0.19	0.22	0.86
HE C	64.4	0.19	0.24	0.79
HE D	67.6	0.20	0.20	1.00
HE E	75.9	0.23	0.22	1.04
H0	78.9	0.24	0.20	1.20

HP A	62.0	0.19	0.23	0.83
HP F	62.1	0.19	0.21	0.90
HP G	65.4	0.20	0.20	0.96
HP D	69.5	0.21	0.21	1.00

Table S2. Data obtained from DSC analysis of classical pHEMA hydrogels.

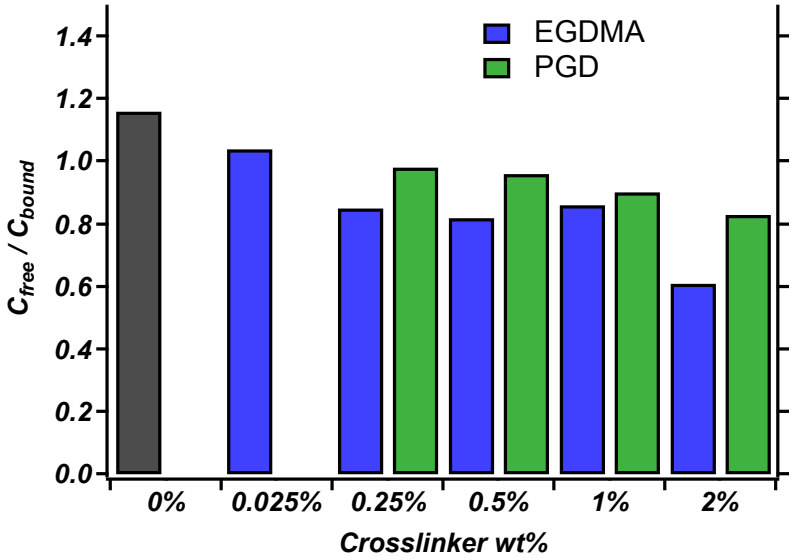

Figure S2. C_{free}/C_{bound} in pHEMA hydrogels with EGDMA (blue) and PGD (green) as a function of cross-linker percentage.

	ΔH_{tr} (J/g)	**C_{free}**	**C_{bound}**	**C_{free}/C_{bound}**
s-IPN60 8:1	141.6	0.42	0.12	3.52
s-IPN50 8:1	62.0	0.19	0.24	0.79
s-IPN38 8:1	57.8	0.17	0.22	0.77
s-IPN38 4:1	56.2	0.17	0.21	0.81

s-IPN38 2:1	57.3	0.17	0.20	0.85

Table S3. Data obtained from DSC analysis of semi-IPN pHEMA/PAA hydrogels.

S5. FRAP experiment

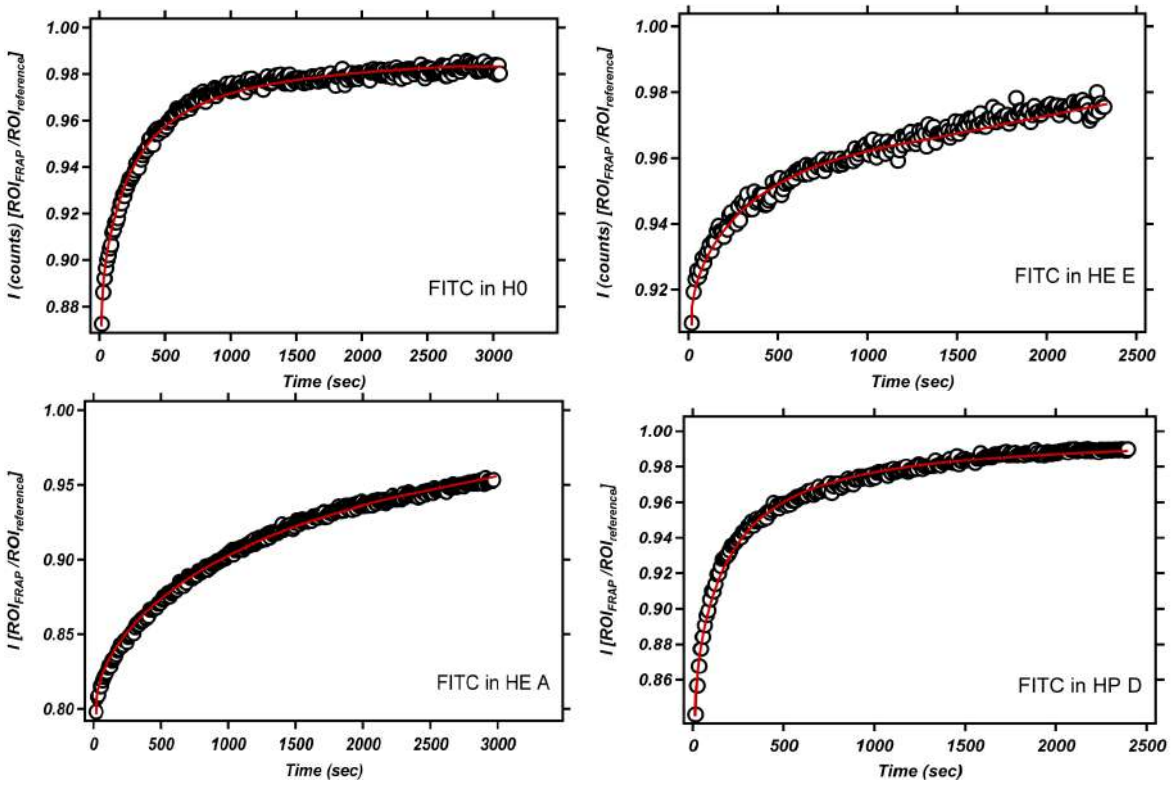

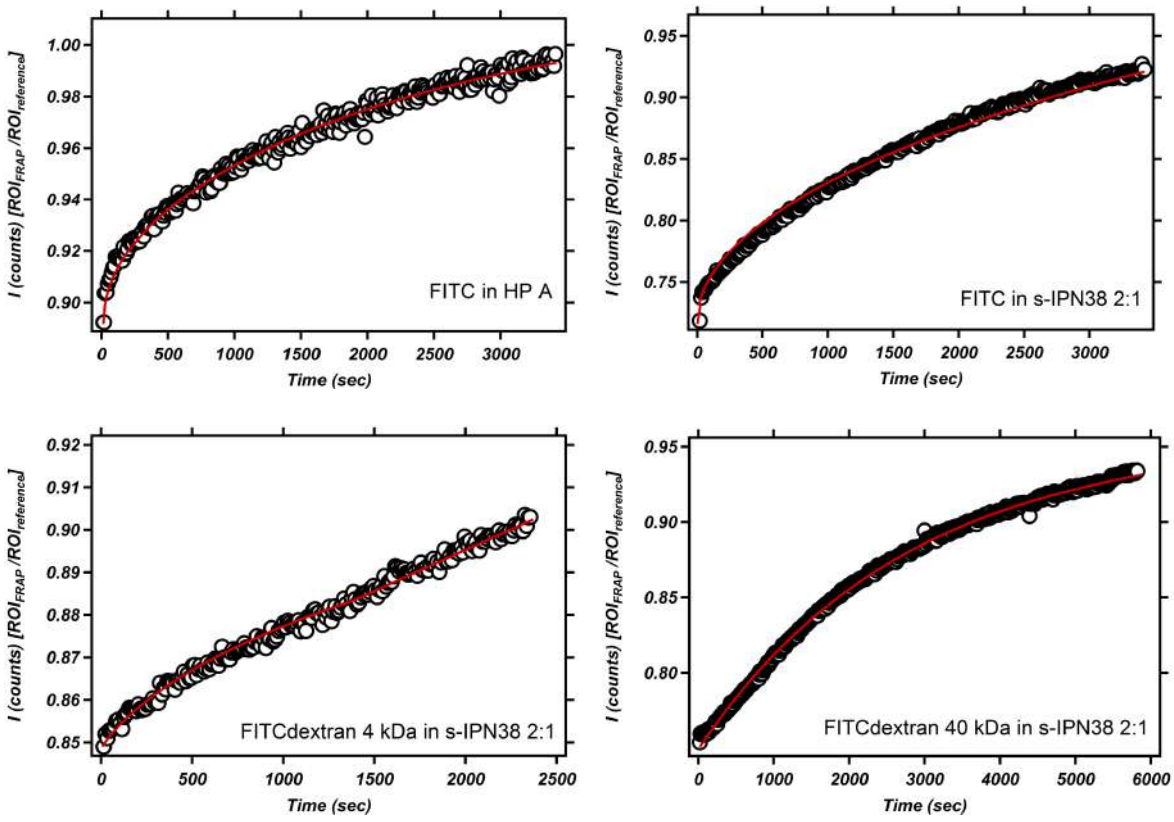

Figure S4. FRAP curves and relative fitting of classical and semi-IPN hydrogels.

Table S4 lists the values of the parameters calculated from the Soumpasis model for classical pHEMA hydrogels loaded with FITC.

	cross-linker/HEMA molar ratio (*10^{-3})	**FITC - D ($\mu m^2/s$)**
Water solution	-	397[a]
H0	0	0.392 ± 0.032
HE A	13.1	0.060 ± 0.005
HP A	13.1	0.091 ± 0.007
HE D	1.6	0.142 ± 0.011
HP D	1.6	0.286 ± 0.023
HE E	0.8	0.373 ± 0.030

Table S4. Diffusion coefficients of FITC in classical pHEMA hydrogels. [a]Diffusion coefficient of FITC in water solution was calculated from the Stokes-Einstein equation at 20 °C $\left(D = \frac{kT}{6\pi\eta R_h}\right)$, where η is the viscosity of the solvent (i.e 1 cP) and R_h hydrodynamic of the fluorophore (i.e 0.54 nm for FITC).

Table S5 reports the calculated diffusion coefficients of the semi-IPN hydrogels.

	FITC D (μm²/s)	**FITC-dextran 4 kDa D (μm²/s)**	**FITC-dextran 40 kDa D (μm²/s)**
Water	397[a]	153[a]	48[a]
s-IPN60 8:1	0.242 ± 0.019	0.028 ± 0.002	0.003 ± 0.001
s-IPN50 8:1	0.107 ± 0.009	0.038 ± 0.003	-
s-IPN38 8:1	0.067 ± 0.005	0.021 ± 0.002	-
s-IPN38 4:1	0.041 ± 0.003	0.015 ± 0.001	-
s-IPN38 2:1	0.034 ± 0.003	0.013 ± 0.001	-

Table S5. Diffusion coefficients of the different probes in semi-IPN pHEMA/PAA hydrogels. [a]Diffusion coefficient of probes in solution are obtained from Stokes-Einstein equation.

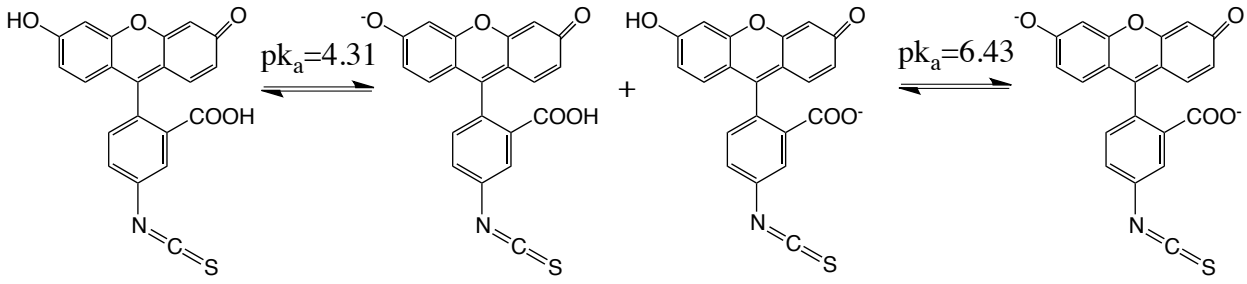

Neutral form Anionic form Dianionic form

Figure S5. Ionization equilibria of FITC as a function of pH.

	a0	**a1**	**τ (s)**	**D (*μ*m2/s)**
H0				
FITC	0.873	0.119	195 ± 16	0.392 ± 0.032
HE E				
FITC	0.719	0.246	205 ± 16	0.373 ± 0.030
HE D				
FITC	0.853	0.136	541 ± 43	0.142 ± 0.011
HE A				
FITC	0.798	0.222	1267 ± 101	0.060 ± 0.005
HP D				
FITC	0.704	0.317	268 ± 21	0.286 ± 0.023
HP A				
FITC	0.728	0.335	839 ± 67	0.091 ± 0.007
s-IPN60 8:1				
FITC	0,803	0,157	317 ± 25	0,242 ± 0,019
FITC-dextran 4 kDa	0,812	0,170	2703 ± 216	0,028 ± 0,002
FITC-dextran 40 kDa	0,833	0,616	23127 ± 1850	0,003 ± 0,001
s-IPN50 8:1				
FITC	0,918	0,071	713 ± 57	0,107 ± 0,009
FITC-dextran 4 kDa	0,907	0,073	2001 ± 160	0,038 ± 0,003
s-IPN38 8:1				

FITC	0,801	0,185	1145 ± 91	0,067 ± 0,005
FITC-dextran 4 kDa	0,930	0,056	3594 ± 287	0,021 ± 0,002
s-IPN38 4:1				
FITC	0,854	0,177	1873 ± 149	0,041 ± 0,003
FITC-dextran 4 kDa	0,888	0,155	5108 ± 409	0,015 ± 0,001
s-IPN38 2:1				
FITC	0,840	0,108	2283 ± 183	0,034 ± 0,003
FITC-dextran 4 kDa	0,719	0,490	5813 ± 465	0,013 ± 0,001

Table S6: Fitting parameters of FRAP curves: classical and semi-IPN hydrogels.

(1) P., Terech. In *Encyclopedia of Surface and Colloid Science*; Marcel Dekker: New York, 2002; pp 2299–2319.

(2) Pezron, I.; Djabourov, M.; Leblond, J. Conformation of Gelatin Chains in Aqueous-Solutions .1. a Light and Small-Angle Neutron-Scattering Study. *Polymer* **1991**, *32* (17), 3201–3210. https://doi.org/10.1016/0032-3861(91)90143-7.

(3) Debye, P.; Bueche, A. M. Scattering by an Inhomogeneous Solid. *J. Appl. Phys.* **1949**, *20* (6), 518–525. https://doi.org/10.1063/1.1698419.

(4) Soumpasis, D. M. Theoretical Analysis of Fluorescence Photobleaching Recovery Experiments. *Biophys. J.* **1983**, *41* (1), 95–97.

Paper IV

Marta Rossi, David Chelazzi, Teresa Guaragnone, Emiliano Fratini, and Piero Baglioni.

Manuscript to be submitted.

List of papers

pHEMA/PAA and pHEMA/PVP semi-IPNs: effect of pH and loading with tetraethylenepentamine for the removal of bronze corrosion products

Marta Rossi, David Chelazzi, Teresa Guaragnone, Emiliano Fratini*, Piero Baglioni*

Department of Chemistry "Ugo Schiff" and CSGI, University of Florence, via della Lastruccia 3-Sesto Fiorentino, I-50019, Florence, Italy.

*email: chelazzi@csgi.unifi.it; emiliano.fratini@unifi.it

KEYWORDS: semi-IPN; hydrogel; pHEMA; PAA; PVP; TEPA; copper ions; cleaning; corroded bronze.

Abstract

Bronze artifacts constitute a fundamental portion of cultural heritage, but there is a lack of effective methodologies for the removal of corrosion layers, such as those produced by the "bronze disease". We propose for the first time networks of poly(2-hydroxyethyl methacrylate) (pHEMA) semi-interpenetrated (semi-IPN) with polyacrylic acid (PAA) or polyvinylpyrrolidone (PVP), loaded with tetraethylenepentamine (TEPA) for the removal of copper corrosion products. Alkaline pH causes the ionization of carboxyls in PAA increasing the swelling and the porosity of the pHEMA/PAA semi-IPN. In pHEMA/PVP, increasing the pH leads to the co-presence of the enol and enolate forms of PVP,

along with significant changes in the macroporosity and a decrease in the mesh size. 2D FTIR imaging indicates that TEPA interacts with carboxylates in PAA, and with polar or charged CO groups in PVP. Upon application of the gels onto corroded bronze, copper oxychlorides dissolve and migrate inside the gels. Cu(II) ions probably form ternary complexes with TEPA and carboxylates in PAA or CO in PVP. The application of the semi-IPNs allowed the gradual and effective removal of oxychlorides, leaving unaltered patinas of cuprite that are needed to passivate bronze against corrosion. Loading the semi-IPNs with TEPA provides a much higher cleaning efficacy than traditional EDTA, opening new perspectives in the restoration of bronze works of art.

INTRODUCTION

The conservation of cultural heritage has deep societal and economic implications, because well preserved and accessible works of art constitute both a drive for social inclusion and an important resource to promote tourism and job creation [1] . Metallic objects and artifacts constitute a vast part of the artistic and architectural production spanning over millennia, however they are typically affected by several degradation processes that can significantly alter their appearance and integrity. In particular, copper-based artifacts are affected by corrosion phenomena that induce the formation of a complex patina on their surface, usually characterized by the presence of copper oxychlorides (atacamite and its polymorphs) responsible of the so called "bronze disease", a cyclic degradative process able to consume the objects up to their complete disgregation[23]. The removal of corrosion products is thus a fundamental operation in conservation practice, but still an open challenge that needs feasible solutions. Traditionally, cleaning is performed by mechanical (vibrating or abrasive tools, ultra-high-pressure water)[4], optical (laser ablation), or chemical wet methods (bases, acids and complexing agents)[5]. However, these approaches involve several risks for the artifacts, unless time consuming protocols are adopted: mechanical treatments and non-confined cleaning fluids are invasive and

scarcely selective, while laser ablation can trigger heating processes on the artifacts' surfaces[6,5]. The confinement of cleaning fluids is an optimal strategy to achieve controlled removal without risks for the objects, but traditional thickeners used in restoration (e.g. cellulose derivatives, viscous dispersions of polyacrylic acid) are either not enough retentive, or exhibit poor mechanical properties and thus tend to leave residues on the treated surfaces [7]. In the last decade, chemical hydrogels have been proposed as optimal matrices to confine fluids for the safe cleaning of works of art [8,9,10,11]. In particular, polymeric networks of poly(2-hydroxyethyl methacrylate) (pHEMA) semi-interpenetrated (semi-IPN) with polyvinylpyrrolidone (PVP) have advantageous properties similar to the average of the two homopolymers characteristics, i.e. the mechanical strength of pHEMA and the hydrophilicity of PVP, resulting in ideal mechanical properties and retentiveness. In this contribution, pHEMA/PVP semi-IPNs were used as confining matrices for cleaning solutions, based on the aforementioned advantages and on the ability of PVP to form complexes with metal ions[1], which is expected to enhance the removal of corrosion patinas. Besides PVP, we also considered polyacryilic acid (PAA) as semi-interpenetrating polymer in the pHEMA network, owing to its ability to give strong coordination bonds at alkaline pH, thanks to the presence of carboxylate groups[13]; the latter also account for the ability of PAA to associate with water molecules and swell extensively at alkaline pH when the polymer deprotonates and unfolds[14]. We chose tetraethylenpentamine (TEPA) as a cleaning fluid to upload in the semi-IPNS owing to its high complexing selectivity to Cu(II) ions, which are typically found in detrimental and defacing corrosion products (Cu(II) oxides and carbonates, copper oxychlorides). In fact, the complex formed by Cu(II) and TEPA has a stability constant ($\log K_f$ = 22.8 at 25°C[15]) four orders of magnitude higher than that of the complex formed with the tetrasodium salt of ethylenediaminetetraacetic acid (EDTA, Y^{4-}) ($\log K_f$ = 18.8 at 25°C and 1 M)[16], the chelating agent traditionally employed by conservators in the removal of copper corrosion products [4, 17].

The pHEMA/PVP and pHEMA/PAA semi-IPNS were swollen in water at different pH values (6, 8, 12), and in a water solution of TEPA (pH 12), and analyzed by small angle X-ray scattering (SAXS) and scanning electron microscopy (SEM), to investigate structural differences at the micron- and nano-scale. Differential scanning calorimetry (DSC) and thermogravimetric analysis (TGA) were employed to evaluate the gels' solvent content, and the properties of water entrapped in the polymeric networks. Fourier Transform Infrared Spectroscopy (FTIR) measurements were performed, using a Focal Plane Array (FPA) detector, to gain information on the composition and structure of the polymers in the semi-IPNS, and on their interaction with TEPA and copper(II) ions. Finally, the semi-IPNS were applied on corroded bronze mock-ups, and their ability to solubilize and remove copper oxychlorides was inquired with FTIR-FPA chemical mapping with spatial resolution at the micron-scale.

EXPERIMENTAL SECTION

Materials 2-Hydroxyethyl methacrylate (HEMA) (purity 99%), poly(acrylic acid) (PAA) (average Mn ≈ 1200 kDa), azoisobutyronitrile (AIBN) (purity 98%), N,N-methylene-bis(acrylamide) (MBA) (purity 99%), poly(vinylpyrrolidone) (PVP) (average Mn ≈ 1300 kDa), tetraethylenepentamine (TEPA) (purity ≥95%), sodium hydroxide pellets (purity 97%), ethylenediaminetetraacetic acid disodium salt dihydrate (EDTA) (purity 98.5-101.5%) were purchased from Sigma-Aldrich and used as received. Water was purified by a Millipore Milli-Q gradient system (resistivity >18 MΩ·cm).

Hydrogels synthesis The pHEMA/PVP semi-IPN was prepared by radical polymerization as reported by Domingues et al [1]. Some variations in the synthetic process were adopted: the HEMA/PVP ratio was changed from 30/70 to 27.5/72.5 (% w/w), the water content in the pre-gel solution was 62.2% instead of 65%, while the cross-linker concentration was halved; these changes were due to the necessity of having slightly softer and more flexible gel sheets to adapt the rough surface of corrosion patinas.

The pHEMA/PAA semi-IPN was synthesized adding an aqueous solution of PAA to HEMA monomer and AIBN. The ratio between the mass of pHEMA and PAA (96.5/3.5 % w/w), was chosen in order to have a molar ratio between -OH and -COOH groups of 16/1, which proved to be an optimal condition to favor the synthetic process, yielding gels with good mechanical properties. After sonication and degassing, the mixture was transferred between two glassy covers and polymerized at 60°C for 4 hours. After the reaction, a 2 mm thick flat hydrogel sheet was obtained; the gel was then washed by renewing water once a day for 7 days to remove residues of unreacted monomers and free PAA molecules. Table 1 shows the composition of the two hydrogels.

Both semi-IPNs were swollen in water, reaching a stable pH of 6.3. Small pieces (5 x 5 x 0.2 cm^3) were cut and swollen with water at pH 8 and 12 (adjusted with a sodium hydroxide solution), and in a water solution of TEPA (20% w/w). In all cases, the gels were placed in the NaOH or TEPA solutions for at least 5 days, using an excess of solution as compared to the gel's mass, to make sure that the semi-IPNs exchanged completely.

Semi-IPN	pHEMA/PAA	Semi-IPN	pHEMA/PVP
HEMA (wt%)	52.5%	HEMA (wt%)	10.3
water (wt%)	45.2%	Water (wt%)	62.2
MBA (wt%)	-	MBA (wt%)	0.4
AIBN (wt%)	0.4%	AIBN (wt%)	0.1
PAA (wt%)	1.8%	PVP (wt%)	27.0
HEMA/PAA ratio (%w/w)	96.5/3.5	HEMA/PVP ratio (%w/w)	27.5/72.5

Table 1. Composition of pHEMA/PAA and pHEMA/PVP semi-IPNs.

Thermal analyses Thermogravimetric analysis (TGA) was carried out with a SDT Q600 (TA Instruments). The balance sensitivity is 0.1 μg. Measurements were performed in a nitrogen atmosphere with a flow rate of 100 mL/min. The samples were put in open alumina pans, and the analyses were performed with a heating rate of 10 °C/min from 25 °C to 450 °C[19].

The equilibrium water content (EWC) and the equilibrium solvent content (ESC) were calculated as follows (Eq. 1):

$$EWC(ESC) = \frac{W - W_d}{W} \quad (1)$$

where W is the weight of the hydrated sample and W_d the weight of the dry sample. The values of W_d were experimentally determined from TGA analysis, considering the weight of the sample at c.a. 200 and 300°C to quantify the EWC (semi-IPNs swollen in water) and the ESC (semi-IPNs swollen in TEPA) respectively.

Differential scanning calorimetry analysis (DSC) was performed with a Q2000 Calorimeter (TA Instruments). The temperature range was from -80 °C to 200 °C with a scan rate of 2 °C/min; sealed stainless steel pans were used. From the DSC curves it is possible to determine the different types of water present in the hydrogels[20]. Water in porous systems like gels can be classified as non-freezing bound water, free or bulk water[21]. The non-freezing water forms hydrogen bonds with the functional groups of the polymer, rather than with other water molecules (as would be necessary for water to freeze); bulk water has the same properties of pure water and can thus bind with other water molecules to form ice crystals when temperature is around 0°C.

Thus, it is possible to determine the free water index (FWI) according to the following equation (Eq. 2):

$$FWI = \frac{\Delta H_{tr}}{\Delta H_f \times EWC} \quad (2)$$

where ΔH_{tr} (J/g) is the heat of transition obtained by the integral of melting peaks around 0°C in the DSC curves, and ΔH_f is the theoretical value of the specific enthalpy of fusion of water at 0 °C (333,6 J/g[22]).

Scanning electron microscopy SEM investigation was performed on the xerogels, obtained by freeze-drying thin slices of the hydrogels. A FEG-SEM ΣIGMA (Carl Zeiss, Germany) was used to acquire the images using an acceleration potential of 2 kV and a working distance of 3 mm. Before carrying out the analysis, the samples were coated with a thin layer of gold using an Agar Scientific Auto Sputter Coater.

Small angle x-ray scattering Small angle x-ray scattering analysis (SAXS) were carried out with a HECUS S3-MICRO SWAXS camera, equipped with a Hecus System3 2D-point collimator and two position-sensitive detectors (PSD-50M) containing 1024 channels with a width of 54 microns. The copper anode from the Oxford 50 W microfocus source emits radiation with the wavelength of the Kα-line given by λ= 1.542 Å. The Kβ-line is removed by FOX-3D single-bounce multilayer point focussing optics (Xenocs, Grenoble). The voltage is generated by the GeniX X-ray generator (Xenocs, Grenoble). The sample-to-detector distance was 281 mm. The volume between sample and detector was kept under vacuum in order to minimize the scattering from the air. This camera was calibrated in the small angle region using silver behenate, which is known to have a well-defined lamellar structure (d = 58.38 Å)[23]. Scattering curves were acquired in the q-range between 0.01 and 0.55 $Å^{-1}$. Samples were placed into demountable cells, with kapton film used as windows. The temperature control was set to 25°C by a Peltier element, with an accuracy of ± 0.1 °C. All the scattering curves were corrected for the empty cell and water contribution considering the relative transmission factors.

2D FTIR imaging 2D FTIR imaging analysis was carried out on xerogels and bronze mock-ups, using a Cary 620-670 FTIR microscope, equipped with an FPA 128 x 128 detector (Agilent Technologies). This set up allows the highest spatial resolution currently available to FTIR

microscopes. The spectra were recorded directly on the surface of the samples (gels, corroded bronze coins, or the Au background) in reflectance mode, with open aperture and a spectral resolution of 4 cm^{-1}, acquiring 128 scans for each spectrum. A ‘‘single-tile” analysis results in a map of 700 x 700 μm^2 (128 x 128 pixels), and the spatial resolution of each imaging map is 5.5 μm (i.e. each pixel has dimensions of 5.5 x 5.5 μm^2). Multiple tiles can be acquired to form mosaics. In order to improve the readability of the spectra, the background noise was reduced using the ‘‘smooth” tool (set at 11) of the Igor Pro software (Wavemetrics), taking care not to alter any diagnostic information deemed useful to this investigation. In each 2D map, the intensity of characteristic bands of the gels, or of bronze corrosion products, was imaged. The chromatic scale of the maps shows increasing absorbance of the bands as follows: blue < green < yellow < red.

Bronze mock-ups and cleaning procedure To evaluate the gels' effectiveness, cleaning tests were carried out on an artificially aged bronze coin, which was provided by CNR-ISMN (Rome, Italy). The artificial aging procedure, developed by Ingo et al., produces corrosion patinas that are similar in appearance and composition to those of archeological bronze artifacts [24]. Small sheets of the two gels (1 x 1 x 0.02 cm^3) were loaded either with a 20% (w/w) TEPA or with a 9.7% (w/w) EDTA aqueous solution, both at pH 12. EDTA was considered as a reference complexing agent in the restoration practice; 9.7% is the maximum concentration of the compound at pH 12. The gels were applied twice on the coin surface for 45 minutes, covered with parafilm to limit evaporation of fluids from the polymer network. During the application, the strong blue color of the gels indicates the absorption of Cu(II) ions and the formation of Cu(II) complexes. After the treatment, the coin substrate was rinsed with water and air-dried. 2D FTIR Imaging was carried out on the coin surface before and after the application of the gels, checking the presence of corrosion products and gel residues.

RESULTS AND DISCUSSION

FEG-SEM images were acquired to understand how the pH influences their microstructure. At pH 6, pHEMA/PAA semi-IPN has a compact structure and does not present any porosity at the microscale (Figure 1 a), while at pH 8 it shows a quite homogeneous porosity in the 7-10 μm range (Figure 1b). A more heterogeneous structure is noted at pH=12, where pores have irregular shape and broad size distribution from 1 to 15 μm (Figure 1c). All pHEMA/PVP semi-IPNs exhibit a microporosity: at pH 6 (Figure 1d) the pores have dimensions of 5-12 μm and fairly regular shape, while at pH 8, (Figure 1e) it is possible to observe three different size distributions (i.e. < 1 μm, 4-5 μm, and 14-20 μm); at pH 12 pores have elongated shapes and are arranged in rows in a more ordered pattern, with dimensions ranging from 2 to 8 μm (Figure 1f). When the gels are loaded with TEPA, the polyethylene amine completely fills the pores, and a plain smooth surface is observed, with no relevant features.

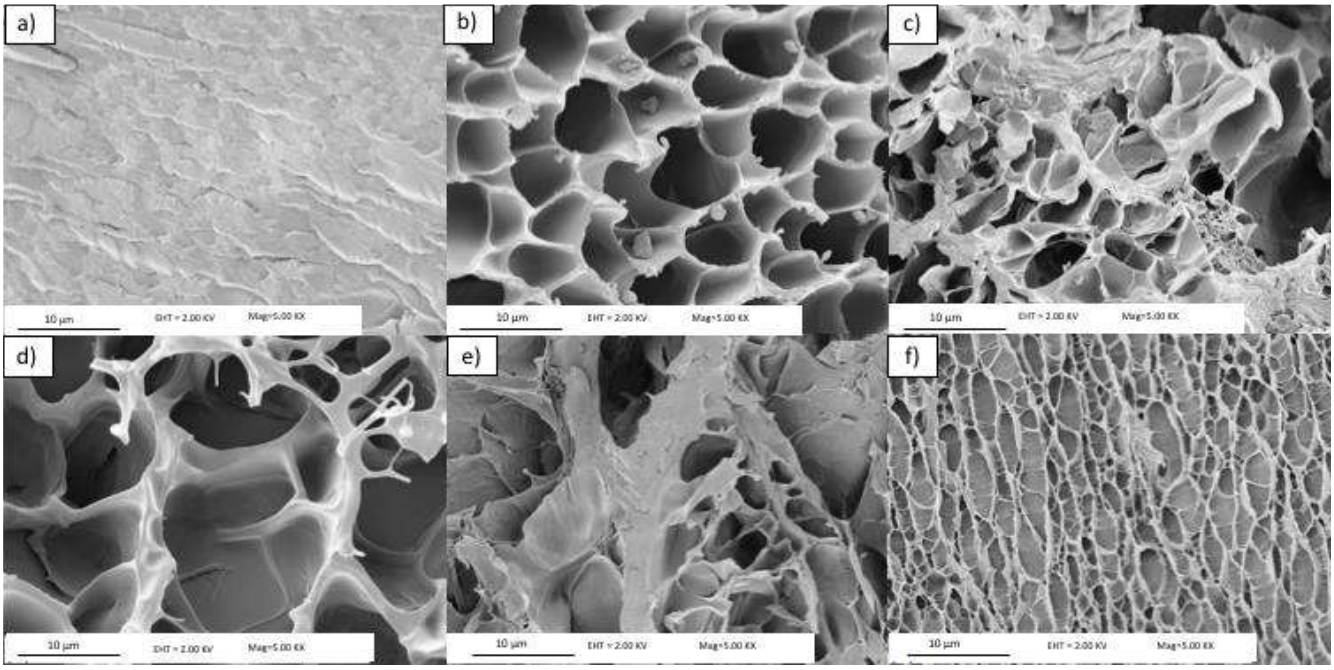

Figure 1. SEM images of pHEMA/PAA and pHEMA/PVP xerogels obtained from the corresponding hydrogels swollen in water at pH 6 (1a, 1d), 8 (1b, 1e), and 12 (1c, 1f). Bar is 10 μm.

SAXS experiments were carried out to investigate changes in the nanostructure of the semi-IPNs due to variations of pH, the presence of TEPA, and the co-presence of TEPA and Cu(II) ions (following the application of the gels onto corroded bronze coins). Figure 2 and 3 show respectively the SAXS curves of pHEMA/PAA and pHEMA/PVP hydrogels at pH 6, 8 and 12 (2a and 3a), and loaded with TEPA (2b) or with TEPA and Cu(II) ions (3b), after subtraction of cell contribution. All the SAXS curves were modelled using a generalized version of the Debye-Bueche approach[25], with two q-dependent contributions and an instrumental flat background [26] (Eq.3):

$$I(q) = I_{sol}(q) + I_{ex}(q) + bkg \qquad (3)$$

The first contribution $I_{sol}(q)$ is a generalized version of the Ornstein-Zernicke equation (Eq.4)

$$I_{sol}(q) = \frac{I_{lor}(0)}{[1+(\zeta q)^{m}]} \qquad (4)$$

where $I_{lor}(0)$ is the scattering intensity at q = 0, dependent from the contrast between the polymer and the solvent and from the volume fraction of the polymer in the gel, ζ is the characteristic average mesh size (or correlation length) of the network, and m is the Porod exponent associated with the solvation term. The second contribution $I_{ex}(q)$ is related to the excess of scattering at low q caused by the solid-like inhomogeneities of the polymeric network (Eq.5):

$$I_{ex}(q) = \frac{I_{ex}(0)}{(1+a^2q^2)^2} \qquad (5)$$

where $I_{ex}(0)$ represents the excess intensity at q = 0 and a is the length scale that characterizes gel inhomogeneities.

The fitting parameters of the SAXS curves of pHEMA/PAA semi-IPNs swollen in water (Figure 2a) are reported in Table 2. The average mesh size increases moving from pH 6 to pH 12, which can be explained considering the electrostatic repulsion between PAA chains when the carboxyl groups are ionized, leading to the stretching of the polymer chains[27]. Consistently, an increase of EWC is observed

with increasing pH values, in agreement with other studies where the mesh dimension is strongly related to the equilibrium water content[28]. The Porod exponent has a value of ca. 3.8 for the hydrogel at pH 6, suggesting that the polymer network is collapsed, while at pH 8 and 12 the exponent is around 2.3 for both systems, indicating that the hydrogels are in a theta solvent. The dimension of spatial inhomogeneities increases from 1.7 nm at pH 6 to 7.3 nm at pH 8, and ca. 5 at pH 12, suggesting that the increase in water content (higher EWC) leads to a less homogeneous semi-IPN at the nanoscale[18].

When pHEMA/PAA is loaded with a water solution of TEPA (20%, pH=12) the mesh size and the dimension of solid-like inhomogeneities are smaller than those of gels simply loaded with water at the same pH, while the Porod exponent is slightly higher. These changes are ascribable to interactions between TEPA and the carboxylic groups in PAA, where molecules of TEPA might interpose between chains of PAA, screening the repulsion between carboxylate groups, and making the semi-IPN tighter. A further decrease of the mesh and inhomogeneities size is observed in the presence of copper II ions. Cheng et al. reported a decrease of the radius of gyration (R_g) for a poly(N-isopropylacrylamide) copolymer hydrogel that adsorbed Cu(II), and such change was ascribed to the formation of complexes between the ions and chelating groups in the polymer chains[29]. In our case, the lower mesh is likely due to the formation of complexes bewteen Cu(II) and ionized carboxylic groups of PAA, e.g. each copper ion coordinating with two $-COO^-$ groups from different chains[30]. Besides, a small decrease in the EWC (about 6%) is observed, in agreement with the lower mesh size value[28]. Finally, the increase in the Porod exponent (see Table 2) indicates a transition to a denser aggregate structure.

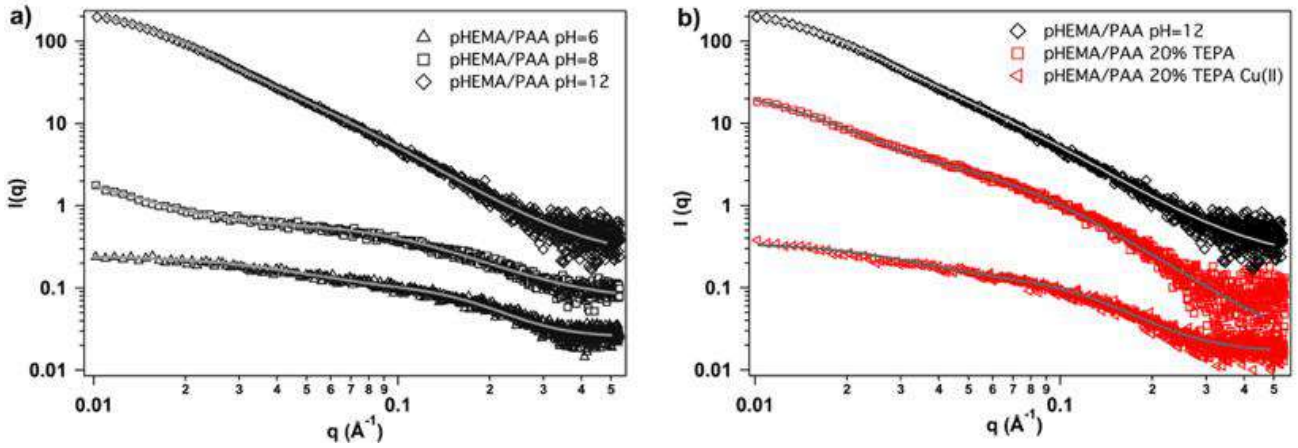

Figure 2. SAXS curves and fitting (grey lines) of pHEMA/PAA semi-IPNs swollen in water (a) at pH 6 (triangles), 8 (squares), and 12 (diamonds), and loaded with TEPA (b, red squares) or TEPA and copper II ions (b, red triangles).

	pH=6	pH=8	pH=12	20%TEPA	20%TEPA Cu(II)
I_0	1.37 ± 0.05	2.77 ± 0.05	11.15 ± 0.58	9.48 ± 0.19	3.36 ± 0.09
ζ (nm)	0.60 ± 0.01	0.83 ± 0.01	1.82 ± 0.06	1.14 ± 0.02	0.78 ± 0.01
m	3.75 ± 0.16	2.29 ± 0.05	2.34 ± 0.04	2.43 ±0.03	3.33 ± 0.07
I_{ex}	2.67 ± 0.05	13.35 ± 0.96	144.33 ± 0.99	79.30 ± 0.89	7.86 ± 0.17
a (nm)	1.67 ± 0.06	7.28 ± 0.03	4.96 ± 0.05	5.54 ± 0.05	2.52 ± 0.07
bkg	0.44 ± 0.01	0.34 ± 0.01	0.11 ± 0.01	0.03 ± 0.01	0.54 ± 0.01

Table 2. Fitting parameters obtained from SAXS curves of pHEMA/PAA semi-IPNs

Regarding pHEMA/PVP semi-IPNs (see Table 3 and Figure 3a), the average mesh size at pH=6 is in agreement with previous studies[18], and remains unchanged at pH=8, while at pH 12 it decreases of about 1 nm. At alkaline pH values (>> 10), the enol tautomer of PVP can lose a proton to form an enolate[31]. The partial deprotonation might lead to an enhancement of inter and intramolecular hydrogen bonds between enol and enolate groups in the PVP chains, resulting in a smaller mesh size and in a

more compact structure, as also suggested by the slight increase of the Porod exponent. The gel swollen in a water solution of TEPA (pH=12) exhibits the smallest value of ζ (ca. 2 nm) and the highest value of m (2.7) (see Table 3). When Cu(II) is absorbed in the hydrogel, similarly low values are found. This behavior can be explained considering that enolate groups are able to interact with TEPA molecules and Cu(II) ions, closing together in the formation of complex structures.

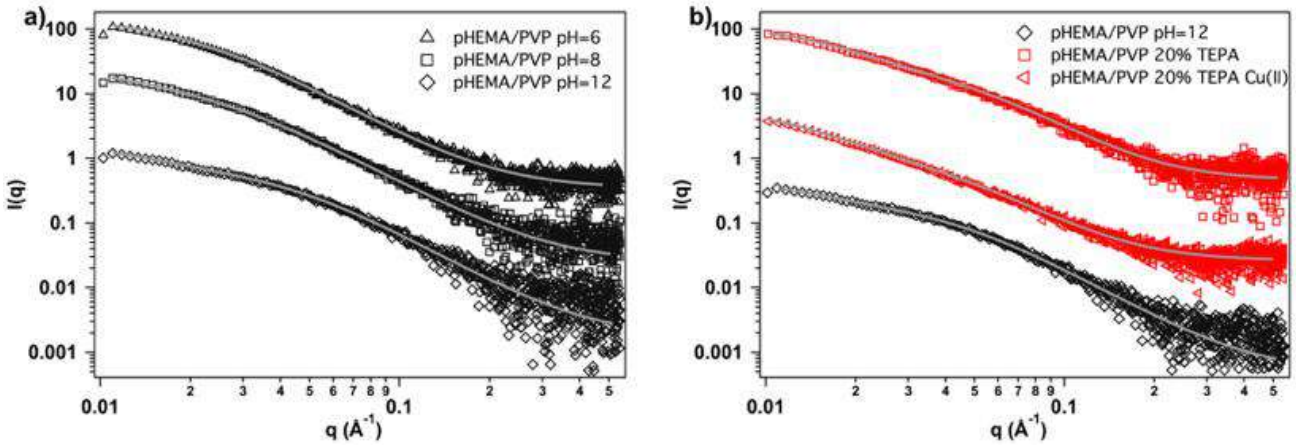

Figure 3. SAXS curves and fitting (grey lines) of pHEMA/PVP semi-IPNs swollen in water (a) at pH 6 (triangles), 8 (squares), and 12 (diamonds), and loaded with TEPA (b, red squares) or TEPA and copper II ions (b, red triangles).

	pH=6	pH=8	pH=12	20%TEPA	20%TEPA Cu(II)
I_0	25.26 ± 11.3	37.70 ± 5.39	15.46 ± 0.63	7.31 ± 0.41	10.78 ± 0.54
ζ (nm)	3.43 ± 0.54	3.81 ± 0.23	2.34 ± 0.06	1.94 ± 0.06	2.28 ± 0.07
m	2.49 ± 0.03	2.44 ± 0.02	2.58 ± 0.03	2.69 ±0.05	2.61 ± 0.05
I_{ex}	68.48 ± 8.84	62.19 ± 2.92	34.90 ± 2.03	46.35 ± 0.62	89.08 ± 0.98
a (nm)	4.93 ± 0.57	6.85 ± 0.83	6.50 ± 0.37	5.05 ± 0.10	6.15 ± 0.09

bkg	0.20 ± 0.01	0.09 ± 0.01	0.04 ± 0.01	0.20 ± 0.01	0.38 ± 0.01

Table 3. Fitting parameters obtained from SAXS curves of pHEMA/PVP semi-IPNs.

The study of the amount and type of water loaded in the hydrogels provided information on the absorption and permeation properties of these systems. The DSC curves of all the gels are reported in the SI (Figure S1 and S2). The EWC in pHEMA/PAA semi-IPNs, swollen at different pH, is mainly due to the gels' porosity and the hydrophilic character of PAA. At pH 6, where the carboxylic group are completely protonated, the EWC is about 43% (see Table 4), similar to that of classical pHEMA chemical gels[32,33], and it increases up to 57 and 79% at pH 8 and 12, owing to the ionization of the carboxyls. When the semi-IPN is loaded with TEPA (pH 12), the solvent content is c.a. 76%. After the absorption of Cu(II) this value decreases to 71%, indicating that some free water and TEPA are lost through evaporation during the application of the gel on the bronze coin, despite having covered the gel with parafilm. The FWI values increase passing from pH 6 to 12 (see Table 4), consistently with the presence of more hydrophilic moieties in the network (carboxylate groups in PAA), and with a higher meso- and microporosity as shown by SAXS and SEM measurements.

	pH 6	pH 8	pH 12	TEPA	TEPA Cu
ΔH_{tr} (J/g)	76.5 ± 1.7	154.3 ± 1.27	293.2 ± 6.1	127.4 ± 4.1	109.0 ± 3.1
EWC	42.9% ± 0.9%	56.8% ± 1.1%	79.1 % ± 3.7%	76.3% ± 1.6%	71.3% ± 1.4%
FWI	0.53 ± 0.02	0.81 ± 0.02	1.11 ± 0.07	0.50 ± 0.03	0.46 ± 0.02

Table 4. Data obtained from DSC and TGA analysis of pHEMA/PAA semi-IPNs swollen in water at pH 6, 8, and 12 and in TEPA water solution before and after Cu(II) uptake.

Both the EWC and FWI of the pHEMA/PVP semi-IPNs remain unchanged when the gels are swollen in water at different pH (Table 5). In any case, these parameters have higher values than those of pHEMA/PAA gels, which is explained considering the high relative content of PVP, a highly

hydrophilic polymer. The EWC does not change significantly in the presence of TEPA and Cu(II) ions, demonstrating the high hydrophilicity of these systems.

It must be noticed that for both systems there is a significant decrease in the heat of the melting transition (ΔH_{tr}, see Table 4 and 5) when Cu(II) ions are absorbed in the gels. The FWI decreases accordingly. This was explained considering that part of the bulk water molecules coordinate with the metal ions, participating in the formation of complexes.

	pH 6	pH 8	pH 12	TEPA	TEPA Cu
ΔH_{tr} (J/g)	296.1 ± 3.9	317.2 ± 1.1	299.5 ± 5.26	154.6 ± 2.5	133.5 ± 4.1
EWC	88.3% ± 0.5%	89.1% ± 1.3%	89.0% ± 2.1%	86.5% ± 0.01%	85.6% ± 0.8%
FWI	1.01 ± 0.02	1.07 ± 0.02	1.01 ± 0.04	0.54 ± 0.01	0.47 ± 0.02

Table 5. Data obtained from DSC and TGA analysis of pHEMA/PVP semi-IPNs swollen in water at pH 6, 8, and 12 and in TEPA water solution before and after Cu(II) uptake.

Further information on the chemical changes of the semi-IPNs at different pH, and upon loading of TEPA and Cu(II) ions, were provided by FTIR 2D Imaging. At pH 6, the spectra of the pHEMA/PAA semi-IPN exhibit features typical of reflective surfaces, with derivative-shaped peaks and distorsions (see Figure 4). In particular, the OH stretching and CH stretching bands of pHEMA and PAA are not observable, and the main peaks are those of C=O stretching (derivative shape, maximum at 1745 cm^{-1}), CH_2 bending (1496 cm^{-1}), C-O stretching (1294 cm^{-1}), and C-O-C stretching (derivative shape, maximum at 1197 cm^{-1}, and 1092 cm^{-1})[34,35]. At alkaline pH values the spectra change significantly, and their aspect resemble much more closely that of standard transmission spectra. This indicates that a change in the refractive index of the gel has occurred, following the neutralization of the carboxyl groups in PAA and the rearrangement of the polymer chains. Both the OH and CH stretching bands are

clearly observable, and the C=O stretching peak shows two components around 1740 (pHEMA) and 1715 (PAA) cm^{-1} [34,35]. Besides, the spectra show a new peak at 1578 cm^{-1}, assigned to the antysimmetric stretching of the $–COO^-$ groups in PAA, whose intensity increases passing from pH 8 to pH 12 (as shown in the FTIR maps in Figure 4). Besides, while at pH 8 the carboxylate groups concentrate in domains ranging from tens to hundreds of microns, at pH 12 they are homogeneously distributed across the gel matrix.

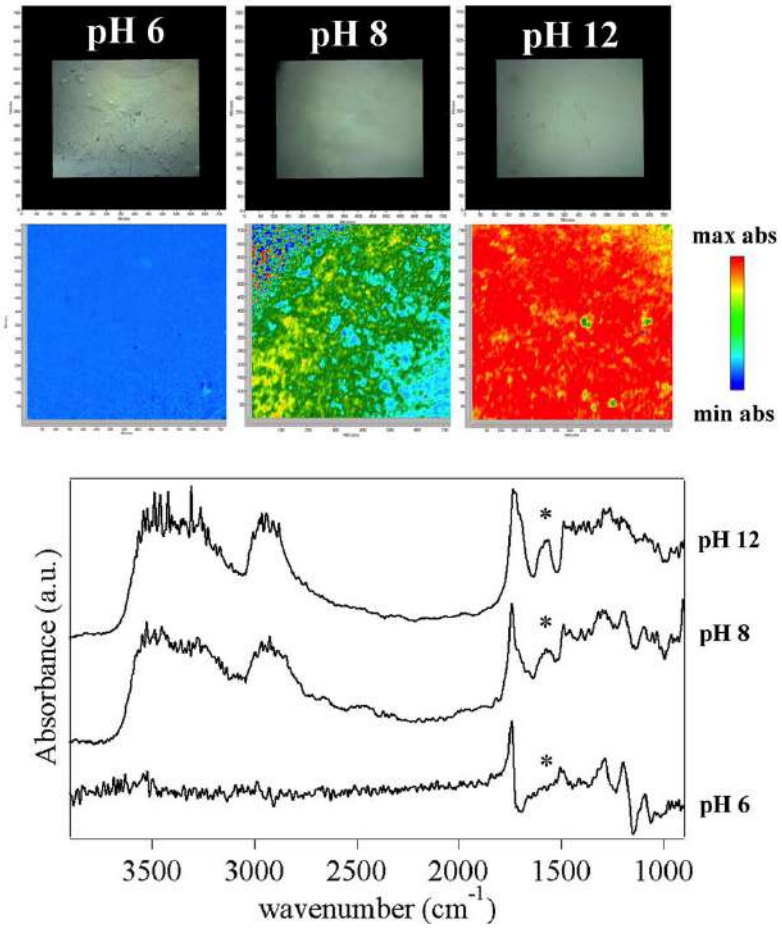

Figure 4. FTIR 2D Imaging of pHEMA/PAA xerogels obtained from hydrogels that were swollen with water at different pH values. Below each visible image, the corresponding 2D FTIR Imaging map shows the intensity of the band at 1578 cm^{-1} ($-COO^-$ antysimmetric stretching of carboxylate groups in

PAA). All maps have dimensions of 700 x 700 μm^2, each axis tick being 50 μm. The bottom panel shows representative spectra of pixels (5.5 x 5.5 μm^2) in the corresponding 2D Imaging map.

Figure 5 shows the FTIR 2D imaging of pHEMA/PAA xerogels obtained from semi-IPNs loaded with TEPA. Loading with the polyethylene amine changes the refractive index of the gels, which show again strongly derivative-shaped C=O and C-O-C stretching bands. The most relevant feature is a composite band that shows two maxima at 1660 and 1610 cm^{-1}. The latter is ascribed to the NH deformation of primary amine in TEPA[36], while the first component can be assigned to the stretching vibration of the carboxylic groups in PAA, when they are neutralized by a polyethylene amine[37]. Namely, the amine group of TEPA interacts with the acid sites of PAA, interfering with the interchain hydrogen bonds; the H atom of the carboxylic group is included in the amine groups, and the carboxylate vibration is shifted to a higher wavenumber with respect to the gels swollen in water solutions at the same pH. As shown by the 2D Imaging maps, in the presence of Cu(II) ions, the peak is no longer clearly observable, all across the gel's surface. Our hypothesis is that the carboxylate vibration is either shifted back to lower wavenumbers (convoluting with the TEPA NH deformation band), or its intensity is decreased, following the formation of a ternary polymer-metal complex by both PAA and TEPA with the copper ions. In fact, Kabanov et al.[38], reported the formation of mixed Cu(II) complexes formed by PAA and polyethylene imines (PEI), where two coordination sites are covered by PAA carboxylates, and two by amine groups. A similar behavior might occur in the case of the PAA-Cu-TEPA complex.

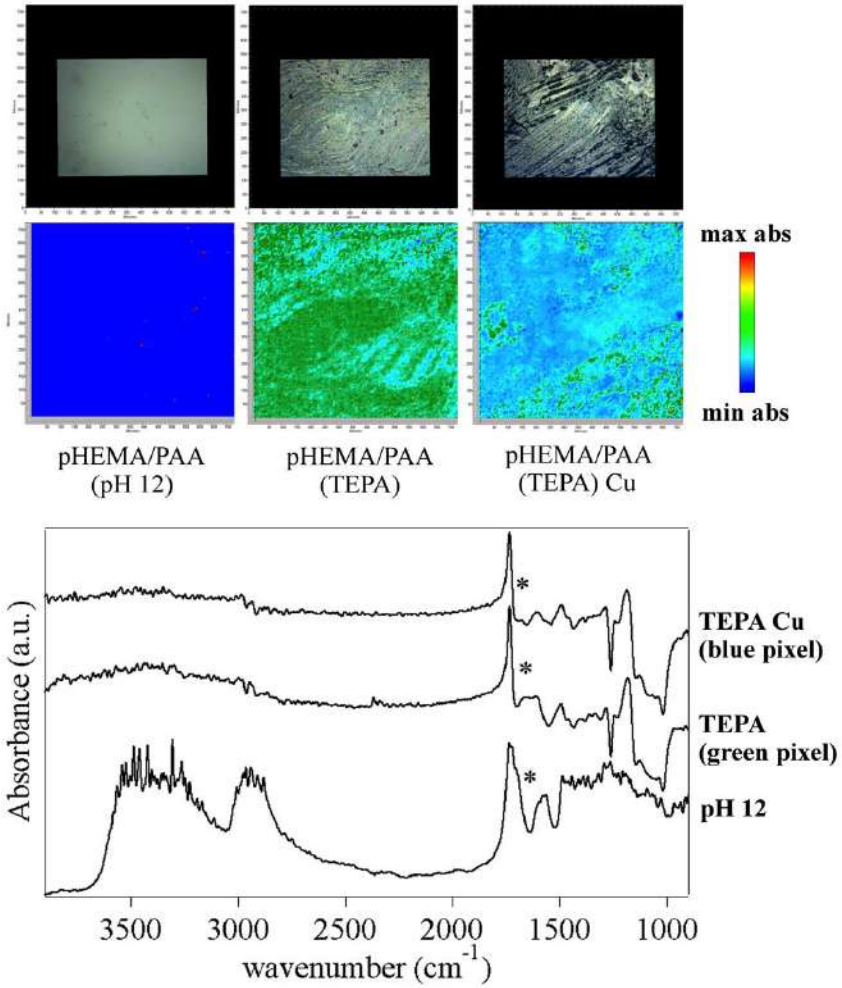

Figure 5. (Top) FTIR 2D Imaging of xerogels obtained from pHEMA/PAA hydrogels: (top left) swollen with water at pH 12; (top center) xerogels obtained from gels swollen with a TEPA solution (20%); (top right) xerogels obtained from gels that were swollen with the TEPA solution and then placed on a bronze coin mock-up containing Cu(II) corrosion products. Below each visible image, the corresponding 2D FTIR Imaging map shows the intensity of the band at 1660 cm^{-1} (assigned to the $-COO^-$ antysimmetric stretching of carboxylate groups in PAA). All maps have dimensions of 700 x 700 μm^2, each axis tick being 50 µm. The bottom panel shows representative spectra of pixels (5.5 x 5.5 μm^2) in the corresponding 2D Imaging map.

Figure 6 shows the FTIR 2D imaging of pHEMA/PVP xerogels obtained from gels swollen in water at different pH values. All the main absorptions of the two polymers are clearly observable[39,34], however a band at 1578 cm^{-1} progressively emerges when pH passes from 6 to 8 and 12, as evidenced in the 2D Imaging maps. This band could be assigned either to a combination of O-H and C-H bending[40], or to the presence of an enolate ion, even if the latter would be expected at slightly higher wavenumbers[41]. In fact, as previously reported, the enolate form of the enol structure of PVP is present at pH >> 10[31]. It must be noticed that the carbonyl band of the lactam form of PVP is also observable at 1655 cm^{-1}.

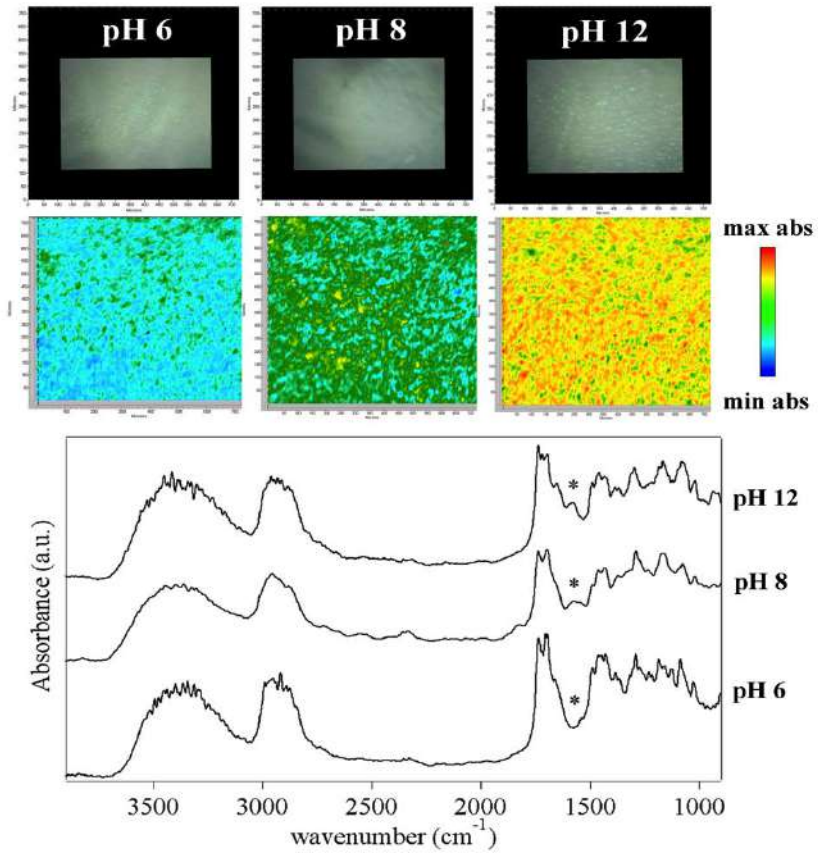

Figure 6. FTIR 2D Imaging of pHEMA/PVP xerogels obtained from hydrogels that were swollen with water at different pH values. Below each visible image, the corresponding 2D FTIR Imaging map shows the intensity of the band at 1578 cm^{-1} (assigned to the stretching of enolate ions in PVP). All

maps have dimensions of 700 x 700 μm^2, each axis tick being 50 μm. The bottom panel shows representative spectra of pixels (5.5 x 5.5 μm^2) in the corresponding 2D Imaging map.

When TEPA is uploaded in the pHEMA/PVP gels, an inhomogeneous pattern is observed in the FTIR 2D Imaging maps of the absorbance intensity in the 1615-1535 cm^{-1} region (see Figure 7). In the main portion of the maps (yellow-red pixels), the NH deformation band of TEPA at 1600 cm^{-1} is clearly observable, as part of a derivative peak whose flexus falls at ca. 1580 cm^{-1}. This band likely includes the contribution from enolate groups in PVP. In some portions (green pixels), no band around 1600 cm^{-1} is detected; instead, a shoulder to the PVP carbonyl peak is observed at ca. 1620 cm^{-1}, along with a derivative band with a maximum at 1500 cm^{-1} and a flexus at ca. 1485 cm^{-1}. We assigned the shoulder to the TEPA NH band (shifted upwards), and the derivative band to the enolate (shifted downwards) and CH_2 vibrations. The bands shifts were ascribed to interactions between the amine groups in TEPA and polar or charged CO groups in PVP. When Cu(II) ions are uploaded in the gel, the shifts are observed in significantly larger portions of the maps, which show a majority of green pixels. It is known that PVP is able to coordinate with copper through the O atom rather than N[42]. Thus, we hypothesized that the interactions between PVP and TEPA are favored by the coordination of Cu(II) with CO groups and amines, which come close together while binding to the ions.

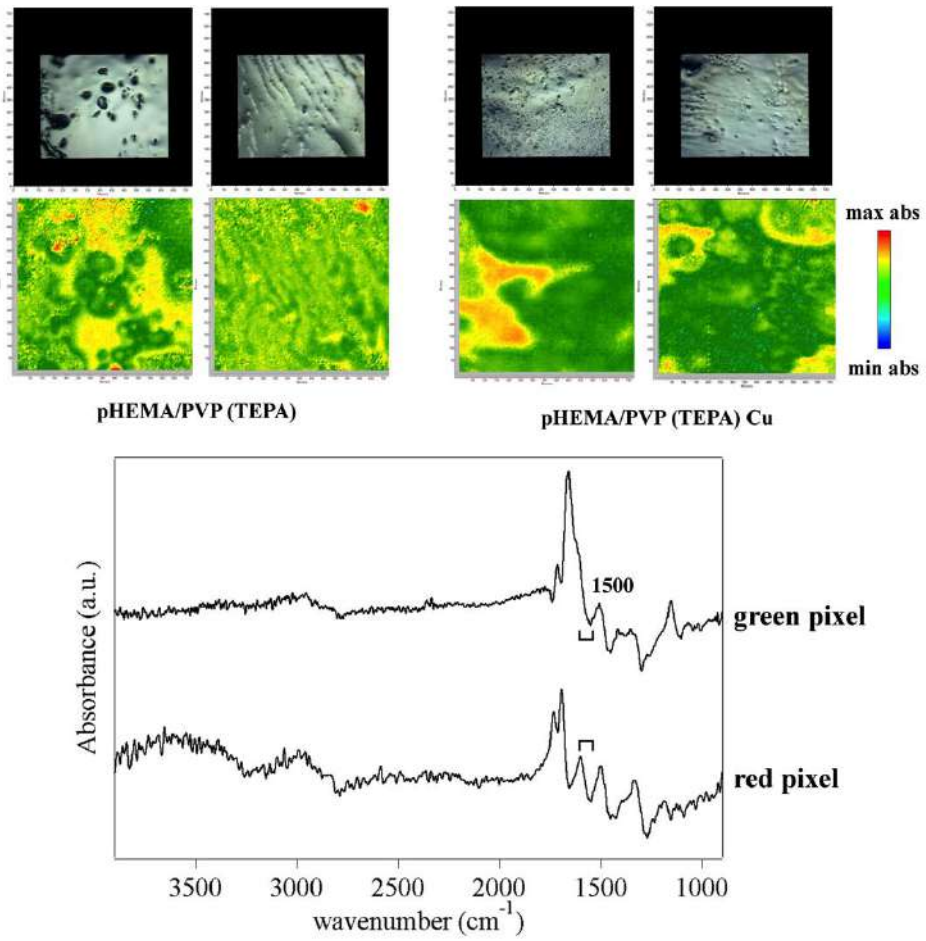

Figure 7. (Top, left panels) FTIR 2D Imaging of xerogels obtained from pHEMA/PVP hydrogels swollen with a TEPA solution (20%); (Top, right panels) xerogels obtained from gels that were swollen with the TEPA solution and then placed on a bronze coin mock-up containing Cu(II) corrosion products. Below each visible image, the corresponding 2D FTIR Imaging map shows the intensity of the 1615-1535 cm^{-1} region. All maps have dimensions of 700 x 700 μm^2, each axis tick being 50 μm. The bottom panel shows representative spectra of high (red) or low (green) intensity pixels (5.5 x 5.5 μm^2) in the corresponding 2D Imaging map.

Figures 8 and 9 show the results of the application of semi-IPNs loaded with TEPA on the surface of a bronze coin that was artificially aged to mimic archaeological bronze artifacts. After aging, the coin surface is covered with a thick and heterogeneous green patina of copper oxychlorides, which show

characteristic IR bands between 3550 and 3300 cm^{-1} (OH stretching[43]) and at 950 cm^{-1} [44]. The application of the gels led to the progressive removal of the oxychlorides, preserving the inner red layer (whose color is indicative of cuprite, Cu_2O[44] inhomogeneously present over the surface. The possibility of controlling the cleaning action, thanks to the use of retentive semi-IPNs, is advantageous from an applicative standpoint; in fact, cuprite can be considered as a protective layer against further corrosion, as it passivates the surface. Where cuprite was not present, the cleaning intervention brought back the bronze surface, and whitish patinas of calcium carbonate (identified thanks to characteristic IR bands at 2512, 1793 and 1463 cm^{-1} [45] that can eventually be removed using a complexing agent selective for calcium. 2D FTIR imaging confirmed the removal of copper oxychlorides at the micron scale (see Figure 9), down to the detection limit of the instrument (< 1 pg/pixel; 1 pixel = 5.5 x 5.5 μm^2). It must be noticed that semi-IPNs of pHEMA/PVP and pHEMA/PAA loaded with TEPA were equally effective in terms of cleaning power and duration of the intervention. In principle, pHEMA/PAA might be expected to remove copper corrosion products more efficiently, owing to the stronger complexing strength of carboxylate groups in PAA as compared to carbonyls in PVP. However, pHEMA/PVP gels have higher ESC, thanks to the hydrophilicity of PVP. Both formulations performed better than semi-IPNs loaded with EDTA (see Figure 8), as expected given the much higher stability constant of TEPA-Cu(II) complexes than those with EDTA.

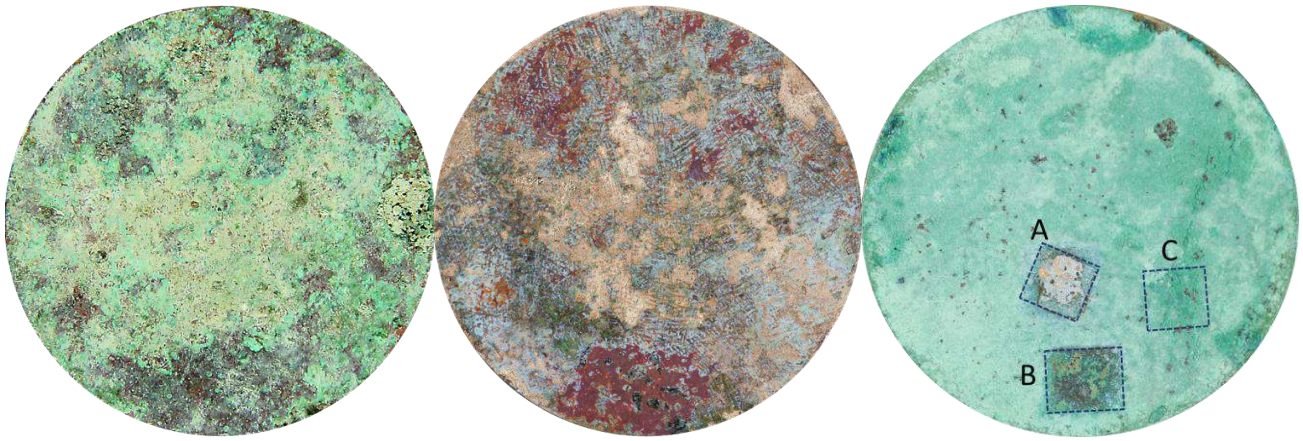

Figure 8. Artificially aged bronze coin before (left) and after (center) cleaning with semi-IPNs loaded with TEPA. The application of the gels (two cleaning rounds, 45 minutes each) led to the removal of the green corrosion products (copper oxychlorides), preserving the red cuprite layer that is inhomogeneously present on the coin surface. In some portions, whitish patinas composed of calcium carbonate were present beneath the oxychlorides layer. (Right) Preliminary cleaning tests showing the progressive removal of corrosion products after the application of semi-IPNs loaded with TEPA for 1 hour (A) or 20 minutes (B). The application of a semi-IPN loaded with EDTA for 1 hour (C) did not remove the corrosion products.

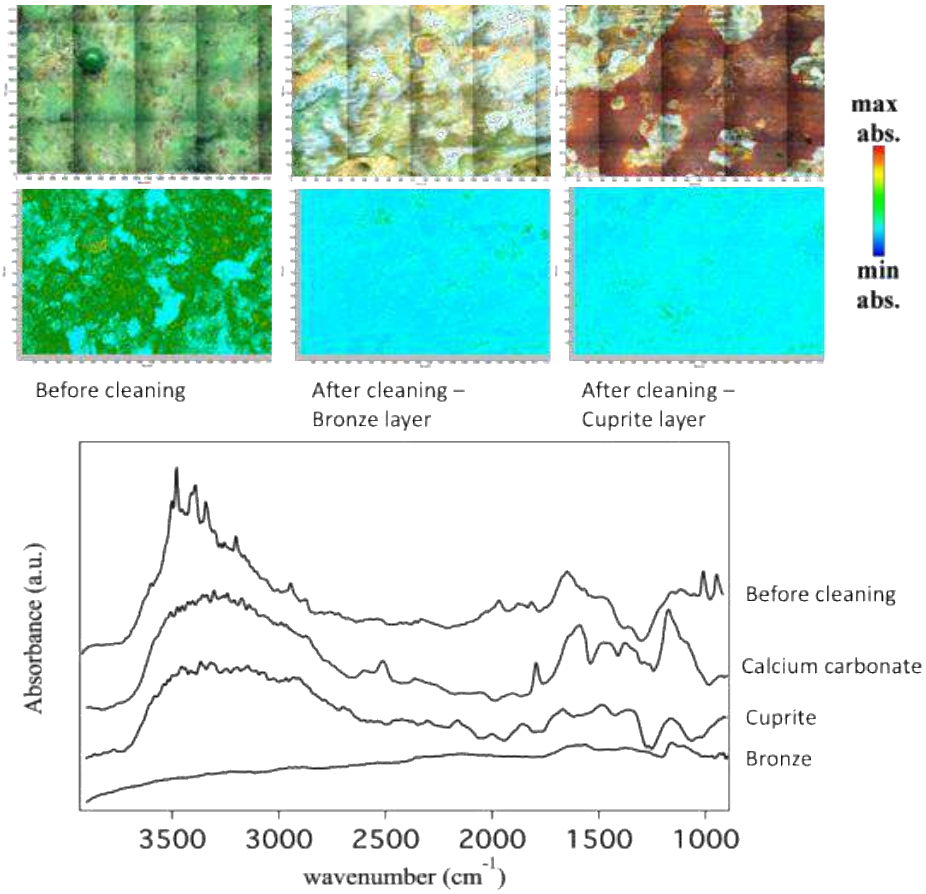

Figure 9. FTIR 2D Imaging of an artificially aged bronze coin before (top, left panel) and after (top, center and right panel) the application of a pHEMA/PVP semi-IPN loaded with TEPA. Below each visible image, the corresponding 2D FTIR Imaging map shows the intensity of the band between 3550 and 3300 cm^{-1} (stretching of OH groups in Cu(II) oxychlorides). All maps have dimensions of 1400 x 2000 μm^2, each axis tick being 50 µm. The bottom panel shows representative spectra of pixels (5.5 x 5.5 μm^2) in the corresponding 2D Imaging maps, from bottom to top: the cleaned bronze surface, the red layer of cuprite, calcium carbonate patinas, and copper oxychlorides (atacamite, paratacamite).

CONCLUSIONS

A pHEMA/PAA semi-IPN was formulated for the first time uploading aqueous solutions at different pH values, and was compared with a pHEMA/PVP semi-IPN. Solutions of TEPA were uploaded in both type of gels to remove corrosion products from aged bronze coins.

Increasing the pH induces changes in the structure of the gels. In the case of pHEMA/PAA, carboxyls in the PAA chains are progressively ionized, as confirmed by 2D FTIR imaging. This results in the swelling of the polymer network, evidenced by an increase in the meso- and macroporosity, and in the amount of free water uploaded in the gels. TEPA molecules interact with carboxyls in PAA, making the semi-IPN tighter (lower mesh size) by screening the repulsion between carboxylate groups. When Cu(II) ions are absorbed in the TEPA-loaded network, ternary PAA-Cu-TEPA complexes are probably formed, where two coordination sites are covered by PAA carboxylates, and two by amine groups. For what concerns pHEMA/PVP semi-IPNs, increasing the pH leads to the partial abstraction of protons from the alcohol group in the enol form of PVP (pH >> 10). Significant changes in the macroporosity are observed at each pH variation step (6; 8; 12). Besides, the mesoporosity decreases at high pH values, as the inter and intramolecular hydrogen bonds between enol and enolate groups in the PVP chains cause a decrease in the mesh size. FTIR 2D Imaging let us hypothesize that the interactions between polar or charged CO groups of PVP and TEPA are favored by the formation of ternary complexes with Cu(II) ions, where CO and amine groups come close together while binding to the metal.

Even though loading with alkaline solutions of water and TEPA changes the micro- and nanostructure of the gels, it does not hinder their applicability for the removal of corrosion products from bronze surfaces. When the TEPA-loaded gels are applied onto corroded bronze coins, they gradually release the polyamine solution on the surface, solubilizing and removing the Cu(II) oxychlorides in the corrosion layers. The dissolved copper ions migrate into the gels and form complexes, which gives the gels an intense blue color. Both pHEMA/PAA and

pHEMA/PVP allowed an effective and controlled removal of corrosion products, while preserving the inner red corrosion layer (cuprite) that is normally left on bronze artifacts as a passivation layer against recurring corrosion. Loading with TEPA dramatically enhanced the cleaning power of the gels as opposed to EDTA, strongly decreasing the time needed for the intervention.

Overall, TEPA-loaded semi-IPNs of pHEMA/PAA and pHEMA/PVP proved to be promising tools for the preservation of archaeological and historical bronze artifacts, overcoming the limitations of traditional restoration practice based on the use of EDTA solutions and mechanical cleaning.

REFERENCES

1. Dümcke, C. & Gnedovsky, M. The Social and Economic Value of Cultural Heritage: literature review. 145 (2013).
2. Scott, D. A. A Review of Copper Chlorides and Related Salts in Bronze Corrosion and as Painting Pigments. *Stud. Conserv.* **45**, 39–53 (2000).
3. Ingo, G. M. *et al.* Combined use of SEM-EDS, OM and XRD for the characterization of corrosion products grown on silver roman coins. *Appl. Phys. A* **83**, 493–497 (2006).
4. Degrigny, C. *Survey of European Experience on Cleaning Procedures*. (Nardini Editore, 2004).
5. Scott, D. A. *Copper and bronze in art*. (The Getty Conservation Institute, 2002).

6. Siano, S. *et al.* Laser cleaning in conservation of stone, metal, and painted artifacts: state of the art and new insights on the use of the Nd:YAG lasers. *Appl. Phys. A* **106**, 419–446 (2012).
7. Baglioni, P., Chelazzi, D. & Giorgi, R. *Nanotechnologies in the Conservation of Cultural Heritage: A compendium of materials and techniques*. (Springer, 2014).
8. Chelazzi, D., Giorgi, R. & Baglioni, P. Microemulsions, Micelles, and Functional Gels: How Colloids and Soft Matter Preserve Works of Art. *Angew. Chem. Int. Ed Engl.* **57**, 7296–7303 (2018).
9. Baglioni, P., Chelazzi, D., Giorgi, R. & Poggi, G. Colloid and Materials Science for the Conservation of Cultural Heritage: Cleaning, Consolidation, and Deacidification. *Langmuir* **29**, 5110–5122 (2013).
10. Baglioni, P., Carretti, E. & Chelazzi, D. Nanomaterials in art conservation. *Nat. Nanotechnol.* **10**, 287–290 (2015).
11. Carretti, E. *et al.* New frontiers in materials science for art conservation: responsive gels and beyond. *Acc. Chem. Res.* **43**, 751–760 (2010).
12. Díaz, E., Valenciano, R. B. & Katime, I. A. Study of complexes of poly(vinyl pyrrolidone) with copper and cobalt on solid state. *J. Appl. Polym. Sci.* **93**, 1512–1518 (2004).
13. Sebastian, N., George, B. & Mathew, B. Metal complexes of poly(acrylic acid): synthesis, characterization and thermogravimetric studies. *Polym. Degrad. Stab.* **60**, 371–375 (1998).

14. Elliott, J. E., Macdonald, M., Nie, J. & Bowman, C. N. Structure and swelling of poly(acrylic acid) hydrogels: effect of pH, ionic strength, and dilution on the crosslinked polymer structure. *Polymer* **45**, 1503–1510 (2004).

15. Critical Stability Constants - Volume 2: Amines | Arthur Martell | Springer. Available at: https://www.springer.com/gp/book/9781461344544. (Accessed: 17th July 2019)

16. Comyns, A. E. Handbook of Copper Compounds and Applications. H.W. Richardson (ed.) Marcel Dekker, New York, 1997 viii + 432 pages $175 ISBN 0-8247-8998-9. *Appl. Organomet. Chem.* **14**, 174–175 (2000).

17. *Ancient & historic metals: conservation and scientific research: proceedings of a symposium organized by the J. Paul Getty Museum and the Getty Conservation Institute, November 1991*. (Getty Conservation Institute, 1994).

18. Domingues, J. A. L. *et al.* Innovative Hydrogels Based on Semi-Interpenetrating p(HEMA)/PVP Networks for the Cleaning of Water-Sensitive Cultural Heritage Artifacts. *Langmuir* **29**, 2746–2755 (2013).

19. Fecchio, B. D., Valandro, S. R., Neumann, M. G. & Cavalheiro, C. C. S. Thermal Decomposition of Polymer/Montmorillonite Nanocomposites Synthesized in situ on a Clay Surface. *J. Braz. Chem. Soc.* (2015). doi:10.5935/0103-5053.20150216

20. Müller-Plathe, F. Different states of water in hydrogels? *Macromolecules* **31**, 6721–6723 (1998).

21. Lele, A. K., Hirve, M. M., Badiger, M. V. & Mashelkar, R. A. Predictions of bound water content in poly(N-isopropylacrylamide) gel. *Macromolecules* **30**, 157–159 (1997).

22. Bhagwan, P. *A Handbook Of Thermodynamics*. (Mittal Publications).

23. T. N. Blanton, T. C. H. JCPDS--International Centre for Diffraction Data round robin study of silver behenate. A possible low-angle X-ray diffraction calibration standard. *Powder Diffr. - POWDER DIFFR* **10**, 91–95 (1995).

24. Ingo, G. M. *et al.* Rebuilding of the Burial Environment from the Chemical Biography of Archeological Copper-Based Artifacts. *ACS Omega* **4**, 11103–11111 (2019).

25. Debye, P. & Bueche, A. M. Scattering by an Inhomogeneous Solid. *J. Appl. Phys.* **20**, 518–525 (1949).

26. Horkay, F. & Hammouda, B. Small-angle neutron scattering from typical synthetic and biopolymer solutions INVITED REVIEW. in (2008).

27. Wang, W. *et al.* Interactions among spherical poly(acrylic acid) brushes: Observation by rheology and small angle X-ray scattering. *Journal of Polymer Science Part B: Polymer Physics* (2016). doi:10.1002/polb.23901

28. Canal, T. & Peppas, N. A. Correlation between mesh size and equilibrium degree of swelling of polymeric networks. *J. Biomed. Mater. Res.* **23**, 1183–1193 (1989).

29. Cheng, J., Shan, G. & Pan, P. Temperature and pH-dependent swelling and copper(II) adsorption of poly(N-isopropylacrylamide) copolymer hydrogel. *RSC Adv.* **5**, 62091–62100 (2015).

30. Hara, K., Sugiyama, M., Annaka, M. & Soejima, Y. Nanostructural characterization of the dehydrated (NIPA/SA+additive ion) gels. *Colloids Surf. B Biointerfaces* **38**, 197–200 (2004).

31. Nikiforova, T. E., Kozlov, V. A. & Islyaikin, M. K. Acid-base interactions and complex formation while recovering copper(II) ions from aqueous solutions using cellulose adsorbent in the presence of polyvinylpyrrolidone. *Russ. J. Phys. Chem. A* **86**, 1836–1846 (2012).

32. Noferini, D. *et al.* Disentangling Polymer Network and Hydration Water Dynamics in Polyhydroxyethyl Methacrylate Physical and Chemical Hydrogels. *J. Phys. Chem. C* (2019). doi:10.1021/acs.jpcc.9b04212

33. Okay, O. Macroporous copolymer networks. *Prog. Polym. Sci.* **25**, 711–779 (2000).

34. Perova, T. S., Vij, J. K. & Xu, H. Fourier transform infrared study of poly (2-hydroxyethyl methacrylate) PHEMA. *Colloid Polym. Sci.* **275**, 323–332 (1997).

35. Dong, J., Ozaki, Y. & Nakashima, K. FTIR studies of conformational energies of poly(acrylic acid) in cast films. *J. Polym. Sci. Part B Polym. Phys.* **35**, 507–515 (1997).

36. Srikanth, C. S. & Chuang, S. S. C. Spectroscopic Investigation into Oxidative Degradation of Silica-Supported Amine Sorbents for CO2 Capture. *ChemSusChem* **5**, 1435–1442 (2012).

37. Todica, M., Stefan, R., Pop, C. V. & Olar, L. IR and Raman Investigation of Some Poly(acrylic) Acid Gels in Aqueous and Neutralized State. *Acta Phys. Pol. A* **128**, 128–135 (2015).

38. Kabanov, N. M., Kokorin, A. I., Rogacheva, V. B. & Zezin, A. B. Study of the structure of a polyacrylic acid-polyethyleneimine-copper (II) ternary polymer-metal complex. *Polym. Sci. USSR* **21**, 230–240 (1979).

39. M. Koczkur, K., Mourdikoudis, S., Polavarapu, L. & E. Skrabalak, S. Polyvinylpyrrolidone (PVP) in nanoparticle synthesis. *Dalton Trans.* **44**, 17883–17905 (2015).

40. Mondal, A. & Mandal, B. CO2 separation using thermally stable crosslinked poly(vinyl alcohol) membrane blended with polyvinylpyrrolidone/polyethyleneimine/tetraethylenepentamine. *J. Membr. Sci. Complete*, 126–138 (2014).

41. Bender, M. L. & Figueras, J. The Infrared Spectra of Enolate Ions. *J. Am. Chem. Soc.* **75**, 6304–6304 (1953).

42. Shahmiri, M., Ibrahim, N. A., Shayesteh, F., Asim, N. & Motallebi, N. Preparation of PVP-coated copper oxide nanosheets as antibacterial and antifungal agents. *J. Mater. Res.* **28**, 3109–3118 (2013).

43. Martens, W., Frost, R. L. & Williams, P. A. Raman and infrared spectroscopic study of the basic copper chloride minerals – implications for the study of the copper and brass corrosion and 'bronze disease'. *Neues Jahrb. Für Mineral. - Abh.* **178**, 197–215 (2003).

44. Di Carlo, G. *et al.* Artificial patina formation onto copper-based alloys: Chloride and sulphate induced corrosion processes. *Appl. Surf. Sci.* **421**, 120–127 (2017).

45. Ricci, C., Miliani, C., Brunetti, B. G. & Sgamellotti, A. Non-invasive identification of surface materials on marble artifacts with fiber optic mid-FTIR reflectance spectroscopy. *Talanta* **69**, 1221–1226 (2006).

Supporting Information

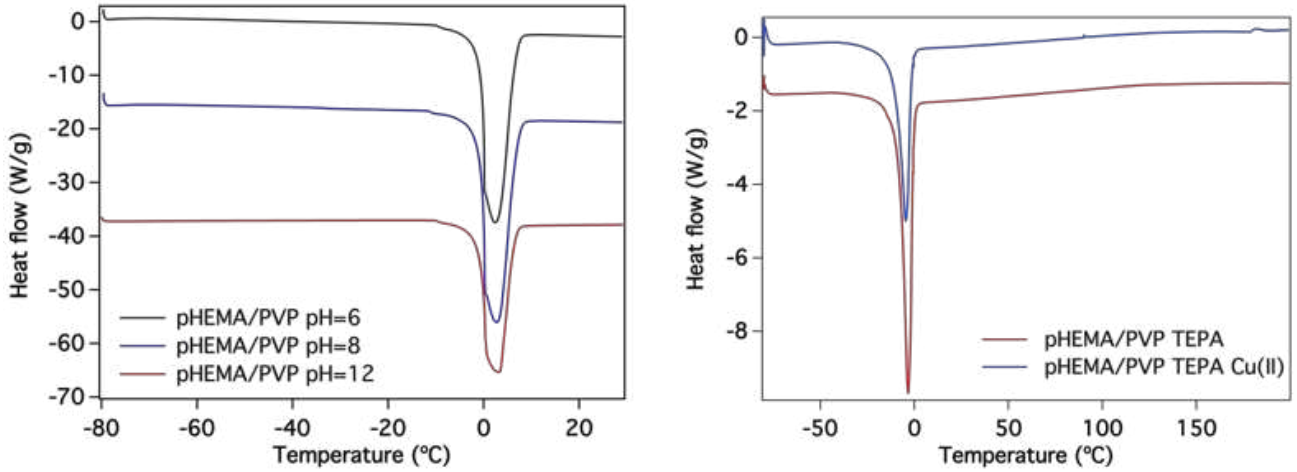

Figure S1. DSC thermograms of pHEMA/PAA hydrogels swollen in water (left panel) and in TEPA (right panel). The reported curves are offset along y-axis for clarity.

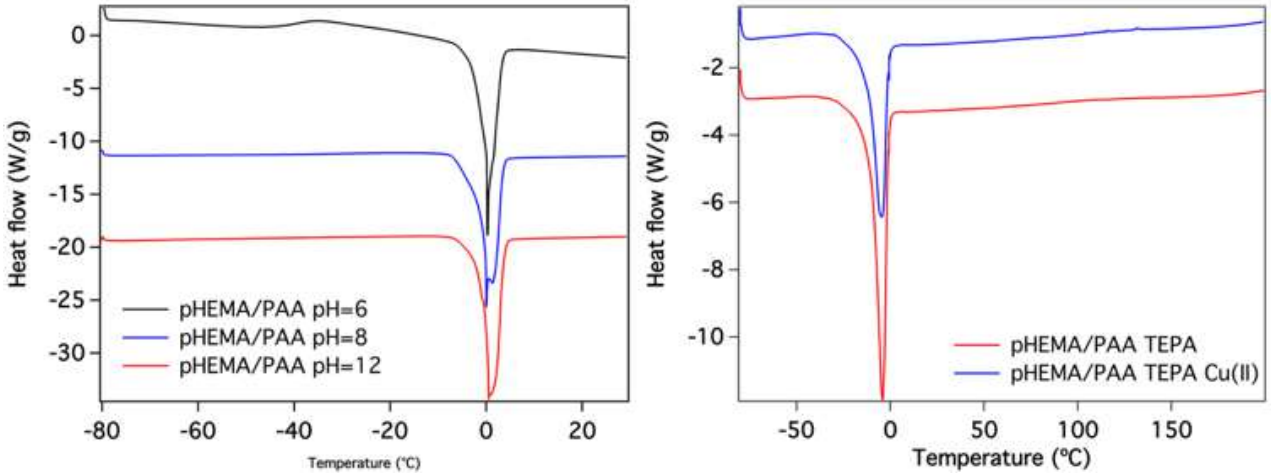

Figure S2. DSC thermograms of pHEMA/VP hydrogels swollen in water (left panel) and in TEPA (right panel). The reported curves are offset along y-axis for clarity.